GEOLOGICAL SURVEY OF CANADA
PAPER 91-9

MINERAL DEPOSIT STUDIES IN NOVA SCOTIA VOLUME 2

edited by
A.L. Sangster

1993

Energy, Mines and Resources Canada
Énergie, Mines et Ressources Canada

Canada

GEOLOGICAL SURVEY OF CANADA
PAPER 91-9

MINERAL DEPOSIT STUDIES IN NOVA SCOTIA VOLUME 2

edited by
A.L. Sangster

1993

Available in Canada through authorized
bookstore agents and other bookstores

or by mail from

Canada Communication Group – Publishing
Ottawa, Canada K1A 0S9

and from

Geological Survey of Canada offices:

601 Booth Street
Ottawa, Canada K1A 0E8

3303-33rd Street N.W.,
Calgary, Alberta T2L 2A7

A deposit copy of this publication is also available for reference
in public libraries across Canada

Cat. No. M44-91/9E
ISBN 0-660-14983-4

Price subject to change without notice

Technical Editor

O.E. Inglis

Cover description

Carbonate dyke or vein cutting interbedded carbonate in carbonaceous argillite, Tangier Gold District, Nova Scotia. This lithology hosts auriferous quartz carbonate veins that are bedding-parallel (long dimension is approximately 20 cm). (GSC 1993-044)

CONTENTS

INTRODUCTION

This is the second and final compendium volume of scientific papers resulting from geoscience research carried out under the Canada-Nova Scotia Mineral Development Agreement, 1984-1989. The volume contains four papers. Three of these papers, authored by K. Ford, J. Kerswill, and F. Hein, M. Graves and A. Ruffman, resulted from studies carried out or sponsored by the Mineral Resources Division of the Geological Survey of Canada. The fourth, co-authored by A. Macdonald and S. Barr, is a study of mineral occurrences, funded by an EMR Research Agreement and an NSERC Operating Grant to S. Barr, that was carried out in conjunction with mapping in the Blue Mountain-French Road area of southeastern Cape Breton Island funded by the Continental Geoscience Division.

The editor wishes to thank all geologists who contributed in any way to the production of this volume. In particular he thanks the Nova Scotia Department of Natural Resources, and members of the Industrial Review Committee of the Nova Scotia Chamber of Mineral Resources who contributed time and effort in monitoring the progress of projects. Gratitude is also expressed to the geologists who reviewed the papers included here. They are as follows:

A.K. Chatterjee, Nova Scotia Department of Natural Resources
R. Boehner, Nova Scotia Department of Natural Resources
B. Ballantyne, Geological Survey of Canada
A. Sangster, Geological Survey of Canada
D.F. Sangster, Geological Survey of Canada
D. Sinclair, Geological Survey of Canada
R. Thorpe, Geological Survey of Canada

INTRODUCTION

Voici le second et dernier volume du compendium d'études scientifiques qui découle des recherches géoscientifiques entreprises dans le cadre de l'Entente Canada - Nouvelle-Écosse sur l'exploitation minérale 1984-1989. Le volume contient quatre études, dont trois, rédigées par K. Ford, J. Kerswill, et F. Heine, M. Graves et A. Ruffman, portent sur des travaux menés ou parrainés par la Division des ressources minérales de la Commission géologique du Canada. La quatrième étude, par A. Macdonald et S. Barr, est un examen des venues minérales qui a été financé par une convention de recherche d'EMR et une subvention de fonctionnement du CRSNG accordées à S. Barr; les travaux ont été effectués dans la région du mont Blue et du chemin French, dans le sud-est de l'île du Cap-Breton, en même temps que des travaux de cartographie financés par la Division de la géologie du continent.

Le rédacteur désire exprimer sa reconnaissance à tous les géologues qui ont contribué à la production du volume et, en particulier, au ministère des Richesses naturelles de la Nouvelle-Écosse et aux membres du comité de révision industrielle de la Nova Scotia Chamber of Mineral Resources (Chambre des ressources minérales de la Nouvelle-Écosse) qui ont surveillé l'avancement des projets. Il remercie aussi les géologues suivants, qui ont passé en revue les études du volume :

A.K. Chatterjee, ministère des Richesses naturelles de la Nouvelle-Écosse
R. Boehner, ministère des Richesses naturelles de la Nouvelle-Écosse
B. Ballantyne, Commission géologique du Canada
A. Sangster, Commission géologique du Canada
D.F. Sangster, Commission géologique du Canada
D. Sinclair, Commission géologique du Canada
R. Thorpe, Commission géologique du Canada

The Blue Mountain polymetallic skarn and associated porphyry dykes, southeastern Cape Breton Island, Nova Scotia

Alan S. Macdonald[1] and Sandra M. Barr[1]

Macdonald, A.S. and Barr, S.M., 1993: The Blue Mountain polymetallic skarn and associated porphyry dykes, southeastern Cape Breton Island, Nova Scotia; in Mineral Deposit Studies in Nova Scotia, Volume 2, (ed.) A.L. Sangster; Geological Survey of Canada, Paper 91-9, p. 3-18.

Abstract

Polymetallic skarn in the Blue Mountain area of southeastern Cape Breton Island occurs within an area of contact metamorphosed Cambrian sedimentary rocks. The skarn forms massive layers, up to 5 m thick, within nodular calc-silicate hornfels. The skarn layers are stratigraphically controlled and are interpreted to have formed from calcareous sedimentary protoliths. They are composed of prograde garnet-rich material consisting of zoned grossularite, andradite, and magnetite, surrounded and partially replaced by retrograde amphibole-rich material consisting of magnesian anthophyllite, epidote, quartz, calcite, and sulphides. Economic elements associated with the skarn include Cu, Co, Bi, Sn, Ag, and Au. The skarn shows features characteristic of Cu-bearing polymetallic calcic skarns associated with barren stocks, and possibly also of gold-bearing skarns.

Porphyry dykes in drill core from the Blue Mountain skarn occurrences are probably related to an underlying Devonian intrusion that produced the hornfels, skarn, and polymetallic mineralization. This postulated intrusion forms part of a transverse, arcuate belt of Devonian plutons that also includes Deep Cove, Gillis Mountain, and Salmon River. The Blue Mountain dykes are chemically similar to granitic units and dykes in the Deep Cove and Gillis Mountain plutons but are less evolved than the Salmon River rhyolite porphyry. Elevated metal abundances in these intrusions reflect the mineralization with which they are associated.

Résumé

Dans la région de Blue Mountain du sud-est de l'île du Cap-Breton, un skarn polymétallique apparaît dans une région de roches sédimentaires d'âge cambrien qui ont subi un métamorphisme de contact. Le skarn forme des couches massives pouvant atteindre 5 m d'épaisseur, à l'intérieur d'une cornéenne nodulaire calco-silicatée. Les couches de skarn montrent un contrôle stratigraphique et se sont sans doute formées à partir de protolithes sédimentaires de composition calcaire. Elles contiennent des matériaux prograde riches en grenat, qui sont constitués de grossularite zonée, d'andradite et de magnétite, entourées et partiellement remplacées par des matériaux rétrogrades riches en amphibole, composés d'anthophyllite magnésienne, d'épidote, de quartz, de calcite et de sulfures. Les éléments d'intérêt économique associés au skarn sont notamment Cu, Co, Bi, Sn, Ag et Au. Le skarn présente certains caractères des skarns calciques polymétalliques cuprifères associés à des stocks stériles, et peut-être aussi des skarns aurifères.

Les dykes porphyriques observés dans les carottes de sondage provenant des venues de skarn de Blue Mountain, sont probablement apparentés à une intrusion dévonienne sous-jacente qui a produit la cornéenne, le skarn et la minéralisation polymétallique. Cette intrusion supposée fait partie d'une zone transversale arquée de plutons du Dévonien qui inclut également les plutons de Deep Cove, de Gillis Mountain et de Salmon River. Les dykes de Blue Mountain présentent une similarité chimique avec les unités et dykes granitiques des plutons de Deep Cove et de Gillis Mountain, mais sont parvenus à un moindre degré d'évolution que le porphyre rhyolitique de Salmon River. La grande abondance des métaux dans ces intrusions reflète la minéralisation à laquelle ils sont associés.

[1] Department of Geology, Acadia University, Wolfville, Nova Scotia, B0P 1X0.

INTRODUCTION

Polymetallic skarn occurs in hornfelsed Cambrian sedimentary rocks in the Blue Mountain area of southeastern Cape Breton Island (Fig. 1). No plutonic source for the contact metamorphic aureole has been found in outcrop but an unexposed pluton of Devonian age has been inferred to underlie the area (Hutchinson, 1952; Macdonald, 1989). Blue Mountain is located in the north-central part of an arcuate zone of Devonian granitoid plutons (Fig. 1) which is transverse to regional structural trends. Polymetallic mineralization is associated with these plutons at Gillis Mountain and Deep Cove (Barr et al., 1982; Barr and Macdonald, 1985; Dennis, 1988), as well as at Blue Mountain.

Exploration of the skarn in the Blue Mountain area began about 100 years ago with the sinking of a shaft into a chalcopyrite-rich occurrence north of French Road (Fig. 2), and has continued in recent years with several programs of diamond drilling and geochemical and geophysical surveys (Bruce, 1969; Sangster, 1977; Forgeron, 1981). Other than those assessment reports, the only descriptions of the occurrences are by Chatterjee (1977) who suggested that the skarn represents metasomatized volcanic layers, and Macdonald (1989) who proposed that they are contact metamorphosed/metasomatized calcareous layers and nodules of sedimentary/diagenetic origin.

The purpose of this paper is to present new information on (i) the form and mineralogy of the skarns, (ii) the geochemistry of a suite of rhyolitic porphyry dykes that is spatially associated with the skarns and that may represent the inferred underlying pluton, and (iii) the age and geological setting of the polymetallic mineralization.

GEOLOGICAL SETTING

The skarn and enclosing hornfels occur within a crudely elliptical area, approximately 3 km by 1 km, in Lower to Middle Cambrian argillite and sandstone of the MacCodrum, Canoe Brook, Trout Brook, and McLean Brook formations (Fig. 2). These formations are folded into north-northeast- to northeast-trending, upright to slightly overturned folds verging toward the northwest. Cleavage is widely developed and varies from fracture to slaty cleavage depending on the lithology involved and its structural position. Although both bedding and cleavage have been obscured by the effects of thermal metamorphism in the Blue Mountain aureole, they can still be detected in many outcrops of hornfels. Black biotite-cordierite hornfels (locally containing abundant calc-silicate nodules) and less abundant grey biotite-quartz granofels are the main metamorphic rock types present within the aureole, although faulting has locally juxtaposed large blocks of essentially unmetamorphosed argillite with the metamorphic rocks (Fig. 3).

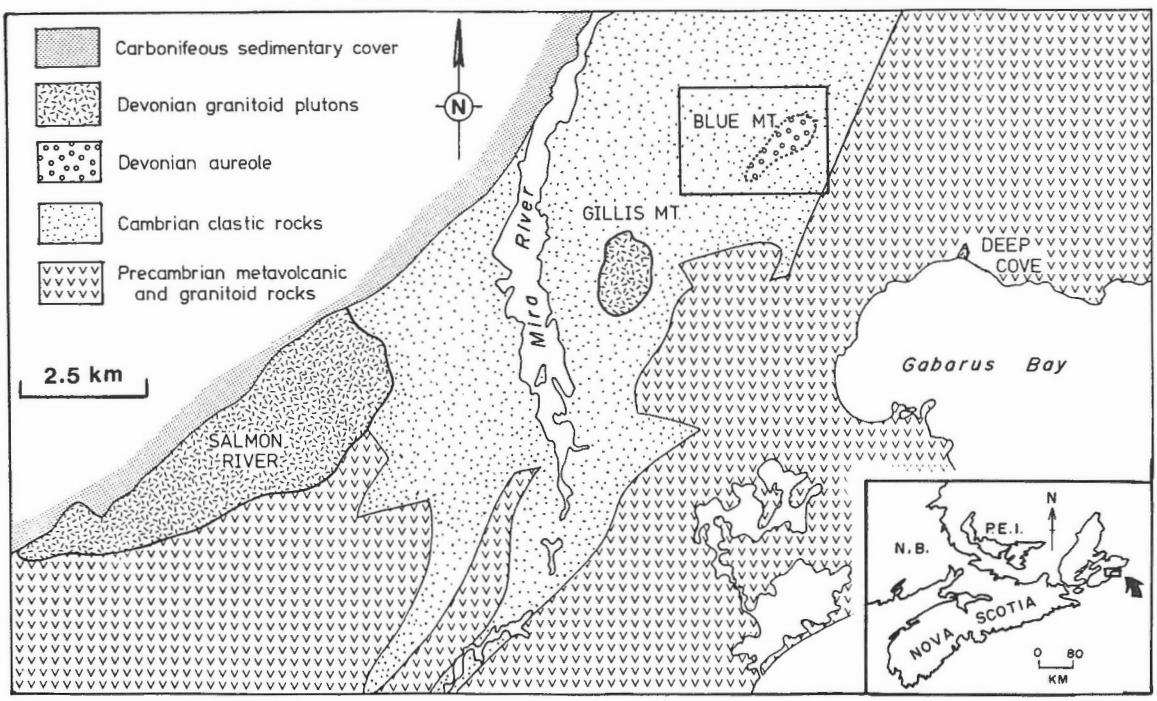

Figure 1. Generalized geological map showing the distribution of Devonian granitoid plutons in southeastern Cape Breton Island and the location of the Blue Mountain contact metamorphic aureole. Area of Figure 2 is outlined in black.

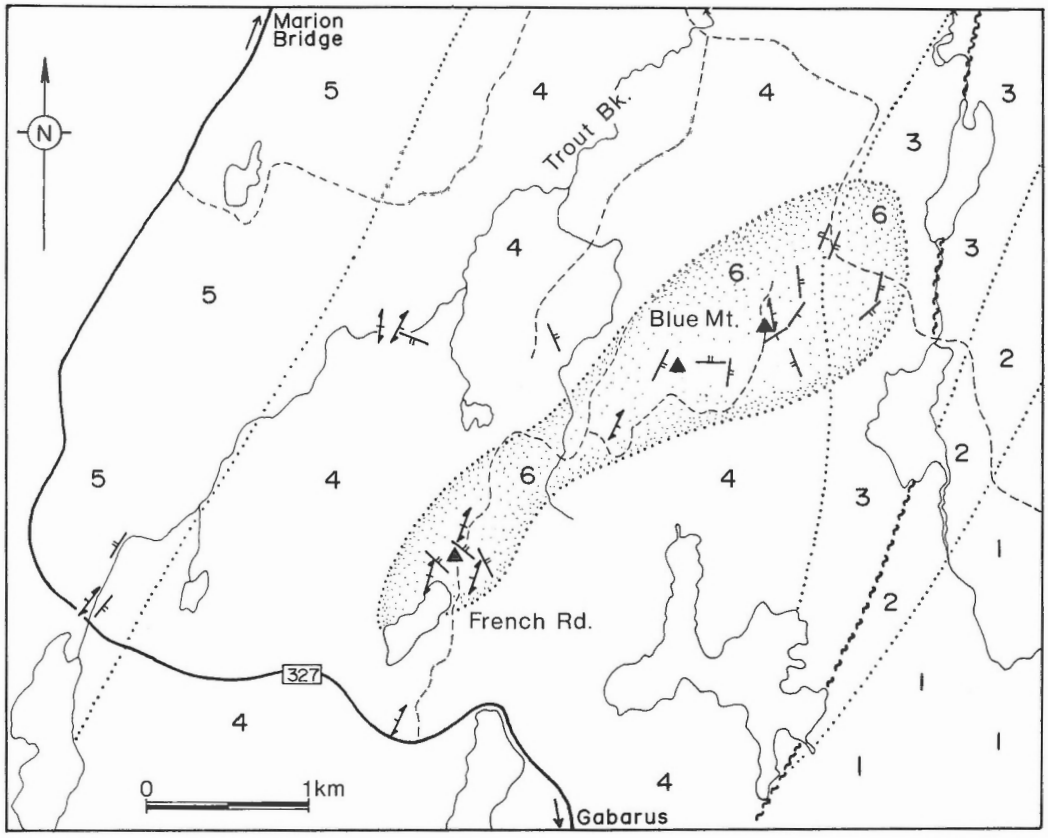

DEVONIAN
Contact aureole

6 hornfels, granofels & skarn

MIDDLE CAMBRIAN
MacLean Brook Formation

5 grey sandstone, siltstone, & argillite

Trout Brook Formation

4 black argillite

LOWER CAMBRIAN
Canoe Brook & MacCodrum Formations

3 red argillite, sandstone

Morrison River Formation

2 conglomerate

LATE HADRYNIAN
Fourchu Group

1 metavolcanic flows & tuffs

▲ mineralized skarn occurrences

bedding (right-way-up, overturned, way-up unknown)

cleavage

fault

Figure 2. Geology of the Blue Mountain area (modified after Macdonald, 1989), showing the locations of the Blue Mountain and French Road skarn occurrences.

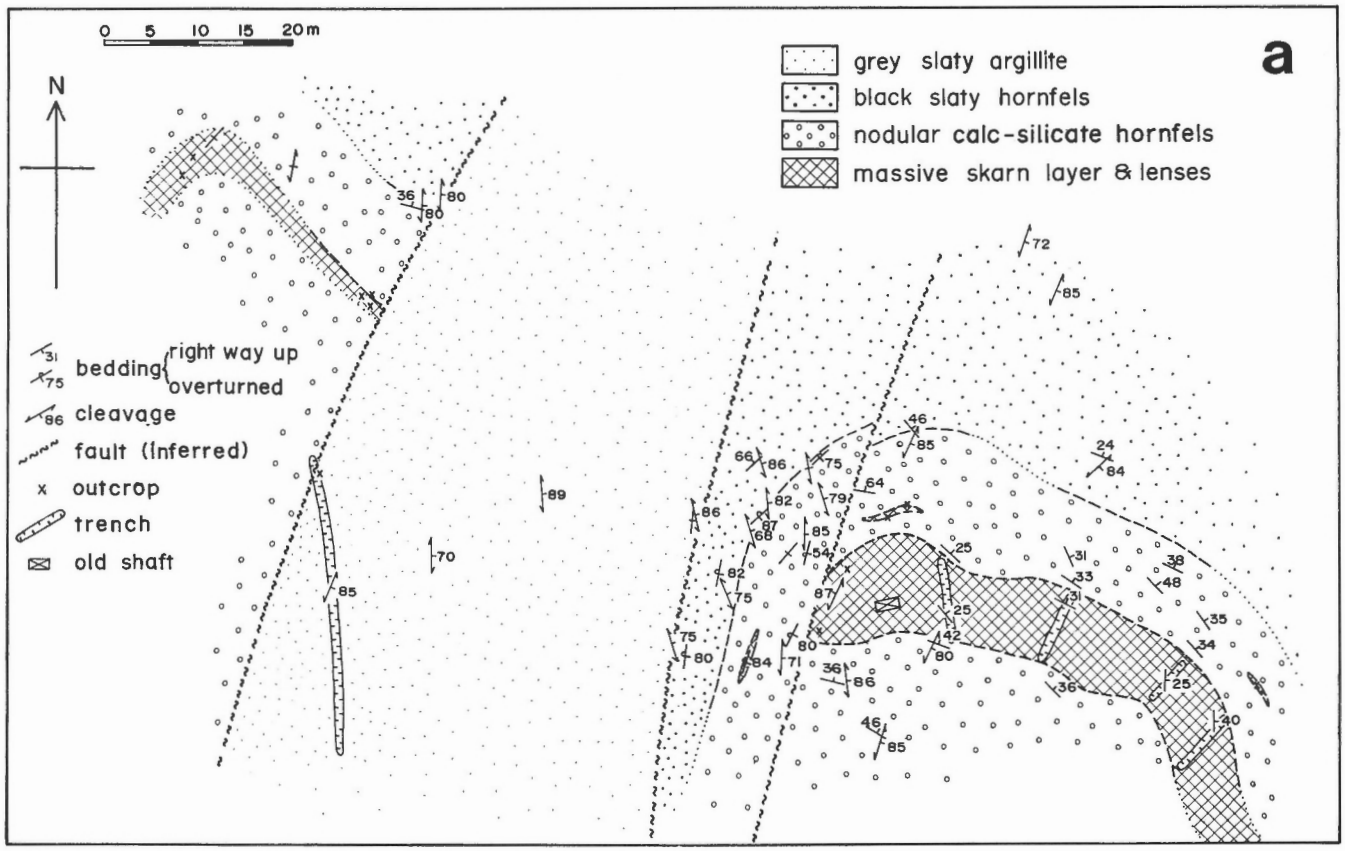

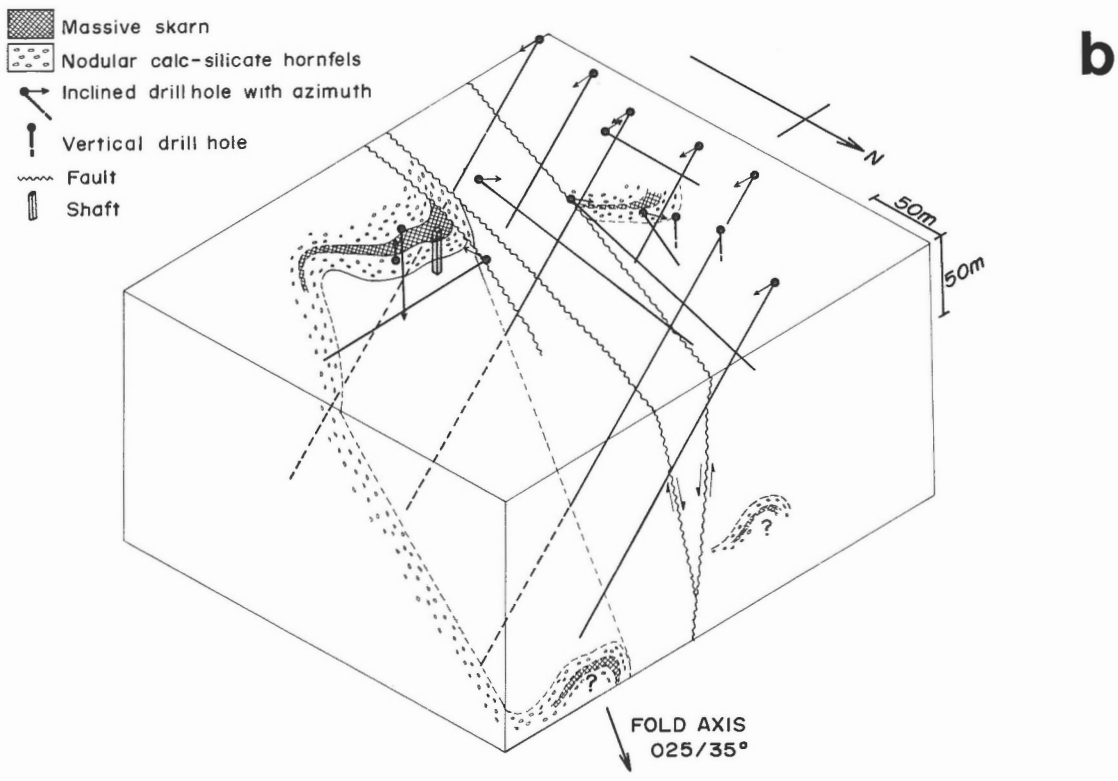

Figure 3. (a) Detailed geology in the vicinity of the French Road skarn occurrence; (b) Isometric block diagram showing down-plunge projection of the French Road skarn, with drill hole locations and orientations after Forgeron (1981).

A biotite concentrate from the hornfels has yielded a K-Ar age of 357 ± 12 Ma (Appendix 1), which is interpreted to represent the time of cooling of the hornfels. Hence it represents a minimum age for the intrusion inferred to underlie the metamorphic aureole.

SKARN OCCURRENCES

Skarn occurs as lenses and massive layers within nodular calc-silicate hornfels. The best exposed and most intensely explored skarn is the French Road occurrence, located between Blue Mountain and French Road (Fig. 2). At this locality, a green and brown massive skarn layer, up to 5 m thick, occurs within an envelope of nodular calc-silicate hornfels, at least 70 m thick, located in a fold structure which plunges at 35° towards the north-northeast (eastern part of Fig. 3a; Fig. 4a). The western limb of the fold structure is slightly overturned and faulted against apparently unmetamorphosed grey-green slaty argillite lacking both skarn and mineralization. Farther west, poorly exposed calc-silicate hornfels with one or more lenses of massive skarn reappear (western part of Fig. 3a). Cleavage orientation is somewhat variable but averages about 015/80°E which is essentially axial planar to the fold structure defined in the area of the occurrence (Fig. 4a, b). Bedding orientations in the enclosing hornfels and the distribution of the massive skarn layer indicate clearly that the skarn is both stratigraphically and structurally controlled (Fig. 3a, b).

Two other massive skarn layers, with associated nodular calc-silicate hornfels, occur to the northeast of the French Road occurrence on Blue Mountain (Fig. 2). Of these, the occurrence on the western flank of the mountain is better exposed and is several metres thick. It appears to have been folded into upright open folds plunging gently toward the north-northeast. The other occurrence, on the north ridge of the mountain, is poorly exposed and appears to be an approximately 1 m thick layer within extensively folded calc-silicate hornfels and biotite-cordierite hornfels.

CALC-SILICATE AND SKARN MINERALOGY

Calc-silicate nodules

The calc-silicate nodules are zoned ovoid masses, 2 to 5 cm in diameter, occurring within biotite or biotite-cordierite hornfels as isolated ovoids and as complex coalesced amoeboid-shaped masses. Abundance of calc-silicate nodules within the host hornfels reaches 30 per cent by volume, but is commonly much less. The nodules outcrop over wide areas but examination of drill core from the vicinity of the French Road occurrence suggests that those areas of calc-silicate hornfels flanking the massive skarn layer are restricted to a discrete stratigraphically controlled zone up to 70 m thick (Macdonald, 1989).

The nodules are typically surrounded by bleached haloes developed in the adjacent hornfels. These haloes are devoid of biotite, presumably because of reaction between the calcareous nodules and their semipelitic host. Internally, the nodules are variegated and zoned inward from quartz-epidote-chlorite through quartz-epidote-actinolite to quartz-epidote-grossularite-diopside-calcite-sulphide assemblages.

Pyrrhotite and chalcopyrite are the main sulphide minerals associated with the calc-silicate nodules, occurring as irregular masses and/or patchy disseminations within the core zones of the nodules. Other minerals present include minor pyrite and magnetite.

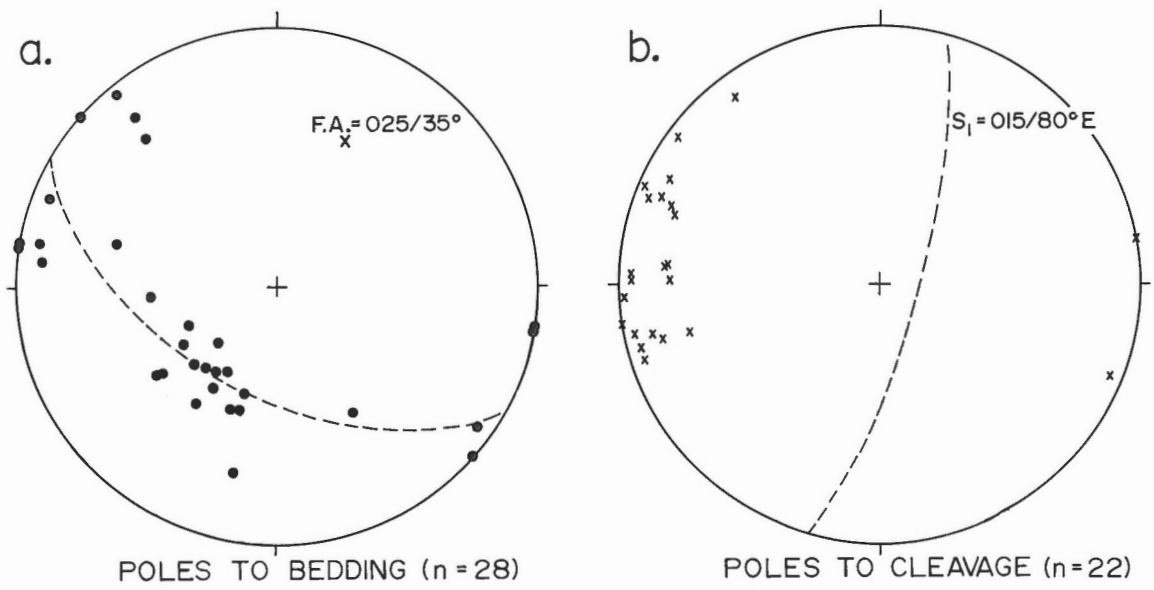

Figure 4. Equal area stereoplots of structural data from the French Road skarn occurrences.

Skarn layers

The skarn layers range from streaky greenish amphibole-rich skarn to granular brownish garnet-rich skarn. The former consist essentially of anthophyllite, epidote, quartz, and calcite, and the latter of strongly zoned euhedral garnet aggregates surrounded by calcite, quartz, epidote, and anthophyllite. Minor minerals include plagioclase, scapolite, idocrase, magnetite, and sulphides. Crosscutting quartz-calcite veinlets locally contain minor amounts of fluorite, tourmaline, chlorite, anthophyllite, and sulphides.

Anthophyllite occurs typically in fine grained, decussate aggregates that are commonly extensively chloritized. Analyses show that anthophyllite has $Mg/(Mg + Fe^{2+})$ ratios between 0.72 and 0.79 (Table 1) and it is therefore magnesian anthophyllite (Leake, 1978).

The garnet is predominantly anisotropic, strongly rim and sector zoned, and grossularite-rich, with the grossularite component ranging between 52 and 77 per cent (Table 1; Fig. 5). However, isotropic garnet is also present, occurring as isolated coarse anhedral to euhedral grains which are locally overgrown by grossularite. This isotropic garnet is andradite-rich with the andradite component ranging between 69 and 83 per cent (Table 1, Fig. 5).

In the skarn layers the most common sulphide species are pyrite and arsenopyrite (commonly intimately intergrown), together with lesser amounts of pyrrhotite and chalcopyrite. Magnetite, although locally abundant, is subordinate to the sulphides. Other minor and more erratically distributed sulphides include sphalerite, molybdenite, and bismuthinite. Although this mineralization may occur in nearly massive concentrations locally, it more typically forms irregular interstitial replacements of the host skarn; euhedral grossularite aggregates and magnetite are commonly enclosed and partially replaced by sulphides and gangue. The main gangue minerals are calcite, anthophyllite, and epidote.

MINERALIZATION

Copper values, from assays of drill core, are commonly about 1 per cent or less, although grades of 2 to 3 per cent Cu over core lengths of less than 1 m are also reported (Forgeron, 1981). Other metals of economic interest associated with Cu include Co, Bi, Mo, Sn, and Ag. Their values vary widely but a 3 m section from drill hole FR81-1 through the skarn layer at the French Road occurrence is representative and contains 0.70% Cu, 0.14% Co, 0.43% Bi, 0.03% Sn, and 16 g/t Ag (Forgeron, 1981). Analyses of

Table 1. Representative analyses* of garnet and amphibole from the French Road occurrence, Blue Mountain.

	GROSSULARITE					ANDRADITE			AMPHIBOLE				
	159-243	159-243	159-243	159-358	BM-11A	159-243	159-243	159-243	159-343	BM-11A	BM-11A	159-358	159-358
SiO_2	37.24	36.58	37.72	35.99	37.20	35.24	36.98	35.03	56.56	52.51	55.93	56.64	55.92
TiO_2	0.13	1.35	0.23	0.67	1.04	0.00	0.04	0.06	0.00	0.00	0.03	0.00	0.02
Al_2O_3	11.73	10.92	14.82	12.46	15.15	0.74	0.52	0.48	0.97	0.73	0.76	0.70	0.66
FeO	12.46	12.89	10.06	12.83	9.11	30.87	28.00	26.74	13.00	15.24	13.96	11.54	10.80
MnO	0.71	1.27	0.45	1.26	0.73	0.67	0.82	0.72	0.09	0.00	0.11	0.22	0.03
MgO	0.00	0.09	0.00	0.00	0.00	0.26	0.07	0.04	23.24	22.94	19.93	22.37	22.37
CaO	37.20	36.12	36.46	35.13	36.12	33.55	35.62	34.40	0.48	0.29	0.03	0.19	0.17
Na_2O	0.00	0.09	0.09	0.04	0.18	0.20	0.00	0.07	0.10	0.20	0.02	0.13	0.10
K_2O	0.01	0.00	0.00	0.00	0.00	0.00	0.03	0.06	0.00	0.00	0.00	0.00	0.00
Cr_2O_3	0.08	0.00	0.00	0.00	0.00	0.00	0.15	0.00	0.00	0.00	0.07	0.05	0.05
TOTAL	99.55	99.31	99.83	98.37	99.53	98.44	102.23	97.61	94.44	91.91	90.84	91.84	90.12
Number of cations		Assuming 24 oxygen								Assuming 23 oxygen			
Si	6.11	6.05	5.88	5.77	5.82	6.29	6.46	6.42	8.08	7.86	8.31	8.24	8.26
Al^{IV}	-	-	-	-	-	-	-	-	-	0.13	-	-	-
Al^{VI}	2.27	2.22	2.72	2.35	2.79	0.16	0.11	0.10	0.24	-	0.44	0.36	0.37
Ti	0.02	0.17	0.03	0.08	0.12	-	0.01	0.01	-	-	-	-	-
Fe^3	1.71	1.70	1.25	1.57	1.09	3.84	3.87	3.89	-	-	-	-	-
Cr	0.01	-	-	-	-	-	0.02	-	-	-	0.01	0.01	0.01
Fe^2	-	0.08	0.06	0.15	0.11	0.76	0.22	0.21	1.55	1.91	1.73	1.40	1.33
Mn	0.10	0.18	0.06	0.17	0.10	0.10	0.12	0.11	0.01	-	0.01	0.03	-
Mg	-	0.02	-	-	-	0.07	0.02	0.01	4.95	5.11	4.41	4.85	4.92
Ca	6.54	6.40	6.09	6.03	6.05	6.41	6.66	6.76	0.07	0.05	0.01	0.03	0.03
Na	-	-	-	-	-	-	-	-	0.03	0.06	0.01	0.04	0.03
K	-	-	-	-	-	-	-	-	-	-	-	-	-
Grossular	0.59	0.54	0.67	0.56	0.68	0.09	0.12	0.09	$\frac{Mg}{Mg+Fe}$ 0.76	0.73	0.72	0.78	0.79
Andradite	0.39	0.42	0.31	0.39	0.29	0.79	0.83	0.79					
Almandine	-	0.01	0.01	0.02	0.02	0.10	0.03	0.10					
Pyrope	-	-	-	-	-	0.01	-	0.01					
Spessart.	0.02	0.03	0.01	-	0.02	0.01	0.02	0.01					

* Analyses by JEOL Superprobe, Department of Geology, Dalhousie University, Halifax.

mineralized skarn sampled during the present study and by Northcote et al. (1989) confirm that Cu, Co, Bi, Sn, and Ag values are elevated, as are As and Zn (Table 2). Trace amounts of Au are also present (Table 2). Similarities of the Blue Mountain occurrences to gold-bearing skarns, as opposed to the richer gold skarns (Orris et al., 1987; Hammarstrom et al., 1989), include their garnet-rich prograde mineralogy, polymetallic sulphide mineralogy, relatively high Cu content, and apparently high Ag/Au ratio.

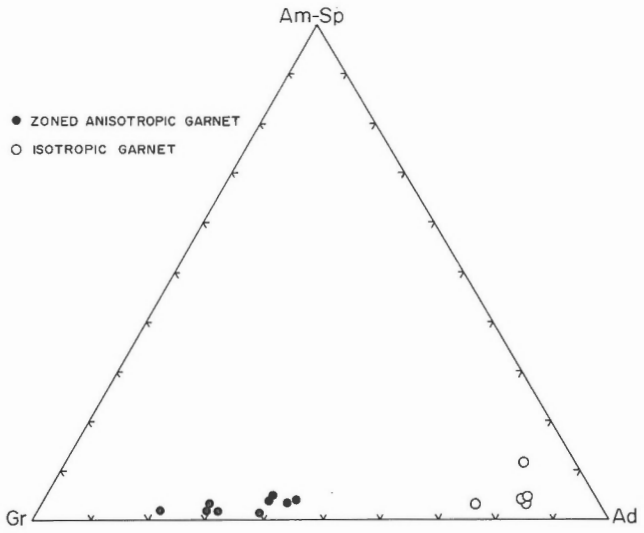

Figure 5. Garnet compositions in skarn samples from the French Road occurrence. Gr, grossularite; Ad, andradite; Am-Sp, almandine-spessartine.

No discrete tin, cobalt, or silver minerals have yet been identified, however electron microprobe analyses of skarn from the French Road occurrence indicate that both epidote and andradite garnet contain up to about 0.2 per cent Sn, whereas zoned grossularite garnet commonly contains less than 0.1 per cent Sn (Fig. 6). This compares with tin values in the range of 0.03 to 2.0 per cent which have been reported in these minerals from Sn-bearing skarn occurrences in general (Kwak, 1987). Elevated cobalt values were detected, also by electron microprobe, in arsenopyrite intergrown with pyrite. The arsenopyrite contains about 1 per cent Co but includes a minor phase (of similar optical properties), which contains 4 to 7 per cent Co and so is believed to be glaucodot. The source of the reported silver values is more problematic: no silver was detected by electron microprobe in the arsenopyrite or in sphalerite. It could, however, be present in galena, although galena is rare within the skarn except in late crosscutting veinlets, or it could occur in some as yet unidentified minor phase, such as a silver-bearing telluride or sulphosalt, both of which have been found associated with chalcopyrite at the Deep Cove occurrence to the east of Blue Mountain (Dennis, 1988).

The close spatial association of most of the mineralization with skarn, the greater abundance of chalcopyrite, pyrrhotite, and pyrite compared to magnetite, and the polymetallic Co-Bi-Mo-Ag association together indicate that the mineralization is of the copper-bearing calcic skarn type, particularly of the more complex polymetallic type associated with some barren granitic stocks (Einaudi et al., 1981).

Table 2. Analyses of mineralized skarn samples from Blue Mountain.

	BM-10A	BM-11A	BM-11C	BM-11D	BM-12	FR-5001*	FR-5002*	FR-5003*
Fe %	16.0	14.9	11.1	14.3	14.1	16.0	10.0	6.5
As %	0.01	10.00	5.30	0.20	0.08	0.08	0.46	0.01
Co ppm	86	3200	1500	78	44	798	4770	39
Ni ppm	<50	<90	<70	<50	<50	45	96	30
Zn ppm	2100	<50	<50	960	1300	1029	92	78
Pb ppm	–	–	–	–	–	51	140	5
Cu ppm	–	–	–	–	–	17300	556	103
Mo ppm	<5	<20	<9	<5	<5	5	16	1
Bi ppm	–	–	–	–	–	1495	7100	247
Ag ppm	31	**	**	19	18	27	<8	<2
Au ppb	<5	<40	<26	14	19	–	–	–
Sn ppm	–	–	–	–	–	220	370	<100
W ppm	<6	<30	<40	<4	<4	–	–	–
U ppm	<0.5	<3.3	<3.6	<0.5	<0.5	–	–	–

* Analyses from Northcote et al. (1989).
FR-5003 is from calc-silicate hornfels.
** Interference
– Indicates element not analyzed

Detection limits for Ni, Mo, Au, W, and U are elevated in samples BM-11A and BM-11C due to high As values.

Analyses by Instrumental Neutron Activation Analysis at Activation Laboratories Ltd., Brantford, Ontario.

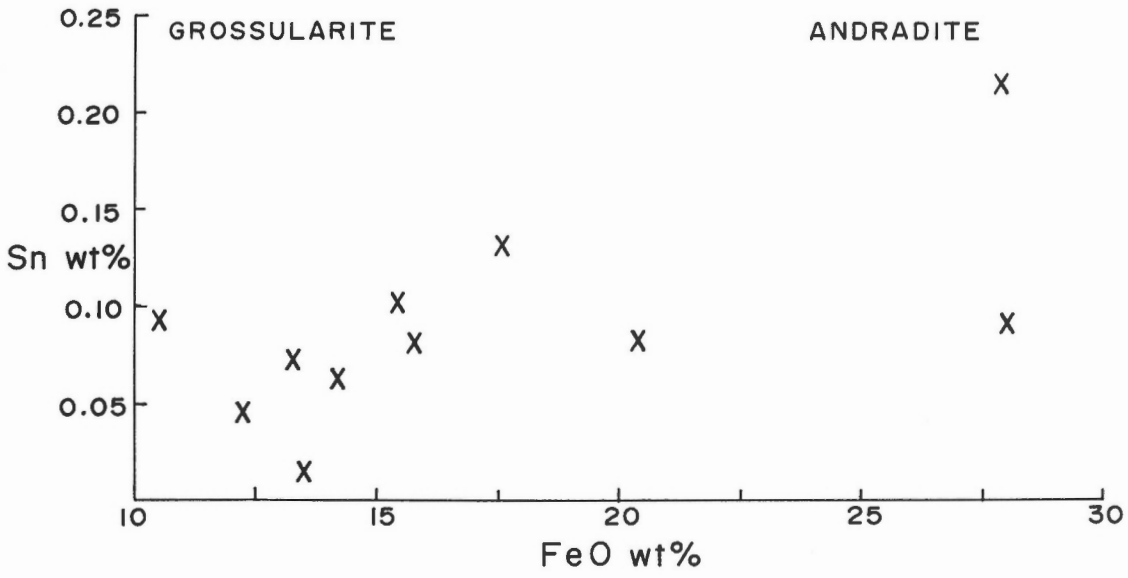

Figure 6. Plot of Sn content versus FeO in garnets from the French Road skarn occurrence.

ORIGIN OF THE SKARN

The nature of the protolith of the skarn has been obscured by metamorphic and metasomatic reactions, and both volcanic and sedimentary/diagenetic protoliths have been proposed (cf. Chatterjee, 1977; Macdonald, 1989). According to the first hypothesis, the massive skarn layer represents localized metasomatic transformation of a mafic volcanic (perhaps tuff) horizon within the argillite sequence, and the calc-silicate nodules in the adjacent hornfels presumably represent more diffuse metasomatic reactions. However, no volcanic rocks have yet been identified within the Cambrian succession east of the Mira River. According to the second hypothesis, the protolith for the skarn was impure calcareous material occurring as one or more layers within the argillite sequence, whereas the protolith for the calc-silicate hornfels was one or more zones of calcareous concretions in the argillite sequence. These calcareous units have been traced out of the aureole as calcareous nodules and limestone beds within the Lower Cambrian sequence in the area (see "Note added in proof", below). Hence a sedimentary protolith for the skarn is considered more likely.

The different mineral assemblages shown by the massive skarn layers and the calc-silicate nodules presumably reflect the higher permeability of the calcareous layers and their subsequent prograde metasomatic transformation; prograde reactions in the nodular calc-silicate hornfels were in contrast essentially metamorphic. However both contain amphibole, epidote, chlorite, and sulphides and so both have been affected by similar retrograde hydrothermal activity.

The abundance and texture of grossularite in the skarn layers, combined with the absence of associated wollastonite, suggests that temperatures during prograde skarn development were between 400 and 600°C (Winkler, 1976, p. 141). A limited episode of iron enrichment during this prograde stage is indicated by the restricted occurrence of andradite which is itself locally overgrown by grossularite. Perhaps magnetite also formed during this episode. Anthophyllite, from its texture and close spatial association with calcite, epidote, quartz, and sulphides, probably formed during the lower temperature hydrothermal stage responsible for mineralization. No pyroxene has been identified within the massive skarn, nor is there any textural evidence to suggest that it did exist and was subsequently retrograded to anthophyllite. However, diopside partly retrograded to actinolite survives in some of the calc-silcate nodules.

Late stage quartz-calcite veinlets, locally containing chlorite, tourmaline, sphalerite, and galena, crosscut skarn layers and nodular calc-silicate hornfels and represent the final stage of the hydrothermal activity that modified the massive skarn.

PORPHYRY DYKES

Although no pluton is exposed in the Blue Mountain-French Road contact metamorphic aureole, numerous rhyolitic porphyry dykes have been intersected in drill holes, and are assumed to be related to a larger intrusion at depth. At least sixteen of these dykes, ranging in apparent thickness from 2 to 12 m, occur in eight exploratory drill holes in the vicinity of the Blue Mountain skarn occurrences. No dykes were encountered in drill holes in the immediate vicinity of the French Road skarn, although a 7 m thick andesitic porphyry dyke was found in a drill hole west of the skarn, outside the contact metamorphic aureole. On the basis of its petrography and chemistry, this dyke does not appear to be related to the rhyolitic porphyry dykes and is not discussed further in this paper.

The rhyolitic dykes are altered and pyritized to varying extents, and range from grey-brown to pinkish or yellowish brown. They are aphanitic to fine grained, with fine- to medium-grained phenocrysts. Most of the phenocrysts are composed of plagioclase crystals that range in size from 1

to 8 mm and commonly form glomeroporphyritic clusters. In places the clusters are enveloped by plagioclase overgrowths. The plagioclase is extensively altered to sericite, chlorite, and calcite; relict twinning indicates albitic compositions (An_{7-12}). Quartz phenocrysts are relatively rare and tend to be small (1 to 2 mm), round, and in some cases clearly resorbed. Rare subporphyritic muscovite, intergrown with chlorite and calcite, may be secondary after biotite.

Groundmass textures range from fine grained spherulitic or granophyric to allotriomorphic. In most samples the groundmass consists mainly of quartz, K-feldspar, and plagioclase, together with sericite, chlorite, calcite, epidote, and opaque minerals (mostly pyrite). However, some samples lack modal K-feldspar, apparently as a result of more intense alteration to albite, sericite, calcite, and other secondary minerals.

GEOCHEMISTRY OF THE PORPHYRY DYKES

Eleven samples were analyzed, representing eight rhyolitic dykes in five drill holes from the Blue Mountain area. Two samples were analyzed from each of three dykes in order to assess internal chemical variation. The samples range in SiO_2 content from about 70 to 74 per cent (Table 3). Variations in major element oxide composition, both within individual dykes and among dykes, are commonly minor, with the exception that three dykes have lower K_2O contents (range 0.9 to 2.3%) compared to the other five dykes (range 3.2 to 4.4%) (Fig. 7). This is reflected in CIPW normative quartz-potassium feldspar-plagioclase ratios, with the samples from the low K_2O dykes plotting in the dacite field whereas samples from the high K_2O dykes plot in or near the rhyolite field (Fig. 8). The low K_2O dykes are those that lack K-feldspar, apparently as a result of more intense alteration. The low K_2O samples commonly contain lower Ba and higher Sr compared to the other samples (Fig. 9), presumably as a result of alkali mobility during alteration. Except for those elements, no systematic trace element variations are apparent between the high K_2O and low K_2O samples. The elements Zr, Y, Nb, V, Ga, Mo, and Cr show little variation in any of the samples. In contrast, Ni, Cu, Pb, Zn, Bi, Ag, and Sn show wide variation, although no sulphide phases other than pyrite were observed in the dykes. Compared to average granite (Turekian and Wedepohl, 1961), the dykes are enriched in Cu, Pb, Zn, Bi, Ag, Mo, and Sn (Fig. 9a). These are the same elements that occur in the Blue Mountain-French Road skarn occurrences, and suggest that both dykes and skarn were affected by the same fluids.

COMPARISON WITH DEVONIAN PLUTONS

Plutonic units of Devonian age in southeastern Cape Breton Island include the Salmon River rhyolite porphyry (Barr et al., 1984; McMullin, 1984), the Gillis Mountain Pluton (Barr and O'Beirne, 1979; Barr and Pride, 1986), and the Deep Cove Pluton (Dennis, 1988). The first two, like the intrusion inferred to underlie the Blue Mountain area, produced hornfels zones in the Cambrian sedimentary rocks that they intruded, whereas the Deep Cove stock intruded, and apparently also hornfelsed metavolcanic rocks of the late Hadrynian Fourchu Group (Fig. 1). Both the Gillis Mountain and Deep Cove intrusions are associated with Cu-Mo dominant, hydrothermal mineralization. In contrast, the Salmon River rhyolite porphyry appears to be largely barren except for rare occurrences of vein-type lead mineralization (Barr et al., 1984), although younger stratabound lead mineralization (Yava deposit) occurs in Pennsylvanian sandstones immediately to the west of the porphyry. It has been suggested that erosion of the Salmon River rhyolite porphyry could have provided the lead for deposition at Yava (Vaillancourt and Sangster, 1984).

With the exception of the Salmon River rhyolite porphyry, the Devonian plutons display geochemical features very similar to those of the Blue Mountain rhyolitic porphyry dykes. Porphyritic granite, which forms the dominant unit of the Gillis Mountain Pluton, and associated late porphyry dykes are characterized by high Ba relative to Rb

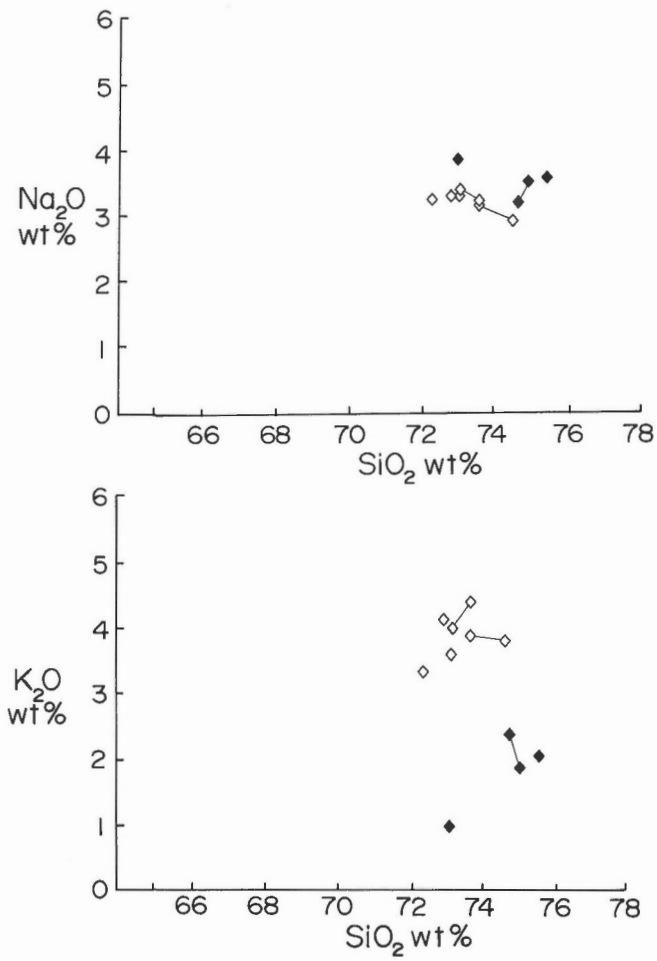

Figure 7. Plots of Na_2O and K_2O versus SiO_2 for rhyolitic porphyry dykes. Open diamonds are high K_2O samples; black diamonds are low K_2O samples. Duplicate samples from the same dyke are joined by tie-lines.

Table 3. Major and trace element analyses* and CIPW normative mineralogies of rhyolitic porphyry dykes from the Blue Mountain area.

	81-5-1a	8-5-1b	81-11-1	81-11-2	81-11-3	81-12-1a	81-12-1b	158-3-1a	158-3-1b	158-3-2	159-6-1
SiO_2	71.73	72.79	71.37	70.19	71.08	72.00	72.47	73.31	72.56	73.99	72.32
TiO_2	0.45	0.43	0.44	0.44	0.43	0.46	0.43	0.48	0.51	0.53	0.49
Al_2O_3	13.63	13.20	13.69	13.62	13.49	13.48	13.13	13.62	13.75	14.03	13.59
$Fe_2O_3^T$	2.79	2.76	3.41	2.94	2.66	2.26	2.27	3.65	3.53	2.52	3.18
MnO	0.06	0.06	0.08	0.07	0.06	0.06	0.05	0.00	0.04	0.04	0.06
MgO	0.78	0.82	1.04	0.87	0.80	0.67	0.66	0.81	0.85	0.86	1.02
CaO	1.28	1.07	2.80	2.36	1.67	1.64	1.49	0.29	0.25	0.29	1.23
Na_2O	3.29	3.16	3.73	3.13	3.18	3.09	2.82	3.44	3.10	3.48	3.23
K_2O	3.92	4.37	0.94	3.21	4.02	3.80	3.70	1.84	2.32	2.01	3.57
P_2O_5	0.06	0.10	0.10	0.12	0.08	0.22	0.10	0.13	0.13	0.13	0.14
LOI	2.01	1.68	2.49	2.90	2.06	2.55	2.66	2.31	2.56	2.34	1.67
TOTAL	100.00	100.44	100.09	99.85	99.53	100.26	99.82	99.96	99.60	100.22	100.50
CIPW normative mineralogy											
Q	34.05	34.38	39.07	34.18	33.02	36.10	38.78	45.15	44.93	45.15	35.96
C	1.83	1.59	1.73	1.03	1.09	1.88	2.08	5.91	6.19	6.05	2.55
Or	23.68	26.19	5.70	19.60	24.41	23.02	22.54	11.16	14.16	12.15	21.38
Ab	28.46	27.12	32.40	27.37	27.65	26.80	24.60	29.87	27.09	30.13	27.70
An	6.09	4.72	13.59	11.29	7.98	6.87	6.95	0.61	0.40	0.60	5.26
Hy	3.23	3.31	4.38	3.63	3.24	2.58	2.61	3.89	3.80	3.08	4.00
Mt	1.65	1.62	2.03	1.76	1.59	1.34	1.36	2.17	2.11	1.50	1.87
Il	0.87	0.83	0.86	0.86	0.84	0.90	0.84	0.94	1.00	1.03	0.94
Ap	0.14	0.24	0.24	0.29	0.19	0.52	0.24	0.31	0.31	0.31	0.33
Trace elements in ppm											
Ba	487	528	260	437	549	446	440	371	378	403	562
Rb	155	151	77	124	159	157	173	122	164	111	115
Sr	108	105	247	162	126	114	98	141	102	132	145
Zr	198	198	197	193	195	196	197	206	205	217	199
Y	33	33	35	32	34	30	32	34	37	36	32
Nb	19	19	19	18	20	19	19	19	20	19	19
Pb	37	35	23	43	76	354	836	7	193	3389	251
Zn	165	303	111	287	260	3493	5305	933	689	6486	286
Cu	15	18	79	34	20	92	28	51	47	55	22
Ni	5	10	4	8	10	9	4	11	12	6	7
V	29	30	33	30	25	28	28	33	36	34	37
Cr	30	31	32	33	35	34	26	46	28	29	38
Th	27	28	25	29	29	34	49	23	32	69	27
Ga	17	18	16	17	16	18	15	17	19	12	17
Mo	5	5	6	6	6	6	6	5	6	5	6
Bi	0.3	0.1	3.5	2.4	0.1	0.6	1.2	0.2	1.4	2.9	0.1
Ag	0.6	0.1	0.2	0.1	0.1	1.8	2.9	0.3	1.0	1.3	0.1
Sn	4.5	3.5	8.7	7.2	5.7	4.0	3.6	8.9	8.7	4.2	3.5

Samples from drill holes indicated by number (e.g. 81-5, 81-11, etc.)

* Analyses by X-ray Fluorescence at the Regional XRF Centre, Department of Geology, St. Mary's University, Halifax. Analyst K. Cameron. FeO is total Fe as FeO. LOI is % weight loss after heating to 1000°C for one hour (= loss-on-ignition). Analyses for Mo, Bi, Ag, and Sn were done by CLIM Laboratories, Technical University of N.S.

and Sr (Fig. 9) and by relatively low Rb/Sr ratios (mean ratios 0.56 and 1.18). Compared with average granite, TiO_2 and the trace metals Cu, Pb, Zn, Ag, Bi, and Mo are elevated (Fig. 10b). The Deep Cove porphyritic monzogranite and associated suite of porphyry dykes are also characterized by relatively high Ba compared to Rb and Sr (Fig. 9) and by low Rb/Sr ratios (mean ratios 1.07 and 1.23). Titanium oxide and the trace metals Cu, Pb, Zn, Ag, Bi, and Mo are high compared with average granite (Fig. 10c).

The Blue Mountain porphyry dyke suite, although slightly lower in Ba, displays an overall Ba-Rb-Sr pattern very similar to those of both the main granites and the porphyry dyke suites at Gillis Mountain and Deep Cove (Fig. 9). The assemblage of trace metals with elevated values is the same, and TiO_2 is elevated compared with average granite (Fig. 10a, b, c).

In contrast, the Salmon River rhyolite porphyry is characterized by lower Ba relative to Rb and Sr (Fig. 9) and by

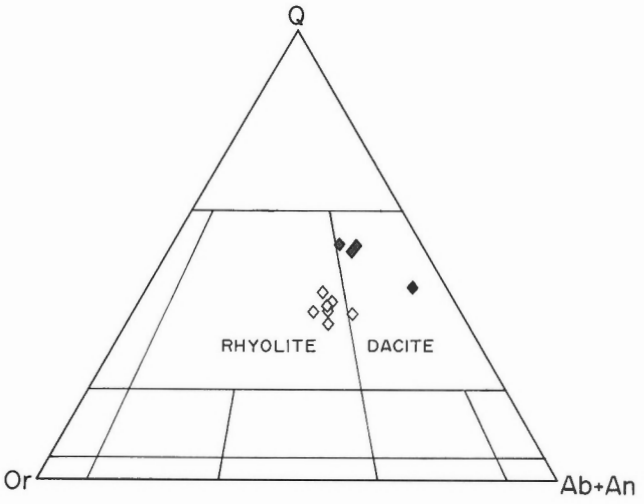

Figure 8. Ternary plot of CIPW normative quartz-orthoclase-albite + anorthite compositions of rhyolitic porphyry dykes. Open diamonds are high K_2O samples; black diamonds are low K_2O samples.

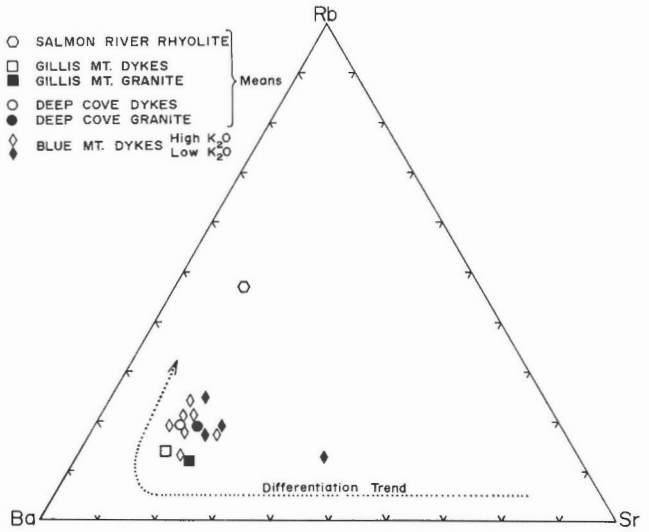

Figure 9. Ternary plot of Ba-Rb-Sr, comparing rhyolitic porphyry dykes from Blue Mountain with rhyolite porphyry and other granites from Gillis Mountain, Deep Cove, and Salmon River plutons. Differentiation trend from El Bouseily and El Sokkary (1975).

high Rb/Sr ratio (mean 3.78) compared to the other Devonian intrusions. These characteristics suggest that it is more highly differentiated, consistent with its higher average SiO_2 content of about 75 per cent (McMullin, 1984). In contrast with the other Devonian intrusions, it has low TiO_2, P_2O_5, and Sr compared with average granite (Fig. 10d), and trace metals do not show the same consistent elevated abundances displayed by the other intrusions (Fig. 10a, b, c). Only Pb, Ag, and Bi values are elevated and less so than those of the other intrusions.

Given the geochemical similarities, there seems little doubt that the Gillis Mountain, Deep Cove, and Blue Mountain intrusions and their diverse hydrothermal effects are related, and represent an important metallogenic episode that affected southeastern Cape Breton Island in the Devonian. The relationship of the Salmon River rhyolite porphyry with the other intrusions is uncertain; however, it may represent a more highly evolved but related magma. The series of intrusions are inferred to represent different levels of emplacement and erosion of related magmatic systems (Fig. 11).

The tectonic environment in which these granites were generated is not clear. Compared with average I-type and A-type granites (Table 4), the rhyolitic dykes are geochemically more similar to I-type granites. This is shown particularly by Sr, Y, and Ga and to a lesser extent by Zr, Nb, and V which are only slightly elevated above I-type values. The I-type characteristics of the Gillis Mountain, Deep Cove, and Salmon River intrusions have been previously noted (McMullin, 1984; Barr and Pride, 1986; Dennis, 1988).

Table 4. Comparison of the average chemical composition of the Blue Mountain rhyolitic porphyry dykes (BM) with average I-type and A-type granites (from Whalen et al., 1987).

	I-TYPE	A-TYPE	BM
%			
SiO_2	73.39	73.81	73.85
TiO_2	0.26	0.26	0.47
Al_2O_3	13.43	12.40	13.88
Fe_2O_3	2.05	2.97	2.97
MnO	0.05	0.06	0.06
MgO	0.55	0.20	0.05
CaO	1.71	0.75	1.34
Na_2O	3.33	4.07	3.32
K_2O	4.13	4.65	3.13
P_2O_5	0.07	0.04	0.12
ppm			
Ba	510	352	441
Rb	194	169	137
Sr	143	48	134
Zr	144	528	200
Y	34	75	33
Nb	12	37	19
Pb	23	24	476
Zn	35	120	4007
Cu	4	2	41
Ni	2	1	9
V	22	6	32
Th	22	23	32
Ga	16	25	16

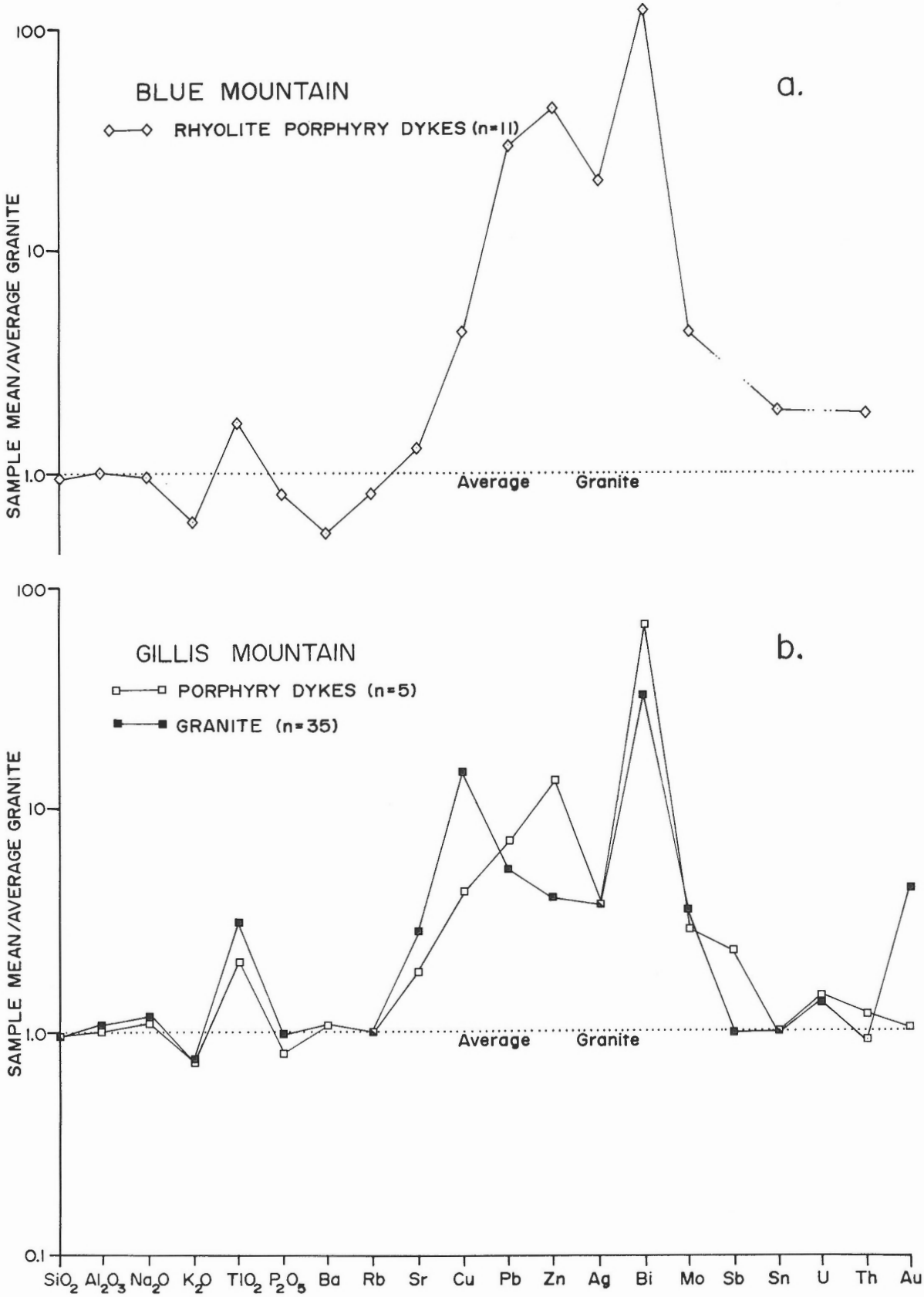

Figure 10. Average compositions compared to the average low Ca granite of Turekian and Wedepohl (1961); (a) Blue Mountain rhyolitic porphyry dykes (this study); (b) Gillis Mountain granite and porphyry dykes (from data in Barr et al., 1982); (c) Deep Cove porphyritic granite and porphyry dykes (from Dennis, 1988); (d) Salmon River rhyolite porphyry (from data in McMullin, 1984). Missing data are indicated by a broken line.

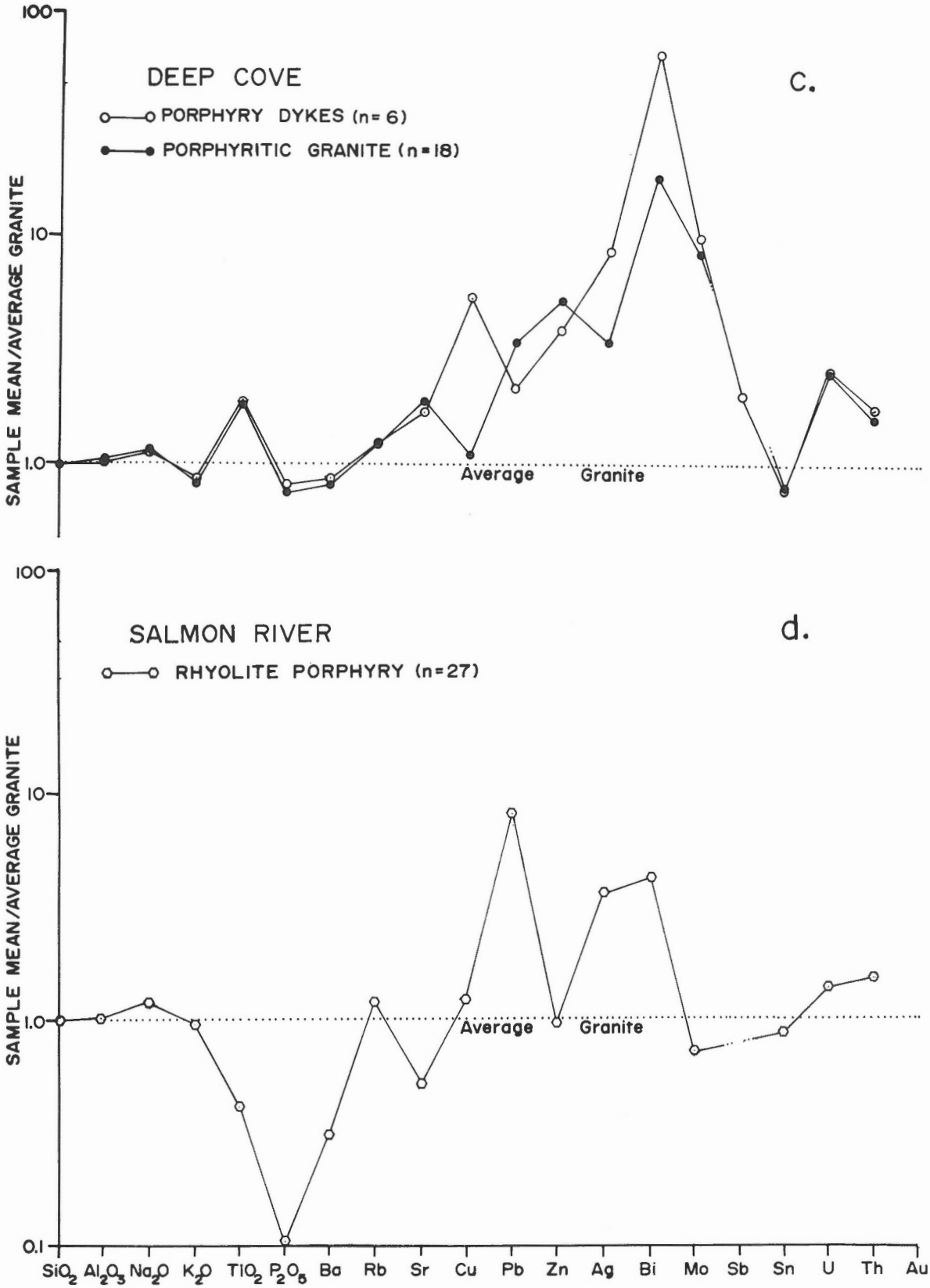
DEEP COVE
C.
PORPHYRY DYKES (n= 6)
PORPHYRITIC GRANITE (n = 18)
SAMPLE MEAN/AVERAGE GRANITE
100
10
1.0
Average
Granite
SALMON RIVER
d.
RHYOLITE PORPHYRY (n=27)
SAMPLE MEAN/AVERAGE GRANITE
100
10
1.0
0.1
Average
Granite
SiO2 Al2O3 Na2O K2O TiO2 P2O5 Ba Rb Sr Cu Pb Zn Ag Bi Mo Sb Sn U Th Au

Figure 10c, d

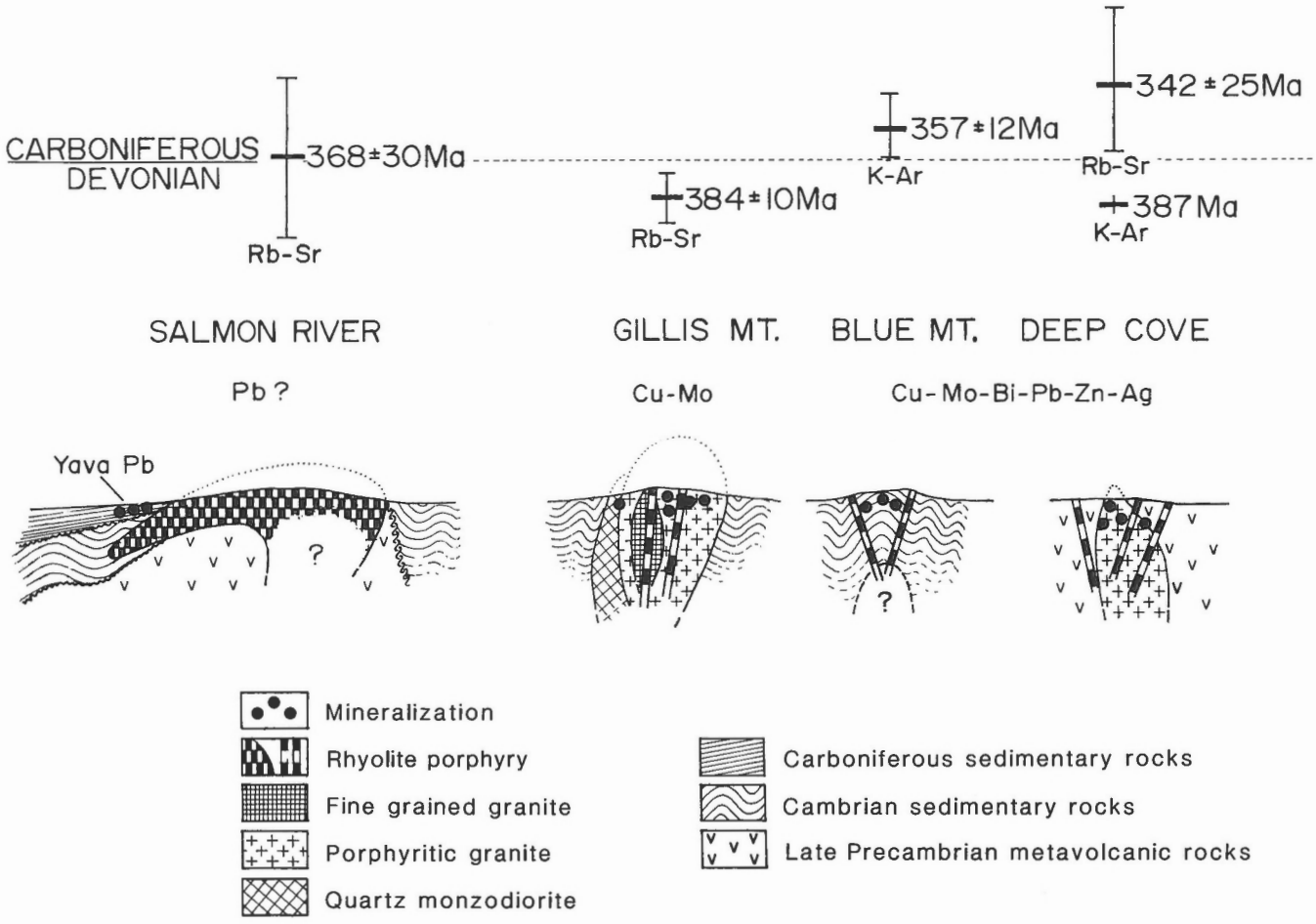

Figure 11. Interpretation of geological setting of Devonian plutons in southeastern Cape Breton Island. Ages from Barr et al. (1984), Cormier (1972, 1979), and M. Zentilli (pers. comm., 1983).

Granitoid plutons with I-type features are commonly formed in association with subduction or with postsubduction uplift (e.g. Pitcher, 1987). However, there is no other evidence for subduction in southeastern Cape Breton Island since the late Precambrian, and the tectonic setting in the Devonian appears to have been anorogenic, a setting typically characterized by A-type granites. The I-type petrological characteristics of these plutons may be related to the nature of the source rocks, inferred to be in the roots of a late Precambrian volcanic arc (McMullin, 1984; Barr and Pride, 1986; Dennis, 1988).

The Devonian plutons occur in an arcuate, easterly trending zone that is transverse to the main structural trends in southeastern Cape Breton Island. However, the zone does parallel, in part, major faults with Carboniferous movement in the Mira River and Mira Bay area 10 km to the north (Gibling et al., 1987). The plutons may reflect the existence of a deep-seated fracture that played a role in their localization and genesis during the Devonian.

On a regional scale, the Devonian plutons in southeastern Cape Breton Island are probably part of a significant episode of posttectonic, high level plutonism that occurred widely in the Avalon Terrane of the northern Appalachian Orogen during the Devonian and that is typically associated with polymetallic mineralization. Other examples include the Ackley Batholith in Newfoundland (e.g. Tuach, 1987) and the Mount Pleasant caldera complex and associated granitic plutons in southern New Brunswick (e.g. Kooiman et al., 1986; Lentz et al., 1988).

CONCLUSIONS

Polymetallic skarn occurrences in the Blue Mountain-French Road area are hosted by contact metamorphosed Lower to Middle Cambrian clastic rocks. A K-Ar age of 357 ± 12 Ma from biotite-rich hornfels is interpreted to be a cooling age, and is compatible with Devonian emplacement of an intrusion at depth that produced the contact aureole. Although this intrusion is not exposed, a swarm of rhyolitic porphyry dykes cutting skarn and hornfels in the Blue Mountain area is interpreted to be directly related to this inferred intrusion.

The polymetallic sulphide assemblage associated with the skarn occurrences, the geochemistry of the porphyry dykes, and the implied Devonian age of plutonic intrusion and associated hydrothermal mineralization strongly suggest that the Blue Mountain-French Road contact aureole and its skarn mineralization are part of an arcuate belt of

Devonian plutons, emplaced at different epizonal levels and subjected to varying degrees of erosional exposure. The Blue Mountain porphyry dykes show strong petrographic and geochemical similarities with granites and associated late porphyry dykes from both the Gillis Mountain and Deep Cove plutons, suggesting that they were all derived from closely related magma systems. The Salmon River rhyolite porphyry, in contrast, appears more highly evolved and more restricted in its metal association.

The presence of these intrusions and their associated, diverse types of mineralization indicate that southeastern Cape Breton Island was affected by an important metallogenic episode in the Devonian, like that associated with the Ackley Batholith in Newfoundland and the Mount Pleasant caldera complex in southern New Brunswick.

NOTE ADDED IN PROOF

Subsequent to completion of this manuscript, an additional Devonian pluton has been recognized in southeastern Cape Breton Island, and a compilation of petrochemistry of the Devonian plutons, including the Blue Mountain dykes, has been published (Barr and Macdonald, 1992). Also, additional mapping has more clearly defined the stratigraphy and distribution of the Lower to Middle Cambrian strata in the general area, and has allowed better recognition of their contact metamorphosed equivalents in the Blue Mountain area (Barr et al., 1992).

ACKNOWLEDGMENTS

This project was funded by an Energy, Mines and Resources Research Agreement and a Natural Sciences and Engineering Research Council of Canada Operating Grant to S.M. Barr. We thank B. MacKay of the Regional Electron Microprobe Facility at Dalhousie University for assistance with the microprobe analyses. The clarity of the text was considerably improved as a result of critical reviews by A.L. Sangster and W.D. Sinclair.

REFERENCES

Barr, S.M. and Macdonald, A.S.
1985: Diverse environments of polymetallic mineralization associated with Devonian granitoid plutons, southeastern Cape Breton Island, Nova Scotia; in Granite-Related Mineral Deposits, (ed.) R.P. Taylor and D.F. Strong; Extended abstracts of papers presented at the CIM conference, September 15-17, Halifax, Nova Scotia, p. 21-24.
1992: Devonian plutons in southeastern Cape Breton Island, Nova Scotia; Atlantic Geology, v. 28, p. 101-113.

Barr, S.M. and O'Beirne, A.M.
1979: Petrology of the Gillis Mountain pluton, Cape Breton Island, Nova Scotia; Canadian Journal of Earth Sciences, v. 18, p. 395-404.

Barr, S.M. and Pride, C.R.
1986: Petrogenesis of two contrasting Devonian granitic plutons, Cape Breton Island, Nova Scotia; Canadian Mineralogist, v. 24, p. 137-14

Barr, S.M., O'Reilly, G.A., and O'Beirne, A.M.
1982: Geology and geochemistry of selected granitoid plutons of Cape Breton Island; Nova Scotia Department of Mines and Energy, Paper 82-1, 176 p.

Barr, S.M., Sangster, D.F., and Cormier, R.F.
1984: Petrology of early Cambrian and Devono-Carboniferous intrusions in the Loch Lomond Complex, southeastern Cape Breton Island, Nova Scotia; in Current Research, Part A; Geological Survey of Canada, Paper 84-1A, p. 203-211.

Barr, S.M., White, C.E., and Macdonald, A.S.
1992: Revision of upper Precambrian-Cambrian stratigraphy, southeastern Cape Breton Island, Nova Scotia; in Current Research, Part D; Geological Survey of Canada, Paper 92-1D, p. 21-26.

Bruce, G.S.W.
1969: French Road drilling project: report on 1969 drilling program; Dome Exploration Limited, Nova Scotia Department of Mines, Assessment Report 11F/16D 13-C-40(03).

Chatterjee, A.K.
1977: Massive sulphide mineralization near Blue Mountain, Cape Breton County, southeast Cape Breton; in Mineral Resources Division Report of Activities 1976, Nova Scotia Department of Mines, Report 77-1, p. 71-81.

Cormier, R.F.
1972: Radiometric ages of granitic rocks, Cape Breton Island, Nova Scotia; Canadian Journal of Earth Sciences, v. 9, p. 1074-1086.
1979: Rubidium/strontium isochron ages of Nova Scotian granitoid plutons; Nova Scotia Department of Mines and Energy, Report 79-1, p. 143-147.

Dennis, F.A.R.
1988: Petrology and mineralization of the Deep Cove Pluton, Gabarus Bay, Cape Breton Island, Nova Scotia; M.Sc. thesis, Acadia University, Wolfville, Nova Scotia, 209 p.

Einaudi, M.T., Meinert, L.D., and Newberry, R.J.
1981: Skarn deposits; in Economic Geology, 75th Anniversary Volume, (ed.) B.J. Skinner; p. 317-391.

El Bouseily, A.M. and El Sokkary, A.A.
1975: The relation between Rb, Ba, and Sr in granitic rocks; Chemical Geology, v. 16, p. 207-219.

Forgeron, D.
1981: Summary report on the French Road-Blue Mountain area; Nova Scotia Department of Mines and Energy, Assessment Report 11F/16D 07-C-40(12).

Gibling, M.R., Boehner, R.C., and Rust, B.R.
1987: The Sydney basin of Atlantic Canada: an Upper Paleozoic strike-slip basin in a collisional setting; in Sedimentary Basins and Basin-forming Mechanisms, (ed.) C. Beaumont and A.J. Tankard; Canadian Society of Petroleum Geologists, Memoir 12, p. 269-285.

Hammarstrom, J.M., Orris, G.J., Bliss, J.D., and Theodore, T.G.
1989: A deposit model for gold-bearing skarns; United States Geological Survey, Circular 1035, p. 27.

Hutchinson, R.D.
1952: The stratigraphy and trilobite faunas of the Cambrian sedimentary rocks of Cape Breton Island, Nova Scotia; Geological Survey of Canada, Memoir 263, 124 p.

Kooiman, G.J.A., MacLeod, M.J., and Sinclair, W.D.
1986: Porphyry tungsten-molybdenum orebodies, polymetallic veins and replacement bodies and tin-bearing greisen zones in the Fire Tower Zone, Mount Pleasant, New Brunswick; Economic Geology, v. 81, p. 1356-1373.

Kwak, T.A.P.
1987: W-Sn skarn deposits; Developments in Economic Geology, Number 24, Elsevier, New York, 451 p.

Leake, B.E.
1978: Nomenclature of amphiboles; Canadian Mineralogist, v. 16, p. 501-520.

Lentz, D.R., Lutes, G., and Hartree, R.
1988: Bi-Sn-Mo-W greisen mineralization associated with the True Hill granite, southwestern New Brunswick; Maritime Sediments and Atlantic Geology, v. 24, p. 321-338.

Macdonald, A.S.
1989: Metallogenic studies, southeastern Cape Breton Island; Nova Scotia Department of Mines and Energy, Paper 89-1, 99 p.

McMullin, D.W.
1984: The Loch Lomond plutonic complex, Cape Breton Island, Nova Scotia; M.Sc. thesis, Acadia University, Wolfville, Nova Scotia, 241 p.

Northcote, K., Demont, G., and Armitage, A.
1989: Open file report on selected mineral occurrences of southern Cape Breton Island, Nova Scotia; Nova Scotia Department of Mines and Energy, Open File Report 89-04, 94 p.

Orris, G.J., Bliss, J.D., Hammarstrom, J.M., and Theodore, T.G.
1987: Description and grades and tonnages of gold-bearing skarns; United States Geological Survey, Open File Report 87-273, 50 p.

Pitcher, W.S.
1987: Granite types and tectonic environment; in Mountain Building Processes, (ed.) K.J. Hsu; Academic Press, London, p. 19-40.

Sangster, A.L.
1977: Report on diamond drilling, Lewis Option, base metals, French Road, Cape Breton County, Nova Scotia, St. Joseph Explorations Limited; Nova Scotia Department of Mines, Assessment Report 11F/16D 07-C-40(05).

Tuach, J.
1987: The Ackley high-silica magmatic/metallogenic system and associated post-tectonic granites, southwest Newfoundland; Ph.D. thesis, Memorial University, St John's, Newfoundland, 455 p.

Turekian, K.K. and Wedepohl, K.H.
1961: Distribution of some major elements in some units of the Earth's crust; Geological Society of America Bulletin, v. 72, p. 175-192.

Vaillancourt, P.D. and Sangster, D.F.
1984: Petrology of mineralization at the Yava sandstone-lead deposit, Nova Scotia; in Current Research, Part A; Geological Survey of Canada, Paper 84-1A, p. 345-352.

Whalen, J.B., Currie, K.L., and Chappell, B.W.
1987: A-type granites: geochemical characteristics, discrimination and petrogenesis; Contributions to Mineralogy and Petrology, v. 95, p. 407-419.

Winkler, H.G.F.
1976: Petrogenesis of metamorphic rocks; Springer-Verlag, New York, 4th edition, 334 p.

APPENDIX 1

K-Ar data for biotite concentrate** from hornfels in the Blue Mountain contact aureole.

K%	^{40}K	$^{40}Ar^*$(ppm)	$^{40}Ar^*/^{40}Ar$	$^{40}Ar^*/^{40}K$	Age (Ma)
6.485	7.736	0.1773	0.833	0.02291	357± 12

* radiogenic ^{40}Ar

** biotite concentrate, -80/+200 mesh. Analysis by Krueger Enterprises Inc., Geochron Laboratories Division, Cambridge, Massachusetts.
Constants used in age calculation: $\lambda_B = 4.962 \times 10^{-10}$/year; $(\lambda e + \lambda' e) = 0.581 \times 10^{-10}$/year; $^{40}K/K = 1.193 \times 10^{-4}$ g/g.

Lithogeochemical indicators of gold potential in the eastern Meguma Terrane of Nova Scotia[1]

J.A. Kerswill[2]

Kerswill, J.A., 1993: Lithogeochemical indicators of gold potential in the eastern Meguma Terrane of Nova Scotia; in Mineral Deposit Studies in Nova Scotia, Volume 2, (ed.) A.L. Sangster; Geological Survey of Canada, Paper 91-9, p. 19-48.

Abstract

Although both sulphur and arsenic appear to be useful indicators of gold potential based on a composite population of 490 samples from nine districts and seven rock types, sulphur is a more reliable guide than arsenic in some districts and rock types. This is at least partly because much of the gold is associated with iron-sulphide minerals in and around prefolding bedding-parallel quartz veins, whereas much of the arsenic occurs in and adjacent to syn- to postfolding quartz veins and structures that are commonly gold-poor. The average gold, sulphur, and arsenic contents of the principal rock types associated with gold occurrences differ among the rock types and from occurrence to occurrence, but are always greater than the regional background contents determined from samples that were collected in areas distant from known occurrences.

Gold concentration can be directly linked to increased K_2O/Na_2O ratios (sericitization) in wacke from Lake Catcha, Tangier, Beaver Dam, Goldenville, and Caribou and in slate from the Touquoy zone, Moose River district and Goldenville, but cannot be correlated with greater CO_2 contents (carbonatization) or higher SiO_2/Al_2O_3 ratios (silicification) in either wacke or slate. At Beaver Dam and Lake Catcha, gold contents are inversely related to the SiO_2/Al_2O_3 ratios in wacke. Small-scale zones of bleaching in wacke were recognized at seven occurrences; these zones are characterized by increased SiO_2/Al_2O_3 ratios only at Beaver Dam and Forest Hill.

A multistage genetic model for gold mineralization is most appropriate. Such a model permits vein-controlled deposition of variable amounts of $SiO_2 \pm S \pm Au \pm As \pm Sb \pm CO_2 \pm Cu \pm Pb \pm Zn \pm W$ from a succession of possibly very different hydrothermal fluids that were generated at various stages during the sedimentary, structural, and metamorphic evolution of the Meguma Terrane. No evidence was collected during this study to support either a syngenetic exhalative model or a late shear-related model for gold mineralization.

[1] Contribution to the Canada-Nova Scotia Mineral Development Agreement, 1984-1989. Project carried by the Mineral Resources Division, Geological Survey of Canada, Project 840003.

[2] Mineral Resources Division, Geological Survey of Canada, 601 Booth St., Ottawa, K1A 0E8

Résumé

Bien que le soufre et l'arsenic soient des indicateurs utiles de la présence de l'or, l'étude d'une population composite de 490 échantillons provenant de neuf districts et de sept lithotypes révèle que le soufre est un repère plus fiable que l'arsenic dans certains districts et dans certains lithotypes. Cette fiabilité accrue du soufre est attribuée en partie au fait qu'une grande partie de l'or est associée à des minéraux à sulfure de fer qui se rencontrent à l'intérieur ou à proximité de filons de quartz parallèles au litage et antérieurs au plissement. Par contre, l'arsenic se rencontre en grande partie dans des structures et des filons de quartz qui sont contemporains du plissement ou postérieurs au plissement et fréquemment pauvres en or. Les teneurs moyennes en or, en soufre et en arsenic des principaux lithotypes associés aux venues aurifères varient en fonction du lithotype et de la venue, mais elles sont toujours supérieures aux teneurs de fond régionales mesurées à partir d'échantillons prélevés loin des venues connues.

Dans le wacke du lac Catcha, de Tangier, de Beaver Dam, de Goldenville et de Caribou et le schiste ardoisier de la zone de Touquoy, du district de la rivière Moose et de Goldenville, il existe un lien direct entre la concentration de l'or et les rapports K_2O/Na_2O accrus (séricitation), mais il n'y a aucune corrélation entre la concentration de l'or et les teneurs plus élevées en CO_2 (carbonatisation) ou les rapports SiO_2/Al_2O_3 plus élevés (silicification). Il y a une relation inverse entre les teneurs en or et les rapports SiO_2/Al_2O_3 dans le wacke à Beaver Dam et au lac Catcha. Le wacke présente de petites zones de blanchiment à sept venues; ces zones ont des rapports SiO_2/Al_2O_3 plus élevés à Beaver Dam et à Forest Hill seulement.

Le modèle préféré de la minéralisation de l'or est un modèle génétique polyphasé. Il prévoit le dépôt contrôlé par des filons de quantités variables de $SiO_2 \pm S \pm Au \pm As \pm Sb \pm CO_2 \pm Cu \pm Pb \pm Zn \pm W$ à partir d'une succession de fluides hydrothermales possiblement très différentes qui ont été produites à divers moments au cours de l'évolution sédimentaire, structurale et métamorphique du terrane de Meguma. On n'a trouvé aucun indice à l'appui d'un modèle exhalatif syngénétique de la minéralisation de l'or ou d'un modèle tardif associé au cisaillement.

INTRODUCTION

The principal goal of this investigation was to document lithogeochemical features of the rocks that host the gold-bearing quartz veins of the eastern Meguma Terrane, Nova Scotia, in an effort to establish useful indicators of gold potential. A related objective was to provide additional constraints for the construction of a predictive genetic model for turbidite-hosted gold deposits. This work builds upon previous studies (Malcolm, 1929, 1976; Graves and Zentilli, 1982, 1986; Smith, 1985; Smith et al., 1985; Crocket et al., 1986; Fueten et al., 1986; Henderson and Henderson, 1986; Mawer, 1986) and should complement other recent investigations (Haynes, 1987; Henderson and Henderson, 1987, 1990; Henderson et al., 1991; Hy and Williams, 1986; Kontak and Smith, 1987a, b, 1988; Kontak et al., 1990; Sangster, 1987, 1990; Smith and Kontak, 1986, 1988; Williams and Hy, 1990).

During the 1986 and 1987 field seasons, more than 800 rock samples were collected from recent drill core and/or underground exposures at seven gold occurrences, namely Beaver Dam, Caribou, Fifteen Mile Stream, Goldenville, Lake Catcha, Moose River, and Tangier (Fig. 1). Several samples were also collected from surface trenches at Beaver Dam, Fifteen Mile Stream, and Forest Hill and from mine dumps at Caribou, Dufferin, Moose River, and Tangier. In addition, more than 50 reference or "regional background" samples were collected from outcrop in areas relatively distant from known mineralization (Fig. 1). After sorting and slabbing, 490 samples were analyzed for their contents of Au, S, As, SiO_2, Al_2O_3, Fe_2O_3(total), CaO, MgO, K_2O, Na_2O, MnO, TiO_2, P_2O_5, H_2O, CO_2, Cu, Pb, Zn, Ni, Co, Cr, Rb, Sr, Ba, Y, Zr, Nb, Mo, Ag, W, Sb, Cd, and LOI. Selected samples were analyzed for C and FeO.

In an attempt to help determine lithogeochemical characteristics that can be directly linked to gold concentration, samples were divided into populations according to lithology, distance from known gold occurrences, and the absence or presence of visible sulphide minerals (pyrrhotite, pyrite, and arsenopyrite). Based on lithology and sulphide mineral content, samples were grouped into seven populations: 1) wacke lacking veins and visible sulphide minerals, 2) slate lacking veins and visible sulphide minerals, 3) wacke with visible sulphide minerals but lacking veins, 4) slate with visible sulphide minerals but lacking veins, 5) wacke with vein material in the sample, 6) slate with vein material in the sample, and 7) quartz veins. Manipulations of the major, minor, and trace element data

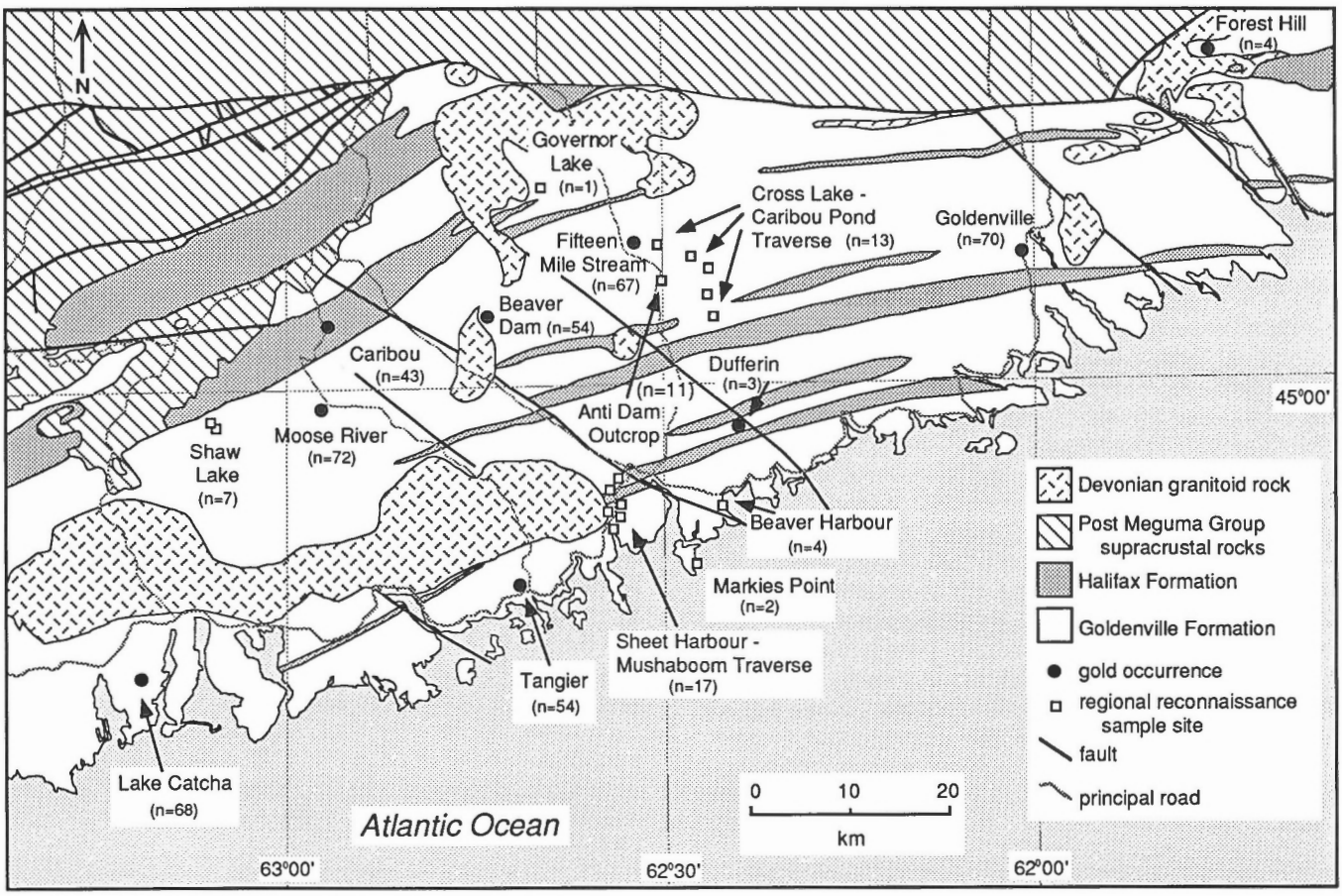

Figure 1. Location map showing distribution of gold occurrences and regional background sites that were sampled in this study as well as the regional geology of the eastern Meguma Terrane. The geological base was created from the 1:500 000 scale geological map of Nova Scotia (Keppie, 1979).

have focused on evaluating differences among districts and rock types in terms of element concentrations and correlations among elements. Initial results of this research have been summarized in two progress reports (Kerswill, 1987, 1988).

GEOLOGICAL SETTING OF GOLD MINERALIZATION

Field observations, combined with a review of the literature, provide a number of constraints in interpreting the lithogeochemical data generated during this study. These constraints are summarized below.

Gold is associated with structurally-controlled quartz-rich veins hosted principally by wacke and slate of the Goldenville Formation. A variety of quartz veins were recognized, but these fall into four principal types: 1) bedding-parallel (BP) veins that typically display crack-seal textures, 2) en échelon veins, 3) true saddle-reef veins, and 4) discordant veins, including ac (late extension veins which occur along ac joints in wacke) and fissure veins. It was not always possible to determine with confidence the actual type of an individual vein, particularly in drill core. Some veins are composite, in that they have the features of more than a single vein type. Although all types can occur in a given volume of rock, and there may be more than one generation of any particular type, the bedding-parallel crack-seal veins are typically the earliest and appear to have formed prior to folding. These were followed by the synfolding en échelon and saddle-reef types and the postfolding discordant types. The vein types identified for this study correspond to those of Henderson and Henderson (1986) as does this writer's interpretation of the relative timing of vein formation. There is no unequivocal field evidence to support formation of all vein types in conjunction with Devonian plutonism.

Much of the gold that has been mined was closely associated with bedding-parallel crack-seal veins that occurred along fold limbs of anticlinal domal structures. However, it was recognized by early miners and researchers that gold was commonly concentrated within ore shoots that were localized where bedding-parallel veins displayed minor folds or were intersected by discordant veins or vein systems. In some districts, as at Caribou, significant gold was mined from late fissure veins (Lake Lode, Dixon, and Elk mines) that apparently did not crosscut gold-bearing bedding-parallel veins. Gold has also been won from a few true saddle-reef veins, as at Dufferin (Henderson and Henderson, 1986, 1987). With respect to this study, it is important to note that most of the samples from known occurrences were collected within a few metres of gold-bearing bedding-parallel veins. Many such samples were also within a few metres of other veins of one or more types. In contrast, none of the regional background samples were collected near gold-bearing veins.

At Tangier, significant gold occurs in the sulphide-bearing Twin lead, a pair of narrow bedding-parallel veins that have been traced for more than 2 km along the south limb of an anticlinal dome. Gold distribution in this ore zone could not be correlated with either shear zones or other vein types. In the Nugget lead at Tangier, gold is restricted to bedding-parallel crack-seal veins, despite the abundance of later en échelon veins. At the main property in the Caribou district, gold occurs in early bedding-parallel veins as well as in a later structure, termed the Main zone, that crosscut the gold-bearing bedding-parallel leads. Some gold also occurs in and adjacent to en échelon vein sets that locally crosscut the bedding-parallel veins; the en échelon sets appear to be more abundant and larger near the Main zone.

Most of the visible gold seen during this study occurs in early bedding-parallel crack-seal veins. Although two generations of quartz are noted in many of the bedding-parallel leads, gold is recognized in both the early, typically oily-lustered, well-laminated quartz and the later, more massive white quartz. Numerous specks of visible gold were seen within narrow (<1 cm in width), sulphide-bearing buckled bedding-parallel veins in core from the Higgins and Lawlor property, Moose River district.

Gold is commonly spatially associated with sulphide minerals, including pyrrhotite, pyrite, arsenopyrite, chalcopyrite, sphalerite, and galena. The sulphides occur within the veins, the slates, and the wackes, but the relative proportions of sulphides in the veins and wall rocks are widely variable. However, economic concentrations of gold are largely restricted to veins or vein-wall rock contacts. Pyrrhotite, the generally dominant iron sulphide, is commonly more abundant than arsenopyrite in both veins and wall rocks; in slate and wacke in which both pyrrhotite and arsenopyrite are present, arsenopyrite commonly overgrows or appears to replace pyrrhotite. Arsenopyrite distribution appears be more closely controlled by quartz veins, particularly those that are later than the bedding-parallel crack-seal veins. This was evident in underground exposures at both Tangier and Caribou. At Tangier, arsenopyrite is abundant adjacent to barren en échelon veins in the Nugget lead, but is rare to absent in the gold-rich Twin and Marker leads and their host rocks. At Caribou, arsenopyrite is abundant in the en échelon vein sets and their adjacent host rocks but is uncommon in either the bedding-parallel leads or their immediately adjacent host rocks. At Beaver Dam, it was not possible to determine the control on arsenopyrite distribution, largely because of the complexity of the vein systems at the occurrence. In drill core from Goldenville, Lake Catcha, Moose River, and Fifteen Mile Stream, much of the arsenopyrite appears to be controlled by late veins or structures. The distribution of most, if not all, fine grained, banded to disseminated pyrrhotite in black carbonaceous slate beds at Beaver Dam, Fifteen Mile Stream, Goldenville, Moose River, and Tangier appears to be unrelated to the distribution of quartz veins. However, narrow pyrrhotite-rich streaks that are locally abundant in wacke-dominated portions of core from Lake Catcha, Goldenville, and Fifteen Mile Stream may have been structurally controlled.

Large hydrothermal alteration zones that can be linked to gold-rich veins were not identified in this study. Many of the arsenopyrite-rich zones that were seen during this investigation can be considered as alteration products related to the introduction of arsenic during formation of

quartz veins, but most of these zones are restricted to narrow haloes immediately adjacent to late quartz veins. Sericite-rich wacke and slate samples were collected from all the districts included in this study. A few small zones of "bleaching" in wacke were recognized by the writer at Beaver Dam, Caribou, Fifteen Mile Stream, Forest Hill, Goldenville, Lake Catcha, and Tangier. All such zones were less than one square metre in area, and most were less than a few square centimetres. Neither the sericite-rich samples nor the bleached zones could be unequivocally linked to early bedding-parallel veins. Tourmaline was not recognized megascopically in any of the samples that were collected during this study.

RESULTS OF LITHOGEOCHEMICAL ANALYSES

Table 1 presents information concerning the analytical methods, detection limits, analytical uncertainties, and standards used in this study. All analytical work was contracted to X-ray Assay Laboratories Limited of Don Mills, Ontario except for the total C (as CO_2) analyses, which were provided by the Geological Survey of Canada, Ottawa.

Examination of scattergrams of gold plotted against other oxides and elements for many sample populations (see Fig. 2 to 9 below) indicates that sulphur and arsenic are the only elements that can be usefully correlated with gold. Summary statistics for gold, sulphur, and arsenic are provided in Tables 2, 3, and 4 for the principal occurrences and regional background sample populations. Because the frequency distributions for gold, sulphur, and arsenic were found to approximate log normality, geometric means are included to provide better estimates of average contents.

Examination of Table 2 indicates that for gold: 1) the regional background in both wacke and slate is less than 1.0 ppb, 2) the average contents in sulphide-poor wacke and slate from occurrences are mostly greater than the regional background but less than 20 ppb, with no consistent difference between wacke and slate, 3) sulphide-bearing wacke and slate typically contain more gold than sulphide-poor wacke and slate, 4) many samples of sulphide-bearing wacke and slate contain more than 100 ppb gold and some have gold contents greater than 1000 ppb, 5) sulphide-bearing wacke contains more gold than sulphide-bearing slate in some occurrences (Beaver Dam, Tangier, and Goldenville), but sulphide-bearing slate contains relatively more gold than sulphide-bearing wacke in other occurrences (Caribou, Lake Catcha, Moose River, and Fifteen Mile Stream), 6) vein-bearing wacke and slate commonly have more gold than vein-poor wackes and slates, and 7) vein-only samples are generally, but not always, enriched in gold. With respect to sample populations lacking veins, sulphide-bearing slate from Lake Catcha possessed the greatest mean gold content (1700 ppb).

With respect to sulphur (Table 3): 1) the regional background sulphur contents for wacke and slate are similar and less than 0.01 wt.%, 2) the average sulphur contents of sulphide-poor wacke and slate from gold occurrences are consistently greater than the regional background contents and are commonly greater by an order of magnitude, 3) the average sulphur contents of sulphide-poor wacke and slate from gold occurrences are similar, 4) sulphide-bearing slate samples from occurrences do not consistently contain more sulphur than sulphide-bearing wacke samples, 5) vein-bearing wacke and slate are not consistently enriched in sulphur with respect to sulphide-bearing samples lacking veins, and 6) vein-only samples have variable sulphur contents.

With respect to arsenic (Table 4): 1) the regional background arsenic contents for wacke and slate are similar and less than 2.0 ppm, 2) the average arsenic contents of sulphide-poor wacke and slate from gold occurrences are consistently greater than regional background values and are commonly two orders of magnitude greater, 3) the average arsenic content of sulphide-poor wacke is greater than that of sulphide-poor slate in the case of some gold occurrences (Beaver Dam, Tangier, and Fifteen Mile Stream), but similar in other cases (Caribou, Lake Catcha, Moose River, and Goldenville), 4) vein-poor sulphide-bearing wacke is enriched in arsenic relative to vein-poor sulphide-bearing slate in some occurrences (Beaver Dam, Fifteen Mile Stream, and Goldenville), but slate is relatively enriched in other cases (Caribou, Lake Catcha, and Tangier), 5) vein-bearing wacke and slate, if compared across different occurrences, are not consistently enriched in arsenic with respect to sulphide-bearing samples that lack veins, and 6) vein-only samples have relatively low arsenic contents.

Although gold is positively correlated with both sulphur and arsenic in a composite population that includes all 490 samples (Fig. 2 and 3), these correlations break down for some individual occurrences and rock types. Both arsenic and sulphur are useful indicators for gold in several occurrences, as at Beaver Dam (Fig. 4). In others, sulphur is more reliable than arsenic as a guide to gold, as at Tangier (Fig. 5). At Moose River, neither sulphur nor arsenic are well correlated with gold. Although gold-rich samples are rarely poor in sulphur, gold-poor samples are in some cases high in sulphur and/or arsenic (Fig. 2 and 3). Samples of black, carbonaceous, pyrrhotite- and/or arsenopyrite-rich slate contain gold contents that range from less than 10 ppb (samples from Beaver Dam, Moose River, Tangier, Fifteen Mile Stream) to greater than 2000 ppb (samples from Beaver Dam and Fifteen Mile Stream). Although the greatest gold content (3300 ppb) for a sulphidic black slate occurs in an arsenopyrite-rich sample from Beaver Dam, there is no consistent positive relationship between gold and arsenic in sulphidic slate samples.

Table 1. Summary information concerning the methods, detection limits, and estimates of precision relevant to the laboratory analyses of rock samples. The precision estimates for S, Au, and As were determined by the writer using information on duplicate pairs and international standards. The precision estimates for the other components were provided by X-ray Assay Laboratories Limited and are based on their control procedures.

Component	Method	Detection Limit	Precision (+/- %)
SiO_2	XRF, fused disk	0.01 %	1.0
Al_2O_3	"	0.01 %	1.0
CaO	"	0.01 %	1.4
MgO	"	0.01 %	1.6
Na_2O	"	0.01 %	2.6
K_2O	"	0.01 %	2.2
Fe_2O_3	"	0.01 %	2.8
MnO	"	0.01 %	1.4
TiO_2	"	0.01 %	2.2
P_2O_5	"	0.01 %	3.0
LOI	Gravimetric	0.01 %	na
H_2O	Combustion/infrared	0.10 %	na
CO_2 (carbonate)	Acid evolution/infrared	0.01 %	na
CO_2 (total)	Combustion/infrared (GSC)	0.10 %	3.0
FeO	Modified Wilson	0.10 %	na
S	Leco (combustion/infrared)	0.01 %	~30.0[3]; ~10[4]
Au	Fire assay/NA (1987)	1.0 ppb	~50.0[3]; ~20[4]
	Fire assay/DCP (1988,89)	1.0 ppb	~50.0[3]; ~20[4]
As	Neutron activation (NA)	1.0 ppm	~30.0[3]; ~10[4]
Sb	"	0.2 ppm	na
W	"	1.0 ppm	na
Co	Direct current plasma (DCP)	1.0 ppm	8.4
Ni	"	1.0 ppm	10.2
Cu	"	0.5 ppm	8.0
Zn	"	0.5 ppm	11.5
Mo	"	1.0 ppm	28.3
Ag	"	0.5 ppm	15.3
Cd	"	1.0 ppm	31.4
Pb	"	2.0 ppm	18.3
Cr	XRF, fused disk	10.0 ppm	na
Rb	"	10.0 ppm	29.8[1]; 8.6[2]
Sr	"	10.0 ppm	6.4
Y	"	10.0 ppm	43.6[1]; 8.8[2]
Zr	"	10.0 ppm	8.0
Nb	"	10.0 ppm	44.0[1]; 8.0[2]
Ba	"	10.0 ppm	9.6

All data provided under contracts to X-Ray Assay Laboratories Limited, Don Mills, Ontario except for CO_2 (total) by the GSC

x^1 = Precision for 10 - 100 ppm
x^2 = Precision for 100- 1000 ppm
x^3 = Precision for 1 - 10 times the detection limit
x^4 = Precision for greater than 10 times the detection limit

Table 2. Summary statistics for gold (ppb) by district and rock type. Dufferin and Forest Hill are not included in this and subsequent tables because only three and four samples, respectively, were analyzed from these occurrences. S = sulphides, Std dev = standard deviation.

	WACKE	WACKE, VISIBLE S	SLATE	SLATE, VISIBLE S	WACKE + VEIN	SLATE + VEIN	VEIN ONLY	SUMMARY
REGIONAL BACKGROUND								
Average	.8	.	.7	.	.	.	.	.8
Geometric mean	0.6	.	0.7	.	.	.	.	0.6
Minimum	.5	.	.5	.	.	.	.	.5
Maximum	3.0	.	2.0	.	.	.	.	3.0
Std dev	.7	.	.5	.	.	.	.	.7
Samples	38		17					55
BEAVERDAM								
Average	9.9	643.4	58.6	399.3	.	900.1	390.1	498.3
Geometric mean	3.7	75.9	13.8	33.9		269.2	123.0	57.5
Minimum	.5	2.0	.5	.5	.	7.0	31.0	.5
Maximum	30.0	2800.0	180.0	3300.0	.	3300.0	2200.0	3300.0
Std dev	12.7	1023.4	83.2	958.6	.	1007.3	799.3	897.1
Samples	5	7	4	17		14	7	54
CARIBOU								
Average	16.4	188.4	8.0	77.7	716.0	1087.5	927.3	390.8
Geometric mean	3.6	41.7	8.0	70.8	562.0	107.2	158.5	50.1
Minimum	.5	3.0	8.0	42.0	210.0	2.0	28.0	.5
Maximum	77.0	1500.0	8.0	120.0	1600.0	3300.0	2700.0	3300.0
Std dev	30.3	389.1		39.4	546.3	1534.9	1535.2	798.6
Samples	6	19	1	3	5	6	3	43
LAKE CATCHA								
Average	24.3	100.3	25.7	331.5	299.0	74.9	.	154.8
Geometric mean	19.1	17.4	17.0	169.8	72.4	20.0	.	35.5
Minimum	9.0	1.0	3.0	25.0	13.0	.5	.	.5
Maximum	53.0	1600.0	67.0	1700.0	850.0	210.0	.	1700.0
Std dev	16.9	329.4	23.5	431.5	477.3	79.2	.	329.3
Samples	8	23	6	19	3	9		68
MOOSE RIVER								
Average	22.7	2.7	3.1	361.2	1.0	6863.9	.	821.1
Geometric mean	10.7	1.8	0.8	14.8	1.0	14.8	.	5.6
Minimum	2.0	.5	.5	.5	1.0	.5	.	.5
Maximum	72.0	9.0	28.0	5100.0	1.0	48000.0	.	48000.0
Std dev	27.0	2.5	8.3	998.8		18139.3	.	5677.1
Samples	7	16	11	30	1	7		72
TANGIER								
Average	17.0	86.8	15.9	7.8	283.3	1213.0	189.5	235.2
Geometric mean	10.7	15.8	2.9	5.5	29.5	100.0	141.3	16.6
Minimum	2.0	.5	.5	.5	3.0	5.0	48.0	.5
Maximum	37.0	450.0	67.0	11.0	1400.0	7500.0	440.0	7500.0
Std dev	15.2	152.2	26.8	4.1	556.2	2778.7	172.0	1031.7
Samples	6	17	8	6	6	7	4	54
FIFTEEN MILE STREAM								
Average	3.2	35.8	.5	740.7	350.0	223.4	150.5	437.1
Geometric mean	2.1	4.5	0.5	33.1	350.0	91.2	56.2	20.0
Minimum	.5	.5	.5	.5	350.0	6.0	11.0	.5
Maximum	5.0	340.0	.5	7400.0	350.0	840.0	290.0	7400.0
Std dev	2.4	92.9		1891.2		280.7	197.3	1401.0
Samples	3	13	3	35	1	10	2	67
GOLDENVILLE								
Average	1.7	44.2	1.0	287.7	220.0	111.6	5.0	78.9
Geometric mean	0.7	20.0	0.8	7.1	220.0	21.9	5.0	4.4
Minimum	.5	.5	.5	.5	220.0	.5	5.0	.5
Maximum	19.0	250.0	2.0	3200.0	220.0	780.0	5.0	3200.0
Std dev	4.0	64.0	.7	918.1		252.3		392.0
Samples	25	18	4	12	1	9	1	70
SUMMARY								
Average	7.0	116.6	10.7	439.2	396.9	1283.5	386.9	333.2
Geometric mean	1.6	13.8	1.6	28.2	87.1	63.1	100.0	11.7
Minimum	.5	.5	.5	.5	1.0	.5	5.0	.5
Maximum	77.0	2800.0	180.0	7400.0	1600.0	48000.0	2700.0	48000.0
Std dev	14.6	358.4	28.5	1230.6	500.1	6145.5	789.2	2320.0
Samples	98	113	54	122	17	62	17	483

Table 3. Summary statistics for sulphur (wt.%) by district and rock type.

	WACKE	WACKE, VISIBLE S	SLATE	SLATE, VISIBLE S	WACKE + VEIN	SLATE + VEIN	VEIN ONLY	SUMMARY
REGIONAL BACKGROUND								
Average	.008	.	.006	.	.	.	.	.007
Geometric mean	.006	.	.005	.	.	.	.	.006
Minimum	.005	.	.005	.	.	.	.	.005
Maximum	.041	.	.015	.	.	.	.	.041
Std dev	.008	.	.002	.	.	.	.	.007
Samples	38		17					55
BEAVERDAM								
Average	.061	.866	.061	.824	.	2.043	1.467	1.102
Geometric mean	.05	.52	.04	.60	.	1.48	1.20	.52
Minimum	.018	.120	.007	.160	.	.480	.630	.007
Maximum	.098	2.050	.160	2.500	.	6.750	3.990	6.750
Std dev	.030	.798	.068	.685	.	1.772	1.163	1.267
Samples	5	7	4	17		14	7	54
CARIBOU								
Average	.078	.456	.009	1.163	.608	.321	.040	.412
Geometric mean	.07	.35	.009	1.05	.47	.21	.04	.23
Minimum	.030	.073	.009	.560	.200	.047	.037	.009
Maximum	.130	1.300	.009	1.630	1.270	.630	.046	1.630
Std dev	.043	.321		.548	.449	.229	.005	.401
Samples	6	19	1	3	5	6	3	43
LAKE CATCHA								
Average	.061	.211	.079	.429	.312	.405	.	.273
Geometric mean	.05	.09	.07	.31	.18	.28	.	.14
Minimum	.006	.008	.028	.069	.056	.083	.	.006
Maximum	.120	1.150	.130	1.660	.730	1.100	.	1.660
Std dev	.037	.318	.033	.411	.365	.356	.	.342
Samples	8	23	6	19	3	9		68
MOOSE RIVER								
Average	.040	.523	.047	.534	.540	.245	.	.381
Geometric mean	.04	.43	.03	.36	.540	.17	.	.20
Minimum	.014	.062	.006	.035	.540	.051	.	.006
Maximum	.065	1.270	.120	2.400	.540	.470	.	2.400
Std dev	.020	.306	.040	.481		.182	.	.403
Samples	7	16	11	30	1	7		72
TANGIER								
Average	.060	.185	.038	.701	.604	.736	.978	.383
Geometric mean	.04	.14	.03	.44	.16	.59	.87	.15
Minimum	.007	.028	.016	.066	.012	.120	.530	.007
Maximum	.180	.560	.100	1.630	2.000	1.270	1.820	2.000
Std dev	.066	.148	.029	.582	.798	.419	.575	.490
Samples	6	17	8	6	6	7	4	54
FIFTEEN MILE STREAM								
Average	.160	.685	.079	.565	.730	1.491	.840	.697
Geometric mean	.09	.45	.08	.41	.730	1.17	.49	.42
Minimum	.020	.060	.058	.050	.730	.170	.160	.020
Maximum	.340	2.320	.110	1.720	.730	2.500	1.520	2.500
Std dev	.164	.632	.027	.440		.745	.962	.632
Samples	3	13	3	35	1	10	2	67
GOLDENVILLE								
Average	.111	.691	.093	.555	.020	.697	.070	.408
Geometric mean	.08	.62	.06	.41	.020	.56	.070	.22
Minimum	.011	.150	.030	.040	.020	.190	.070	.011
Maximum	.380	1.640	.270	2.000	.020	1.460	.070	2.000
Std dev	.097	.338	.118	.490		.460		.415
Samples	25	18	4	12	1	9	1	70
SUMMARY								
Average	.056	.464	.042	.593	.523	1.003	.944	.455
Geometric mean	.02	.28	.02	.41	.23	.58	.47	.15
Minimum	.005	.008	.005	.035	.012	.047	.037	.005
Maximum	.380	2.320	.270	2.500	2.000	6.750	3.990	6.750
Std dev	.074	.443	.050	.509	.545	1.138	.975	.649
Samples	98	113	54	122	17	62	17	483

Table 4. Summary statistics for arsenic (ppm) by district and rock type.

	WACKE	WACKE, VISIBLE S	SLATE	SLATE, VISIBLE S	WACKE + VEIN	SLATE + VEIN	VEIN ONLY	SUMMARY
REGIONAL BACKGROUND								
Average	1.9	.	3.5	.	.	.	.	2.4
Geometric mean	1.3	.	1.9	.	.	.	.	1.5
Minimum	.5	.	.5	.	.	.	.	.5
Maximum	10.0	.	16.0	.	.	.	.	16.0
Std dev	1.9	.	4.2	.	.	.	.	2.9
Samples	38		17					55
BEAVERDAM								
Average	625.8	14917.6	165.3	6854.0	.	42490.7	434.4	15234.1
Geometric mean	489.8	3388.4	117.5	2290.9		10000.0	275.4	1862.1
Minimum	99.0	33.0	47.0	38.0	.	180.0	71.0	33.0
Maximum	1000.0	44000.0	410.0	37000.0	.	150000.0	1100.0	150000.0
Std dev	357.0	18325.9	165.9	9737.0	.	47289.4	407.1	30002.9
Samples	5	7	4	17		14	7	54
CARIBOU								
Average	191.2	6801.1	130.0	19450.0	12260.0	835.2	390.0	5961.1
Geometric mean	104.7	4677.4	130.0	6606.9	7413.1	229.1	346.7	1513.6
Minimum	35.0	420.0	130.0	350.0	3100.0	36.0	250.0	35.0
Maximum	580.0	17000.0	130.0	32000.0	38000.0	2900.0	660.0	38000.0
Std dev	221.4	5032.4		16810.9	14834.0	1224.1	233.9	8662.0
Samples	6	19	1	3	5	6	3	43
LAKE CATCHA								
Average	321.5	1556.1	120.0	1780.6	1670.0	808.8	.	1237.0
Geometric mean	91.2	478.6	114.8	1000.0	1479.1	407.4		426.6
Minimum	33.0	53.0	91.0	100.0	810.0	99.0	.	33.0
Maximum	2100.0	15000.0	210.0	4900.0	2600.0	3000.0	.	15000.0
Std dev	719.7	3297.7	44.7	1611.1	897.1	1052.5	.	2214.1
Samples	8	23	6	19	3	9		68
MOOSE RIVER								
Average	17.4	3361.0	34.7	2299.9	68.0	485.7	.	1760.3
Geometric mean	17.0	125.9	15.8	173.8	68.0	64.6		79.4
Minimum	11.0	10.0	2.0	6.0	68.0	7.0	.	2.0
Maximum	23.0	27000.0	220.0	36000.0	68.0	3000.0	.	36000.0
Std dev	5.1	7497.3	62.2	7287.2		1111.4	.	5944.1
Samples	7	16	11	30	1	7		72
TANGIER								
Average	283.3	2018.1	82.5	12548.3	2076.8	9991.5	28.9	3601.4
Geometric mean	131.8	691.8	38.9	3467.4	245.5	1202.3	10.7	316.2
Minimum	20.0	37.0	5.0	170.0	.5	.5	.5	.5
Maximum	990.0	13000.0	250.0	42000.0	6500.0	29000.0	54.0	42000.0
Std dev	369.6	3273.3	89.7	15734.3	2865.2	11450.7	27.6	7862.8
Samples	6	17	8	6	6	7	4	54
FIFTEEN MILE STREAM								
Average	315.0	5164.2	369.0	2259.2	12000.0	20675.0	205.0	5483.9
Geometric mean	100.0	891.3	18.6	331.1	12000.0	4073.8	107.2	489.8
Minimum	5.0	56.0	1.0	9.0	12000.0	150.0	30.0	1.0
Maximum	610.0	17000.0	1100.0	14000.0	12000.0	55000.0	380.0	55000.0
Std dev	302.8	7301.2	633.1	3988.9		22666.2	247.5	11504.5
Samples	3	13	3	35	1	10	2	67
GOLDENVILLE								
Average	112.8	12111.1	43.0	4331.0	4.0	6696.7	810.0	4772.1
Geometric mean	34.7	8912.5	41.7	478.6	4.0	1513.6	810.0	380.2
Minimum	4.0	1000.0	27.0	39.0	4.0	170.0	810.0	4.0
Maximum	970.0	31000.0	58.0	39000.0	4.0	28000.0	810.0	39000.0
Std dev	227.2	8021.7	13.2	11096.0		10505.6		8519.6
Samples	25	18	4	12	1	9	1	70
SUMMARY								
Average	127.6	5687.2	72.1	4003.9	5343.7	15282.6	326.3	4539.4
Geometric mean	13.8	1174.9	15.1	549.5	851.1	1288.2	128.8	223.9
Minimum	.5	10.0	.5	6.0	.5	.5	.5	.5
Maximum	2100.0	44000.0	1100.0	42000.0	38000.0	150000.0	1100.0	150000.0
Std dev	304.5	8200.9	162.9	8385.5	9243.9	29076.9	342.6	12868.8
Samples	98	113	54	122	17	62	17	483

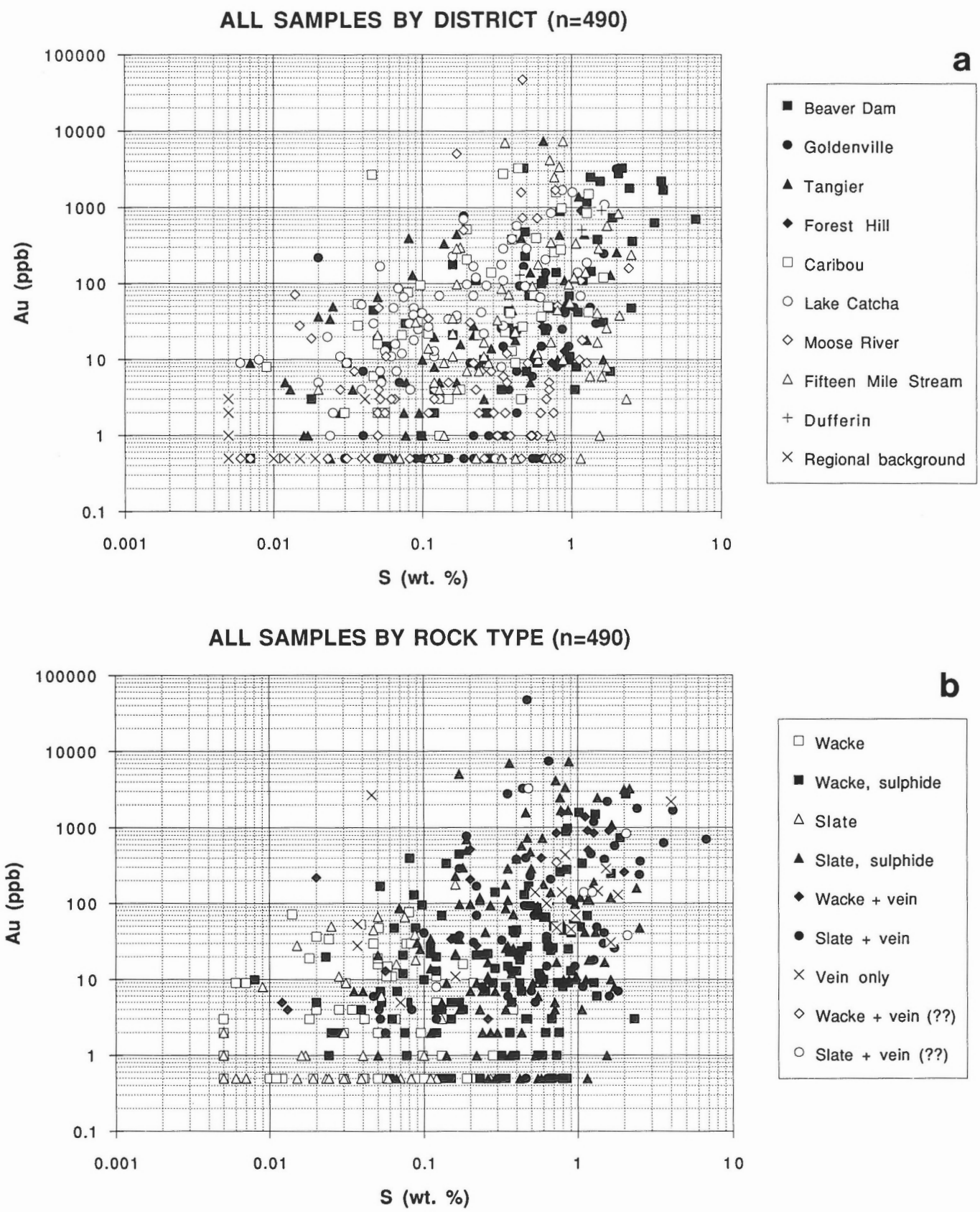

Figure 2. Scattergrams for gold versus sulphur for a composite sample population (all 490 samples) in which the data have been plotted by a) district and b) rock type. The correlation coefficient for each plot is 0.57 and is highly significant. All data were log transformed prior to correlation analysis.

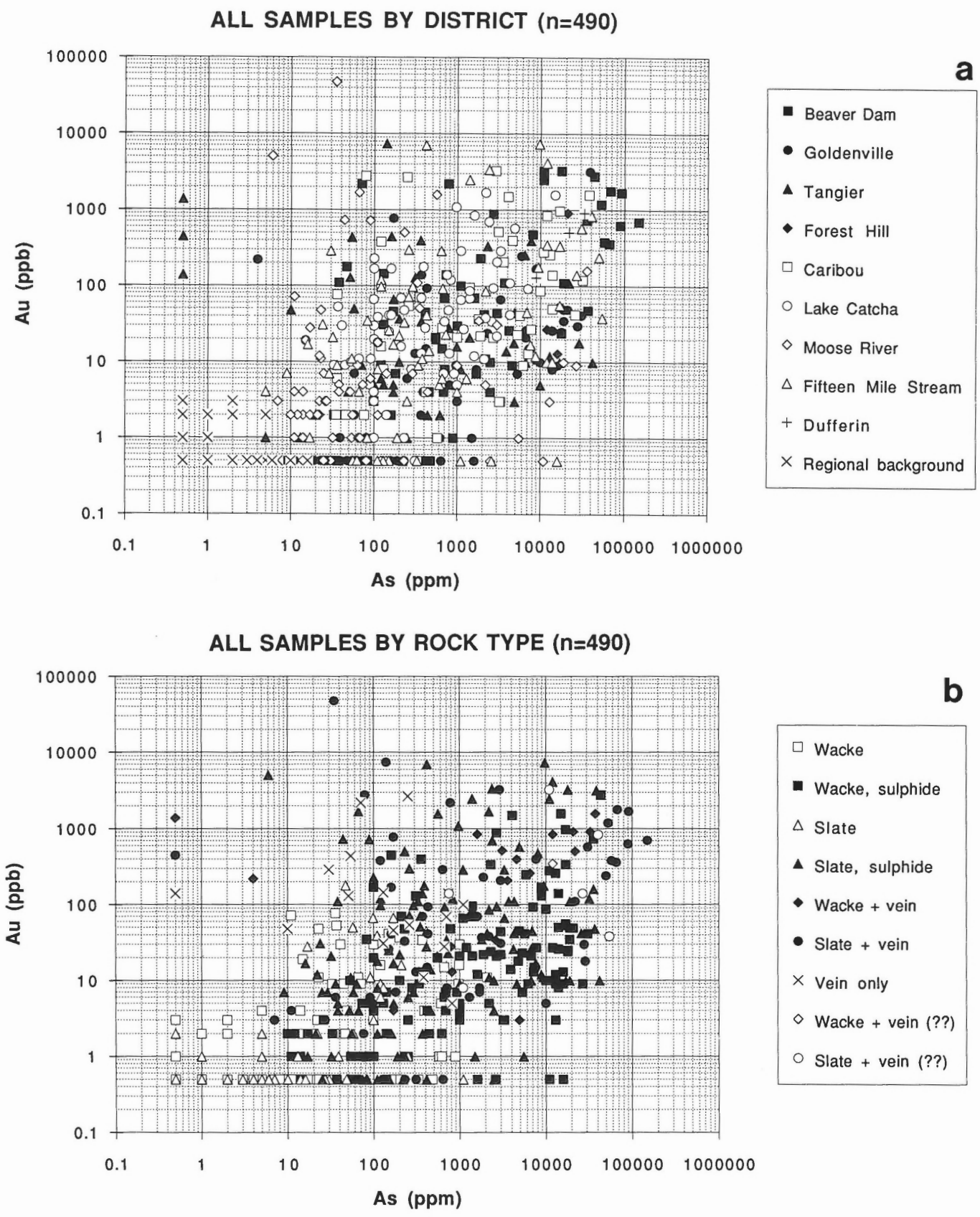

Figure 3. Scattergrams for gold versus arsenic for a composite sample population (all 490 samples) in which the data have been plotted by a) district and b) rock type. The correlation coefficient for each plot is 0.56 and is highly significant. All data were log transformed prior to correlation analysis.

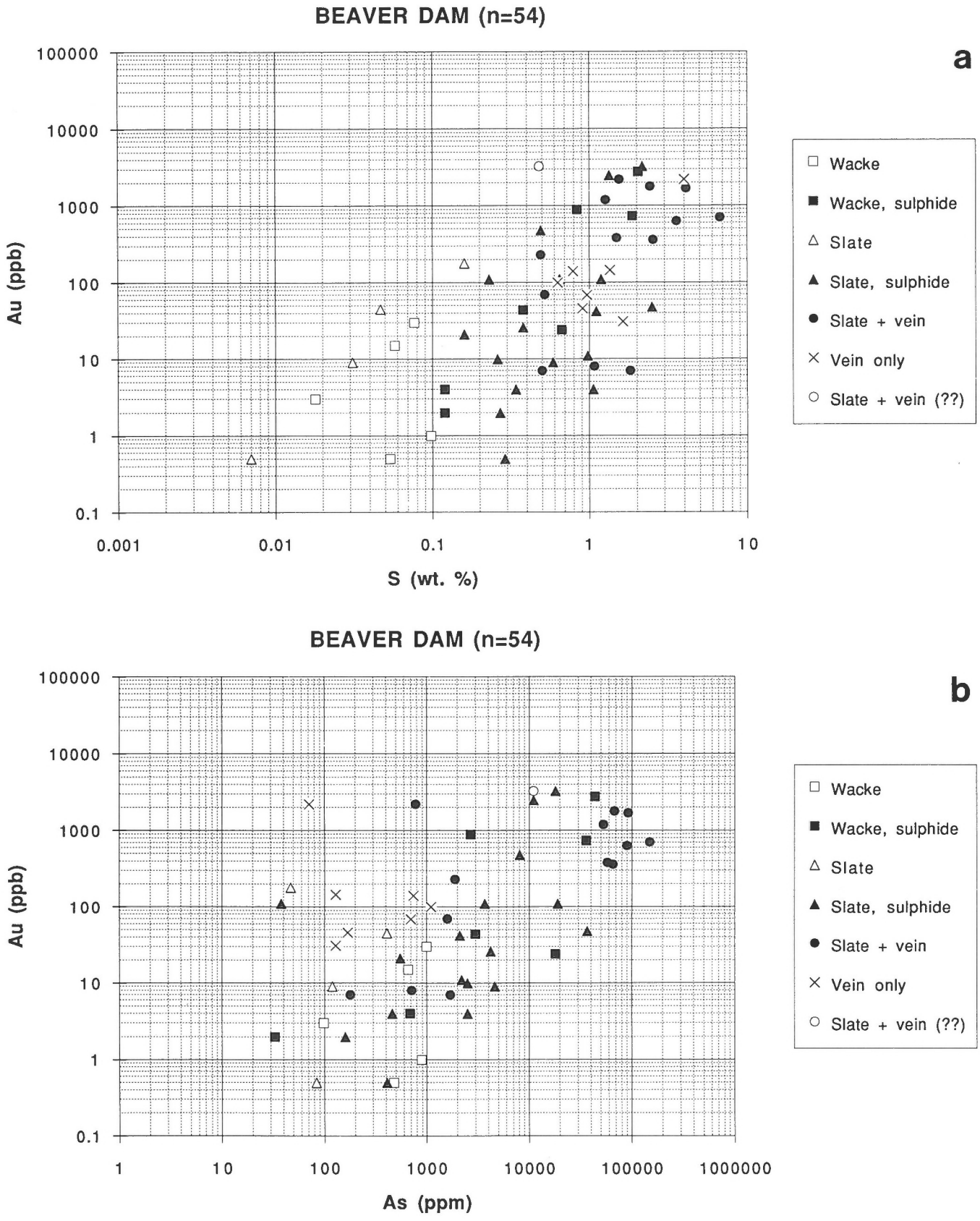

Figure 4. Scattergrams for gold versus a) sulphur and b) arsenic for Beaver Dam. The Au-S and Au-As correlation coefficients are 0.66 and 0.56, respectively, and both are highly significant. All data were log transformed prior to correlation analysis.

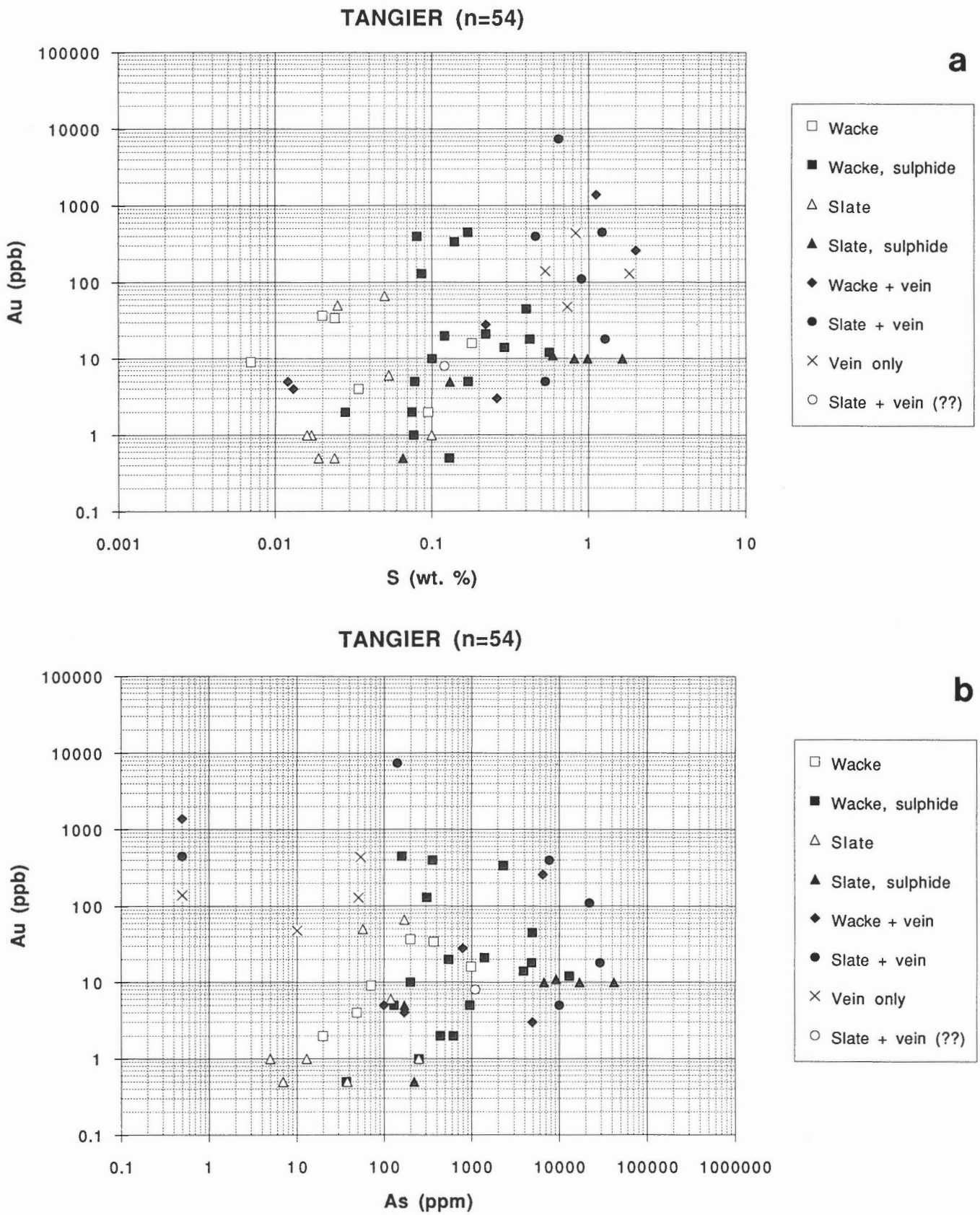

Figure 5. Scattergrams for gold versus a) sulphur and b) arsenic for Tangier. The Au-S and Au-As correlation coefficients are 0.51 and -0.02, respectively; the Au-S coefficient is highly significant, but the Au-As coefficent clearly indicates a lack of correlation between gold and arsenic. All data were log transformed prior to correlation analysis.

Correlation coefficients are presented in Tables 5 and 6 for the main rock types across the principal districts. The composite wacke and slate populations of Table 6 were created by combining all the sulphide-poor, sulphide-bearing, and vein-bearing samples of wacke and slate, respectively. There are numerous examples of intriguing differences among sample populations. Despite a highly significant correlation of 0.44 between gold and sulphur across all samples from occurrences, the coefficients for different subpopulations of wacke samples range from -0.26 for the sulphide-poor subpopulation through 0.29 for the sulphide-bearing subpopulation to 0.60 for the vein-bearing subpopulation. Although the Au-S correlation coefficient is only 0.29 for all sulphide-bearing wacke samples from occurrences, the coefficient ranges from -0.23 at Moose River to much greater values at Lake Catcha (0.67), Goldenville (0.70), and Beaver Dam (0.94). The Au-S coefficient for the composite wacke sample population from Moose River (-0.67) is markedly different from that for the composite slate sample population from Moose River (0.41). With respect to Au-As correlations there are also considerable differences among different rock types and among districts. This is particularly true for the different rock types at Caribou and of populations of vein-bearing slate samples for different districts. These contrasts among the Au-S and Au-As correlation coefficients suggest that different processes may have controlled the distributions of gold, sulphur, and arsenic, not only in the different rock types but also in the same rock type in different districts.

The K_2O/Na_2O ratio appears to be a potentially useful indicator of gold-related hydrothermal alteration in wacke, and possibly in slate. Samples with high ratios are relatively rich in sericite (white mica). Summary statistics for the K_2O/Na_2O ratio are provided in Table 7. The regional background is less than 1.0 for wacke and less than 6.0 for slate. Correlation coefficients for gold contents versus K_2O/Na_2O ratios for a variety of sample populations are provided in Tables 5 and 6. Gold contents are plotted against the K_2O/Na_2O ratios for wacke, slate, and vein samples in Figure 6.

Only 4 of 38 or 10.5% of wacke samples from the regional background population and just 7 of 60 or 11.7% of sulphide-poor wacke samples from occurrences possess K_2O/Na_2O ratios greater than 1.0. In marked contrast, 43 of 117 or 36.8% of sulphide-bearing wacke samples, and 8 of 20 or 40.0% of vein-bearing wacke samples possess K_2O/Na_2O ratios greater than 1.0. None of the regional background wacke samples and only 2 of the 60 or 3.3% of sulphide-poor wacke samples from occurrences have K_2O/Na_2O ratios greater than 2.0. However, 12 of 117 or 10.3% of sulphide-bearing wacke samples and 4 of 20 or 20% of vein-bearing wacke samples have K_2O/Na_2O ratios greater than 2.0. With respect to gold contents, 10 of 12 or 83% of wacke samples with gold greater than 700 ppb have K_2O/Na_2O ratios greater than 1.0; 5 of the 12 or 41.7% have K_2O/Na_2O greater than 2.0. Only 48 of 223 or 21.5% of those wacke samples containing less than 700 ppb gold have K_2O/Na_2O ratios greater than 1.0 and just 13 or 5.8% have K_2O/Na_2O ratios greater than 2.0. Examination of the correlation coefficients for gold contents versus K_2O/Na_2O ratios for wacke populations in Table 6 indicates very strong positive correlations for the occurrence-wide composite population (0.38) and the Lake Catcha population (0.54), as well as moderately strong coefficients for the Tangier (0.49), Beaver Dam (0.63), Goldenville (0.34), and Caribou (0.37) populations.

In contrast to wacke samples, 5 of 17 or 29.4% of slate samples from the regional background population and 15 of 37 or 40.5% of sulphide-poor slate samples possess K_2O/Na_2O ratios greater than 6.0. However, only 25 of 122 or 20.5% of sulphide-bearing slate samples and 13 of 62 or 21.0% of vein-bearing slate samples possess K_2O/Na_2O ratios greater than 6.0. There is no clear relationship between anomalous K_2O/Na_2O values and gold contents in most slate sample populations. However, all six sulphide-bearing slate samples from the Touquoy Zone, Moose River district possess K_2O/Na_2O ratios greater than 6.0. Four of the six (67%) contain gold contents greater than 700 ppb; three of these have K_2O/Na_2O ratios greater than 10.0. A direct relationship between gold contents and the K_2O/Na_2O ratios for slate samples is also suggested by the moderately strong correlation coefficient of 0.46 for the composite slate sample population from Goldenville.

Data from this study suggest that SiO_2 and/or CO_2 variations in the rocks hosting gold-bearing veins cannot be consistently correlated with either gold contents or hydrothermal alteration. Summary statistics for the SiO_2/Al_2O_3 ratio, a useful index of possible silicification, are provided in Table 8. The average SiO_2/Al_2O_3 ratios for sulphide-poor wacke samples lacking veins are less than the average for the regional background wacke population in all gold occurrences except Beaver Dam. Furthermore, the average SiO_2/Al_2O_3 ratios in sulphide-bearing wacke are less than the average ratios in sulphide-poor wacke for all districts except Tangier. The average SiO_2/Al_2O_3 ratios for the populations of both sulphide-poor and sulphide-bearing slate samples from occurrences are either less than or similar to the average for the regional background slate population. Sulphide-bearing slate samples contain similar or lower SiO_2/Al_2O_3 ratios relative to sulphide-poor slate in all occurrences except Beaver Dam.

Table 5. Summary table of correlation coefficients by district and rock type. Coefficients flagged with two asterisks (**) are significant at the 0.001 or better level, indicating that the probability of exceeding the calculated correlation coefficent in a random sample of observations taken from an uncorrelated parent population is only 0.1% or less. Coefficients flagged with one asterisk (*) are significant at the 0.005 to 0.002 level, indicating that the probability of exceeding the calculated correlation coefficent in a random sample of observations taken from an uncorrelated parent population is 0.5% to 0.2%. RKNA = K_2O/Na_2O ratio; RSiAl = SiO_2/Al_2O_3 ratio.

	WACKE	WACKE, VISIBLE S	SLATE	SLATE, VISIBLE S	WACKE + VEIN	SLATE + VEIN	VEIN ONLY	COMPOSITE
REGIONAL BACKGROUND								
Au vs S	.19	-	-.13	-	-	-	-	.13
Au vs As	-.20	-	-.17	-	-	-	-	-.18
Au vs CO_2	.04	-	.05	-	-	-	-	.04
Au vs RKNa	-.27	-	.17	-	-	-	-	.03
Au vs RSiAl	-.08	-	-.15	-	-	-	-	-.05
Samples	38		17					55
BEAVER DAM								
Au vs S	.07	.94*	.98	.50	-	.33	.69	.66**
Au vs As	.23	.78	.03	.52	-	.67	-.35	.56**
Au vs CO_2	-.63	.25	-.52	.28	-	.01	-.80	-.01
Au vs RKNa	.54	.48	.39	.08	-	-.29	.27	-.03
Au vs RSiAl	-.90	-.63	.27	-.07	-	-.11	-.13	.06
Samples	5	7	4	17		14	7	54
CARIBOU								
Au vs S	-.25	.56	x	.21	.70	.75	.99	.47**
Au vs As	-.56	.51	x	.05	.88	.41	-.63	.36
Au vs CO_2	-.89	-.34	x	-.74	-.33	-.31	.90	-.15
Au vs RKNa	-.43	.06	x	.11	.33	-.05	-.63	.05
Au vs RSiAl	.77	-.26	x	-.08	-.29	-.41	.56	.17
Samples	6	19	1	3	5	6	3	43
LAKE CATCHA								
Au vs S	.38	.67**	-.12	.65	.99	.04	-	.57**
Au vs As	-.15	.55*	.04	.33	.31	.42	-	.48**
Au vs CO_2	.11	-.30	.55	-.27	.97	.50	-	-.12
Au vs RKNa	.43	.62*	.07	.02	.98	-.34	-	.32
Au vs RSiAl	-.60	-.48	.18	-.12	-.99	.10	-	-.43**
Samples	8	23	6	19	3	9		68
MOOSE RIVER								
Au vs S	-.53	-.23	-.17	.18	x	.39	-	.20
Au vs As	-.11	.32	.05	-.01	x	.01	-	.13
Au vs CO_2	.24	.08	-.07	.32	x	-.76	-	.09
Au vs RKNa	.26	.12	.02	.55	x	.74	-	.44**
Au vs RSiAl	.53	-.15	-.55	.22	x	.43	-	.03
Samples	7	16	11	30	1	7		72
TANGIER								
Au vs S	-.27	.23	.29	.85	.79	.34	.06	.51**
Au vs As	.81	.25	.53	.74	-.49	-.48	.29	-.02
Au vs CO_2	-.38	-.20	.78	-.44	-.09	-.14	.05	-.04
Au vs RKNa	.63	.06	-.25	.42	.95	-.59	.84	-.04
Au vs RSiAl	-.36	-.12	-.15	-.33	.81	.50	-.20	.36
Samples	6	17	8	6	6	7	4	54
FIFTEEN MILE STREAM								
Au vs S	-.72	.31	x	.014	x	-.02	x	.34*
Au vs As	-.31	.42	x	.50	x	.56	x	.46**
Au vs CO_2	.90	-.10	x	-.20	x	-.10	x	-.20
Au vs RKNa	-.16	-.09	x	-.07	x	-.28	x	.06
Au vs RSiAl	.17	-.35	x	.23	x	-.69	x	.08
Samples	3	13	3	35	1	10	2	67
GOLDENVILLE								
Au vs S	.26	.70**	-.52	.44	x	-.26	x	.58**
Au vs As	.41	.54	.65	.77	x	-.09	x	.67**
Au vs CO_2	.27	.01	-.60	-.26	x	.28	x	-.14
Au vs RKNa	.23	.03	-.51	.66	x	.04	x	.35*
Au vs RSiAl	.01	-.14	.44	-.72	x	.18	x	-.02
Samples	25	18	4	12	1	9	1	70
COMPOSITE (occurrences only)								
Au vs S	-.26	.29*	.17	.23	.60*	.38*	.32	.44**
Au vs As	.22	.52**	.46*	.35**	.29	.31	-.26	.44**
Au vs CO_2	.17	-.05	.31	.08	-.01	-.20	-.16	-.03
Au vs RKNa	.30	.20	.06	.12	.48	-.08	-.24	.11
Au vs RSiAl	-.15	-.14	-.21	-.03	-.01	.20	-.10	.11
Samples	60	117	37	122	20	62	17	435

Table 6. Summary table of correlation coefficients for composite sample populations. An explanation for the asterisks which accompany some of the correlation coefficients is provided in the caption for Table 5. RKNA = K_2O/Na_2O ratio; RSiAl = SiO_2/Al_2O_3 ratio.

	Au vs S	Au vs As	Au vs CO_2	Au vs RKNa	Au vs RSiAl
all samples					
background in (490)	.57**	.56**	.26**	.14*	.11
background out (435)	.44**	.44**	-.03	.11	.11
all wacke samples					
background in (235)	.56**	.65**	.37**	.40**	-.21**
background out (197)	.38**	.53**	.02	.38**	-.12
all slate samples					
background in (238)	.55**	.54**	.23**	.08	.15
background out (221)	.46**	.46**	.03	.07	.15
Beaver Dam					
all samples (54)	.66**	.56**	-.01	-.03	.06
all wacke (12)	.84**	.77*	-.19	.63	-.80*
all slate (35)	.56**	.63**	.23	-.19	.18
Caribou					
all samples (43)	.47**	.36	-.15	.05	.17
all wacke (30)	.63**	.59*	.01	.37	-.12
all slate (10)	.55	.23	-.21	-.09	-.22
Lake Catcha					
all samples (68)	.57**	.48**	-.12	.32	-.43**
all wacke (34)	.66**	.42	-.11	.54**	-.48*
all slate (32)	.37	.52*	-.03	-.18	-.12
Moose River					
all samples (72)	.20	.13	.09	.44**	.03
all wacke (24)	-.67**	-.07	-.07	-.22	.55
all slate (48)	.41*	.19	.20	.44*	.18
Tangier					
all samples (54)	.51**	-.02	-.04	-.04	.36
all wacke (29)	.40	-.01	-.24	.49	.29
all slate (21)	.56	.15	-.07	-.04	.50
Fifteen Mile Stream					
all samples (67)	.34*	.46**	-.20	.06	.08
all wacke (17)	.28	.45	-.04	.18	-.40
all slate (48)	.33	.55**	-.15	-.15	.03
Goldenville					
all samples (70)	.58**	.67**	-.14	.35*	-.02
all wacke (44)	.65**	.72**	-.04	.34	-.14
all slate (25)	.42	.61**	-.04	.46	-.48

Table 7. Summary statistics for the K_2O/Na_2O ratio by district and rock type.

	WACKE	WACKE, VISIBLE S	SLATE	SLATE, VISIBLE S	WACKE + VEIN	SLATE + VEIN	VEIN ONLY	SUMMARY
REGIONAL BACKGROUND								
Average	.70	.	4.55	.	.	.	.	1.89
Minimum	.30	.	1.35	.	.	.	.	.30
Maximum	1.57	.	8.98	.	.	.	.	8.98
Std dev	.27	.	2.26	.	.	.	.	2.19
Samples	38		17					55
BEAVER DAM								
Average	.52	1.43	8.77	3.99	.	3.69	.90	3.21
Minimum	.25	.36	6.24	.77	.	.98	.47	.25
Maximum	1.08	3.34	11.03	8.79	.	13.61	1.46	13.61
Std dev	.33	.98	2.15	2.34	.	3.44	.35	3.06
Samples	5	7	4	17		14	7	54
CARIBOU								
Average	.69	.95	24.39	5.09	1.75	16.61	2.23	4.12
Minimum	.54	.61	24.39	2.42	.60	1.56	2.13	.54
Maximum	.99	1.39	24.39	9.59	3.95	33.00	2.40	33.00
Std dev	.17	.25		3.92	1.33	15.35	.15	8.26
Samples	6	19	1	3	5	6	3	43
LAKE CATCHA								
Average	1.22	1.26	3.96	3.55	1.01	3.51	.	2.42
Minimum	.59	.50	2.24	2.02	.66	2.38	.	.50
Maximum	3.08	3.27	5.49	4.44	1.68	5.40	.	5.49
Std dev	.89	.86	1.34	.62	.59	1.07	.	1.47
Samples	8	23	6	19	3	9		68
MOOSE RIVER								
Average	.50	1.23	5.59	6.67	1.01	4.58	.	4.41
Minimum	.39	.60	1.48	1.77	1.01	2.40	.	.39
Maximum	.67	3.31	18.00	44.43	1.01	6.92	.	44.43
Std dev	.11	.77	5.04	9.78		1.80	.	7.02
Samples	7	16	11	30	1	7		72
TANGIER								
Average	.82	.85	4.77	30.58	1.43	12.86	6.53	6.77
Minimum	.50	.47	1.11	5.52	.48	3.07	1.06	.47
Maximum	1.17	2.51	9.69	71.08	3.31	29.37	17.50	71.08
Std dev	.26	.53	2.67	26.35	1.33	11.24	7.56	13.13
Samples	6	17	8	6	6	7	4	54
FIFTEEN MILE STREAM								
Average	.59	.74	5.81	4.51	1.55	3.52	.92	3.36
Minimum	.36	.40	5.09	1.43	1.55	2.07	.57	.36
Maximum	.75	2.06	6.30	17.41	1.55	5.49	1.26	17.41
Std dev	.20	.43	.64	3.30		1.04	.49	2.95
Samples	3	13	3	35	1	10	2	67
GOLDENVILLE								
Average	.67	1.15	5.05	9.89	.48	10.86	24.00	4.26
Minimum	.43	.02	2.74	1.82	.48	1.51	24.00	.02
Maximum	1.04	3.34	10.68	46.33	.48	45.32	24.00	46.33
Std dev	.14	.73	3.77	15.83		14.35		9.43
Samples	25	18	4	12	1	9	1	70
SUMMARY								
Average	.71	1.07	5.52	6.64	1.38	7.06	3.82	3.78
Minimum	.25	.02	1.11	.77	.48	.98	.47	.02
Maximum	3.08	3.34	24.39	71.08	3.95	45.32	24.00	71.08
Std dev	.36	.69	4.09	10.57	1.08	9.17	6.58	7.06
Samples	98	113	54	122	17	62	17	483

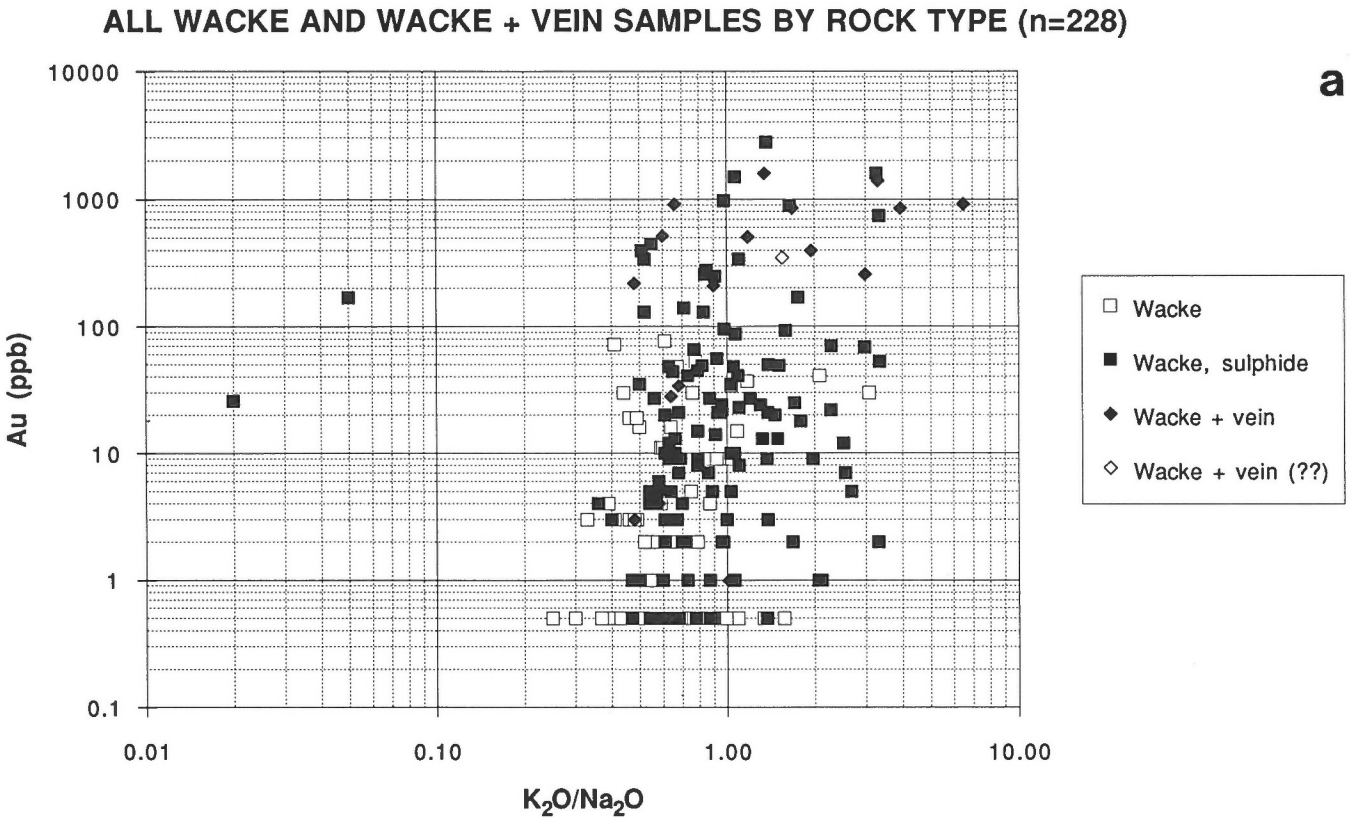

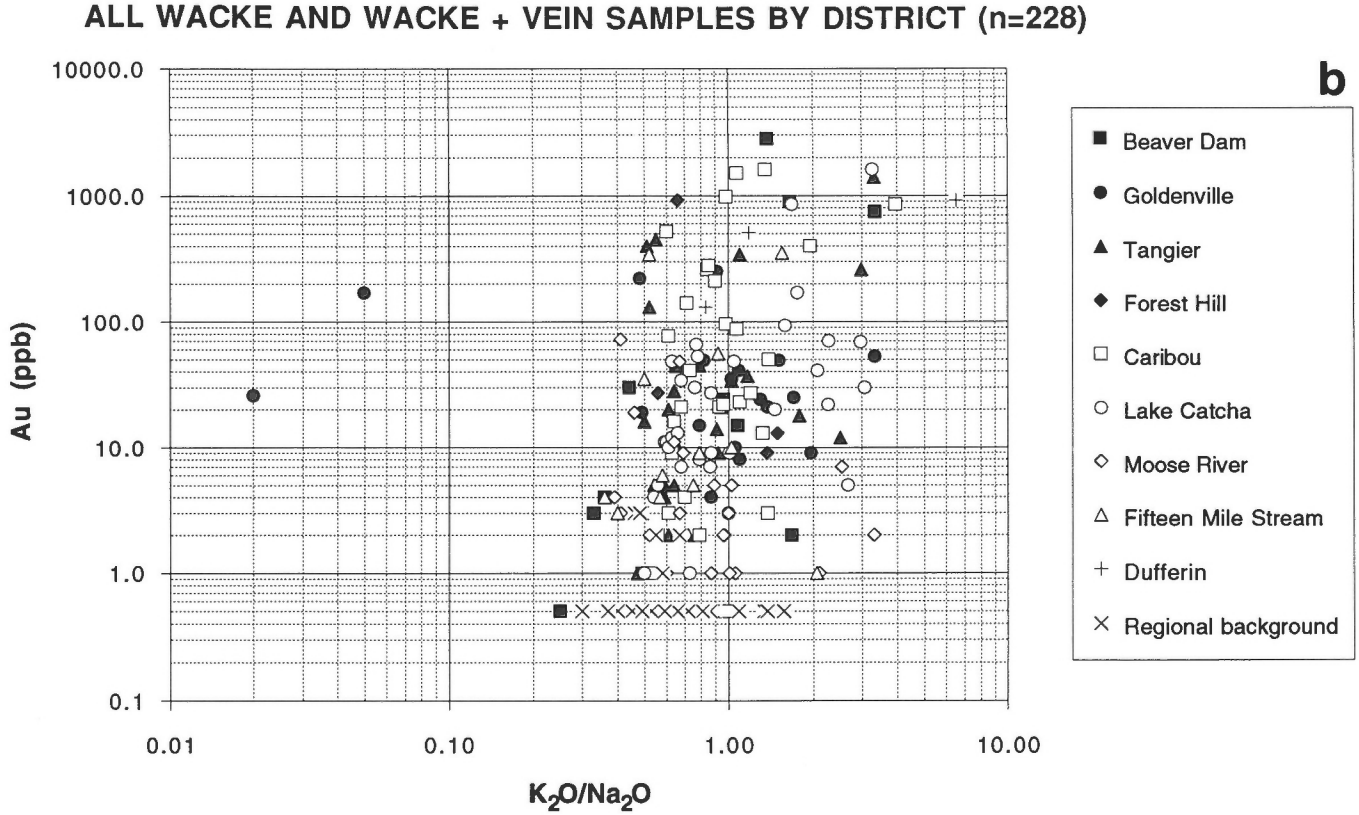

Figure 6. Scattergrams for gold versus K_2O/Na_2O ratio for wacke samples by a) rock type and b) district, as well as for slate and vein samples by c) rock type and d) district. Samples from the Touquoy zone, Moose River district are indicated by a T symbol. Slate + vein = slate containing small quartz veinlets.

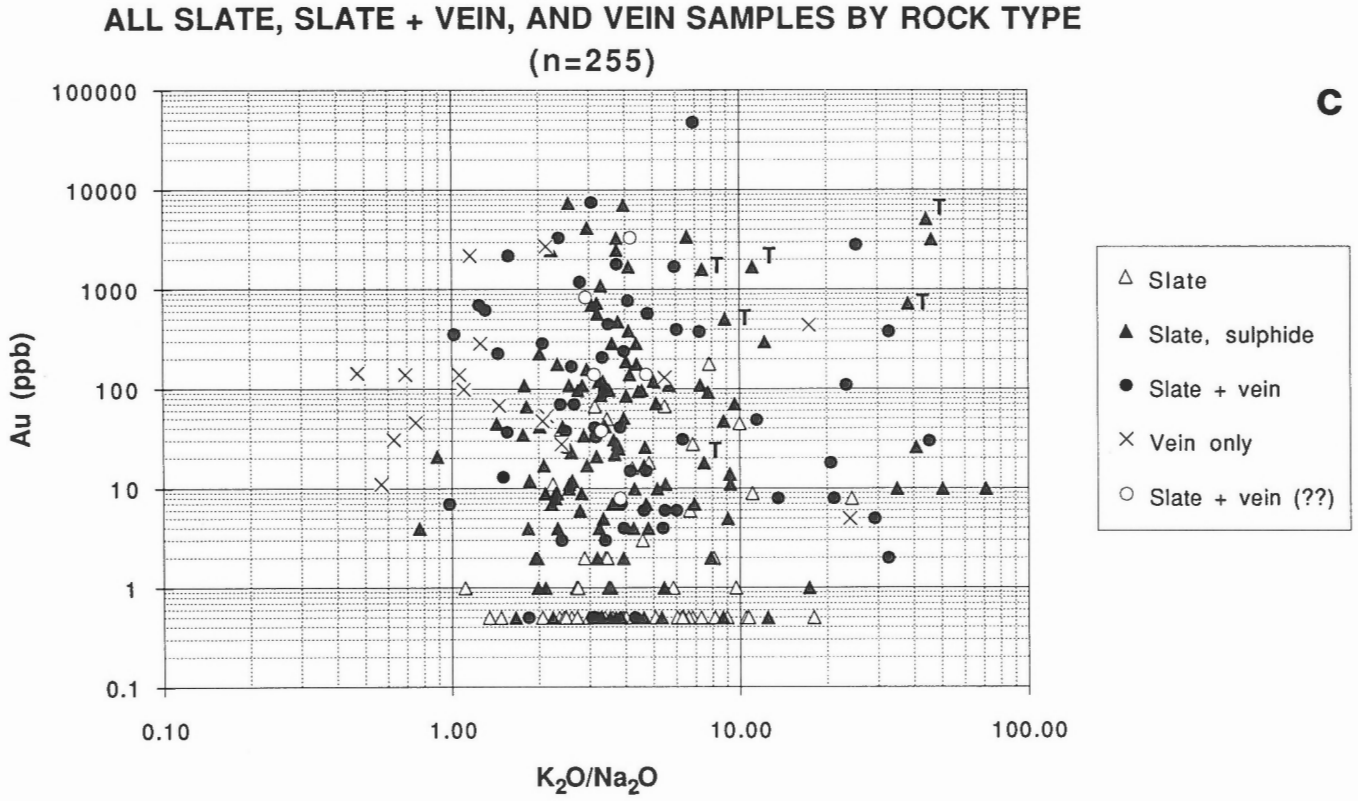
ALL SLATE, SLATE + VEIN, AND VEIN SAMPLES BY ROCK TYPE
(n=255)
c
100000
10000
1000
100
10
1
0.1
Au (ppb)
0.10
1.00
10.00
100.00
K2O/Na2O
Slate
Slate, sulphide
Slate + vein
Vein only
Slate + vein (??)

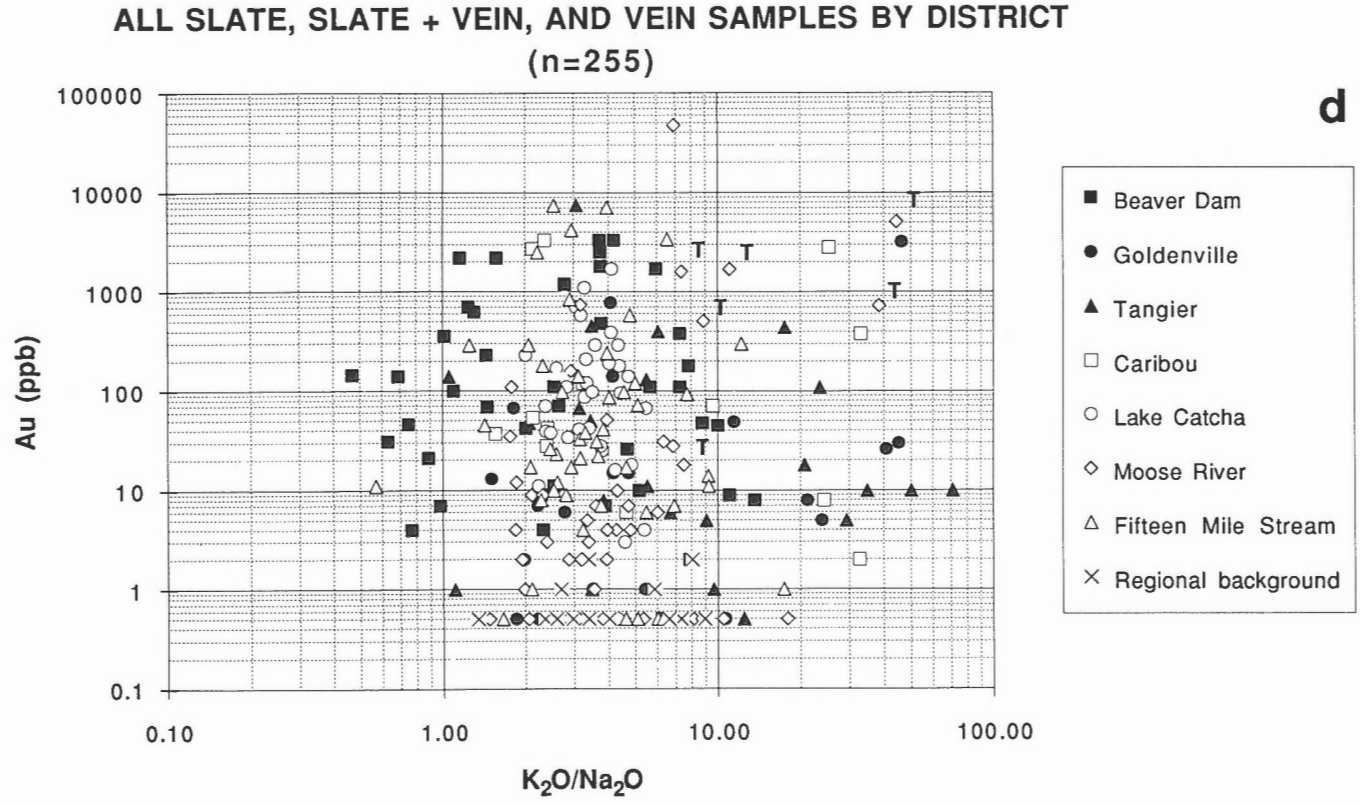
ALL SLATE, SLATE + VEIN, AND VEIN SAMPLES BY DISTRICT
(n=255)
d
100000
10000
1000
100
10
1
0.1
Au (ppb)
0.10
1.00
10.00
100.00
K2O/Na2O
Beaver Dam
Goldenville
Tangier
Caribou
Lake Catcha
Moose River
Fifteen Mile Stream
Regional background

Figure 6c, d

Table 8. Summary statistics for the SiO_2/Al_2O_3 ratio by district and rock type.

	WACKE	WACKE, VISIBLE S	SLATE	SLATE, VISIBLE S	WACKE + VEIN	SLATE + VEIN	VEIN ONLY	SUMMARY
REGIONAL BACKGROUND								
Average	6.93	.	3.04	.	.	.	.	5.73
Minimum	4.33	.	2.52	.	.	.	.	2.52
Maximum	10.36	.	4.28	.	.	.	.	10.36
Std dev	1.36	.	.48	.	.	.	.	2.15
Samples	38		17					55
BEAVER DAM								
Average	9.28	4.57	2.25	3.11	.	5.88	95.93	16.56
Minimum	5.96	2.24	1.52	1.44	.	2.22	15.83	1.44
Maximum	11.76	11.37	3.44	4.83	.	15.07	248.46	248.46
Std dev	2.79	3.09	.89	.71	.	4.07	81.17	41.37
Samples	5	7	4	17		14	7	54
CARIBOU								
Average	6.61	5.80	3.09	2.66	6.13	5.41	88.23	11.37
Minimum	4.72	4.50	3.09	2.01	2.86	3.26	35.15	2.01
Maximum	7.77	9.12	3.09	3.80	9.01	10.73	117.80	117.80
Std dev	1.20	1.35		.99	2.62	2.70	46.07	23.63
Samples	6	19	1	3	5	6	3	43
LAKE CATCHA								
Average	5.35	5.27	2.67	2.58	5.34	2.71	.	3.96
Minimum	2.68	2.84	2.48	2.05	3.97	2.50	.	2.05
Maximum	7.60	7.56	2.99	3.54	6.19	3.19	.	7.60
Std dev	1.76	1.68	.21	.31	1.20	.22	.	1.77
Samples	8	23	6	19	3	9		68
MOOSE RIVER								
Average	6.55	4.32	3.02	3.13	4.32	3.07	.	3.72
Minimum	5.15	2.56	2.03	2.20	4.32	2.59	.	2.03
Maximum	8.21	6.27	3.84	4.44	4.32	3.52	.	8.21
Std dev	.96	.84	.54	.58		.37	.	1.25
Samples	7	16	11	30	1	7		72
TANGIER								
Average	6.04	6.26	3.06	1.90	9.07	11.51	64.16	10.56
Minimum	4.77	3.40	2.45	1.41	6.31	1.55	13.59	1.41
Maximum	8.16	7.33	4.48	2.54	13.74	49.56	96.06	96.06
Std dev	1.29	1.33	.64	.53	3.06	18.00	35.55	18.77
Samples	6	17	8	6	6	7	4	54
FIFTEEN MILE STREAM								
Average	5.55	4.54	2.47	2.96	3.07	3.42	40.38	4.55
Minimum	4.17	3.19	2.21	2.15	3.07	2.37	14.03	2.15
Maximum	7.44	6.25	2.67	3.85	3.07	7.73	66.72	66.72
Std dev	1.69	.87	.24	.34		1.58	37.25	7.90
Samples	3	13	3	35	1	10	2	67
GOLDENVILLE								
Average	6.40	4.79	2.75	2.86	14.20	2.32	188.65	7.36
Minimum	4.89	2.05	2.43	1.45	14.20	1.47	188.65	1.45
Maximum	10.01	6.73	2.90	4.24	14.20	3.19	188.65	188.65
Std dev	1.06	1.35	.22	.78		.58		22.09
Samples	25	18	4	12	1	9	1	70
SUMMARY								
Average	6.65	5.17	2.89	2.89	7.21	4.78	86.01	7.51
Minimum	2.68	2.05	1.52	1.41	2.86	1.47	13.59	1.41
Maximum	11.76	11.37	4.48	4.83	14.20	49.56	248.46	248.46
Std dev	1.55	1.58	.54	.60	3.43	6.64	64.36	19.29
Samples	98	113	54	122	17	62	17	483

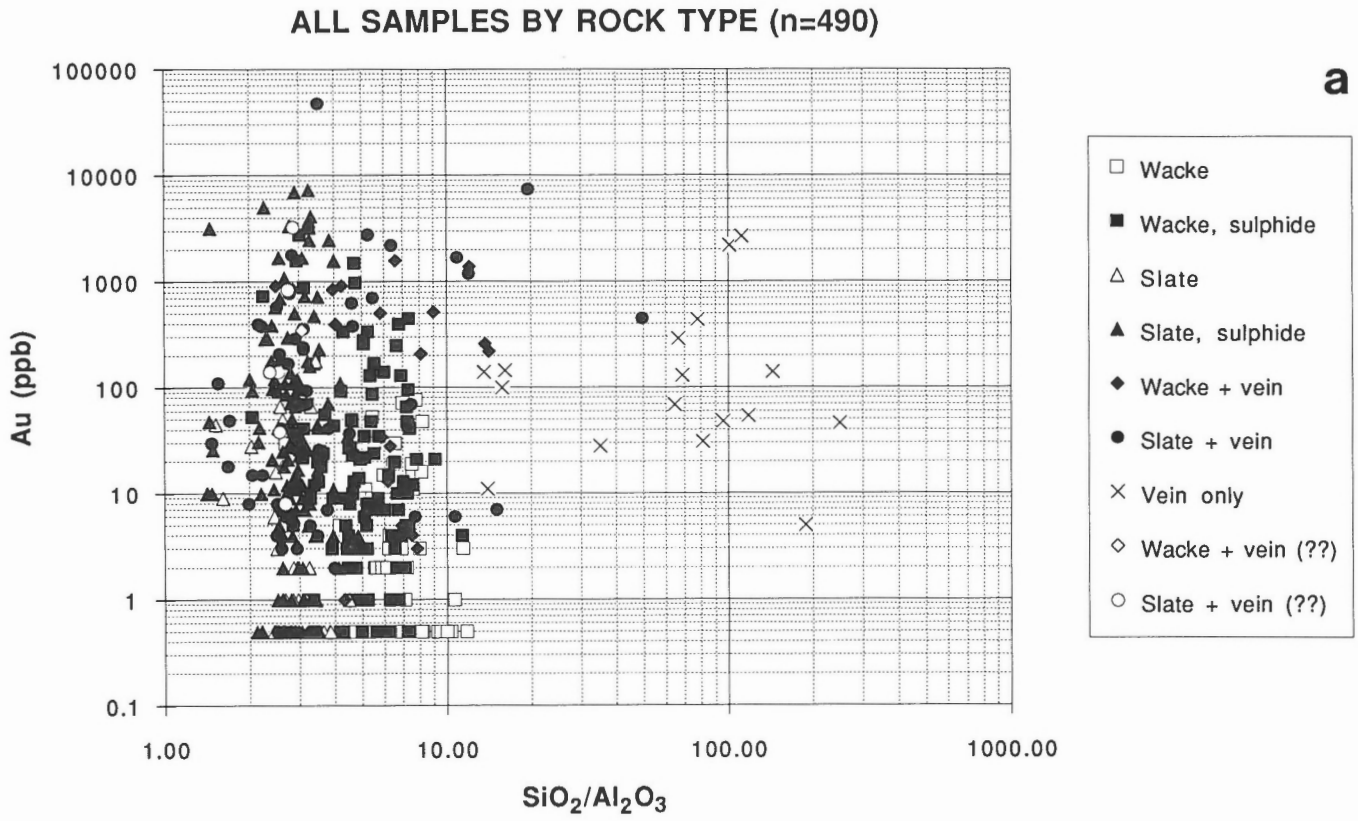

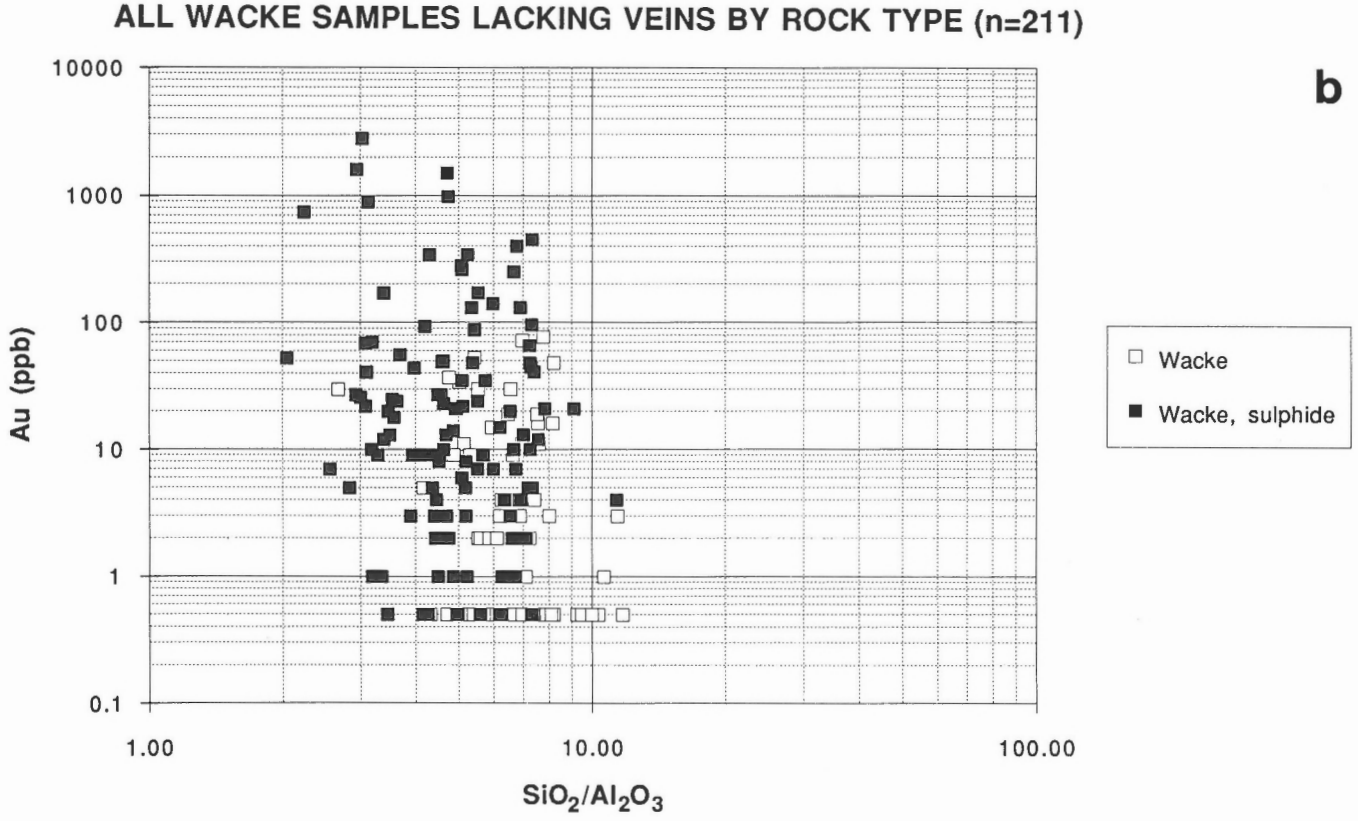

Figure 7. Scattergrams for gold versus SiO_2/Al_2O_3 ratio for a) all samples, wacke samples lacking veins by b) rock type and c) district, as well as for slate samples lacking veins by d) rock type and e) district. Slate + vein = slate containing small quartz veinlets.

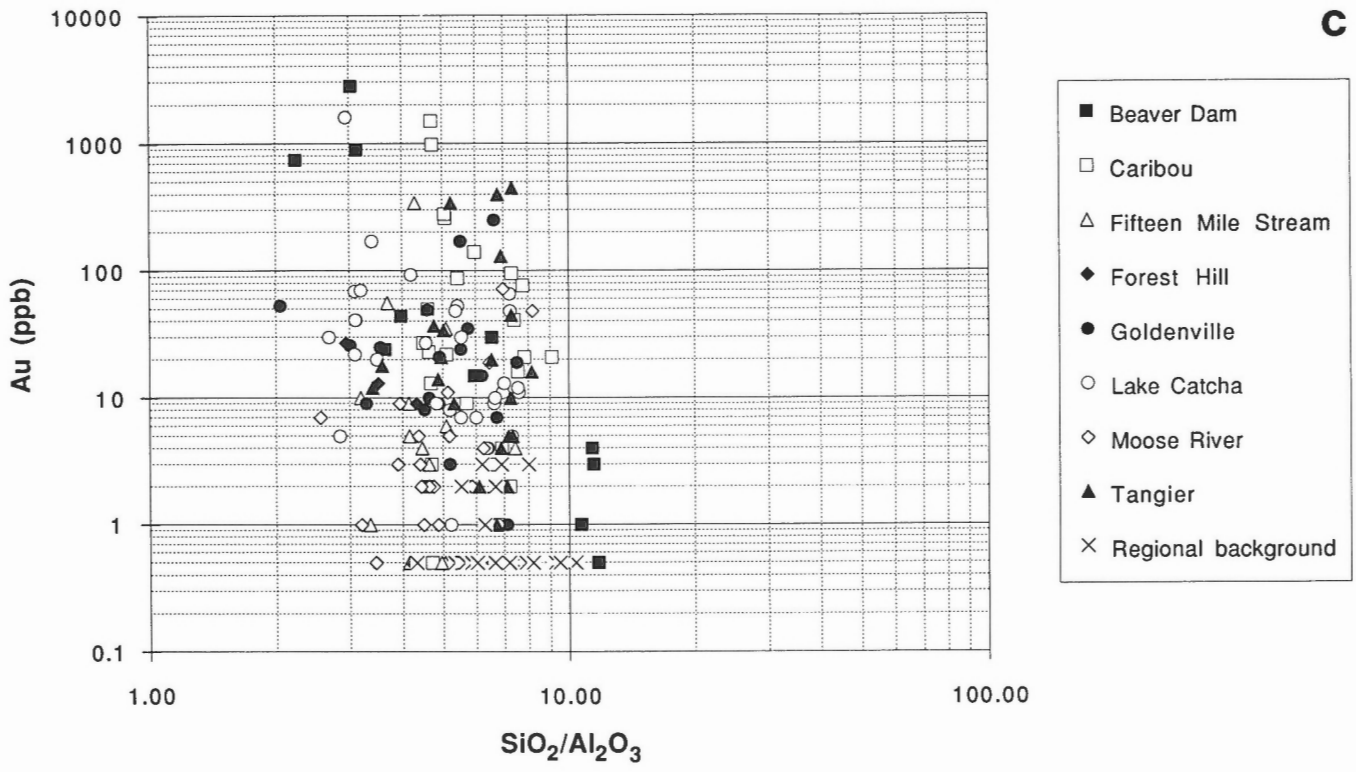
ALL WACKE SAMPLES LACKING VEINS BY DISTRICT (n=211)
c
10000
1000
100
10
1
0.1
Au (ppb)
1.00
10.00
100.00
SiO2/Al2O3
Beaver Dam
Caribou
Fifteen Mile Stream
Forest Hill
Goldenville
Lake Catcha
Moose River
Tangier
Regional background

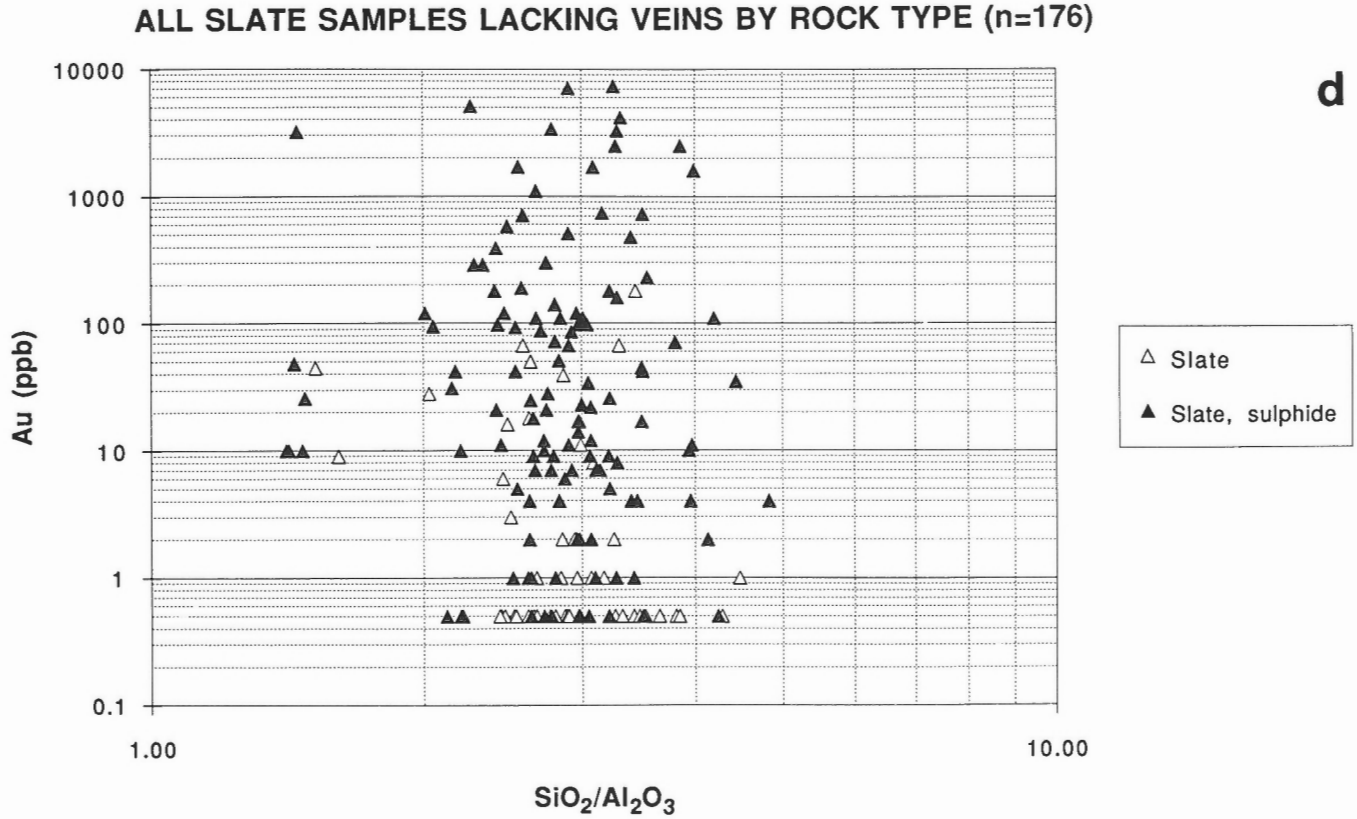
ALL SLATE SAMPLES LACKING VEINS BY ROCK TYPE (n=176)
d
10000
1000
100
10
1
0.1
Au (ppb)
1.00
10.00
SiO2/Al2O3
Slate
Slate, sulphide

Figure 7c, d

Correlation coefficients for gold contents versus SiO_2/Al_2O_3 ratios for a variety of sample populations are given in Tables 5 and 6. The SiO_2/Al_2O_3 ratios for three sample populations (all samples, wacke-lacking veins, and slate-lacking veins) are plotted against gold contents in Figure 7. Less than 5% of wacke samples from known gold occurrences possess SiO_2/Al_2O_3 ratios greater than 8.0; all such "anomalous" samples contain background contents of gold, sulphur, and arsenic, as well as K_2O/Na_2O ratios of less than 1.0. No slate samples contain SiO_2/Al_2O_3 ratios greater than 5.0. The scattergrams and correlation coefficients reveal a lack of significant positive correlation between gold contents and SiO_2/Al_2O_3 ratios in both wacke and slate across all districts. At Beaver Dam and Lake Catcha, there is a strong inverse relationship between gold and the SiO_2/Al_2O_3 ratio in wacke. However, it is possible to correlate the SiO_2/Al_2O_3 ratio directly with "bleaching" in wacke samples from Beaver Dam and Forest Hill (Fig. 8). In both these areas, the bleached samples contain the least gold. At Lake Catcha and Caribou there is no apparent correlation between bleaching and either the SiO_2/Al_2O_3 ratios or gold contents. The two bleached samples from Tangier contain relatively high SiO_2/Al_2O_3 ratios but were not enriched in gold. There is no apparent correlation between bleaching and the SiO_2/Al_2O_3 ratio in the Goldenville samples, but two of the bleached samples contain the highest gold contents for wacke from the occurrence.

Summary statistics for CO_2 are provided in Table 9. Scattergrams for gold against CO_2 are displayed in Figure 9. Correlation coefficients for gold contents versus CO_2 contents for a variety of sample populations are given in Tables 5 and 6. Although wacke and slate from gold occurrences contain at least an order of magnitude more CO_2 than the background populations, there is no significant correlation between CO_2 contents and gold contents in any of the rock types or occurrences. This is despite the existence of significant positive correlations for the three composite sample populations in which background samples were combined with occurrence samples (Table 6). It is noteworthy that the CO_2 contents of sulphide-rich wackes and slates are less than or similar to the CO_2 contents of sulphide-poor wackes and slates at Beaver Dam, Caribou, Lake Catcha, Tangier, and Goldenville.

Although the analytical method chosen for antimony and tungsten resulted in an incomplete data set for these elements, inspection of the available data indicates a strong positive correlation between antimony and arsenic. Gold versus antimony scattergrams plotted using the available data suggest that antimony could be a useful indicator for gold in both the sulphide-bearing and vein-bearing wacke populations. Tungsten, however, does not appear to correlate with gold, sulphur, or arsenic in any sample population.

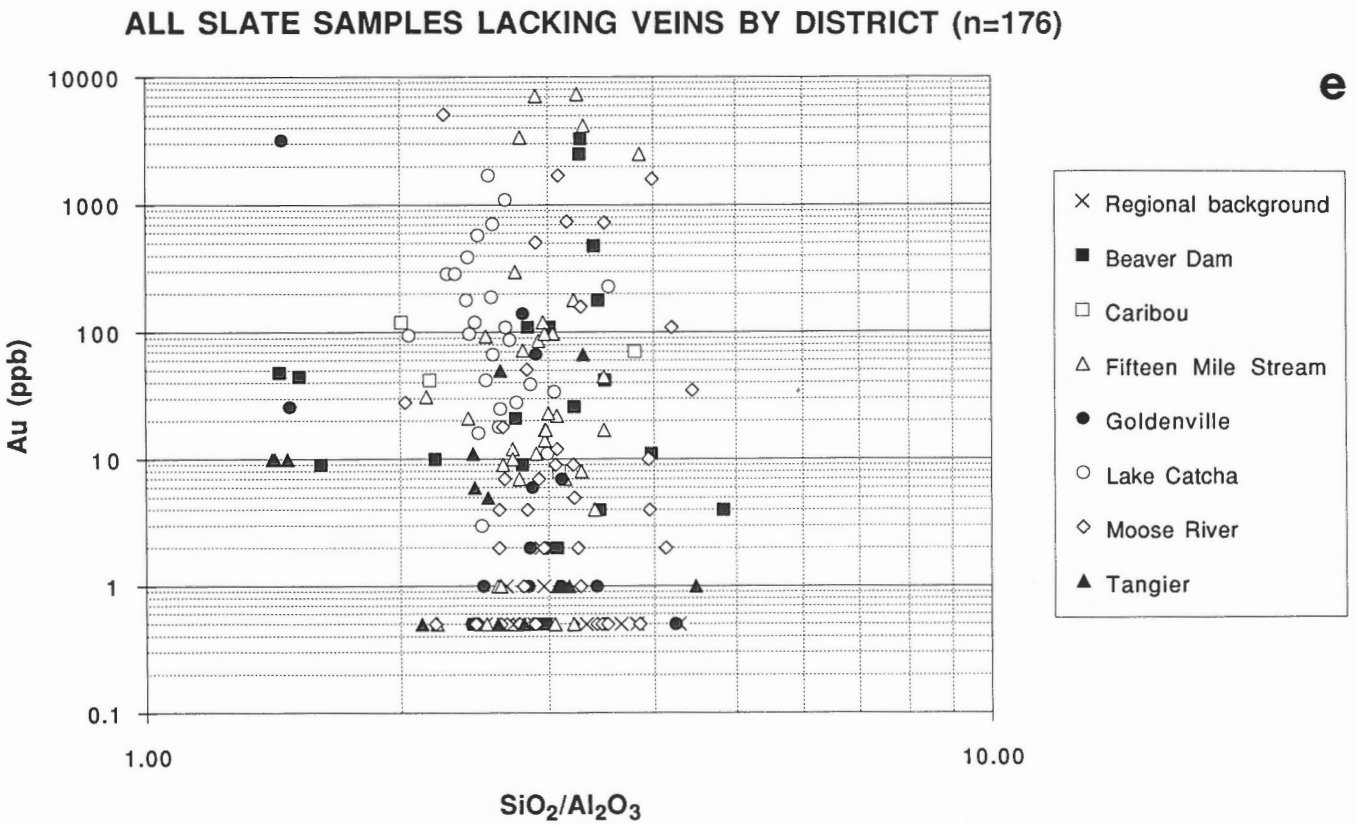

Figure 7e

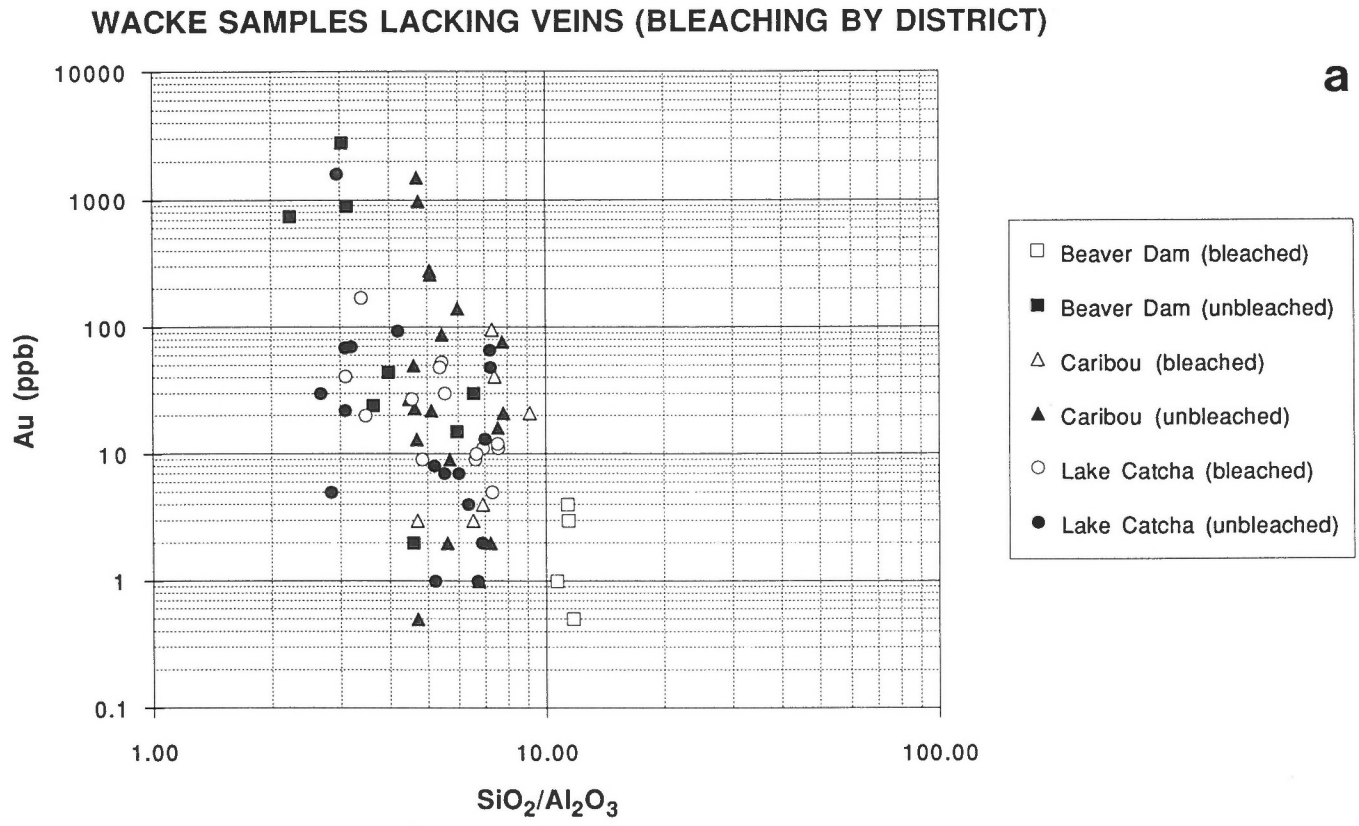

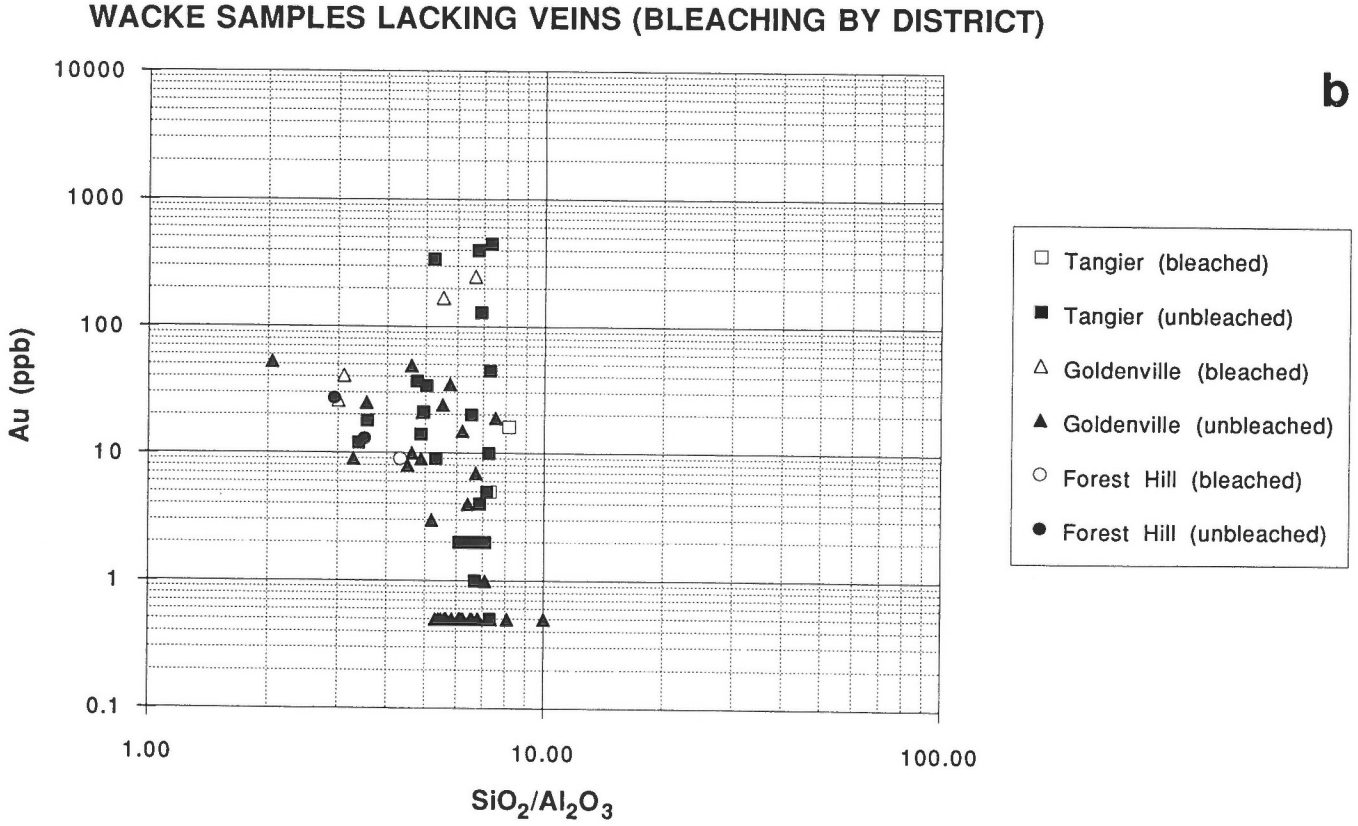

Figure 8. Scattergrams for gold versus SiO_2/Al_2O_3 ratio for a) bleached and unbleached wacke samples lacking veins from Beaver Dam, Caribou, and Lake Catcha, and b) bleached and unbleached wacke samples lacking veins from Tangier, Goldenville, and Forest Hill.

Table 9. Summary statistics for CO_2 (wt.%) by district and rock type.

	WACKE	WACKE, VISIBLE S	SLATE	SLATE, VISIBLE S	WACKE + VEIN	SLATE + VEIN	VEIN ONLY	SUMMARY
REGIONAL BACKGROUND								
Average	.049	.	.009	.	.	.	.	.037
Geometric mean	.012	.	.008	.	.	.	.	.010
Minimum	.005	.	.005	.	.	.	.	.005
Maximum	.390	.	.020	.	.	.	.	.390
Std dev	.103	.	.006	.	.	.	.	.088
Samples	38		17					55
BEAVER DAM								
Average	3.328	.541	.178	.209	.	.489	.517	.651
Geometric mean	.567	.313	.152	.105	.	.242	.252	.202
Minimum	.050	.050	.070	.005	.	.030	.010	.005
Maximum	14.270	1.370	.340	.760	.	2.180	1.930	14.270
Std dev	6.153	.536	.115	.226	.	.635	.643	1.954
Samples	5	7	4	17		14	7	54
CARIBOU								
Average	1.922	2.361	1.030	1.357	3.162	3.642	.367	2.331
Geometric mean	1.912	2.285	1.030	1.301	2.716	2.017	.351	1.857
Minimum	1.630	1.460	1.030	.860	1.320	.460	.260	.260
Maximum	2.180	3.250	1.030	1.720	5.550	7.590	.520	7.590
Std dev	.211	.592		.445	1.839	3.254	.136	1.576
Samples	6	19	1	3	5	6	3	43
LAKE CATCHA								
Average	2.013	2.213	1.995	1.702	3.537	2.318	.	2.099
Geometric mean	1.932	1.940	1.726	1.398	3.432	2.008	.	1.804
Minimum	.920	.300	.510	.520	2.860	1.010	.	.300
Maximum	2.640	5.090	2.980	4.920	4.810	5.420	.	5.420
Std dev	.533	1.048	.937	1.178	1.103	1.439	.	1.123
Samples	8	23	6	19	3	9		68
MOOSE RIVER								
Average	1.326	2.897	.463	1.361	2.150	2.757	.	1.708
Geometric mean	1.219	1.756	.302	.985	2.150	1.513	.	1.006
Minimum	.480	.510	.050	.100	2.150	.180	.	.050
Maximum	2.040	16.090	1.130	4.990	2.150	5.640	.	16.090
Std dev	.514	4.221	.412	1.074		2.524	.	2.357
Samples	7	16	11	30	1	7		72
TANGIER								
Average	1.867	1.693	1.448	1.042	.997	1.126	3.280	1.570
Geometric mean	1.767	1.439	1.274	.822	.903	.856	2.261	1.247
Minimum	.890	.230	.590	.240	.450	.290	.500	.230
Maximum	2.790	4.020	3.240	2.070	1.490	2.580	7.190	7.190
Std dev	.622	.902	.846	.715	.446	.861	2.820	1.145
Samples	6	17	8	6	6	7	4	54
FIFTEEN MILE STREAM								
Average	.373	1.236	.340	.347	.620	.516	2.170	.604
Geometric mean	.371	.747	.257	.227	.620	.298	2.169	.332
Minimum	.320	.200	.080	.030	.620	.070	2.090	.030
Maximum	.420	5.810	.570	1.840	.620	2.410	2.250	5.810
Std dev	.050	1.643	.246	.388		.691	.113	.911
Samples	3	13	3	35	1	10	2	67
GOLDENVILLE								
Average	.888	1.226	.135	.231	1.890	.277	.160	.744
Geometric mean	.850	.611	.085	.085	1.890	.158	.160	.367
Minimum	.350	.005	.020	.005	1.890	.020	.160	.005
Maximum	1.680	3.810	.280	.890	1.890	.700	.160	3.810
Std dev	.261	1.028	.122	.285		.235		.701
Samples	25	18	4	12	1	9	1	70
SUMMARY								
Average	.918	1.883	.594	.836	2.180	1.361	1.314	1.202
Geometric mean	.185	1.251	.804	.392	1.699	.558	.561	.433
Minimum	.005	.005	.005	.005	.450	.020	.010	.005
Maximum	14.270	16.090	3.240	4.990	5.550	7.590	7.190	16.090
Std dev	1.573	1.919	.834	.959	1.546	1.829	1.799	1.584
Samples	98	113	54	122	17	62	17	483

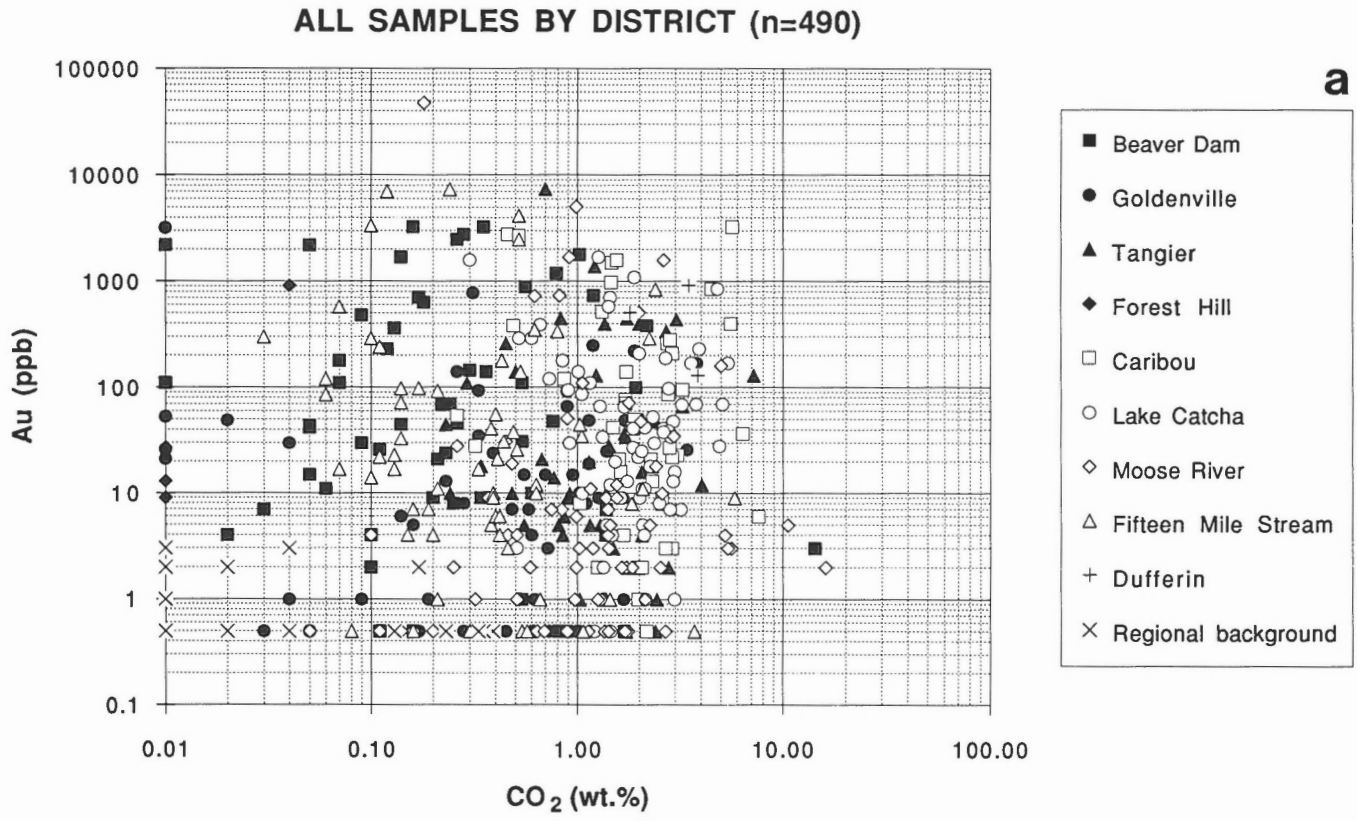

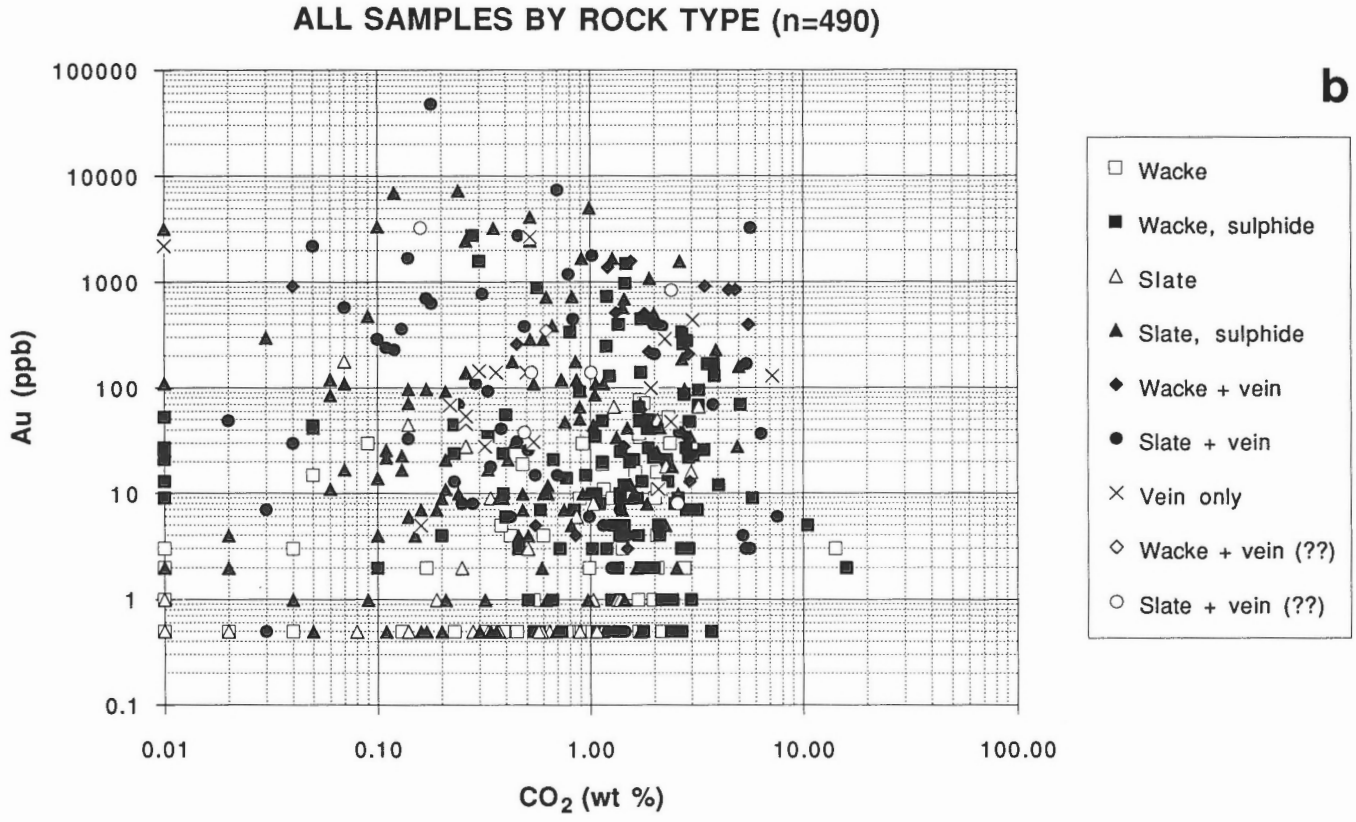

Figure 9. Scattergrams for gold versus CO_2 for a composite sample population (all 490 samples) in which the data have been plotted by a) district and by b) rock type. All data were log transformed prior to correlation analysis. Slate + vein = slate containing small quartz veinlets.

DISCUSSION

The estimates of regional background gold contents of wacke and slate obtained during this investigation (0.6 ppb for wacke and 0.7 ppb for slate) compare favourably with those reported by others for wacke and slate samples from unmineralized areas. Thorpe and Thomas (1976) determined that the best estimates of average gold contents in wacke and slate samples collected from core several hundreds of metres from nearest known mineralization in the Oldham area are 0.62 and 2.0 ppb, respectively. Crocket et al. (1983) concluded that the background gold contents of greywacke from the Ruth Falls syncline and slate from the Ecum Secum area (Liscomb Point and nearshore islands) are 1.19 and 1.39 ppb, respectively. Brooks et al. (1982) reported an average gold content of 1.0 ppb for a mixed population of samples that included both wackes and slates from the Sherbrooke area, as well as samples from the Wine Harbour gold district.

The gold contents that are significantly greater than regional background values for both wacke and slate from the seven principal gold districts chosen for this study are consistent with enhanced average gold contents of wacke and slate samples from other gold-rich areas. Boyle (1979, p. 244, 245) reported that each of five chip samples collected from wacke within one foot of a gold-rich vein in the Caribou gold mine contained 10 ppb gold, whereas a composite chip sample of wacke collected from one to fifty feet from the vein contained less gold. Calculation of arithmetic means for gold contents of wacke and slate samples from a trench at the Mount Uniacke occurrence (Thorpe and Thomas, 1976) indicate average contents of 24.8 and 59.3 ppb, respectively. At the Cochrane Hill occurrence, Smith et al. (1985, p. 59) reported average gold contents for wacke sample populations ranging from 700 to 3740 ppb, and average gold contents for slate sample populations ranging from 720 to 1320 ppb. For the Harrigan Cove occurrence, Crocket et al. (1986) reported average gold contents of 8.7 and 8.0 ppb for wacke and slate, respectively.

The estimates of regional background arsenic contents of wacke and slate obtained during this investigation (1.3 ppm for wacke and 1.9 ppm for slate) are also similar to those reported by others. Crocket et al. (1983) determined that the background arsenic contents of greywacke from the Ruth Falls syncline and slate from the Ecum Secum area are 2.30 and 2.12 ppm, respectively. The enhanced arsenic contents of both wacke and slate from the seven principal districts that were sampled in this study are consistent with the results obtained by Smith et al. (1985) for Cochrane Hill and by Crocket et al. (1986) for Harrigan Cove. At Harrigan Cove, the average arsenic contents for wacke and slate are 972 and 549 ppm, respectively; at Cochrane Hill, the average arsenic contents for wacke populations range from 6402 to 7477 ppm, and the average arsenic contents for slate sample populations range from 9188 to 10 176 ppm. Boyle (1979) reported arsenic contents ranging from 1250 to 1500 ppm in the five wacke samples adjacent to the gold-rich quartz vein at Caribou compared to a content of only 15 ppm in the composite wacke sample collected farther from the vein.

The limited scale of alteration in the gold districts as determined in this study is similar to that reported by Boyle (1979, 1986, 1992) for most turbidite-hosted gold-quartz vein deposits, but is markedly different from that described by some others. Smith and Kontak (1986), Kontak and Smith (1987a, b), and Kontak et al. (1989) have reported extremely large-scale (kilometre-scale) alteration zones in Meguma gold occurrences that are comparable in scale to those observed in other hydrothermal systems, including epithermal and porphyry Cu-Mo deposits. They also recognized several widespread alteration types, including silicification, carbonatization, tourmalinization, sulphidization, and phyllic alteration. Of these, silicification of greywacke was reported as the most pervasive and prevalent of the alteration types associated with gold districts. Data provided by Kontak and Smith (1987b; Cochrane Hill sample PQ142) and Kontak et al. (1991; Beaver Dam sample 116.1) indicate that silicified wacke samples contain 80.0 to 89.4 wt.% SiO_2 with corresponding SiO_2/Al_2O_3 ratios of 9.0 and 18.8. Examination of Table 8 and the scattergrams of Figure 7 indicates, with respect to wacke samples collected from gold occurrences during this study, that only 4 of the 60 samples (6.7%) lacking visible sulphide minerals, and only 1 of the 117 samples (0.85%) containing visible sulphide minerals have SiO_2/Al_2O_3 ratios of 10.0 or greater. None of these wacke samples have SiO_2/Al_2O_3 ratios greater than 11.76. Kontak and Smith (1987b) reported that strongly altered wacke of the Cochrane Hill area exhibits not only marked enrichment in silica, but also strong depletion of alumina. However, examination of their data suggests that the apparent strong depletion of alumina may reflect increased silica content rather than actual loss of alumina. This interpretation is consistent with the results of this study which indicate that significant amounts of alumina were typically neither lost nor gained during alteration. Kontak and Smith (1987b) and Kontak et al. (1991) also reported that the presence of bleaching in wacke reflects silicification. However, as noted in the previous section of this paper, the distribution of data points in Figure 8 indicates that bleached wacke samples collected during this investigation do not have consistently high SiO_2/Al_2O_3 ratios.

Smith and Kontak (1986), Kontak and Smith (1987a, b), Kontak et al. (1989), and Kontak et al. (1990) suggested that there is a direct relationship between alteration intensity and gold mineralization. As noted in the previous section of this paper, evaluation of the results presented in Figures 7, 8, and 9 and Tables 5, 6, 8, and 9 indicates that gold contents in wacke and slate cannot be directly correlated with increased SiO_2/Al_2O_3 ratios (possible silicification), enhanced contents of CO_2 (possible carbonatization), or bleaching. Although relatively great K_2O/Na_2O ratios may be potentially useful indicators of gold-related hydrothermal alteration (sericitization) in wacke, and possibly in slate, this alteration may not correspond to the phyllic alteration type identified by Kontak and Smith (1987b) and Kontak et al. (1990, 1991). Figure 1 of Kontak et al. (1991) provides analytical data for a wacke (Beaver Dam 116.2) that has undergone intense phyllic alteration. The K_2O/Na_2O ratio of this sample is only 0.83, a value which is not greatly different from the average K_2O/Na_2O ratio of

the regional background wacke sample population (0.70) and possibly not indicative of intense sericitization. Sericite-rich wacke samples that were collected during this investigation typically have K_2O/Na_2O ratios greater than 2.0. The relatively great CaO and LOI contents reported for Beaver Dam 116.2 suggest that the alteration may have included carbonatization as well as sericitization.

The close spatial association between late quartz veins and arsenic distribution that was observed in this study was also recognized by Haynes (1987). He reported a lack of arsenopyrite adjacent to stratiform (early bedding-parallel) veins, but noted arsenopyrite haloes adjacent to relatively late semi-concordant veins, step veins, and side veins. The apparent lack of a clear association between sericite and early bedding-parallel veins that was recognized during this investigation is also consistent with work by Haynes (1987). He concluded that sericite was absent adjacent to early bedding-parallel veins, but characteristically associated with later semi-concordant veins, step veins, side veins, and postfolding veins. With respect to the direct correlation between gold contents and high K_2O/Na_2O ratios in host rocks to gold-bearing veins that was determined in this study, Boyle (1986) also reported that K_2O/Na_2O ratios in wall rocks immediately adjacent to gold-bearing veins in turbidite-hosted deposits are commonly greater than the ratios in samples relatively distant from gold-bearing veins.

GENETIC MODEL

As noted in earlier publications (Kerswill, 1987, 1988), a predictive genetic model for Meguma gold deposits must account for the occurrence of much of the gold in early bedding-parallel (BP) crack-seal veins. A successful working hypothesis should also explain the apparently strong structural control on ore shoot distribution, as well as the presence of significant gold in late fissure veins. A multistage model that permits vein-controlled deposition of variable amounts of $SiO_2 \pm S \pm Au \pm As \pm Sb \pm CO_2 \pm Cu \pm Pb \pm Zn \pm W$ from a succession of possibly very different hydrothermal fluids that were generated at various stages during the sedimentary, structural, and metamorphic evolution of the Meguma Terrane seems most appropriate. The sediments were the most likely source of the vein components, but transport distances from source to site of deposition may have been at the kilometre scale. Early hydrothermal fluids were most probably generated by a combination of basinal fluid release during burial, diagenesis, pressure solution, and prograde metamorphic dehydration reactions of the greenschist facies. Fluids evolved during higher grade metamorphism associated with intrusion of the Devonian granitoid rocks may have contributed to the later veins. Such fluids probably had a magmatic component. Remobilization of gold from early bedding-parallel veins into later veins may have occurred, but was probably not sufficient to account for the varied styles of gold distribution.

The model presented herein is similar to that proposed by a variety of workers, including Graves and Zentilli (1982), Henderson and Henderson (1986), and Sangster (1990, 1992), but is markedly different from the late shear zone model proposed by Kontak and Smith (1987a, b, 1988) and Kontak et al. (1990). The reader is referred to Henderson et al. (1991) and Sangster (1991) for detailed comments on the paper by Kontak et al. (1990). No evidence was found during this study to support the syngenetic model of Haynes (1987) in which the gold-rich bedding-parallel veins were interpreted as siliceous sinters exhaled directly onto the seafloor.

The differences in the distributions of gold, sulphur, and arsenic from district to district and from rock type to rock type that have been documented in this study can be related, at least in part, to different histories of vein formation. Not all stages of veins (early bedding-parallel, en échelon, true saddle reef, late discordant) occur in all districts; different stages are not equally developed. Although much gold may have been deposited during formation of the early bedding-parallel veins, abundant arsenic appears to have been introduced by later veins or structures. This could help explain the lack of correlation between gold and arsenic in those districts where most of the gold occurs in early bedding-parallel veins. The relatively strong positive correlation between gold and sulphur in most districts, combined with the ubiquitous presence of bedding-parallel veins, suggests that gold distribution was largely controlled by sulphur-bearing bedding-parallel veins. The lack of a strong relationship between gold and sulphur in some districts may be related to the presence of mixed sulphur populations ("synsedimentary" sulphur deposited prior to vein formation and "hydrothermal" sulphur introduced or remobilized during vein formation).

CONCLUSIONS

Although the best geochemical indicator of gold potential is clearly gold itself, sulphur and arsenic appear to be useful guides for gold. This reflects the common association between gold, pyrrhotite, and arsenopyrite that was noted during field work and sample preparation. Ranges and average contents of gold, sulphur, and arsenic, as well as interrelationships among the three elements, are variable in different rock types and from district to district. Sulphur is more reliable than arsenic in some districts. This is at least partly because much of the gold occurs in iron-sulphide-bearing early bedding-parallel quartz veins and their adjacent iron-sulphide-rich host rocks, whereas much of the arsenic occurs adjacent to later veins that commonly contain less gold.

The average gold, sulphur, arsenic, and CO_2 contents of wacke and slate samples collected from all seven gold districts are significantly greater than the average gold, sulphur, arsenic, and CO_2 contents of samples collected in areas distant from known mineralization. Many of the sulphide-bearing wacke and slate samples from gold districts contain greater than 100 ppb gold. None of the wacke and slate samples from unmineralized areas contain greater than 3 ppb gold.

Gold cannot be directly linked to either increased SiO_2/Al_2O_3 ratios (possible silicification) or CO_2 contents (possible carbonatization) in the host rocks to gold-bearing veins, but can be correlated with increased K_2O/Na_2O

ratios (sericitization) in wacke from five districts and in slate from two districts. K_2O/Na_2O ratios greater than 1.0 and 6.0 are considered anomalous for wacke and slate, respectively. Large-scale silicification was neither recognized during sample collection nor revealed by geochemical analyses. Bleached wacke samples are not consistently enriched in silica relative to alumina.

Work to date confirms that several of the different stages of vein formation had the potential to deposit gold, and also suggests that each of the different stages may have produced a diagnostic geochemical and mineralogical signature in the host rock. Additional work is required to better document the latter possibility and to more clearly identify those chemical and mineralogical changes that are most closely linked to deposition of potentially mineable gold concentrations.

ACKNOWLEDGMENTS

Many individuals and companies in the exploration and geoscience communities have contributed to this project. The writer would like to thank Seabright Resources Inc., Coxheath Gold Holdings Limited, and MPH Consulting Ltd. for access to properties and permission to sample drill core and underground workings. Special thanks go to Paul Beliveau, Bob Chataway, Mike Cullen, Dave Duncan, Dennis Forgeron, Bruce Hudgins, Alistair MacIntyre, Don Pollock, Al Sexton, Derek Thomas, and Peter Webster for their support, encouragement, and exchange of information and ideas. Al Sangster, Jack Henderson, and Mariette Henderson of the Geological Survey of Canada provided useful guidance and insight throughout the course of this project, not only in the field but also in the office. The author also benefitted from discussions with Paul Smith, Dan Kontak, and John McMullen of the Nova Scotia Department of Mines and Energy, Charlotte Hy and Paul Williams of the University of New Brunswick, Tom Wright of the National Science Foundation, Marcos Zentilli of Dalhousie University, and Milton Graves of Cuesta Research Ltd. Ralph Thorpe and Al Sangster provided many constructive comments that greatly improved this manuscript.

REFERENCES

Boyle, R.W.
1979: The geochemistry of gold and its deposits; Geological Survey of Canada, Bulletin 280, 584 p.
1986: Gold deposits in turbidite sequences: their geology, geochemistry and history of theories of their origin; in Turbidite-hosted gold deposits, (ed.) J.D. Keppie, R.W. Boyle, and S.J. Haynes; Geological Association of Canada, Special Paper 32, p. 1-14.
1992: Auriferous Archean greenstone-sedimentary belts; in Historical perspectives of genetic concepts and case histories of famous discoveries, (ed.) R.W. Hutchinson and R.I. Graugh; Economic Geology Monograph 8, p. 164-191.

Brooks, R.R., Chatterjee, A.K., Smith, P.K., Ryan, D.E., and Zhang, H.F.
1982: The distribution of gold in rocks and minerals of the Meguma Group of Nova Scotia, Canada; Chemical Geology, v. 35, p. 87-95.

Crocket, J.H., Clifford, P.M., Fueten, F., and Kabir, A.
1983: Distribution and localization of gold in Meguma Group rocks, Nova Scotia. Part 2: Implications of background geochemistry and cleavage development – a preliminary report; in Current Research, Part B; Geological Survey of Canada, Paper 83-1B, p. 285-290.

Crocket, J.H., Fueten, F., Kabir, A., and Clifford, P.M.
1986: Distribution and localization of gold in Meguma Group rocks, Nova Scotia: Implications of metal distribution patterns in quartz veins and host rocks on mineralization processes at Harrigan Cove, Halifax County; Maritime Sediments and Atlantic Geology, v. 22, no. 1, p. 15-33.

Fueten, F., Clifford, P.M., Pryer, L.L., Thompson, M.J., and Crocket, J.H.
1986: Formation of spaced cleavage and concurrent mass removal of SiO_2, Meguma Group metagreywackes, Goldenville, Nova Scotia; Maritime Sediments and Atlantic Geology, v. 22, p. 35-50.

Graves, M.C. and Zentilli, M.
1982: A review of the geology of gold in Nova Scotia; in Geology of Canadian Gold Deposits, (ed.) R.W. Hodder and W. Petruk; Canadian Institute of Mining and Metallurgy, Special Volume 24, p. 233-242.
1986: Geochemical characterization of the Goldenville-Halifax transition of the Meguma Group of Nova Scotia: Progress Report; Nova Scotia Department of Mines and Energy, Program and Summaries, Tenth Annual Open House and Review of Activities, Information Series No. 12, p. 170.

Haynes, S.J.
1987: Classification of quartz veins in turbidite-hosted gold deposits, greenschist facies, eastern Nova Scotia; Canadian Institute of Mining and Metallurgy, Bulletin, v. 80, no. 898, p. 37-51.

Henderson, J.R.
1983: Harrigan Cove Mine; in Gold Deposits in the Meguma Terrane of Nova Scotia; Canadian Institute of Mining and Metallurgy, Geology Division Excursion Guidebook, p. 28-30.

Henderson, J.R. and Henderson, M.N.
1987: Meguma gold deposits; nested saddle reefs or early hydraulic extension fractures?; in Mines and Minerals Branch Report of Activities 1987, Part A, Nova Scotia Department of Mines and Energy, Report 87-5, p. 213-215.
1990: Crack-seal texture in bedding-parallel, gold-bearing, columnar-quartz veins; evidence of fossil water sills; in Mineral Deposit Studies in Nova Scotia, Volume 1, (ed.) A.L. Sangster; Geological Survey of Canada, Paper 90-8, p. 163-168.

Henderson, J.R., Henderson, M.N., Kerswill, J.A., Wright, T.O., and Zentilli, M.
1991: Comment and reply on "Integrated model for Meguma Group lode gold deposits, Nova Scotia, Canada"; Geology, v. 19, no. 5, p. 534-536.

Henderson, M.N. and Henderson, J.R.
1986: Constraints on the origin of gold in the Meguma Zone, Ecum Secum area, Nova Scotia; in Contributions to the Geology of the Meguma Terrane, Nova Scotia, Maritime Sediments and Atlantic Geology, v. 22, no. 1, p. 1-13.

Hy, C. and Williams, P.F.
1986: Meguma quartz veins, Tangier area; Nova Scotia Department of Mines and Energy, Program and Summaries, Tenth Annual Open House and Review of Activities, Information Series No. 12, p. 202-204.

Keppie, J.D. (comp.)
1979: Geological map of Nova Scotia; Nova Scotia Department of Mines and Energy, scale 1:500 000.

Kerswill, J.A.
1987: Mineralogy and chemistry of metawackes and slates as a guide to gold in the Eastern Meguma Terrane of Nova Scotia: a progress report; in Mines and Minerals Branch Report of Activities 1987, Part A, Nova Scotia Department of Mines and Energy, Report 87-5, p. 209-212.

1988: Lithogeochemical indicators of gold potential in the eastern Meguma terrane of Nova Scotia: second progress report; in Mines and Minerals Branch Report of Activities 1988, Part A, (ed.) D.R. MacDonald, and Y. Brown; Nova Scotia Department of Mines and Energy, Report 88-3, p. 215-217.

Kontak, D.J. and Smith, P.K.

1987a: Meguma gold: the best kept secret in the Canadian mining industry; Prospectors and Developers Association of Canada, Annual Meeting, March 1987, 14 p.

1987b: Alteration haloes and their implications for gold mineralization in the Meguma Zone, Nova Scotia; in Report of Activities 1987, Nova Scotia Department of Mines and Energy, Report 87-1, p. 65-74.

1988: Meguma gold studies VI; integrated model for the genesis of Meguma-hosted lode gold deposits; in Mines and Minerals Branch, Report of Activities 1987, Part B, Nova Scotia Department of Mines and Energy, Report 88-1, p. 111-119.

Kontak, D.J., Smith, P.K., Chatterjee, A.K., and Giles, P.S.

1989: Meguma gold studies: an integrated model for the genesis of Meguma-hosted lode gold deposits; paper presented at the Prospectors and Developers association of Canada, Annual Meeting, Toronto, Ontario, March 1989, 8 p.

Kontak, D.J., Smith, P.K., Kerrich, R., and Williams, P.F.

1990: Integrated model for Meguma Group lode gold deposits, Nova Scotia, Canada; Geology, v. 18, p. 238-242.

1991: Reply, Comment and Reply on ''Integrated model for Meguma Group lode gold deposits, Nova Scotia, Canada''; Geology, v. 19, no. 5, p. 534-536.

Malcolm, W.

1929: Gold fields of Nova Scotia; Geological Survey of Canada, Memoir 156, 253 p.

1976: Gold fields of Nova Scotia; Geological Survey of Canada, Memoir 385 (reprint of Memoir 156 without plates or maps), 253 p.

Mawer, C.K.

1986: The bedding-concordant gold-quartz veins of the Meguma Group, Nova Scotia; in Turbidite-hosted gold deposits, (ed.) J.D. Keppie, R.W. Boyle, and S.J. Haynes; Geological Association of Canada, Special Paper 32, p. 135-148.

Sangster, A.L.

1987: Sulphur isotope studies, Meguma terrane, Nova Scotia: A preliminary report; in Report of Activities 1987, Part A, Nova Scotia Department of Mines and Energy, Report 87-5, p. 207-208.

1990: Metallogeny of the Meguma Terrane, Nova Scotia; in Mineral Deposit Studies in Nova Scotia, Volume 1, (ed.) A.L. Sangster; Geological Survey of Canada, Paper 90-8, p. 115-162.

1991: Comment and reply on "Integrated model for Meguma Group lode gold deposits, Nova Scotia, Canada"; Geology, v. 19, no. 7, p. 764-766.

1992: Light stable isotope evidence for a metamorphogenic origin for bedding-parallel, gold-bearing veins in Cambrian flysch, Meguma Group, Nova Scotia; Exploration and Mining Geology, v. 1, p. 69-79.

Smith, P.K.

1985: Meguma gold project; Nova Scotia Department of Mines and Energy, Program and Summaries, Ninth Annual Open House and Review of Activities, Information Series No. 9, p. 51-52.

Smith, P.K. and Kontak, D.J.

1986: Meguma Gold Studies: advances in geological insight as an aid to gold exploration; Tenth Annual Open House and Review of Activities, Program and Summaries, Nova Scotia Department of Mines and Energy, Information Series No. 12, p. 105-113.

1988: Meguma gold studies II: vein morphology, classification and information, a new interpretation of "crack-seal" quartz veins; in Mines and Minerals Branch, Report of Activities 1987, Part B, Nova Scotia Department of Mines and Energy, Report 88-1, p. 61-76.

Smith, P.K., Haynes, S.J., and Reilly, B.A.

1985: Turbidite hosted gold deposits, Meguma Domain, eastern Nova Scotia; Geological Association of Canada-Mineralogical Association of Canada Joint Annual Meeting, Fredericton, New Brunswick, Excursion 11, 67 p.

Thorpe, R.I. and Thomas, G.M.

1976: Gold content of greywacke and slate of the Goldenville Formation, Nova Scotia, as determined by neutron activation analysis; in Report of Activities, Part A, Geological Survey of Canada, Paper 76-1A, p. 319-326.

Williams, P.F. and Hy, C.

1990: Origin and deformational and metamorphic history of gold-bearing quartz veins on the Eastern Shore of Nova Scotia; in Mineral Deposit Studies in Nova Scotia, Volume 1, (ed.) A.L. Sangster; Geological Survey of Canada, Paper 90-8, p. 169-194.

The Jubilee Zn-Pb deposit, Nova Scotia: the role of synsedimentary faults[1]

F.J. Hein[2], M.C. Graves[3], and A. Ruffman[4]

Hein, F.J., Graves, M.C., and Ruffman, A., 1993: The Jubilee Zn-Pb deposit, Nova Scotia: the role of synsedimentary faults; in Mineral Deposit Studies in Nova Scotia, Volume 2, (ed.) A.L. Sangster; Geological Survey of Canada, Paper 91-9, p. 49-69.

Abstract

The Jubilee Zn-Pb deposit is hosted by brecciated Carboniferous limestone of the Windsor Group where the contact with underlying Horton Group conglomerates is offset by synsedimentary faults. Reserves of the Jubilee deposit are estimated at 900 000 metric tonnes of 5.2% Zn and 1.4% Pb over thicknesses of 7.6 to 9.4 m in three zones along the downthrown (northeast) side of the Jubilee Fault.

The order of hydrothermal mineral deposition is pyrite, sphalerite, galena, barite/anhydrite. Calcite is mostly of postsulphide age. Only traces of silver and copper occur. Sulphide textures include both fine grained, disseminated (as replacement of limestone clasts) and coarser grained open-space filling. Fluid salinities were low; depositional temperatures were low; the deposit is stratabound; and alteration is absent.

Hydrocarbon fluid and bitumen solid inclusions are ubiquitous throughout the porous limestone, and occur within sphalerite and barite. Hydrocarbon-aided reduction of dissolved sulphate occurred before mineralized fluid migration and sulphide sulphur was preserved for subsequent mineralization in the subevaporite trap as H_2S gas or H_2S dissolved in hydrocarbon.

Synsedimentary faults influenced the evolution of the Jubilee deposit: (1) by controlling the distribution of footwall clastic sediments; (2) by venting fluids which localized thicker accumulations of carbonate; (3) by controlling the geometry of limestone brecciation through sulphate dissolution, liquid hydrocarbon migration after brecciation, and deposition of sulphides.

The synsedimentary fault setting on thick Horton Group clastics during basal Windsor carbonate sedimentation opens much more of the Horton/Windsor surface for potential mineral exploration.

[1] Contribution to the Canada-Nova Scotia Mineral Development Agreement, 1984-1989. Project carried by the Mineral Resources Division, Geological Survey of Canada, Project 860008.

[2] Dept. of Geology and Geophysics, University of Calgary, Calgary, Alberta. T2N 1N4

[3] Cuesta Research Ltd., 154 Victoria Rd., Dartmouth, Nova Scotia. B3A 1V8

[4] Geomarine Associates Ltd., 5112 Prince Street, 3rd floor, P.O. Box 41, Station M, Halifax, Nova Scotia. B3J 2L4

Résumé

Le gisement de Zn-Pb de Jubilee est contenu dans le calcaire bréchique d'âge carbonifère du Groupe de Windsor où le contact avec les conglomérats sous-jacents du Groupe de Horton est déplacé par des failles synsédimentaires. Les réserves du gisement de Jubilee sont estimées à 900 000 tonnes métriques de minerai à 5,2 % de Zn et 1,4 % de Pb sur une épaisseur de 7,6 à 9,4 m dans trois zones qui suivent le compartiment affaissé (nord-est) de la faille de Jubilee.

Les minéraux du gisement hydrothermal ont été mis en place selon l'ordre suivant: pyrite, sphalérite, galène, barytine/anhydrite. La calcite s'est en majorité formée après les sulfures. L'argent et le cuivre n'apparaissent qu'à l'état de traces. Les textures des sulfures comprennent à la fois des minéraux de granulométrie fine, disséminés (remplaçant des clastes de calcaire) et des matériaux plus grossiers comblant les cavités. La salinité des fluides était faible, et les températures de sédimentation basses, le gîte est de type stratiforme et il n'y a pas d'altération.

Des inclusions liquides d'hydrocarbures et des inclusions solides de bitume sont partout présentes dans le calcaire poreux, et se manifestent dans la sphalérite et la barytine. La réduction des sulfates dissous, favorisée par les hydrocarbures, a eu lieu avant la migration des fluides minéralisants, et le soufre que contenaient les sulfures a subsisté dans le piège sous-jacent aux évaporites sous forme de H_2S gazeux ou de H_2S dissous dans les hydrocarbures, avant de contribuer aux minéralisations.

Les failles synsédimentaires ont influencé l'évolution du gisement de Jubilee: (1) en contrôlant la distribution des sédiments clastiques au mur des failles; (2) en laissant s'échapper des fluides qui ont formé des accumulations localisées, plus épaisses, de carbonates; (3) en contrôlant la géométrie de la bréchification des calcaires par dissolution des sulfates, migration des hydrocarbures liquides après la bréchification, et mise en place des sulfures. Des failles synsédimentaires ayant traversé les épaisses roches clastiques du Groupe de Horton pendant la sédimentation carbonatée de la partie inférieure du Groupe de Windsor, une bien plus grande partie de la surface des groupes de Horton et de Windsor se prête à la prospection minérale.

INTRODUCTION

The Jubilee Zn-Pb deposit (latitude 45°59′N, longitude 60°57′ W; Fig. 1) occurs near Little Narrows, on the Iona Peninsula, Cape Breton Island. In the area of the Jubilee deposit, Lower Carboniferous (Tournaisian and Visean) rocks unconformably overlie Devonian intrusive rocks (Bell, 1929) that form the resistant rocks that underlie the upland terrain to the northwest of the study area (Kelley, 1967; Stewart, 1978). The Tournaisian rocks consist of the Horton Group, comprised mainly of continental sandstones, siltstones, and conglomerates, and the overlying Visean Windsor Group, consisting predominantly of marine limestone and evaporite (Bell, 1944; Geldsetzer, 1977; Isenor et al., 1980). A review of the stratigraphy and regional correlations is given in Hamblin (1989b) and Hein et al. (1988). Hamblin's (1988, 1989a, b) recent study of the sedimentology, tectonic control, and resource potential of the Horton Group on Cape Breton Island focused on outcrops in the Mabou/Lake Ainslie/Baddeck areas of western Cape Breton Island, including the Jubilee area. Toward the basin centre (near Mabou River), the Horton Group attains a composite thickness of 2700 m, which thins to 1000 m near the eastern margin of the basin. Facies associations within the Horton Group maintain their identity across the basin, although they have been interpreted as being diachronous and deposited within fault-bounded basins (Hamblin, 1988, 1989a, b).

In the Jubilee area, the main structural feature is a northwesterly elongated horst, originally called the "Jubilee dome" (Fig. 2). Conglomerate of the Horton Group is exposed in the core of the horst. At Jubilee, Horton conglomerate is abruptly overlain by limestone of the basal Windsor Group. The limestone is succeeded by a transitional unit of interstratified limestone and evaporite that is capped by a thick anhydrite unit. At the northeastern margin of the horst is a normal fault called the Jubilee Fault (Hein et al., 1988). Zinc and lead sulphide mineralization occur in the limestone, particularly where it is brecciated in a narrow band parallel with the Jubilee Fault (Fig. 2).

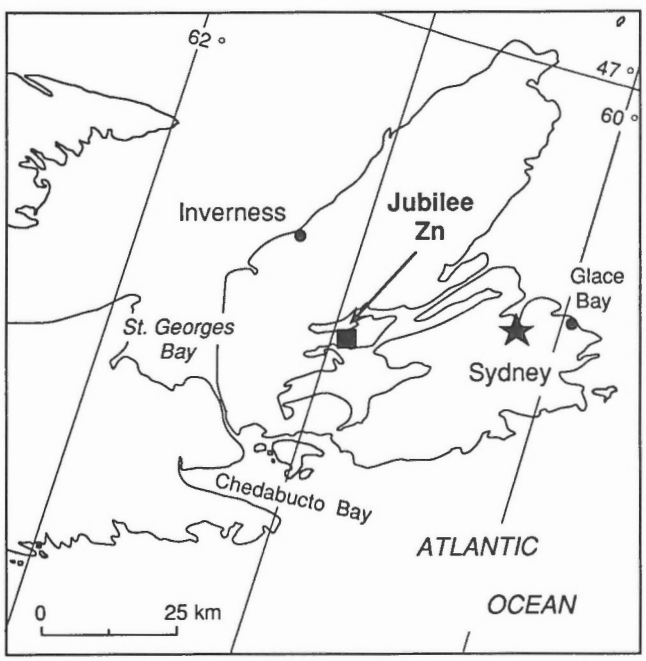

Figure 1. Location map, Jubilee deposit, Cape Breton Island, Nova Scotia.

EXPLORATION AND DEVELOPMENT HISTORY

In the 1930s several adits were driven to test subcrop near mineralized outcrop discovered earlier in the decade. A record exists of only the longest adit. It was driven about 40 m south-southeast of the mineralized outcrop through overburden and then along the subcrop. This adit was sampled in 1936/1937 with assays averaging 12.73% Zn and 0.79% Pb.

Drilling in 1937 and trenching and drilling from 1945 to 1948 failed to define a larger zone of mineralization. The most recent work on the deposit began in 1972 and culminated in 1979, with a drilling program of 89 holes carried out by the Texam Joint Venture. This program tested the host rock downdip from outcrop on the north side of the Jubilee dome to a depth of 62 m along a width of 550 m between the Jubilee Fault and the Road Fault (Fig. 2, 3). The Jubilee Fault was sampled over a length of 1600 m and to a depth of 352 m; the Road Fault was sampled less systematically over a length of 1800 m and to depths of 225 m. A further 30 holes were drilled by Falconbridge Ltd. from 1989 to 1991 after this study was completed.

Grade and tonnage estimates were not attempted in the present study. A formal estimate of the grade and tonnage was done by F.J. Sugden (unpublished internal memorandum, Amax Resources Incorporated, 1978). He estimated that there was potential for just under 900 000 metric tonnes of 5.2 per cent Zn and 1.4 per cent Pb over average cumulative thicknesses of 7.6 to 9.4 m in three zones along the Jubilee Fault. The three zones extend 1000 m along the fault and are up to 100 m wide.

An oil seep near the site of the original showing was used to position three holes drilled in 1946-1948 to test the structural target presented by the Jubilee dome. The holes were dry and no base metal mineralization was reported. The Little Narrows Gypsum Company Limited has continuously operated a gypsum mine for 54 years immediately north of the Zn-Pb occurrence.

PURPOSE AND METHODS

Rigorous documentation of exploration activity on the Jubilee deposit and the synthesis of previous work is presented in Hein et al. (1988) and Graves et al. (1989). In the present study, 38 drill cores were described on a bed-by-bed basis. Detailed facies description and interpretation are given in Hein et al. (1988) and Graves et al. (1989). This paper presents: (1) a general lithological

description and interpretation; (2) an outline of the nature of the contact between the Windsor and the Horton groups in the study area, and the effect of this contact on sedimentary distributions, subsequent faulting, and mineralization; (3) a discussion of the timing, distribution, and origin of the limestone breccia that hosts the mineralization with respect to development of other sediment types; (4) a discussion of the relationship of mineralization to sedimentary patterns; and, (5) the timing of mineralization with respect to diagenetic and epigenetic history of the sediments.

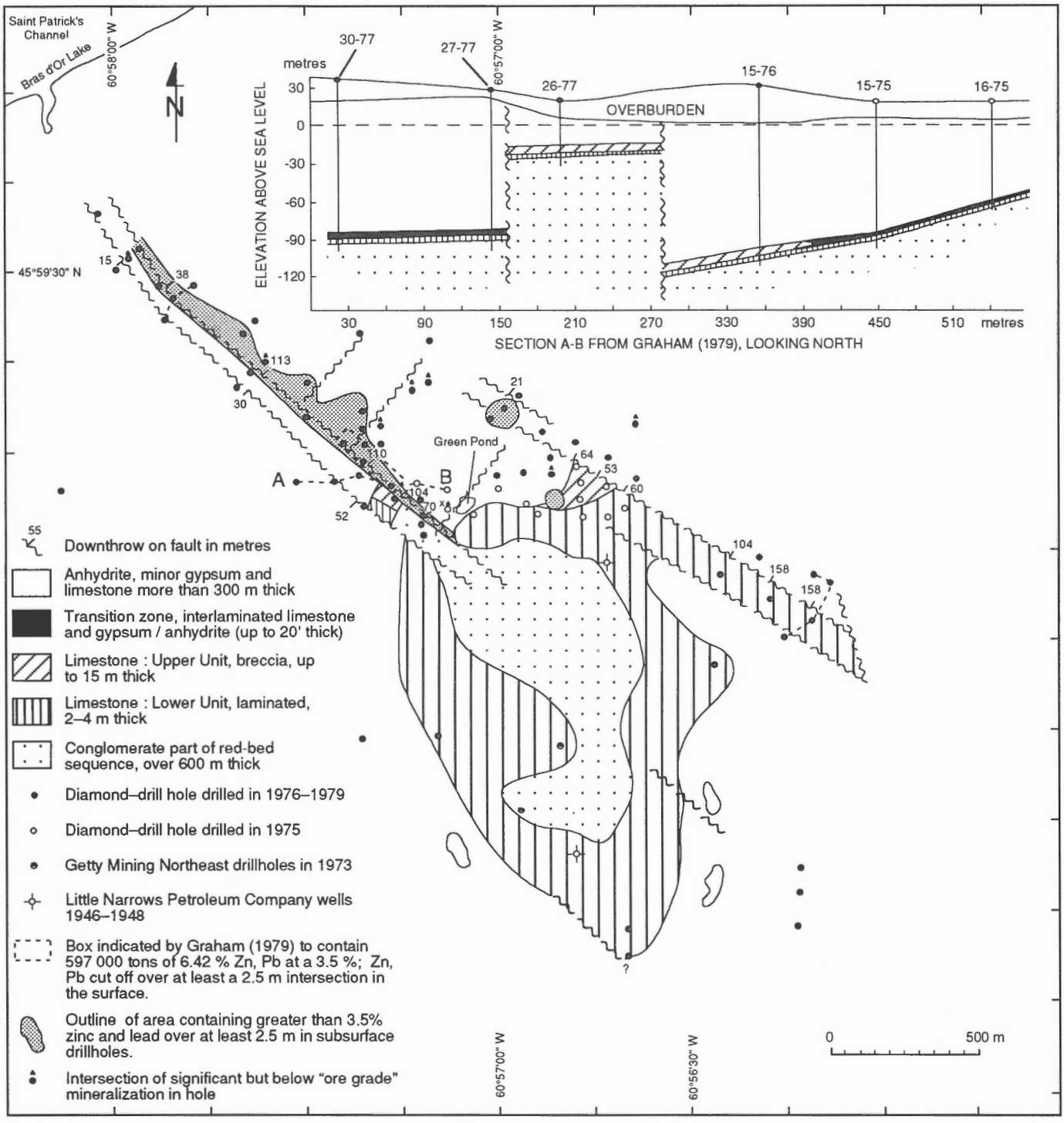

Figure 2. Surface geology, Jubilee deposit (modified after R.A.F. Graham, unpublished report for Texas Gulf Canada Limited, 1979); wavy line indicates fault, thin dashed line shows drilling of oblique holes.

LITHOLOGICAL DESCRIPTION AND INTERPRETATION

The footwall to the Jubilee mineralization consists of red and green conglomerate of the Horton Group overlain by laminated dark grey limestone of the basal Windsor Group (Fig. 4). In contrast with most other carbonate-hosted Zn-Pb deposits, dolomite is conspicuously absent. The lithologies in the Jubilee area are, in ascending order, Horton Group: (1) conglomerate; and Windsor Group: (2) laminated, grey to black micritic limestone with pisolitic textures; (3) convolute-laminated micrite; (4) interbedded limestone and evaporite; and, (5) thick evaporites (Fig. 4). Detailed descriptions of drill core are given in Hein et al. (1988) and Graves et al. (1989), and are summarized below.

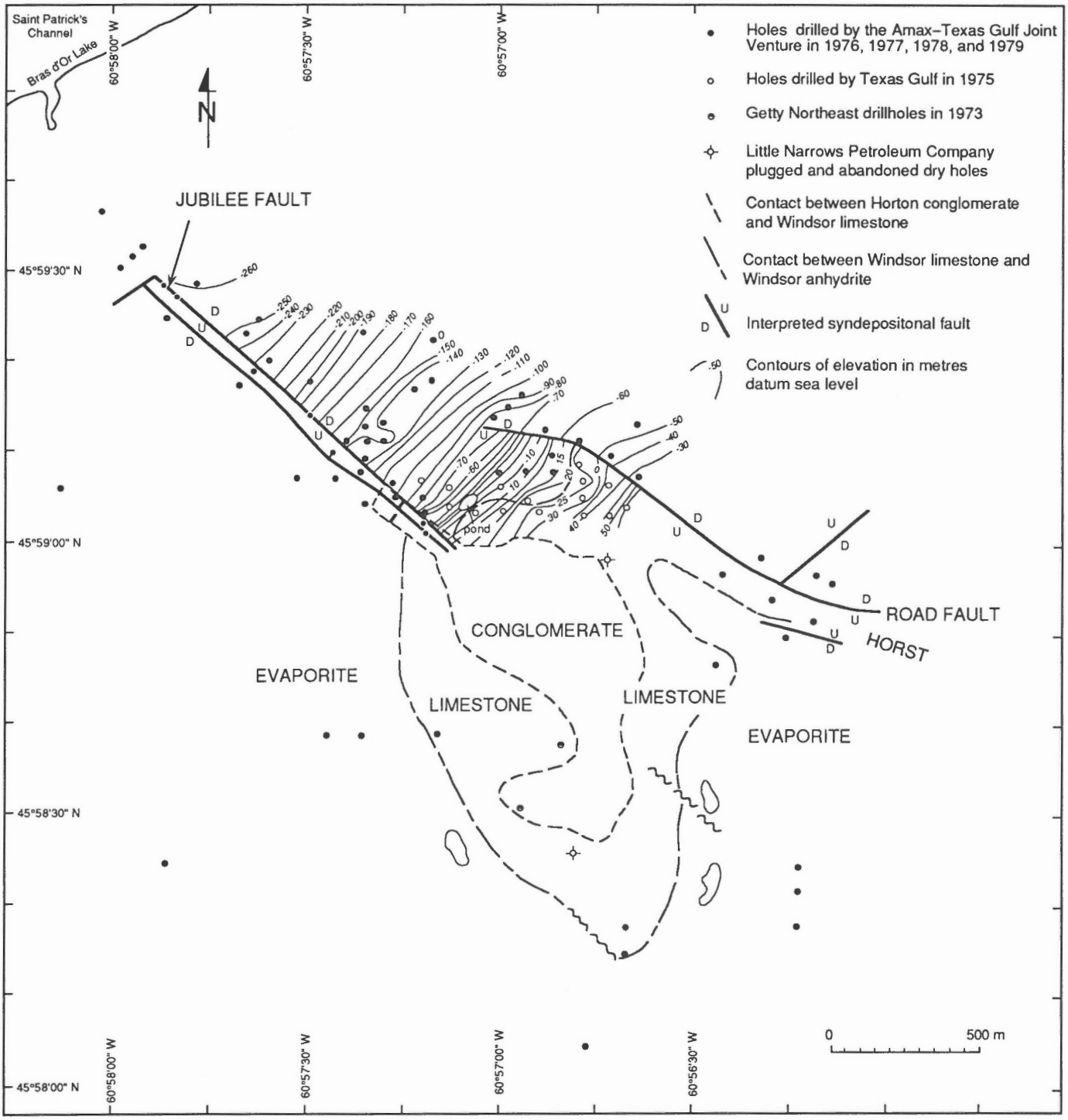

Figure 3. Structure contour map, Jubilee deposit. Present-day elevations on top of the Horton Group conglomerate; U indicates relative upward fault displacement, D indicates relative downward fault displacement.

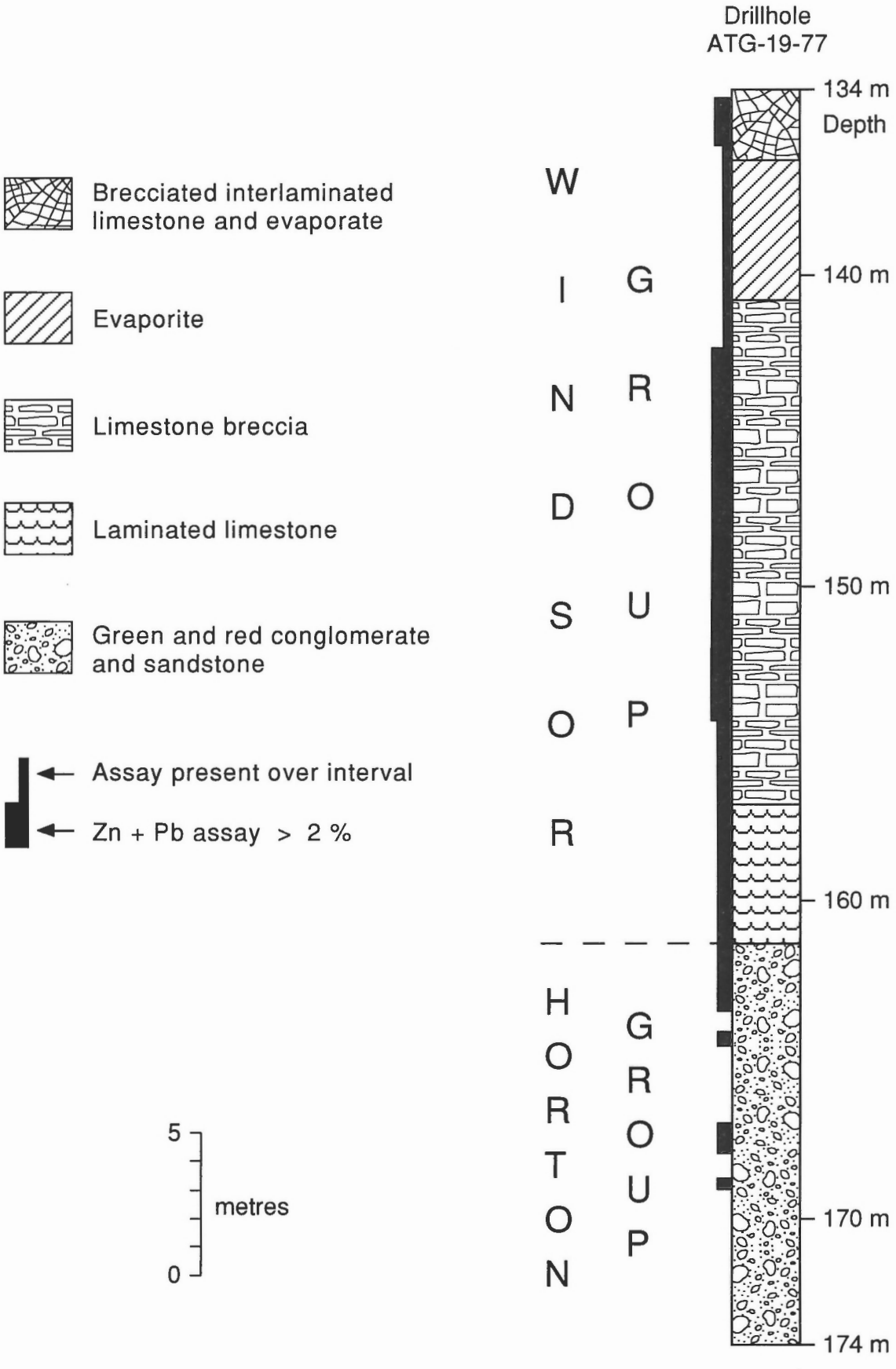

Figure 4. Stratigraphic profile, drillhole ATG-19-77, Jubilee deposit.

Horton Group

The most common lithology seen in drill core is ungraded and massive conglomerate to pebbly sandstone. Lack of stratification, poor sorting, and coarse grain size indicate very rapid rates of deposition from high energy flood flows. Stratified conglomerate to pebbly sandstone is also common. Here the well defined stratification indicates deposition from coarse grained bedforms, including diagonal bars or diffuse gravel sheets (cf. Gustavson, 1974; Hein and Walker, 1977), under high discharge levels in a fluvial setting. Less common lithologies include inverse and normally graded to stratified conglomerate. The variable grading patterns, lack of well defined stratification, poor sorting, and coarse grain size indicate that these facies were probably deposited by sediment-gravity flows.

Only the uppermost units of the Horton Group have been examined in drill core in the Jubilee area. The Horton rocks obtained in core correspond to the Ainslie Formation (Hamblin, 1988, 1989a, b), which in northern and central Cape Breton Island includes up to 500 m of grey and red sandstone and siltstone with conglomerate. Red conglomerate is a predominant lithology locally in the Bras d'Or Lakes area (Kelley, 1967). All previous work indicates that the Horton is continental in origin. In particular, the upper Ainslie Formation shows facies patterns interpreted as representing alluvial fan and low to high sinuosity fluvial settings, bordering high relief, fault-bounded basin margins (Hamblin, 1989b). All palynological evidence (Hamblin, 1989b; Utting et al., in press) indicates that the Horton is Tournaisian in age.

Windsor Group

The base of the Windsor Group consists of a laminated limestone (equivalent to the Macumber Formation) (Fig. 4), the top of which also has a pisolitic texture. Within the laminated and pisolitic limestones, variable grading patterns, poor sorting, absence of bioturbation, and lack of bidirectional crossbedding, wave ripple marks, flaser structures or algal microfilaments suggest that these limestones are neither shallow marine nor algal in origin. The occurrence of grading and the general lack of shallow-water features indicates a depositional environment probably below wave base. The types of grading patterns resemble those described in deep water (i.e. below wave base) resedimented carbonates (McIlreath, 1977; Whisonant, 1987). Carbonates were most likely resedimented by various sediment-gravity flows, including slumps, debris flows, and turbidity currents. Bioturbation features and shelly material are generally lacking within the limestones indicating that the depositional environment was probably ecologically stressed (i.e. high salinity, anoxia or dysaerobia combined with a high sedimentation rate).

The ungraded laminite and pisolitic laminite may have originated as microbial mats which, upon compaction and diagenesis, underwent shortening and stylolitization to produce the alternating dark organic residue and lighter carbonate bands. Such mats have been reported from an equivalent Macumber facies in Newfoundland (von Bitter et al., 1988) and were interpreted by these authors as representing possible deep water vent communities. Recent submersible dives on the Oregon subduction zone show that dense faunal populations and authigenic carbonates are associated with venting sites of methane and hydrocarbons at water depths in excess of 2000 m (Kulm et al., 1986). Other dense biological communities occur in water depths exceeding 3800 m on the Laurentian Fan and are sustained by chemosynthetic processes operating on organic-rich sediments (Mayer et al., 1988). Thus, there are no depth constraints on the occurrence of such vent communities, and the laminite and pisolitic laminite in the study area may also be deep water in origin.

The laminated limestone is overlain by a transitional interstratified limestone-evaporite in which the evaporite is gypsum or anhydrite (Fig. 4). Capping the succession is a massive blue anhydrite, with rare thin (up to decimetre thickness) interbeds of halite and limestone with a relict chickenwire texture (perhaps representing dissolution of original evaporite). Although the evaporites were not examined in detail in the present study, earlier work by Stewart (1978) interpreted most of the massive evaporite as forming from a deep water brine.

Elsewhere within Atlantic Canada, the Windsor Group is more variable, consisting of fossiliferous marine carbonates and evaporites, with minor red clastic interbeds. The Windsor Group in the Jubilee area corresponds to the Major Cycle 1 of Giles (1981), which consists of a lowermost 3 to 50 m of laminated dolostone (Macumber Formation) that is conformably overlain by a maximum of 300 m of massive anhydrite, and up to 300 m of stratified halite and red siltstone (Boehner, 1986). Palynological data indicate a Visean age for the Macumber (Utting, 1980; Utting et al., in press). The Windsor has been interpreted as representing a rapid marine transgression into a continental basin (Geldsetzer, 1977; Kirkham, 1978; Giles, 1981), associated with eustatic sea level rise (Geldsetzer, 1977) or tectonic downfaulting of a basin margin (Kirkham, 1978).

The Pembroke breccia and other secondary limestone textures

Secondary limestone textures occur on scales ranging from a few millimetres to tens of metres thick. The most common secondary texture occurs as a thick limestone breccia (Fig. 4), which resembles the Pembroke Formation (collapse breccia) described by Smith and Collins (1979) from bore holes at Coxheath and Kaiser, central Cape Breton Island, and from Walton, north-central Nova Scotia. The Pembroke breccia is comprised mainly of clasts of Macumber lithologies, with a mixed matrix, including calcareous sand, red mudstone, local anhydrite, with some coarse calcite filling. The Pembroke breccia directly overlies the lower Macumber laminated limestone (Fig. 4) or may completely replace the Macumber (Smith and Collins, 1979). This breccia has been variously interpreted as a karstic collapse breccia (Clifton, 1967; Smith and Collins, 1979), an evaporite solution breccia (Smith and Collins, 1979), or an intraclast storm deposit (Schenk, 1969). In the Jubilee cores examined in the present study, secondary textures

within the limestone include: thick brecciated limestone and open-space filling texture (the Pembroke breccia), thin solution intraclasts, and rare karstic breccia.

The Pembroke breccia

In the Jubilee deposit, the most common secondary texture developed in the thick limestone (Pembroke) breccia is a 'rock-matrix breccia'. This limestone breccia is composed of subrounded to angular, centimetre-scale limestone clasts of Macumber lithologies. Most commonly, clasts are unrecrystallized, with original lamination and pisolitic texture preserved. Breccia clasts are in a clast-support framework and are commonly chaotically rotated with respect to one another (Fig. 5C). Individual clasts seem to have fallen into spaces created by dissolution of original evaporite interbeds and interlaminae. This texture is best developed in mineralized cores (ATG-49-78 (Fig. 5B), 39-77 (Fig. 5E), 53-78 (Fig. 5D), 51-78 (Fig. 5A), and 20-77, Hein et al., 1988; Graves et al., 1989), and all gradations exist between unaffected interbedded limestone/evaporite and well developed breccia texture (Hein et al., 1988). Matrix most commonly consists of finely comminuted Macumber rock fragments.

Less commonly, the brecciated limestone is matrix-supported, in which the matrix consists of gangue and sulphide minerals with open-space (vein and cavity) filling textures. This type of breccia is termed a 'mineralized-matrix breccia'. Limestone clasts are recrystallized and corroded, often containing finely disseminated sphalerite. The vein- and cavity-infills consist of banded sphalerite, pyrite, and calcite (Fig. 5D, E). This texture is particularly well developed in the thickened portions of the brecciated limestone and is characteristic of the more highly mineralized parts of the deposit.

Solution intraclasts

A less common secondary limestone texture consists of a solution texture, termed 'solution intraclasts'. Small limestone 'intraclasts' (< 1 cm long) have irregular margins and appear to have undergone dissolution (Fig. 5B). Solution intraclasts always occur within a dark, organic-rich, fine grained matrix, at the basal centimetre or less of individual laminated limestone beds. This secondary texture is most common within an upper laminated limestone near the contact with the overlying succession of interbedded limestone and evaporite. The solution intraclast texture is particularly well developed in the more mineralized zones in the Jubilee deposits, and is rarely observed in less mineralized drill core samples.

Karstic breccia

A rare limestone breccia, which consists of chaotically-oriented limestone clasts in a fine grained, dark (possibly organic-rich) clastic matrix is interpreted as a collapse breccia formed by karstification (Fig. 5A). This texture was observed only in the core from drillhole ATG-51-78, in the northwest part of the study area (Hein et al., 1988; Graves et al., 1989).

STRUCTURAL GEOLOGY

Detailed structural features in the study area are described in Hein et al. (1988) and Graves et al. (1989), and are summarized as follows. The Jubilee Fault extends northwest from the Jubilee dome (Fig. 3). A number of other faults strike parallel to the Jubilee Fault. One of the more prominent faults is the Road Fault, which is 450 m northeast of the Jubilee Fault, and forms the northeastern boundary of the study area (Fig. 2, 3). Although most of the drilling was concentrated along the Jubilee Fault, 20 drillholes were spaced over a length of 1350 m along the Road Fault (Fig. 2, 3). The Road Fault has a downthrow to the northeast, which increases from 10 m at the northwestern end to 165 m to the southeast. Although not discussed by R.A.F. Graham (unpublished report for Texasgulf Canada Limited, 1979) and G.P. Isenor (unpublished reports Texam Joint Venture, 1978, 1979), their maps indicate that the dome is 'horst-like' where it meets the Jubilee Fault and could be interpreted as a horst rather than a monocline or fold structure.

Structural features are not well documented northwest of the study area. There a major fault strikes perpendicular to the Jubilee Fault, and places lower Windsor strata in contact with the Precambrian strata. Due to a lack of drilling, there is no evidence that the Jubilee Fault extends north of St. Patrick's Channel (Fig. 2, 3).

The paleotopography of the Horton Group was determined by contouring the subsurface elevation of the Windsor/Horton Group contact (Fig. 2) from 1975-79 drill data (G.P. Isenor, unpublished report to Canamax, 1979). The resultant map (Fig. 3) shows a major northwest-trending horst bounded on the northeast by the Jubilee Fault. A second parallel horst occurs on the eastern flank of the central conglomerate area bounded to the northeast by the Road Fault. The structural contours indicate possible valleys trending subparallel to the faults between the two horsts. The northeastern edges of both horsts contain the more prominent faults, suggesting that they initiated as half-grabens bounded by the major faults. The dip of the paleosurface of the top of the Horton Group in the area bounded by the faults is parallel to the strike of the faults and shallows downdip from about 20° on the northern flank of the Jubilee dome to about 10° at the northwestern limit of drilling.

FACIES VARIATIONS

Rocks were classified into facies, defined on the basis of lithology, sedimentary structure, the presence or absence of grading, and the occurrence of a matrix- versus clast-supported framework. Because facies are defined mainly on the basis of lithology and physical aspects, the term "facies" in this paper refers to lithology.

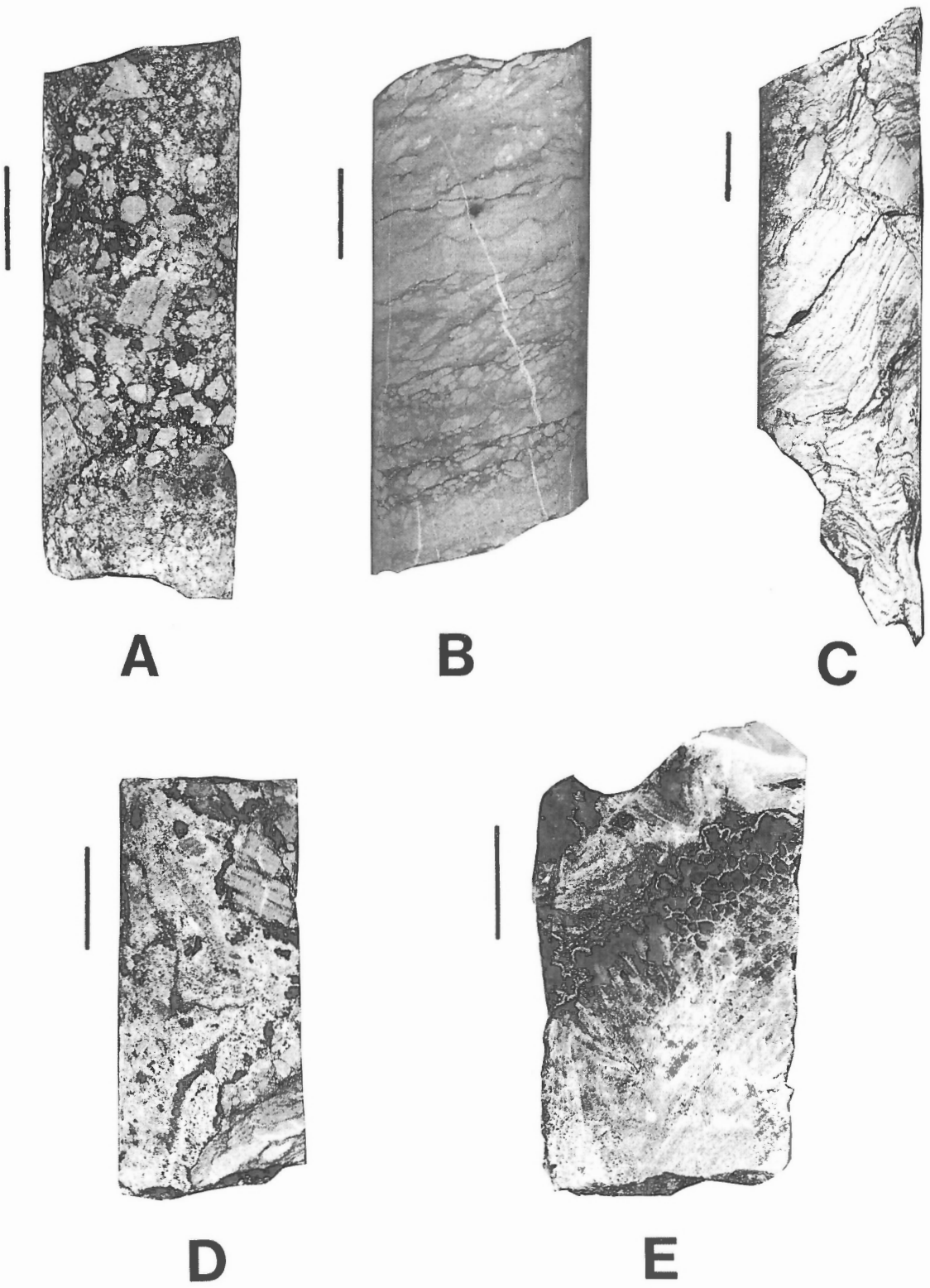

Figure 5. Secondary limestone and breccia textures:
A) karstic breccia, sample J035, core ATG-51-78, depth 236.57 to 236.67 m;
B) "solution intraclast" texture, sample J013, core ATG-49-78;
C) breccia texture in a rock-matrix breccia, sample J008, core ATG-49-78, depth 326.48 to 326.73 m;
D) mineralized, vein-infilled breccia texture in a mineralized-matrix breccia, sample J028, core ATG-53-78, depth 235.12 to 235.19 m;
E) mineralized, veined breccia texture in a mineralized-matrix breccia, sample J083, core ATG-39-77, depth 252.50 to 252.58 m.

Vertical facies patterns

Preferred vertical facies patterns were compiled by Markov chain analysis of the Horton Group clastics and Windsor Group carbonates and evaporites (cf. Hein et al., 1988; Graves et al., 1989). For the Horton Group succession, the pattern of the vertical sequences reflects proximal-to-distal trends in sediment-gravity flow deposition for conglomerates, with transitions from inversely graded to inverse-to-normally graded to normally graded conglomerate. More inversely graded and inverse-to-normally graded conglomerates occur within the mineralized zone than elsewhere. This suggests that the mineralization is in the more proximal conglomerate areas.

For the Windsor Group carbonate and evaporite successions, two significant patterns occur: (1) There is a tendency for the convoluted limestone to be succeeded by the laminated limestone. This transition may possibly reflect proximal-to-distal trends within a deep carbonate basin, with the convolute facies developed in high slope areas susceptible to mass-wasting; and, (2) There is a tendency for the brecciated limestone (Pembroke Formation) and massive evaporite to be associated with one another. The only other facies that shows a close association with the massive evaporite is the interbedded limestone and evaporite.

Lateral facies patterns

The facies percentages of the various lithologies show both an increase of mass-flow clastic facies and an increase of brecciated and laminated limestone facies on the downthrown side of the Jubilee Fault (cf. Hein et al., 1988). These data suggest that the Jubilee Fault may have been active during deposition of the uppermost Horton and lowermost Windsor groups. Moreover, the enhanced carbonate section observed in some of the cores may reflect deposition on the downthrown side of faults which were active during deposition of the Windsor Group (cf. Hein et al., 1988). To test a correlation between enhanced carbonate deposition and the occurrence of faults in the area, three isopach maps were constructed of the Windsor carbonate and evaporite facies, including laminated limestone (Fig. 6), interbedded limestone and evaporite (Fig. 7), and brecciated limestone and evaporite (Fig. 8).

The distribution of total limestone reflects the similar distribution of the laminated limestone and the brecciated limestone (Hein et al., 1988; Graves et al., 1989). Both the laminated limestone (Fig. 6) and the brecciated limestone (Fig. 8) are markedly thicker along the downthrown side of the Jubilee Fault. This would be the case if fault displacement affected not only breccia formation but limestone accumulation as well.

The patterns along the parallel Road Fault to the east are less obvious (Fig. 6, 8), perhaps indicating a shorter period of fault activity during sedimentation. The laminated limestone only shows influence of sediment accumulation on the downthrown side at the northwestern extension of the Road Fault (Fig. 6). The isopach of the brecciated limestone shows little correlation with displacement of the Road Fault (Fig. 8).

The irregular distribution of the brecciated limestone may also reflect irregularities in the underlying clastic surface (compare Fig. 3 and 8). Such irregularities could be the result of small orthogonal cross faults; however, a sedimentary control is more strongly suggested by the coincidence of the mineralized zone with depressions in the underlying clastic surface and the tendency of the host rocks to consist of proximal conglomerate. If the top of the brecciated limestone is contoured over the mineralized zone, the thickest mineralized intersections indicate poorly controlled closure in the updip direction (cf. Graves et al., 1989). This coincidence could be the result of relict depositional topography affecting deposition of the Windsor interbedded limestone and evaporite which then, through dissolution, were transformed into the brecciated limestone.

Contours on the interbedded limestone and evaporite isopach map (Fig. 7) are much less regular, suggesting that multiple factors controlled the thickness-distribution of this facies. There are three thicker portions of this facies: one parallels the horst extension of the Jubilee dome downdip from the outcrop; a second parallels the Road Fault to the east of the Jubilee dome; and a third occurs as an extension of the northeastern end of the Road Fault. These trends suggest that both the Jubilee and Road faults affected deposition of the interbedded limestone and evaporite facies. Thus, it may be inferred that subsidence along synsedimentary faults was pronounced on both sides of the study area during deposition of the interbedded facies (Fig. 9).

The most pronounced feature of the interbedded limestone and evaporite facies is not the thickening, but the thinning corresponding firstly, to the area along the Jubilee Fault with enhanced brecciation and mineralization; and, secondly, on the downthrown and downdip end of the Jubilee Fault, which is also an area of enhanced breccia development. The absence of the interbedded facies in areas of enhanced breccia development suggests that the breccia may have formed by solution of evaporite from a pre-exisiting interbedded limestone and evaporite unit that was thicker on the downthrown side of synsedimentary faults. In addition, the outline of the area where the interbedded unit is absent has a shape consistent with dissolution by a fluid flowing laterally along and away from the Jubilee Fault (Fig. 7).

PALEOGEOGRAPHIC MODEL

The simplest paleogeographic model for the study area, which accounts for all the facies variations, vertical sequences, and isopach trends consists of sedimentation within an active small half-graben (or later full-graben) (Fig. 9). During active tectonism, small alluvial fan deltas built up a series of mass-flow deposits along the boundary faults of horsts. During periods of active faulting, local paleogeographic highs were exposed and served as sources for the upper coarse conglomerates noted in the northwestern part of the study area (drillholes ATG-51-78, 53-78, Hein et al., 1988; Graves et al., 1989). In the deeper central parts of the graben or half-graben, laminated limestones and/or pisolitic limestones were deposited during Windsor time.

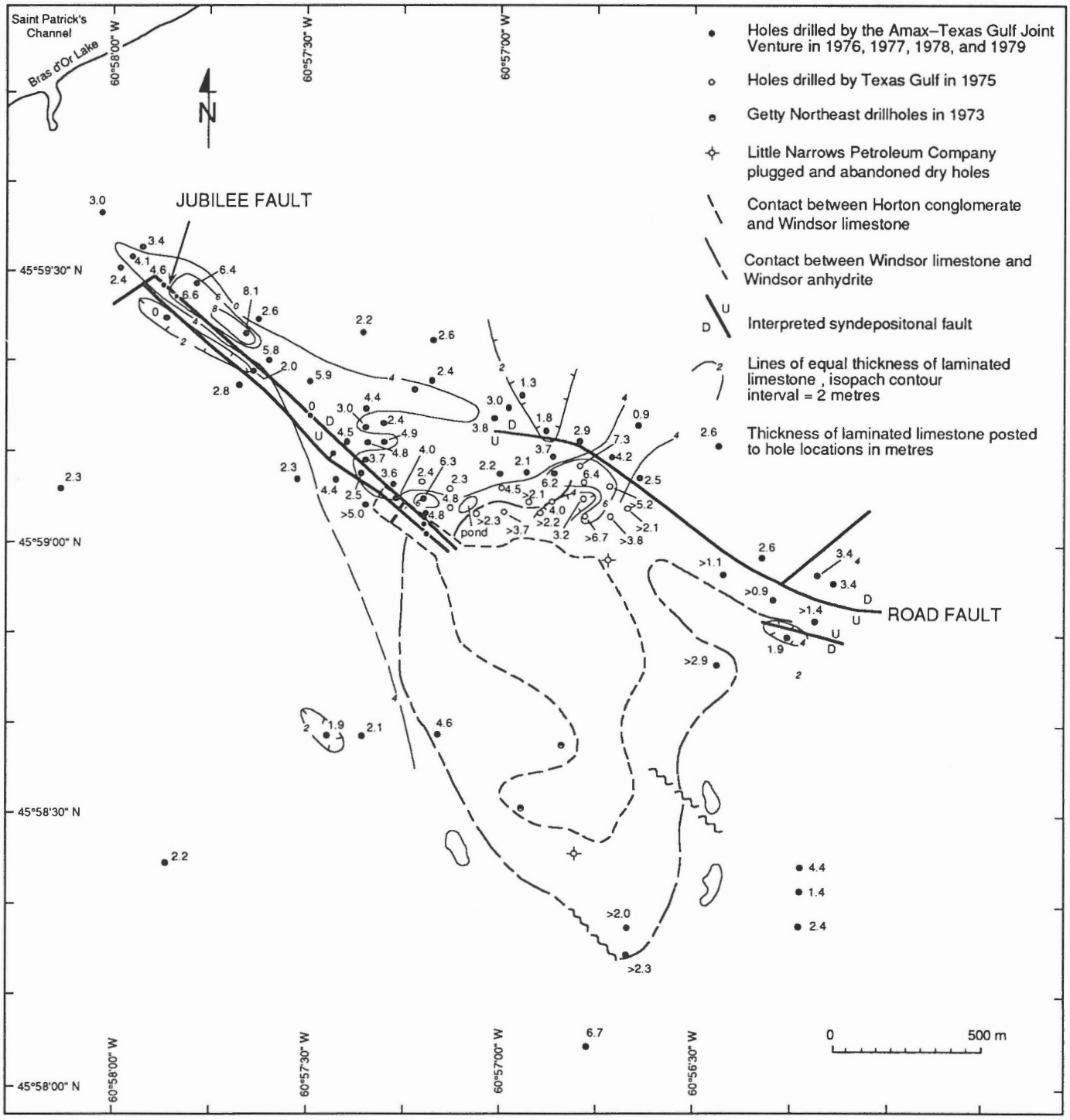

Figure 6. Thickness of laminated limestone in metres; U indicates relative upward fault displacement, D indicates relative downward fault displacement.

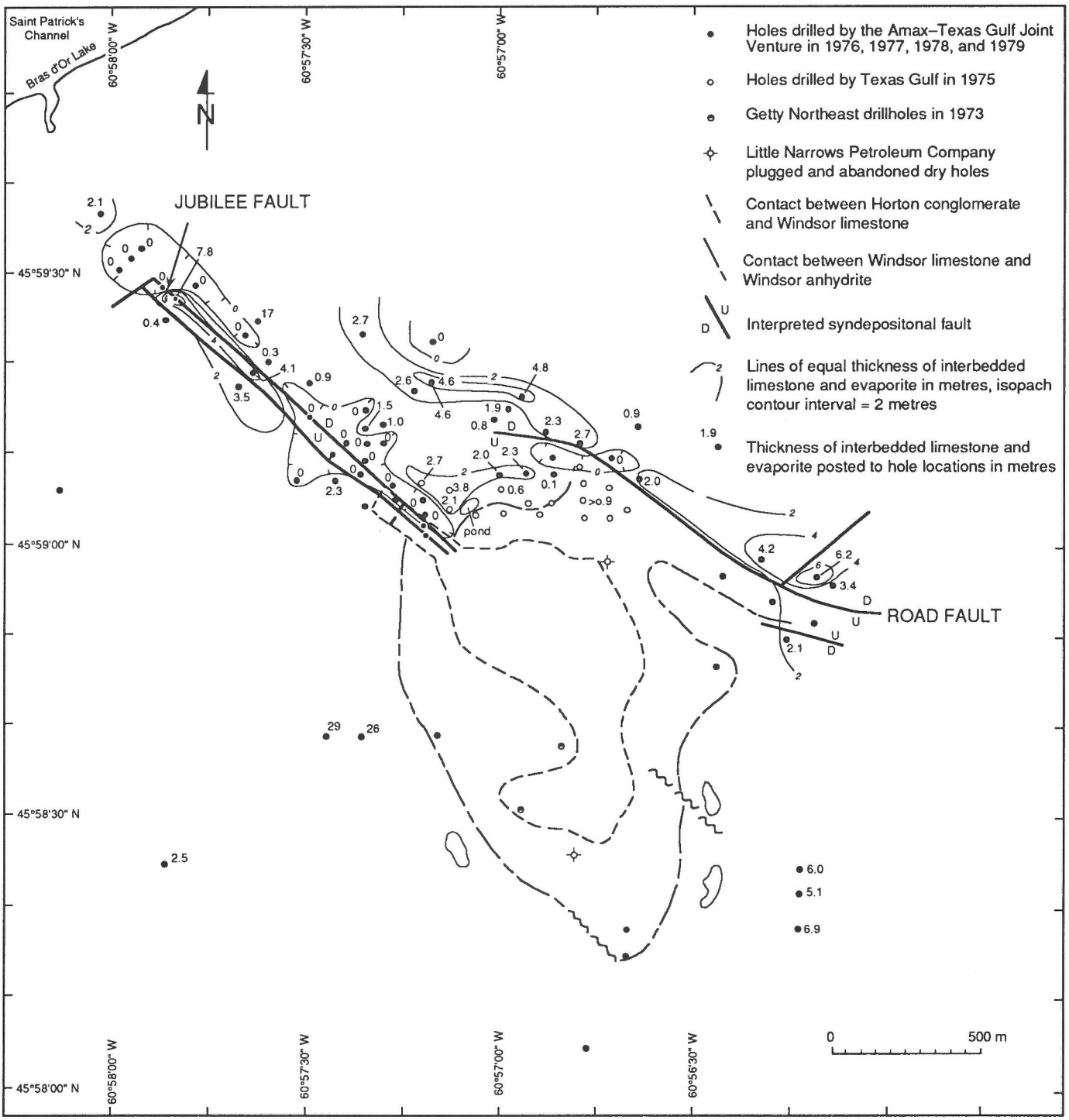

Figure 7. Thickness of interbedded limestone and evaporite in metres; U indicates relative upward fault displacement, D indicates relative downward fault displacement.

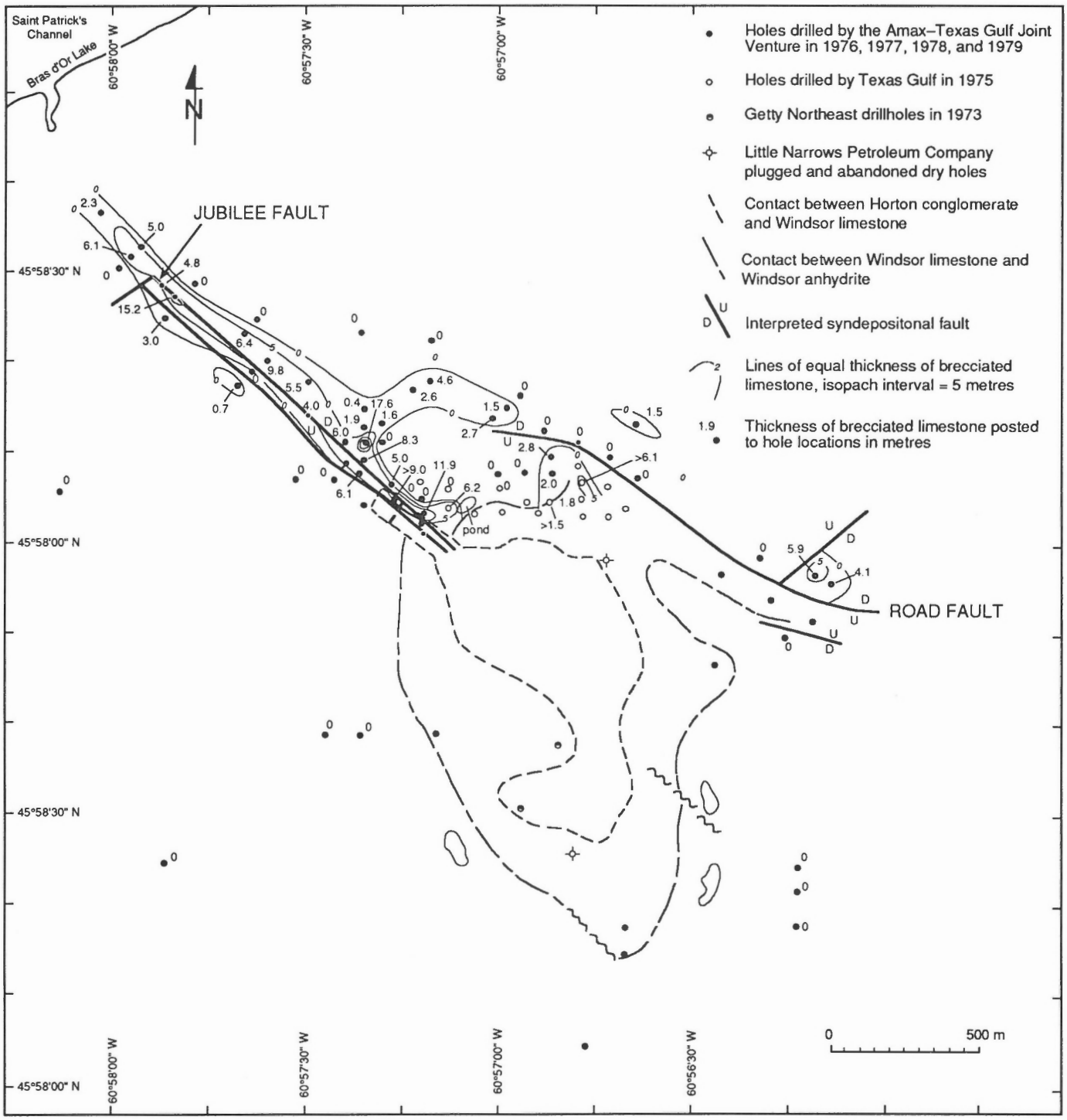

Figure 8. Thickness of brecciated limestone in metres; U indicates relative upward fault displacement, D indicates relative downward fault displacement.

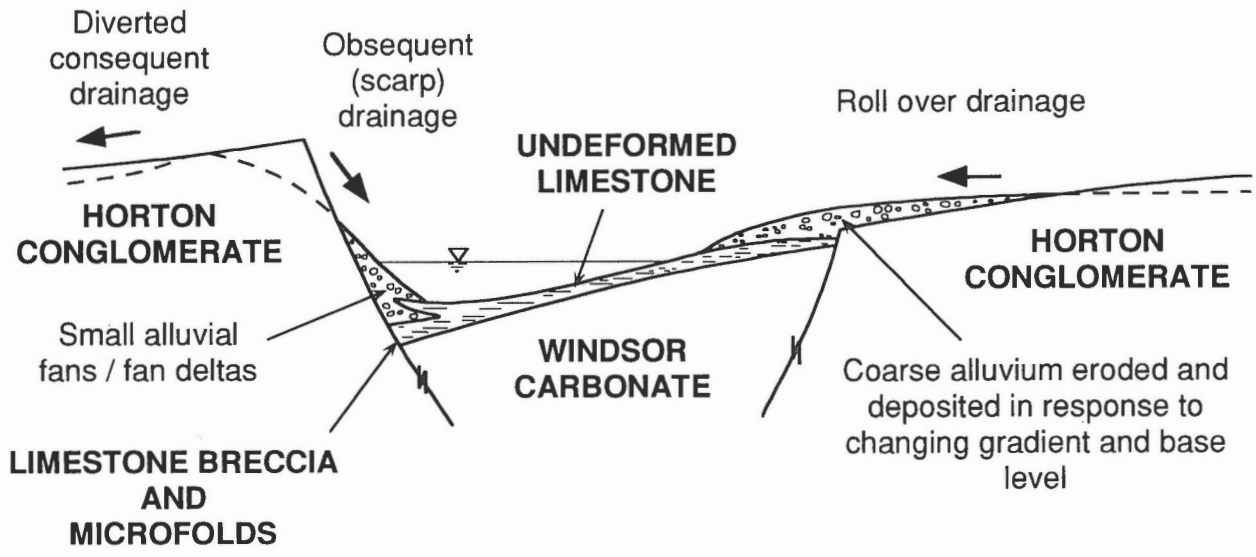

Figure 9. Paleogeographic model of small graben, Jubilee area (based on models for the East African Rift Valley, after Frostick and Reid, 1987) (modified from Hein et al., 1988).

Data from drillholes located near the Jubilee Fault indicate interfingering of Horton conglomerates and Macumber (Windsor) intraclasts. This suggests that, during part of Macumber carbonate deposition, Horton clastic sediments were being deposited adjacent to the boundary Jubilee Fault (Fig. 9). Jubilee Fault activity was initiated during upper Horton clastic deposition and continued during deposition of the Windsor laminated limestone (Macumber) and the overlying interbedded limestone and evaporite facies. During deposition of the interbedded facies, the Road Fault also influenced facies development. Thus, the basin may have originated as a small half-graben structure, which evolved through time into a full graben. Later, during periods of tectonic quiescence and subsidence, widespread massive evaporites with thin limestone and rare halite interbeds, more typical of the Windsor, were deposited.

The model discussed here is virtually identical to the simple half-graben model developed by Frostick and Reid (1987) for Tertiary to Recent successions of the great East African rift system. A similar model has been proposed for the Triassic sediments of the Inner Moray Firth of Scotland (Frostick et al., 1988). The Jubilee half-graben or graben structure is small, 0.5 to 1 km wide by 2 to 5 km long, within a larger rift basin (10 to 20 km wide by 50 km long) (cf. Hamblin, 1988, 1989a, b). The scale of the Jubilee half-graben or graben corresponds to the third order basins of Large (1983), which have lateral dimensions ranging from several hundreds of metres to several kilometres.

GEOLOGY OF THE SULPHIDE ZONE

Minerals and mineralization textures

Zinc is the most abundant commodity in the Jubilee deposit, with lead of secondary, but significant, importance. Although silver is commonly mentioned in the assessment reports, only three assays (of eighty in the 1975-79 program; complete assays are tabulated in Hein et al., 1988) have detectable Ag (0.02 to 0.06 troy ounces per ton; 0.6-1.7 g/tonne). Murphy (1937) reported 1.4 oz/ton (3.9 g/tonne), presumably from outcrop; however, a location is not given.

Minor commodities of interest include Cd in sphalerite (up to 0.54 weight per cent within single sphalerite grains), and Sr in barite (1 to 4 weight per cent) (reported both in assay results and in the present study). Limited assays for Cu (as chalcopyrite inclusions in pyrite) in the conglomerate were low (maximum of 0.08 weight per cent). Potential economic minerals are sphalerite and galena; other sulphides include pyrite, marcasite, and chalcopyrite. Sparry calcite, anhydrite, and barite are associated spatially and paragenetically with the economic minerals. A few occurrences of fluorite were observed in the drill core.

Vug fillings and joint coatings of liquid hydrocarbons and solid bituminous matter are ubiquitous in the drill core and are particularly common in zones of both high present porosity and zones of sulphide mineralization. Hydrocarbon-bearing fluid inclusions and bitumen solid inclusions are abundant in sphalerite. Gaucher (1977) and G.P. Isenor (pers. comm., 1988) reported the flow of liquid hydrocarbons in a drillhole undergoing geophysical examination.

Sphalerite is pale yellow to white and transparent with rare light reddish bands. It occurs as either disseminated small crystals on the periphery of cavities filled with calcite or as disseminations throughout rounded and recrystallized limestone clasts. Visual examination of grade is difficult due to poor colour contrast between sphalerite and the host carbonate. Sphalerite also occurs as reddish banded fans growing from pyrite or limestone walls into calcite-filled cavities. In this latter form, it tends to be strongly yellow and to have numerous solid bitumen inclusions. Microprobe analysis indicates that the red bands are high in Fe, whereas the yellow sphalerite is low in Fe and high in Cd (cf. Hein et al., 1988).

Galena occurs as euhedral and equant crystals of various sizes. It is commonly associated with sphalerite-galena-calcite veins. The only significant trace metal observed in reconnaissance microprobe analyses of galena was Bi (up to 0.20 weight per cent). Pyrite, marcasite, and calcite commonly fill cavities. Some drillcore exhibits massive pyrite/marcasite mineralization (Stewart, 1978). The internal texture of these pyrite-rich zones consists of a delicate colloform lacework of pyrite and calcite. Chalcopyrite, although frequently reported during exploration (especially from the top of the Horton conglomerate), occurs as a trace mineral in pyrite inclusions.

Barite occurs as an accessory mineral in several drill cores and as a significant mineral in core from drillhole ATG-51-78 and at the mouth of the adit located at the original showing. At the adit, barite occurs as radiating aggregates in postsulphide cavity fillings, where it is accompanied by earlier sphalerite and galena.

Paragenetic sequence

The paragenesis is simple and universal in the Jubilee deposit, consisting of: pyrite → sphalerite → galena → barite and/or anhydrite. Calcite can occur throughout the paragenetic sequence but generally occurs late, after the sulphides and sulphates. Galena and sphalerite commonly show mutual inclusion textures and thus commonly crystallized together. Fractured sphalerite fans growing on pyrite and cemented together with sparry calcite is a common texture. The paragenetic position of the hydrocarbons is uncertain. Hydrocarbons fill present-day porosity and occur as fluid inclusions in both sphalerite and barite, whereas they are absent in postmineralization calcite. Thus, two periods of hydrocarbons emplacement are clearly indicated – one during sphalerite crystallization and one after the final calcite crystallization.

Fluid inclusions

Fluid inclusion temperatures reported by Stewart (1978) from sphalerite and barite obtained from the main surface showing are in excess of 300°C. These temperatures were not confirmed quantitatively in the present study, but several significant qualitative observations do not support Stewart's (1978) determinations. The fluid/vapour ratios in sphalerite two-phase inclusions are inconsistent with filling temperatures as high as those reported by Stewart (1978). Seven homogenization temperatures from primary inclusions derived from barites in two samples averaged 89.1°C (range: 81.6°C and 98.3°C; standard deviation: 5.2°C).

Fluid inclusions in sphalerite fall into several populations:

1) Ubiquitous small (largest about 1 μm) inclusions defining growth bands;

2) Secondary irregular liquid (or perhaps liquid/gas) inclusions of hydrocarbons;

3) Secondary solid bitumen inclusions with irregular shapes and variable size; and,

4) Rare two-phase liquid-gas inclusions (presumably water) (largest about 2 μm). Larger inclusions in barite with a similar setting are three-phase inclusions with liquid water, liquid hydrocarbon and gas.

Fluid inclusions in barite are larger and also can be classed into several types:

1) Primary, liquid-dominated three-phase hydrocarbon inclusions that occur along crystal and cleavage faces and have relatively constant liquid/gas ratios. Light brown, immiscible liquid hydrocarbon wets the cavity walls. The inclusions are commonly filled with a clear liquid and have a vapour bubble. Freezing behaviour is dominated by liquid hydrocarbon. Homogenization of the vapour bubble is similar in the inclusions measured at 81.6°C to 96.0°C.

2) Liquid-dominated, two-phase hydrocarbon inclusions with vapour bubble in a light brown liquid hydrocarbon.

3) Secondary liquid-dominated, two-phase inclusions with variable vapour bubble size and clear liquid. Inclusions in paragenetically later calcite are predominantly secondary two-phase inclusions with low vapour/liquid ratios.

Although the fluid inclusion investigation was of a reconnaissance nature, some limitations to the fluid composition can be made. Firstly, fluids present during sphalerite, galena, and barite precipitation were most likely at a temperature less than 150°C. Secondly, fluids entrapped during sphalerite and barite precipitation were not of sufficient salinity to result in the common halite/sylvite solid phase in water inclusion, although small inclusion size and the high hydrocarbon content may have prohibited crystallization of salt.

Mineral zoning

Stewart (1978) considered the Jubilee deposit to be zoned both vertically and laterally. The footwall conglomerate and the laminated limestone contain only minor sulphide mineralization in calcite veins. Pyrite is the most common sulphide in these veins, although both sphalerite and galena are usually present. Chalcopyrite occurs as inclusions in pyrite, but was nowhere seen to be a significant phase. Galena content varies with sphalerite content, and becomes coarser grained and more visible when the vein or breccia porosity is sufficient for significant sulphide mineralization.

Vertical profiles of Zn/(Zn + Pb) ratios in any given hole are commonly linear with major breaks at lithological boundaries. Compilation of mineral exploration assay data (G.P. Isenor, unpublished report for Canamax, 1979; Hein et al., 1988) show that 12 of 23 breccia sections are more Pb-rich at the base and become increasingly Zn-rich upward. Higher grade sections tend to be Zn-rich and have more openwork breccia. Of the remaining holes with significant breccia, two have no pattern, two are Zn-rich at the base, and seven have complex patterns.

Stewart (1978) cited a subtle increase in maximum Pb content over Zn farther from the Jubilee Fault as evidence for subtle lateral zoning of lead and zinc. In the present study, mapping of Zn/(Zn + Pb) was attempted at many grades and failed to show any lateral zoning patterns.

R.A.F. Graham (unpublished report for Texasgulf Canada Limited, 1979) noted that the northernmost drill core along the Jubilee Fault is more pyritic and that this may indicate lateral zoning of Fe along the fault. It was difficult to assess this observation as no quantitative record of Fe or pyrite content was included in the company logs.

Metal distribution maps, plotted as metre per cent metal, are a common tool for analyzing mineralization trends and have been constructed in this study for the Jubilee deposit. Data for the metal distribution maps are from the assays of Texasgulf Canada Limited and the Texam Joint Venture drilling programs of 1975 to 1979 inclusive (reported in Table 4 of Hein et al., 1988, after assay reports on drill logs from G.P. Isenor, unpublished report for Canamax, 1979). In each assay report, per cent Zn and per cent Pb were multiplied by the interval of the assay in metres to give metre percentage values. The metre percentage values from the assay reports were then summed for each hole, which were then contoured on Figure 10 (metre per cent Zn) and Figure 11 (metre per cent Pb).

The zinc and lead metal distribution maps are similar and mirror the brecciated limestone thickness patterns (Fig. 8). The positive correlation between metal distribution and breccia occurrence confirms the primary role of breccia paleoporosity on metal distribution. No strong metal zoning is evident in these maps.

Mineralization processes and models

Many of the characteristics of the Jubilee deposit are similar to those of Mississippi Valley-type (MVT) deposits (Sangster, 1983, 1988): the grade is low, mineralogy is simple, there is negligible Ag, the Zn/(Zn + Pb) is high and relatively constant, depositional temperatures are low, the deposit is stratabound, and alteration is absent.

Some important differences exist between the Jubilee deposit and other MVT deposits. The first is the strong fault control of mineralization and host rock lithology and geometry. There may be a subtle zinc-to-lead zoning related to the Jubilee Fault and a tendency for a vertical zoning within the mineralized breccia, from a weakly mineralized, more Pb-rich base to a more metal-rich and Zn-rich top. Although there is evidence of high fluid flux (emplacement of hydrocarbons and sulphides in breccia paleoporosity, dissolution of sulphate, and dissolution and replacement of breccia clasts), dolomitization is absent. Both fine grained, disseminated and coarser grained, open-space filling textures are present. Fluid salinities are not as high as MVT deposits, although the very small fluid inclusion size precludes definitive conclusions. The stratigraphy is unusual, with clastic rocks occurring immediately below the mineralized zone and evaporites immediately above it. There is no premineralized karst surface in the evaporite succession overlying the mineralized zones. Examples of virtually all of these features are recognized in accepted MVT deposits. Consequently, the following discussion will consider the Jubilee deposit in terms of MVT models.

The breccias that host sulphide minerals in the Jubilee deposit are important in consideration of any model for mineralization. Most of the brecciation in the deposit was caused by sulphate dissolution and subsequent collapse of the remaining laminated limestone in a unit originally made of laminated limestone interbedded with sulphate. Two main types of breccia occur – rock-matrix breccia and mineralized-matrix breccia. The breccias are confined between a sulphate-free laminated limestone footwall and a massive sulphate hanging wall. Dissolution of the sulphate is complete where it is a subordinate component of the original interbedded rock. If the breccia did not grade upward into sulphate, it would be difficult to recognize the evidence of sulphate dissolution in vertical section and to distinguish the process from later carbonate dissolution. Thus, the processes of breccia formation by sulphate dissolution may be an unrecognized factor in carbonate host rocks in other deposits that contain less original sulphate. Thin beds of interlaminated sulphate and limestone occur within the massive sulphate. Where these are adjacent to the Jubilee Fault or mineralized-matrix breccia, they are replaced by sulphide minerals.

Sphalerite contains solid inclusions of galena and hydrocarbon-bearing fluid inclusions indicating that Zn, Pb, sulphide S, and hydrocarbons were all present at the time of mineralization. The unbrecciated limestone may have been a potential source of hydrocarbon; however, it is not discoloured by thermal maturation in the mineralized zone. Maturation studies in the Jubilee area indicate that mobile liquid hydrocarbons are from a high salinity marine source, but that the commonly carbonaceous Macumber limestone has limited total organic carbon (TOC) at Jubilee, and thus, is not a potential source (P. McMahon, pers. comm., 1989). Further maturation and biomarker data will test these relationships, but it is currently believed that the liquid hydrocarbon was not derived from a local source.

According to Anderson (1983), a general hydrothermal fluid carrying metals and chloride accounts for the MVT fluid inclusion data. Although metal transport in basinal brines with sulphide (Sverjensky, 1981) or organic-metal complexes (Barnes, 1983) has been proposed for other MVT deposits, Anderson's (1983) analysis and rejection of these processes is supported by evidence at the Jubilee deposit.

It is unnecessary to transfer sulphur to the site of potential mineralization if sulphate from the evaporite is available for reduction. Basinal fluids (i.e. water and hydrocarbons) could be channelled beneath the impermeable sulphate from the time there was enough sulphate to make an effective cap. It seems most practical to invoke microbial sulphate reduction in the presence of hydrocarbons to produce enough sulphur or H_2S to lower the effective temperature of sulphate reduction, as suggested by Macqueen (1986) for the mineralization at Pine Point. Sulphate would be preferentially reduced in structural traps at sites of hydrocarbon accumulation (i.e. the Jubilee Fault) under the caprock (provided by the sulphate). Porosity and permeability would be enhanced throughout the fluid his-

tory by hydrofracturing beneath the impermeable cap, especially during gypsum dehydration and periods of active burial. Hydrogen sulphide produced would be preserved beneath sulphate caprock with or without liquid hydrocarbon. An accumulation of elemental sulphur could also serve to store the products of sulphate reduction for later maturation to H_2S and subsequent reaction with metal-bearing fluids (Ruckmick, 1986).

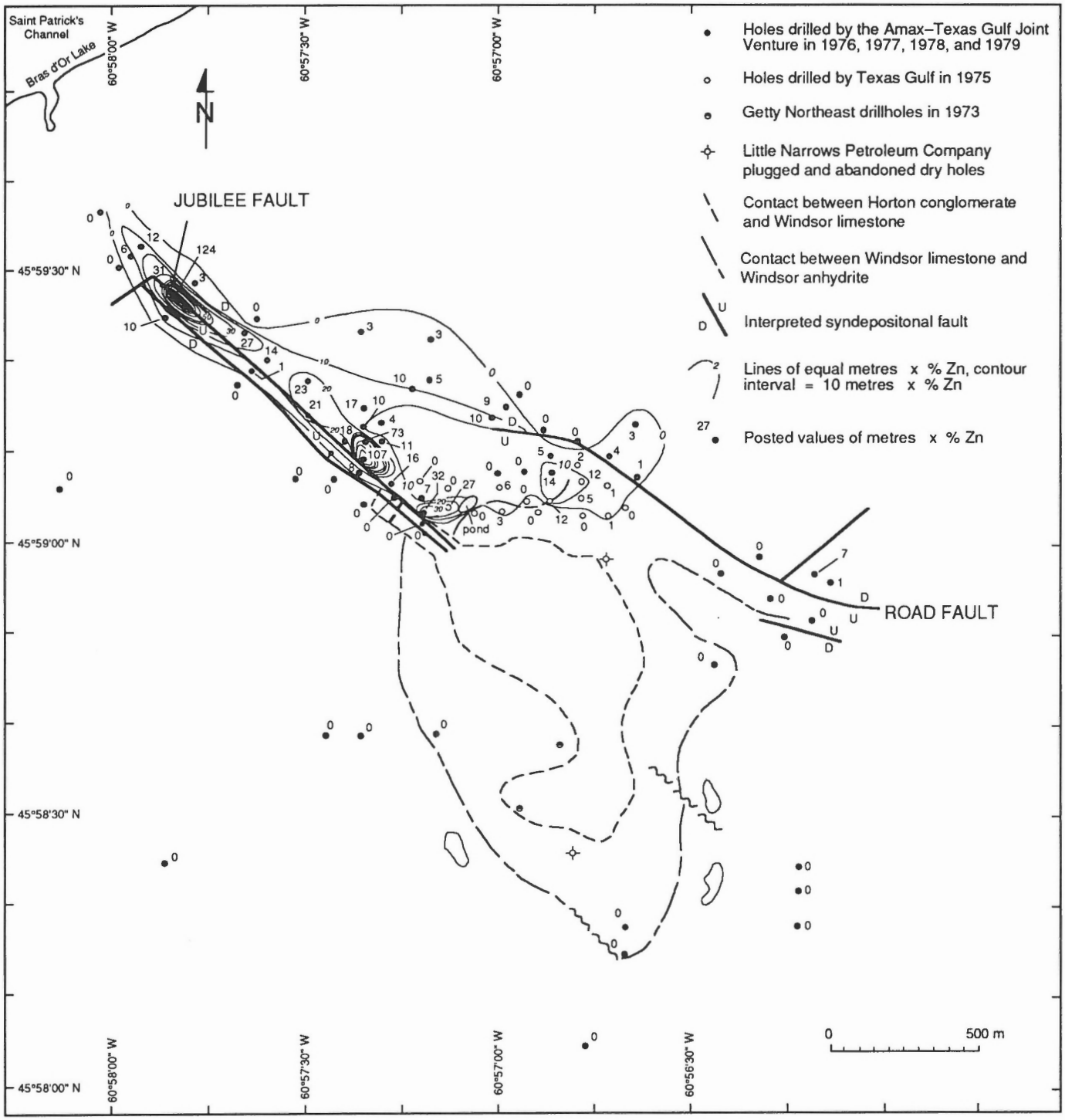

Figure 10. Metre per cent Zn, Jubilee deposit; U indicates relative upward fault displacement, D indicates relative downward fault displacement.

A possible sequence of mineralization events for Jubilee is proposed for a fluid which does not contain significant sulphur but which transports metals to the site of mineralization as follows:

1) Fluids venting along synsedimentary faults provided nutrients for biota resulting in the development of localized thick accumulations of carbonate.

2) Fluids dissolved sulphate from a unit of interbedded sulphate and limestone under a solid sulphate cap.

3) Liquid hydrocarbon migrated to the site and was structurally trapped in the breccia.

4) Bacterial reduction of sulphate to sulphide (or elemental sulphur) occurred, consuming liquid hydrocarbon and sulphate.

5) The rate of inorganic reduction of sulphate was increased by the presence of sulphur and hydrocarbons.

6) Further burial slowed sulphate dissolution and reduction reactions.

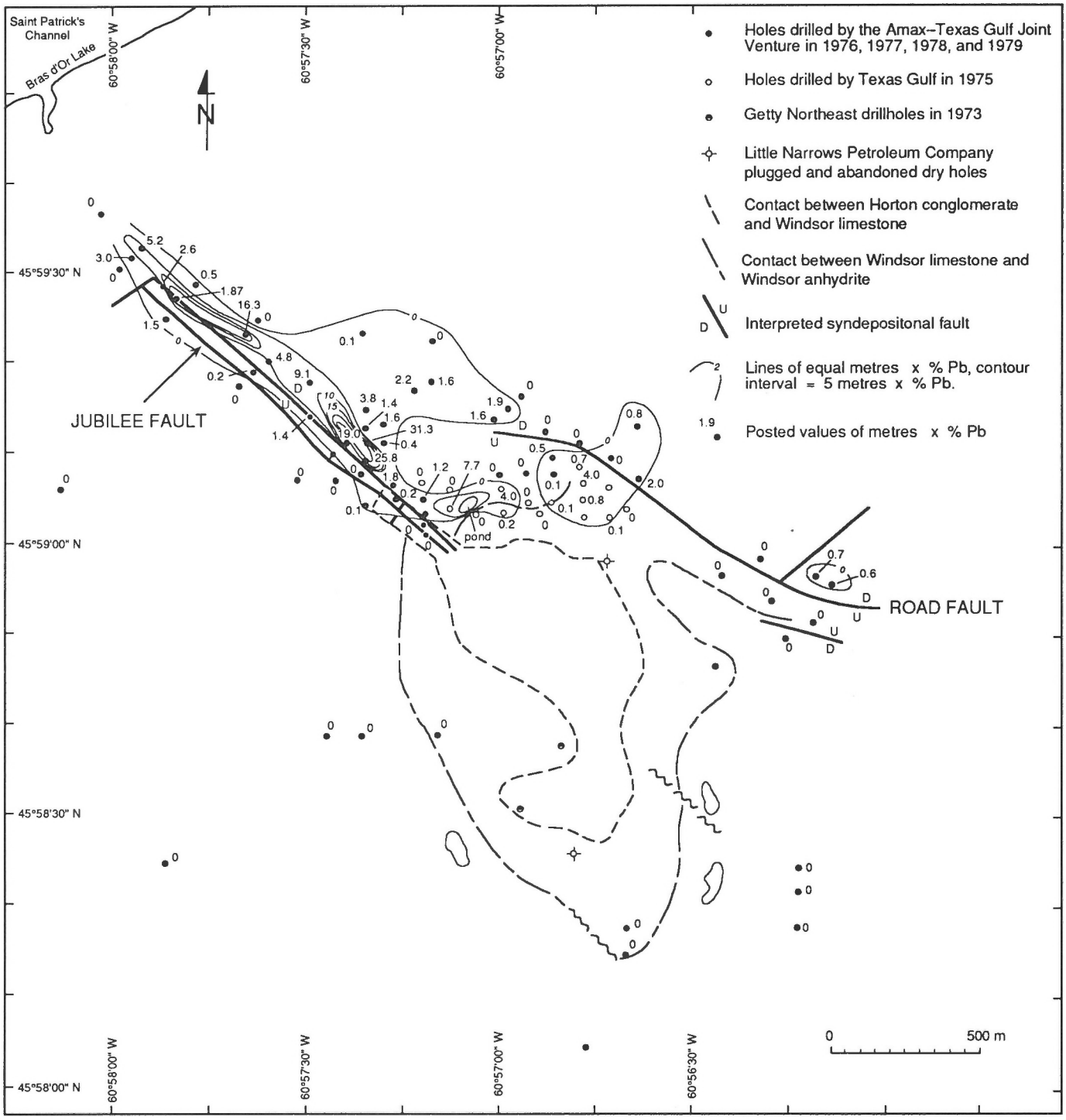

Figure 11. Metre per cent Pb, Jubilee deposit; U indicates relative upward fault displacement, D indicates relative downward fault displacement.

7) Porosity was maintained by a pore fluid of liquid and gas hydrocarbons.

8) Zinc-, lead-, and barium-bearing hydrothermal fluid (basinal brine from deeper and hotter parts of the basin or epigenetic basement fluid) was introduced into the reservoir.

9) Metal sulphide precipitation occurred when the metal-bearing fluid reacted with the sulphide sulphur or sulphur-bearing hydrocarbon. Carbonate dissolution (pH decreased as metal reacted with H_2S) further increased porosity (hydrothermal brecciation).

10) Completion of the reactions resulted in precipitation of sulphate (barite or anhydrite) and carbonate. At Jubilee there was sufficient hydrocarbon to partially fill the remaining porosity.

MINERALIZATION MODELS: DISCUSSION AND CONCLUSIONS

The importance of liquid hydrocarbons in sulphide deposition is not known with certainty. They could have provided a reductant for mineralizing fluids, a media for biogenic and abiogenic sulphur production from sulphate at the deposition site, and a media to preserve porosity for mineralizing fluids if the geometry of the reservoir was that of an oil trap prior to economic mineral precipitation. If the latter were important, economic mineral accumulation should be favoured in the localization of premineralization oil accumulations. Although the drilling density is insufficient to test this, contours of the base of the evaporite indicate closure around the thickest mineral-grade intersections (cf. Graves et al., 1989). If the hydrocarbons prove to be essential to the deposition of economic minerals or ground preparation of host rock, joint exploration for economic minerals and hydrocarbons may be a fruitful line of investigation.

Textural features obtained from drill core at the Jubilee deposit indicate that brecciation was caused by sulphate dissolution that predated sulphide mineralization. The brecciation is not associated with either early karst formation (soon after deposition) or karst formation of Tertiary age that controls the present landscape. Brecciation at Jubilee could be associated with subevaporite fluid flux that occurred early in the basin history or with thermal events of Permian or Triassic age (cf. Ravenhurst et al., 1989). Consequently, the brecciation at the Jubilee deposit must: 1) be younger than deposition of sufficient evaporite to seal the breccia porosity; 2) precede sulphide and calcite deposition (which filled much of the porosity); and, 3) predate the karst development which controls present topography.

Fluid localization along synsedimentary faults played a key role throughout the entire evolution of the Jubilee deposit. Although exploration company reports contain specific recommendations for drill sites to test for possible extensions of the Jubilee deposit, it is more interesting to consider the regional potential of Jubilee-type mineralization in the basal Windsor Group limestone. The best known exploration target in the Windsor Group carbonate is the biohermal carbonate buildups on sub-Windsor basement highs at the Gays River deposit (Akande and Zentilli, 1984). The Jubilee synsedimentary fault setting over thick Horton Group clastics opens much more of the Windsor/Horton contact for potential mineralization. The identification of the synsedimentary fault control is fundamental to successful exploration of Jubilee-type deposits.

ACKNOWLEDGMENTS

We thank Don F. Sangster of the Geological Survey of Canada (Ottawa), who initiated the study, arranged funding, and provided useful comments and guidance throughout the project. We recognize the essential co-operation of Fred J. Johnson, Vice President of Canamax Resources Inc. (Toronto) for assistance in the release of detailed reports and maps. To this end, Greg P. Isenor, a former Amax (Canamax) geologist, has been co-operative and helpful. He and Terry A. Goodwin of Seabright Resources Inc. (Lower Sackville, Nova Scotia), led a valuable field trip to the original Green Pond adit and showing, as well as other mineralized zones in the area. Marcos Zentilli and Casey Ravenhurst (Dalhousie University, Halifax), Sam Akande (University of Ilorin, Nigeria), and Al Sangster (Geological Survey of Canada, Ottawa) are thanked for their input dealing with mineralization in the Carboniferous of Nova Scotia. Debbie Kelley assisted in the fluid inclusion descriptions and thermometric data analysis.

Francis Kelly drafted the figures and Gerry Hickman assisted in word processing. Jim Langille of the Nova Scotia Department of Mines and Energy Core Storage Facility in Stellarton provided informed and enthusiastic co-operation during the core logging phases of this study.

REFERENCES

Akande, S.O. and Zentilli, M.
1984: Geological, fluid inclusion, and stable isotope studies of the Gays River lead-zinc deposit, Nova Scotia, Canada; Economic Geology, v. 79, p. 1187-1211.

Anderson, G.M.
1983: Some geochemical aspects of sulfide precipitation in carbonate rocks; in Proceedings of the International Conference on Mississippi Valley-Type Lead-Zinc Deposits, (ed.) G. Kisvarsanyi, S.K. Grant, W.P. Pratt, and J.W. Koenig; University of Missouri-Rolla, Rolla, Missouri, p. 61-76.

Barnes, H.L.
1983: Ore depositing reactions in Mississippi Valley-type deposits; in Proceedings of the International Conference on Mississippi Valley-Type Lead-Zinc Deposits, (ed.) G. Kisvarsanyi, S.K. Grant, W.P. Pratt, and J.W. Koenig; University of Missouri-Rolla, Rolla, Missouri, p. 77-85.

Bell, W.A.
1929: Horton-Windsor district, Nova Scotia; Geological Survey of Canada, Memoir 155, 268 p.
1944: Carboniferous rocks and fossil floras of northern Nova Scotia; Geological Survey of Canada, Memoir 238, 277 p.

Boehner, R.A.
1986: Salt and potash resources in Nova Scotia; Nova Scotia Department of Mines and Energy, Bulletin 5, 346 p.

Clifton, H.F.
1967: Solution-collapse and cavity filling in the Windsor Group, Nova Scotia, Canada; Geological Society of America Bulletin, v. 78, p. 819-832.

Frostick, L.E. and Reid, I.
1987: Tectonic control of desert sediments in rift basins ancient and modern; in Desert Sediments: Ancient and Modern, (ed.) L.E. Frostick and I. Reid; Geological Society of London, Special Publication No. 35, p. 53-68.

Frostick, L., Reid, I., Jarvis, J., and Eardley, H.
1988: Triassic sediments of the Inner Moray Firth, Scotland: early rift deposits; Journal of the Geological Society of London, v. 145, p. 235-248.

Gaucher, E.
1977: Drill hole induced polarization survey, Little Narrows, Cape Breton, Nova Scotia; Amax Potash Limited, Nova Scotia Department of Mines and Energy, Assessment File 11F/15C, 07-Q-09(02), 15 p.

Geldsetzer, H.H.J.
1977: The Windsor Group of Cape Breton Island, Nova Scotia; Geological Survey of Canada, Paper 77-1A, p. 425-428.

Giles, P.S.
1981: Major transgressive-regressive cycles in Middle to Late Visean rocks of Nova Scotia; Nova Scotia Department of Mines and Energy, Paper 81-2, 27 p.

Graves, M.C., Hein, F.J., and Ruffman, A.
1989: Geology of the Jubilee zinc-lead deposit, Victoria County, Cape Breton Island, Nova Scotia – supplementary data; Geomarine Associates Ltd., Halifax, Nova Scotia, Project 88-14, unpublished contract report, Geological Survey of Canada, Ottawa, 80 p.

Gustavson, T.C.
1974: Sedimentation on glacial outwash fans, Malaspina Glacier foreland, Alaska; Journal of Sedimentary Petrology, v. 44, p. 374-389.

Hamblin, A.P.
1988: A preliminary report on the sedimentology, tectonic control and resource potential of the Upper Devonian – Lower Carboniferous Horton Group, Cape Breton Island; in Current Research, Part B; Geological Survey of Canada, Paper 88-1B, p. 17-22.
1989a: Basin configuration, sedimentary facies, and resource potential of the Lower Carboniferous Horton Group, Cape Breton Island, Nova Scotia; in Current Research, Part B; Geological Survey of Canada, Paper 89-1B, p. 115-120.
1989b: Sedimentology, tectonic control and resource potential of the Upper Devonian – Lower Carboniferous Horton Group, Cape Breton Island, Nova Scotia; Ph.D. thesis, University of Ottawa, Ottawa, Ontario, 300 p.

Hein, F.J. and Walker, R.G.
1977: Bar evolution and development of stratification in the gravelly braided Kicking Horse River, B.C.; Canadian Journal of Earth Sciences, v. 14, p. 562-570.

Hein, F.J., Graves, M.C., and Ruffman, A.
1988: Geology of the Jubilee zinc-lead deposit, Victoria County, Cape Breton Island, Nova Scotia; Geological Survey of Canada, Open File 1891, 135 p.

Isenor, G.P., Stewart, E., and Chatterjee, A.K.
1980: Jubilee lead-zinc deposit; in Mineral Deposits and Mineralogenic Provinces of Nova Scotia, Field Trip 6, Field Trip Guidebook, Halifax '80, (ed.) A.K. Chatterjee et al.; Joint Annual Meeting of the Geological Association of Canada and the Mineralogical Association of Canada, p. 60-63.

Kelley, D.G.
1967: Baddeck and Whycocomagh map-areas, with emphasis on Mississippian stratigraphy of central Cape Breton Island, Nova Scotia (11K/2 and 11F/14); Geological Survey of Canada, Memoir 351, 65 p.

Kirkham, R.V.
1978: Base metal and uranium distribution along the Windsor-Horton contact central Cape Breton Island, Nova Scotia; in Current Research, Part B; Geological Survey of Canada, Paper 78-1B, p. 121-135.

Kulm, L.D., Suess, E., Moore, J.C., Carson, B., Lewis, B.T., Ritger, S.D., Kadko, D.C., Thornburg, T.M., Embley, R.W., Rugh, W.D., Massoth, G.J., Langseth, M.G., Cochrane, G.R., and Sammon, R.L.
1986: Oregon subduction zone: venting, fauna, and carbonates; Science, v. 231, p. 561-566.

Large, D.E.
1983: Sediment-hosted massive sulphide lead-zinc deposits: an empirical model; in Sediment-Hosted Stratiform Lead-Zinc Deposits, (ed.) D.F. Sangster; Mineralogical Association of Canada, Short Course Notes, p. 1-29.

Macqueen, R.W.
1986: Origin of Mississippi Valley-type lead-zinc ores by organic matter-sulfate reactions: the Pine Point example; in Organics and Ore Deposits, Proceedings of the Denver Region Exploration Geologists Society Symposium, (ed.) W.E. Dean; Denver, Colorado, p. 151-156.

Mayer, L.A., Shor, A.N., Hughs Clarke, J., and Piper, D.J.W.
1988: Dense biological communities at 3850 metres on the Laurentian Fan and their relationship to the deposits of the 1929 Grand Banks earthquake; Deep Sea Research, v. 35, p. 1235-1246.

McIlreath, I.A.
1977: Accumulation of a Middle Cambrian, deep-water limestone debris adjacent to a vertical, submarine carbonate escarpment, Southern Rocky Mountains, Canada; in Deep-Water Carbonate Environments, (ed.) H.E. Cook and P. Enos; Society of Economic Paleontologists and Mineralogists, Special Publication 25, p. 113-124.

Murphy, G.F.
1937: Gilmac Mine, Jubilee, Victoria County, Nova Scotia: Letters addressed to Gilbert D. Hedden (Chester, Nova Scotia) dated July 2, 20, 29 and August 9, 1937; Nova Scotia Department of Mines and Energy, Assessment File 11F/15C, 27-Q-09(00).

Ravenhurst, C.E., Reynolds, P.H., Zentilli, M., Krueger, H.W., and Blenkinsop, J.
1989: The formation of Carboniferous Pb-Zn and barite mineralization from basin-derived fluids, Nova Scotia, Canada; Economic Geology, v. 84, p. 1471-1488.

Ruckmick, J.C.
1986: Elemental sulfur deposits and their relation to metal sulfide deposits; in Organics and Ore Deposits, Proceedings of the Denver Region Exploration Geologists Society Symposium, (ed.) W.E. Dean; Denver, Colorado, p. 165-169.

Sangster, D.F.
1983: Mississippi Valley-type deposits: a geological melange; in Proceedings of the International Conference on Mississippi Valley-Type Lead-Zinc Deposits, (ed.) G. Kisvarsanyi, S.K. Grant, W.P. Pratt, and J.W. Koenig; University of Missouri-Rolla, Rolla, Missouri, p. 7-19.
1988: Breccia-hosted lead-zinc deposits in carbonate rocks, in Paleokarst, (ed.) N.P. James and P.W. Choquette; Springer-Verlag, New York, p. 102-116.

Schenk, P.E.
1969: Carbonate-sulfate-redbed facies and cyclic sedimentation of the Windsorian Stage (Middle Carboniferous) Maritime Provinces; Canadian Journal of Earth Sciences, v. 6, p. 1037-1066.

Smith, L. and Collins, J.A.
1979: Unconformities, sedimentary copper mineralization, and thrust faulting in the Horton and Windsor groups, Cape Breton Island and central Nova Scotia; Neuvieme Congres International de Stratigraphie et de Geologie du Carbonifere, Washington and Champaign-Urbana, v. 3, Southern Illinois University Press, p. 105-116.

Stewart, E.B.
1978: A study of the lead-zinc mineralization at Jubilee, Victoria County, Nova Scotia; M.Sc. thesis, Department of Geology, Acadia University, Wolfville, Nova Scotia, 190 p.

Sverjensky, D.A.
1981: The origin of Mississippi Valley-type deposits in the Viburnum trend southeast Missouri; Economic Geology, v. 76, p. 1848-1872.

Utting, J.
1980: Palynology of the Windsor Group (Mississippian) in a borehole at Stewiacke, Shubenacadie Basin, Nova Scotia; Canadian Journal of Earth Sciences, v. 17, p. 1031-1045.

Utting, J., Keppie, J.D., and Giles, P.S.
in press: Palynology and the age of the Lower Carboniferous Horton Group, Nova Scotia; in Contributions to Canadian Paleontology, Geological Survey of Canada, Bulletin.

von Bitter, P.H., Scott, S.D., and Schenk, P.E.
1988: Hydrothermal vent animals in carbonate mounds in bacterial laminites, Lower Codroy Group (Lower Carboniferous), Port au Port Peninsula, Newfoundland, Canada; Geological Association of Canada, Mineralogical Association of Canada, and Canadian Society of Petroleum Geologists Joint Annual Meeting, Program with Abstracts, St. John's, Newfoundland, p. A130.

Whisonant, R.C.
1987: Paleocurrent and petrographic analysis of imbricate intraclasts in shallow-marine carbonates, Upper Cambrian, southwestern Virginia; Journal of Sedimentary Petrology, v. 57, p. 983-994.

Radioelement mapping of parts of the Musquodoboit Batholith and Liscomb Complex, Meguma Zone, Nova Scotia [1]

K.L. Ford[2]

Ford, K.L., 1993: Radioelement mapping of parts of the Musquodoboit Batholith and Liscomb Complex, Meguma Zone, Nova Scotia; in Mineral Deposit Studies in Nova Scotia, Volume 2, (ed.) A.L. Sangster; Geological Survey of Canada, Paper 91-9, p. 71-111.

Abstract

Follow-up investigations in parts of the Musquodoboit Batholith and the eastern part of the Liscomb Complex of the Meguma Zone, Nova Scotia, confirm that airborne gamma ray spectrometry surveys can be a valuable aid in mapping large, composite granitic intrusions. Direct correlations were noted between the highest eU/eTh ratio values, as measured by the airborne surveys, and the most evolved phases, including some types of porphyry and small leucogranite bodies. The airborne radioelement distribution patterns suggest that the more evolved phases are more extensive than previously recognized. Correlations between the airborne and ground gamma ray spectrometric data and various petrographic and lithogeochemical indicators suggest that the elevated eU/eTh ratios are mainly a result of decreased levels of thorium, and/or increased levels of uranium, associated with increasing magmatic differentiation. This study and the studies of others also show that some of the more evolved phases of the peraluminous granites, which are characterized by unusually high eU/eTh ratios, also contain elemental variations that suggest varying degrees of late- and/or postmagmatic metasomatism and hydrothermal alteration. The common association of granophile-element mineralization with areas of pervasive alteration and anomalous radioelement signatures has important applications to mineral exploration.

Résumé

L'étude complémentaire de certaines parties du batholite de Musquodoboit et de la partie est du complexe de Liscomb de la zone de Meguma, en Nouvelle-Écosse, confirme que la spectrométrie gamma aéroportée peut s'avérer utile pour cartographier les grandes intrusions granitiques composées. On a observé des corrélations directes entre les rapports eU/eTh les plus élevés, mesurés au cours des levés aéroportés, et les phases les plus évoluées, y compris certains types de porphyres et des petits massifs de leucogranite. La répartition des radioéléments déterminée au cours des levés aéroportés porte à croire que les phases plus évoluées sont plus étendues que prévu. Les corrélations établies entre les données de spectrométrie gamma aéroportée et de spectrométrie gamma au sol et divers indicateurs pétrographiques et lithogéochimiques portent à croire que les rapports eU/eTh élevés sont principalement le résultat de teneurs réduites en thorium, de teneurs accrues en uranium, ou les deux, associées à une différenciation magmatique croissante. Cette étude et d'autres révèlent en outre que certaines des phases plus évoluées des granites hyperalumineux, qui se caractérisent par des rapports eU/eTh exceptionnellement élevés, présentent aussi des variations élémentaires qui semblent indiquer qu'il y a eu divers degrés de métasomatisme et d'altération hydrothermale tardimagmatiques ou postmagmatiques. L'association fréquente de la minéralisation en éléments granophiles et des zones d'altération pénétrative et de signatures radioélémentaires anormales revêt une certaine importance pour la prospection minérale.

[1] Contribution to the Canada-Nova Scotia Mineral Development Agreement, 1984-1989. Project carried by the Mineral Resources Division, Geological Survey of Canada, Project 840062.

[2] Mineral Resources Division, Geological Survey of Canada, 601 Booth St., Ottawa, Canada, K1A 0E8

INTRODUCTION

Between 1976 and 1986, the Geological Survey of Canada systematically collected approximately 46 000 line kilometres of 1 km line spaced airborne gamma ray spectrometric data over the Province of Nova Scotia (Ford et al., 1989). The general principles of gamma ray spectrometry, including instrumentation, electronics, and operational procedures, have been described elsewhere by Bristow (1979, 1983), Grasty (1979), Grasty et al., (1988, 1991), and Killeen (1979).

Previous studies (Chatterjee and Muecke, 1982; Ford, 1982; Ford and Ballantyne, 1983; Ford and O'Reilly, 1985; Ford and Carson, 1986; Corey, 1987; O'Reilly, 1988; O'Reilly et al., 1988) have demonstrated that variations in the radioelement concentrations and their associated ratios, as measured by airborne gamma ray spectrometry, are useful indicators of areas of specialization and associated mineralization within the granitic rocks of Nova Scotia. They have shown that these surveys can be used as reliable regional mapping tools, accurately reflecting various aspects of the regional bedrock and surficial geology.

The purpose of this paper is to demonstrate the application of gamma ray spectrometry (airborne and ground) as a suitable geophysical technique for mapping and subdividing various phases of a composite suite of granitic rocks, some of which may have undergone varying degrees of late- and/or postmagmatic metasomatism and hydrothermal alteration. This report will examine the relationship of radioelement distribution patterns, as measured by airborne gamma ray spectrometry and confirmed by ground gamma ray spectrometry, with some of the associated petrographic and lithogeochemical variations for selected parts of the Musquodoboit Batholith and eastern part of the Liscomb Complex of central Nova Scotia (Fig. 1).

REGIONAL GEOLOGY

The geology of mainland Nova Scotia south of the Cobequid-Chedabucto Fault Zone (Meguma Zone; Williams, 1978) consists of a thick sequence of Cambrian to Early Devonian metasedimentary and metavolcanic rocks intruded by a suite of Devono-Carboniferous peraluminous granitic rocks. This sequence is overlain by Carboniferous sedimentary and Triassic volcanic rocks.

Most metasedimentary rocks in the Meguma Zone belong to the Meguma Group. The older Goldenville Formation is composed predominantly of metawacke and quartzite with minor slate, and the younger Halifax Formation is composed predominantly slate with minor metawacke and quartzite. These rocks were deformed into a series of tight, upright east-northeast-trending folds

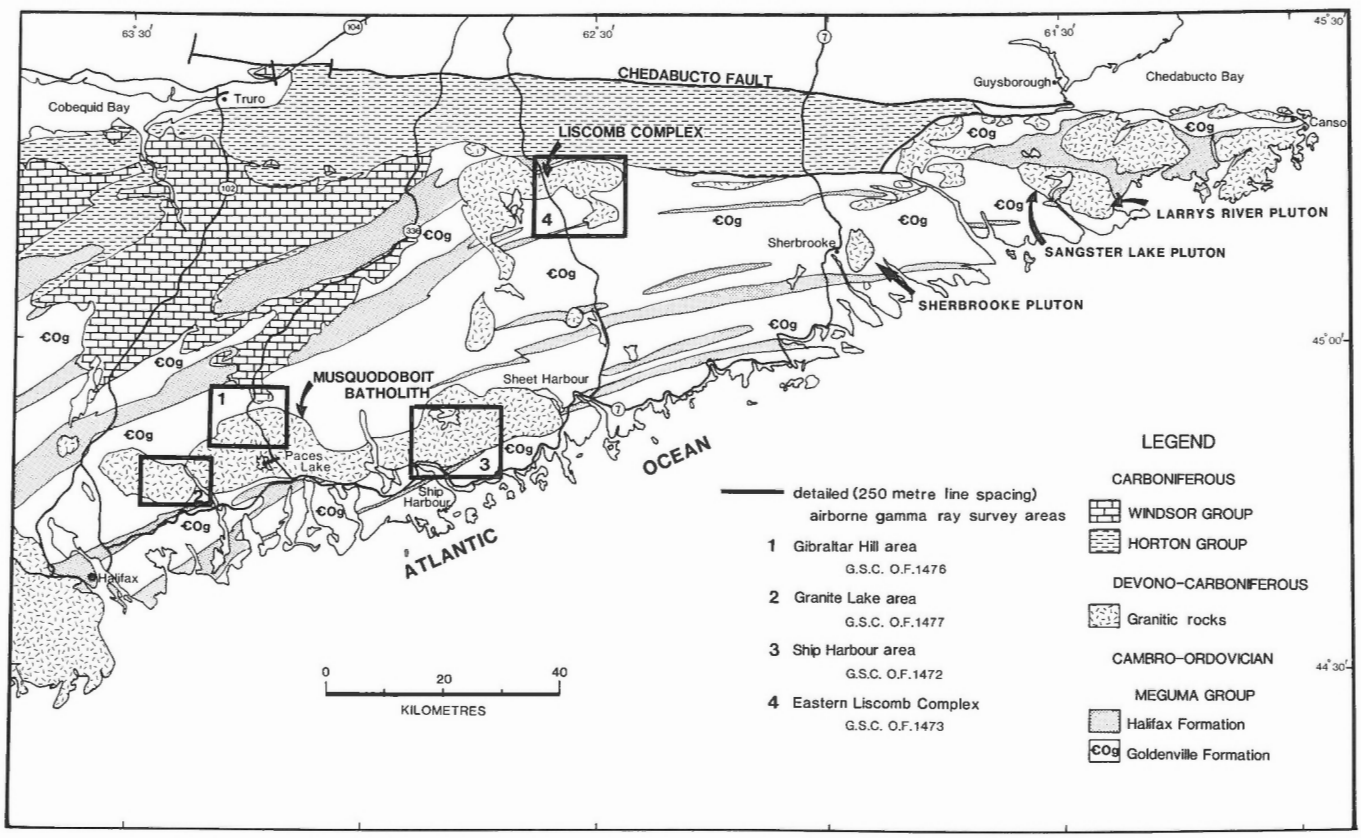

Figure 1. Geology of the eastern Meguma Zone showing the locations of the four detailed airborne gamma ray spectometric surveys.

during the Acadian Orogeny (Fyson, 1966). Regional greenschist-amphibolite grade metamorphism accompanied the middle to late stages of the Acadian Orogeny (Keppie and Muecke, 1979).

A suite of peraluminous granitic rocks are intruded discordantly into the Meguma Group. The largest of these granitic massifs is the South Mountain Batholith, which occupies an area of about 7300 km^2. MacDonald et al. (1992) summarized much of the recent work done on the granitic rocks of the South Mountain Batholith, which range in composition from tonalite to leucogranite with biotite monzogranite predominating.

Chatterjee and Muecke (1982) have documented the presence of a paraintrusive suite of rocks composed of biotite leucogranite, argillitized and sericitized granite, albitized granite, albitite, and various greisens, which they suggest are the product of the interaction of a fluid phase with residual magma and/or previously crystallized rock. This "specialized" paraintrusive suite of rocks, which is volumetrically quite small, is of particular interest because of a close spatial and genetic association with prominent Sn and U mineralization. Radiometric age determinations for the bulk of the granitoid units fall in the range of 370 ± 5 Ma (Clarke and Halliday, 1980; Reynolds et al., 1981, 1987). Recent work has produced younger ages in the 260-340 Ma range (O'Reilly et al., 1985) for granitic rocks associated with significant Sn and U mineralization (paraintrusive suite). Results of detailed Rb/Sr and $^{40}Ar/^{39}Ar$ analyses on rocks from the East Kemptville leucogranite by Kontak et al. (1989) suggest that the younger ages reflect the effects of variably pervasive tectonothermal events at 330, 300, and 250 Ma which postdate the emplacement at 370 Ma of the East Kemptville leucogranite and the associated mineralization.

In the eastern Meguma Zone (Fig. 1), the largest granitic massif is the Musquodoboit Batholith, covering an area of approximately 800 km^2. MacDonald and Clarke (1985) reported that the batholith is characterized by a restricted variety of rock types composed primarily of medium- to coarse-grained monzogranite intruded by two small, porphyritic aplites and numerous aplite and aplite-pegmatite dykes. MacMichael (1975) reported a $^{40}Ar/^{39}Ar$ age of 368.7 ± 3.2 Ma on biotite from a monzogranite.

The Liscomb Complex (Fig. 1) covers an area of approximately 350 km^2. Recent mapping of the western half of the complex (Giles and Chatterjee, 1987) documented a composite intrusion consisting of: (1) a suite of seven discrete plutons ranging from granodiorite to biotite monzogranite and leucocratic two-mica monzogranite; (2) a suite of high-grade metamorphic rocks composed of felsic and mafic gneisses; and (3) two xenolith-rich diatremes/breccia pipes of quartz-gabbro and quartz-diorite composition. Ford and Carson (1986) noted that the eastern half of the Liscomb Complex (referred to as the Governor Lake Pluton in older terminology) was composed predominantly of two-mica monzogranite and muscovite leucomonzogranite.

AIRBORNE GAMMA RAY SPECTROMETRIC SURVEYS

This investigation uses the results of airborne gamma ray spectrometric surveys with line spacings of 1 km and 250 m that were flown between 1976 and 1986 by the Geological Survey of Canada. Survey data were acquired with a high sensitivity gamma ray spectrometer system consisting of 50 litres of NaI detectors flown at a mean terrain clearance of 125 m at a ground speed of 190 km/h. Unless otherwise stated, the terms "low ratio" and "high ratio" refer to the eU/eTh ratio measured by airborne gamma ray spectrometry.

Charbonneau et al. (1976) noted that relationships between the airborne radioelement distribution patterns, which represent an averaged surface concentration, and corresponding bedrock concentrations depend on several factors: (1) the percentage of outcrop; (2) whether the overburden is derived locally and thus representative of the underlying bedrock, or from sources external to the survey area; and (3) the percentage of marshland or surface water, soil moisture, and density of vegetation within the field of view of the airborne spectrometer system. They concluded that these factors have the combined effect of diluting the airborne radioelement values of a particular area with respect to the corresponding bedrock values. However, relative radioelement concentrations are similar, so variations in the airborne ratios closely reflect the absolute variations in the radioelement ratios of the bedrock.

Examination of the airborne gamma ray spectrometric data from Nova Scotia indicates that areas of anomalously high radioactivity commonly correspond to areas underlain by granitic rocks (Ford, 1982). An unusual feature of the radioelement distribution patterns in Nova Scotia is the extensive areas of granitic rocks characterized by high eU/eTh ratios compared with the normal crustal ratio of 0.25 (Clarke et al., 1966). These high ratio areas correspond to portions of composite batholiths or plutons and are the result of the cumulative effects of varying intensities of increased magmatic differentiation and/or late- or postmagmatic metasomatism and hydrothermal alteration (Ford and O'Reilly, 1985).

This study focuses primarily on an evaluation of the eU, eTh, and eU/eTh ratio patterns for selected portions of the Musquodoboit Batholith and the eastern half of the Liscomb Complex (Fig. 1). These radioelements generally show the greatest variation between and within the granites of the Meguma Zone and commonly permit subdivision of the granites despite little or no recognizable petrographic or textural variation. Within the eastern Meguma Zone, five areas were selected to study airborne and in situ radioelement distribution patterns and the associated petrographic and lithogeochemical variations. Four of these areas, shown on Figure 1, have been covered by airborne gamma ray spectrometric surveys flown with line spacings of both 1 km and 250 m. These include: Granite Lake; Gibraltar Hill; Ship Harbour-Tangier Grand Lake; and the eastern part of the Liscomb Complex. A fifth area, the Paces Lake area, was covered at a line spacing of 1 km only.

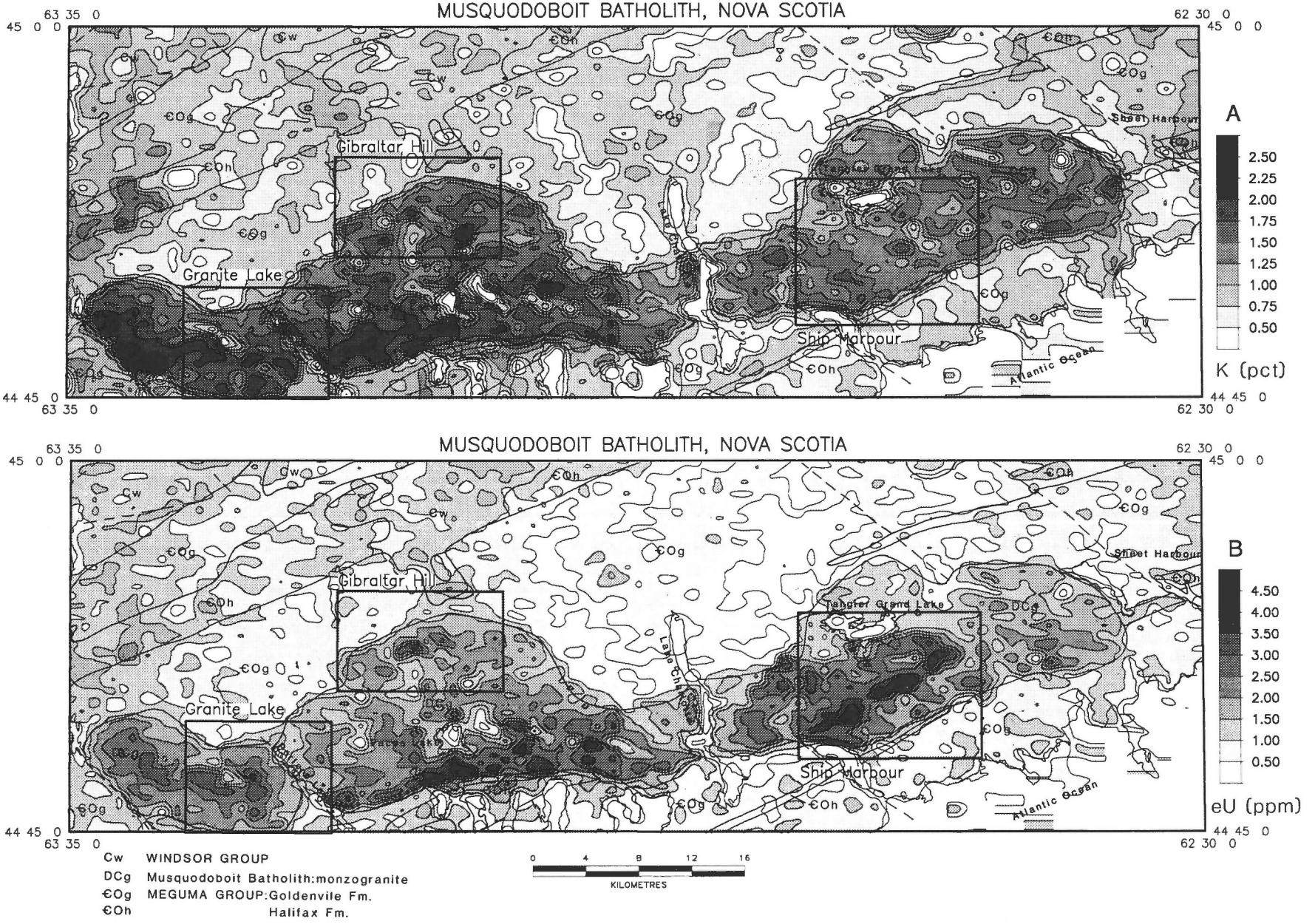
MUSQUODOBOIT BATHOLITH, NOVA SCOTIA
63 35 0
62 30 0
45 0 0
44 45 0
Gibraltar Hill
Granite Lake
Ship Harbour
Sheet Harbour
Atlantic Ocean
Cw
€Og
€Oh
A
2.50
2.25
2.00
1.75
1.50
1.25
1.00
0.75
0.50
K (pct)
MUSQUODOBOIT BATHOLITH, NOVA SCOTIA
B
4.50
4.00
3.50
3.00
2.50
2.00
1.50
1.00
0.50
eU (ppm)
Cw WINDSOR GROUP
DCg Musquodoboit Batholith:monzogranite
€Og MEGUMA GROUP:Goldenvile Fm.
€Oh Halifax Fm.
0 4 8 12 16
KILOMETRES

Figure 2A, B

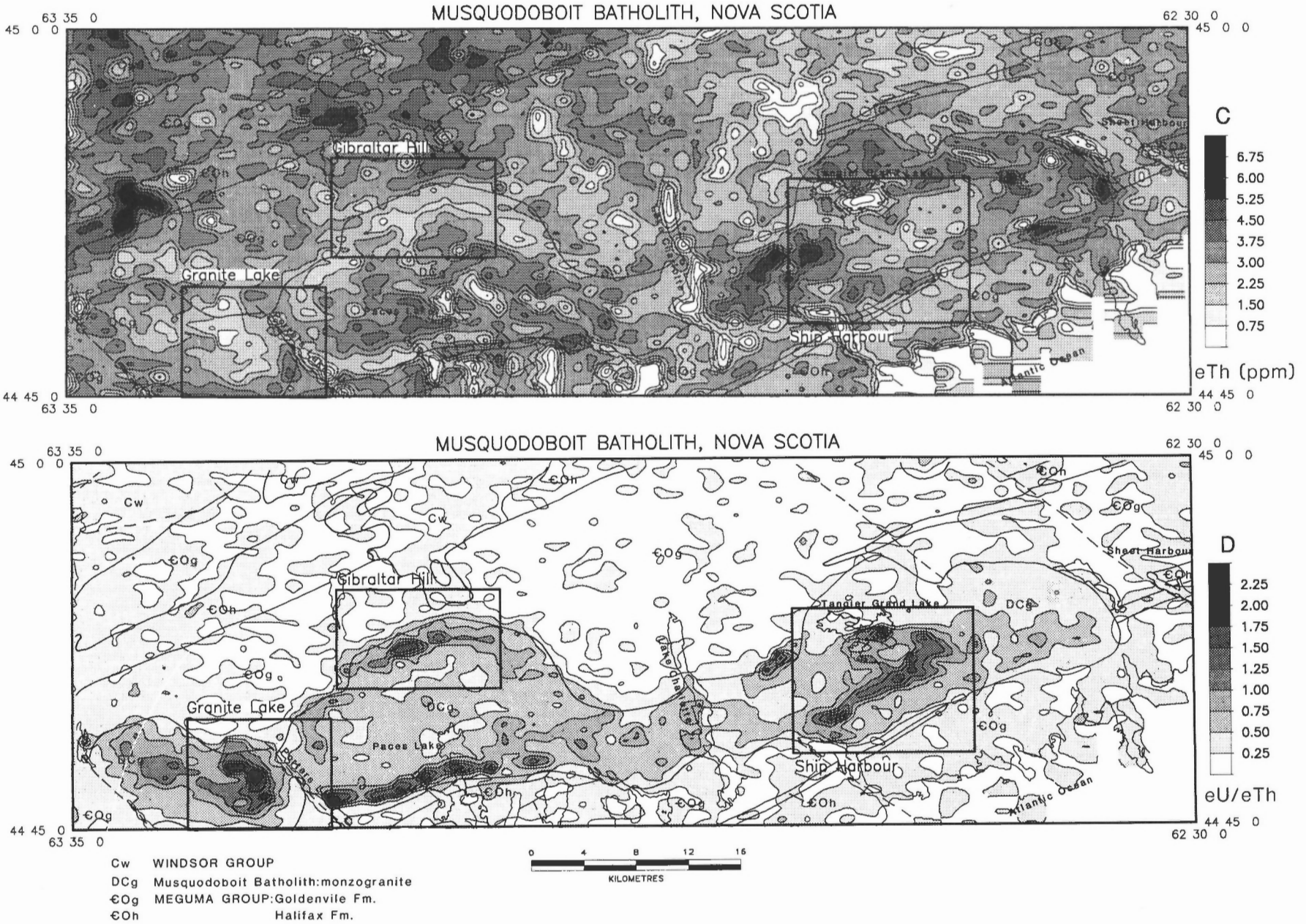

Figure 2. Radioactivity maps for the Musquodoboit Batholith compiled from 1 km line spaced airborne gamma ray spectrometric data; A) K(pct); B) eU (ppm); C) eTh (ppm); D) eU/eTh ratio.

Each area has high (>1.0) eU/eTh ratios which occur at (Paces Lake) or near (Gibraltar Hill) contacts with the Meguma Group metasedimentary rocks, or well within the granitic intrusions (Granite Lake and Ship Harbour-Tangier Grand Lake areas).

MUSQUODOBOIT BATHOLITH

Regional airborne gamma ray spectrometric surveys

As documented on the Radioactivity Maps of Nova Scotia (Ford et al., 1989), the Musquodoboit Batholith contrasts sharply with metawacke and quartzite of the Goldenville Formation and displays significant internal radioelement variation. Airborne K concentrations (Fig. 2A) are highest (1.75-2.25% K) over the southern halves of the western and central parts of the batholith west of Lake Charlotte, moderate in the northern halves of each area (1.50-1.75% K), and lowest (1.25-1.75% K) east of Lake Charlotte. As shown by other authors, (Charbonneau et al., 1976; O'Reilly et al., 1988), till provenance and thickness can influence the airborne gamma ray spectrometric estimate of bedrock composition. It is possible that the lower K concentrations over the northern halves of the western and central parts of the batholith result from the incorporation of quartzite till, derived from the Goldenville Formation north of the batholith, into the local granite till overlying these areas of the batholith. Stea and Fowler (1979) mapped a quartzite till south of the granite/sediment contact along the northern margins of the batholith for distances of up to 2 km from the contact. The moderate K concentrations over the eastern part of the batholith may be the result of thicker till cover, less outcrop, and a slightly larger proportion of foreign (nongranitic) material in the overburden (R.R. Stea, pers. comm., 1991). Although the incorporation of foreign material into the local granite till has a diluting effect, the bedrock geological contacts, in particular the northern contacts, are sharply defined by the airborne gamma ray spectrometric data.

Elevated eU concentrations within the batholith (Fig. 2B) are restricted to: 1) the central region of the western part of the batholith, west of Porters Lake; 2) the northern (Gibraltar Hill area) and southern (Paces Lake area) margins of the central part of the batholith; and 3) the central region of the eastern part of the batholith between Ship Harbour and Tangier Grand Lake. Maximum eU concentrations in these areas range from 3.4 ppm to 4.6 ppm. The remainder of the Musquodoboit Batholith is characterized by eU concentrations of 2.0 to 3.0 ppm with the exception of the eastern part of the batholith north of Tangier Grand Lake, where eU concentrations are noticeably lower, ranging from 1.0 to 2.0 ppm (Fig. 2B).

Most of the Musquodoboit Batholith contains low eTh concentrations (Fig. 2C) coincident with elevated eU values, as observed in large parts of other Meguma Zone granitoids. Minimum eTh concentrations for these areas are between 1.5 and 2.5 ppm. The remainder of the Musquodoboit Batholith has eTh concentrations between 2.0 and 5.0 ppm, with a maximum eTh concentration of just in excess of 6.0 ppm east of Lake Charlotte.

The eU/eTh ratio map for the Musquodoboit Batholith (Fig. 2D) highlights this inverse relationship between eU and eTh. Areas of the batholith characterized by elevated eU concentrations and lower eTh concentrations have maximum eU/eTh ratio values that range from 1.50 to 3.25. The remainder of the batholith contains a more restricted range of ratio values, from 0.25 to 0.75. The maximum ratio values are similar to those elsewhere within the Meguma Zone (i.e. Sangster Lake, New Ross, East Kemptville) where granitic rocks have been affected by pervasive, late- and/or postmagmatic metasomatism and hydrothermal alteration (Ford and O'Reilly, 1985; O'Reilly et al., 1988).

Detailed airborne gamma ray spectrometric surveys

Detailed (250 m line spaced) airborne gamma ray spectrometric surveys flown in the Granite Lake, Gibraltar Hill, and Ship Harbour-Tangier Grand Lake areas (Geological Survey of Canada, 1987b, c, d) not only provide increased resolution of radioelement distribution patterns outlined previously by 1 km line spacing surveys (Fig. 2A, B, C, D) but they also highlight features not defined by the earlier surveys.

The 1.0 contour on the eU/eTh ratio map for each area in this study is used as an approximate division between low and high ratio areas or phases of the batholith. This is approximately twice the average ratio value for the Musquodoboit Batholith and four times the average crustal ratio of 0.25 (Clark et al., 1966).

In the Granite Lake area (Fig. 3A), eU/eTh ratio contrasts (Fig. 3B) permit subdivision of this part of the batholith into a central core characterized by elevated eU/eTh ratios (maximum 2.5), and a marginal zone containing low eU/eTh ratios (average 0.50). In the marginal zone average eU and eTh concentrations are 2.0 and 3.5 ppm respectively, whereas in the core zone eU concentrations reach a maximum of 5.0 ppm and eTh concentrations diminish to a minimum of 1.2 ppm.

In the Gibraltar Hill area (Fig. 4A), the 1.0 contour on the eU/eTh ratio map (Fig. 4B) defines an almost continuous arcuate zone which, for more than 10 km, parallels the northern contact of the granite with the Meguma Group metasedimentary rocks. The axis of this zone is situated between 1 and 1.5 km from the contact and the zone varies from 0.5 to 1 km wide. Within this zone are several discrete high eU/eTh ratio anomalies with values greater than 2.0 and a maximum of 2.85. On the eU/eTh ratio map compiled from the regional 1 km line spaced data (Fig. 2D), the high ratio zone continues westward, parallel to the granite-Meguma Group contact, to a location just east of Porters Lake, where it bends southward, parallel to the shoreline of the lake. This 20 km long Gibraltar Hill zone is offset to the south along a northwest-trending sinistral fault which crosses the southwest corner of the detailed survey area. A recent aeromagnetic survey (Geological Survey of Canada, 1986a, b) confirms this offset, which may be as much as 1.5 km.

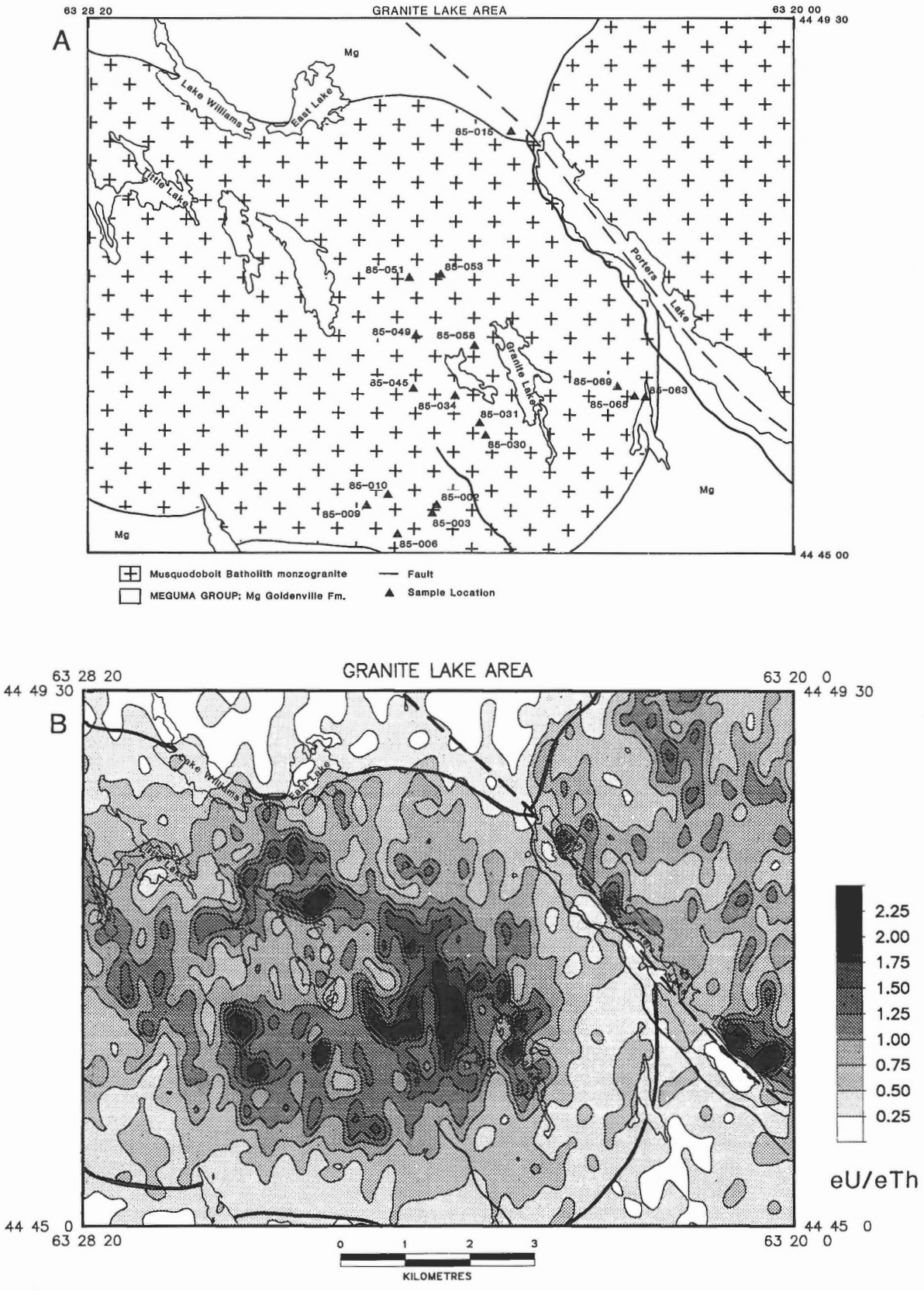

Figure 3. A) Geology of the Granite Lake area (Keppie, 1979) with B) airborne gamma ray spectrometric data for the eU/eTh ratio collected with a line spacing of 250 m (Geological Survey of Canada, 1987c).

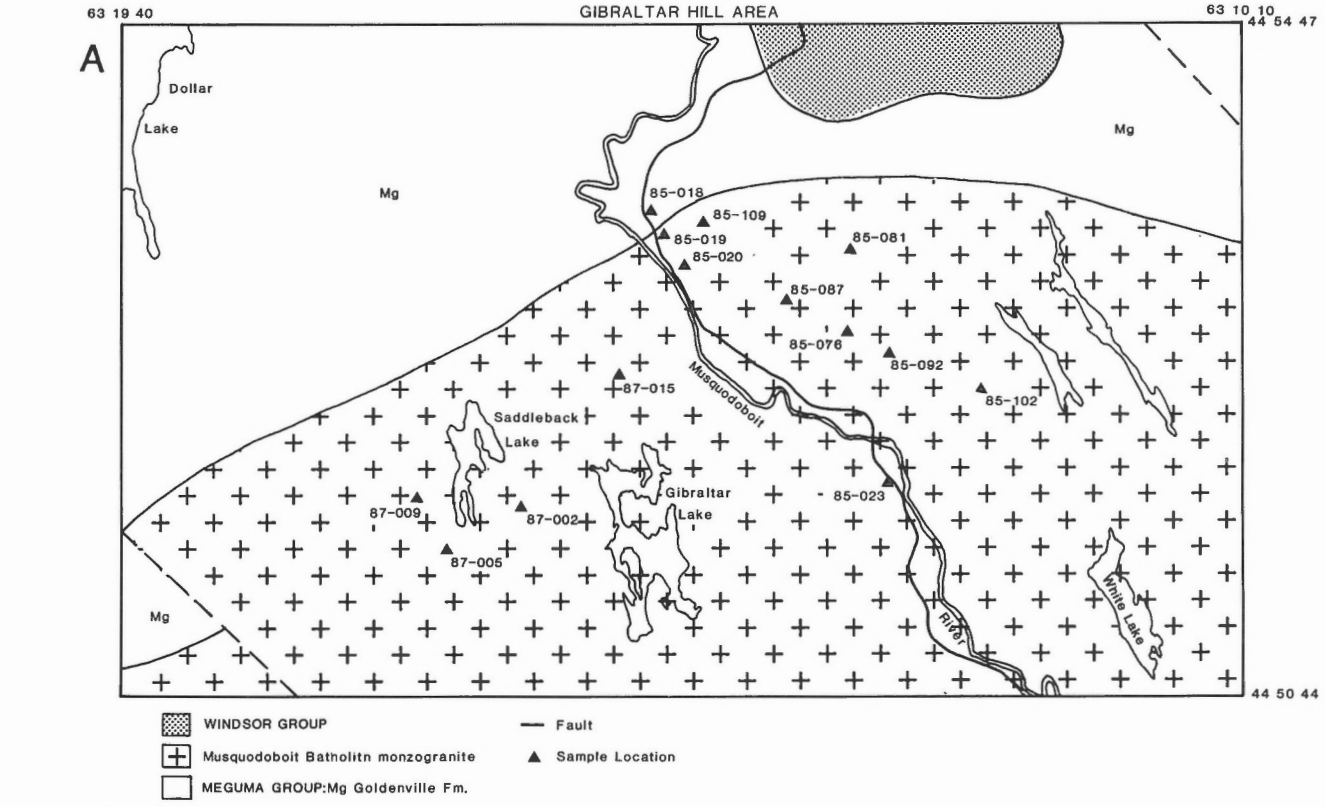

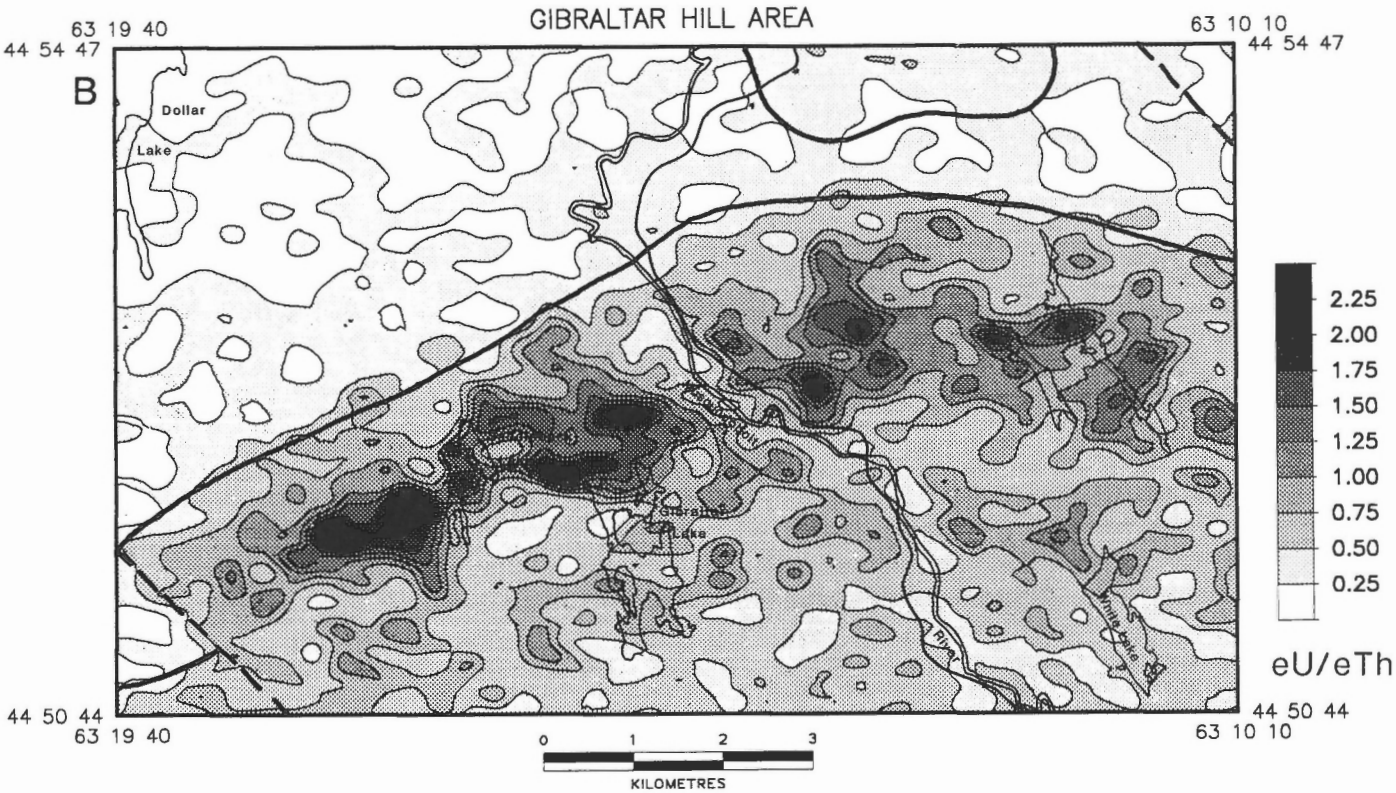

Figure 4. A) Geology of the Gibraltar Hill area (Keppie, 1979) with B) airborne gamma ray spectrometric data for the eU/eTh ratio collected with a line spacing of 250 m (Geological Survey of Canada, 1987b).

One to 1.5 km south of the main eU/eTh ratio anomaly, a series of small, discontinuous eU/eTh ratio anomalies define a second, parallel, less anomalous zone. As discussed for the Granite Lake area, the high eU/eTh ratio zone contains elevated eU concentrations (maximum 4.4 ppm) and low eTh concentrations (minimum 1.0 ppm). Adjacent areas of the batholith average 2.0 ppm eU, 3.5 ppm eTh, with an average eU/eTh ratio of 0.50.

In the Paces Lake area (Fig. 5A, B) the 1.0 eU/eTh contour compiled from regional, 1 km line spaced, airborne gamma ray spectrometric data outlines an 11 km long zone from west of Conrod Lake to east of Scots Lake. Isolated high eU/eTh ratio anomalies to the east and west of this zone extend the length to more than 17 km. Flight line profile data show that the zone width varies between 0.5 and 2.0 km and averages approximately 1.0 km. As in the Gibraltar Hill area this linear, high eU/eTh ratio zone parallels the granite-Meguma Group contact but unlike the Gibraltar Hill area it occurs at the contact. As observed in the Gibraltar Hill and Granite Lake areas, the high eU/eTh ratios (maximum 1.90) are the results of elevated eU (maximum 4.0 ppm) combined with lower eTh concentrations (minimum 2.0 ppm). Adjacent areas of the batholith average 2.5 ppm eU, 4.0 ppm eTh, with eU/eTh ratios between 0.50 and 0.75.

In the Ship Harbour-Tangier Grand Lake area, four radioelement zones are apparent (Fig. 6A, B, C, D). The most prominent zone is characterized by high eU/eTh ratios (maximum 2.80), high eU (maximum 6.2 ppm), and low eTh (minimum 1.0 ppm). This 13 km long zone extends northeasterly from southwest of Trout Lake to northeast of O'Brien Lake. Additional elevated eU/eTh ratio values extend westward along the southern shore of Tangier Grand Lake for an additional 6 km. The northeast-trending part of this high eU/eTh ratio zone subparallels the southeastern granite-Meguma Group contact.

A second radioelement zone forms a roughly triangular shaped area northwest of the high eU/eTh ratio zone and south of Tangier Grand Lake. This zone is characterized by variable eU and eTh concentrations that increase gradually from O'Brien Lake in the east to the west side of the survey area. Compared with the high eU/eTh ratio zone, this zone contains higher eTh and slightly lower eU and eU/eTh ratio values between 0.50 and 0.75. The highest concentrations occur in the Acadia Lake area northwest of Trout Lake where values of 4.0 ppm eU and 7.0 ppm eTh are contoured.

A third radioelement domain is situated between the high eU/eTh ratio zone and the granite-Meguma Group contact to the southeast. This zone has relatively low eU, variable eTh, and eU/eTh ratio values between 0.50 and 0.75, with the exception of a series of weak, isolated ratio highs that occur along the granite-Meguma Group contact between Ship Harbour and the east end of Tangier Lake.

The fourth radioelement zone, situated north and west of Tangier Grand Lake, has anomalously low eU (average <2.0 ppm), low eU/eTh ratio values (0.25-0.50), and moderate eTh concentrations (4.5 ppm).

Compared with other areas of the Musquodoboit Batholith, the radioelement patterns in the Ship Harbour-Tangier Grand Lake area display greater variability, particularly for eU and eTh.

Geology

In general, the granitic rocks in the low eU/eTh ratio (<1.0) areas are dominated by a medium- to coarse-grained porphyritic, biotite monzogranite. High ratio areas are dominated by fine- to coarse-grained, heterogeneous, two-mica monzogranite, porphyry, aplite, and aplite-pegmatite dyke rocks. The high ratio granitic rocks display greater textural inhomogeneity, ranging from porphyritic to seriate to inequigranular to equigranular. Contact relationships between rock types with low and high ratios are enigmatic, ranging from gradational to sharp and intrusive.

The low ratio, porphyritic, biotite monzogranite is medium- to coarse-grained, and in places megacrystic, hypidiomorphic-granular. It is typically light grey and generally massive, although locally it may have a weak to strong foliation defined by parallel alignment of alkali-feldspar phenocrysts. Phenocryst content, which varies from 0% to 50% locally and averages between 5% and 15%, accounts for most textural variations (porphyritic (megacrystic) to seriate and inequigranular). A QAP plot (Fig. 7) indicates that all but one sample with a low eU/eTh ratio are monzogranitic in composition. Modal abundances were determined from point counting cut slabs stained for potassium feldspar only. All unstained feldspar was counted as plagioclase. In the eastern Musquodoboit Batholith samples from the three low ratio zones show only minor differences in their modal mineralogy except for samples from north of Tangier Grand Lake (Fig. 8A, C; 9B, D), which have higher biotite contents and contain low eU and eU/eTh ratio values.

The major constituents are quartz, alkali feldspar as perthitic phenocrysts and groundmass grains, plagioclase (occasional phenocrysts), and biotite (5-15% modal). Cordierite, which is invariably pinitized to some degree, locally occurs as an important constituent (up to 5% modal). Cordierite is abundant in the Paces Lake area and portions of the Ship Harbour-Tangier Grand Lake area, including parts of the high eU/eTh ratio domain and present only in trace amounts in the Granite Lake area. Although muscovite contents may equal biotite, biotite is typically the dominant micaceous phase. Accessory phases comprise cordierite, muscovite, chlorite as an alteration product of biotite, garnet, tourmaline, andalusite, apatite, zircon, and ilmenite. Monazite has been recognized recently by several authors (O'Reilly, 1988; M.A. MacDonald, pers. comm., 1991) as minute inclusions along with zircon in biotite. Inclusions are quite common in the biotite from the low ratio monzogranite of the Musquodoboit Batholith and it is possible that many of these are monazite.

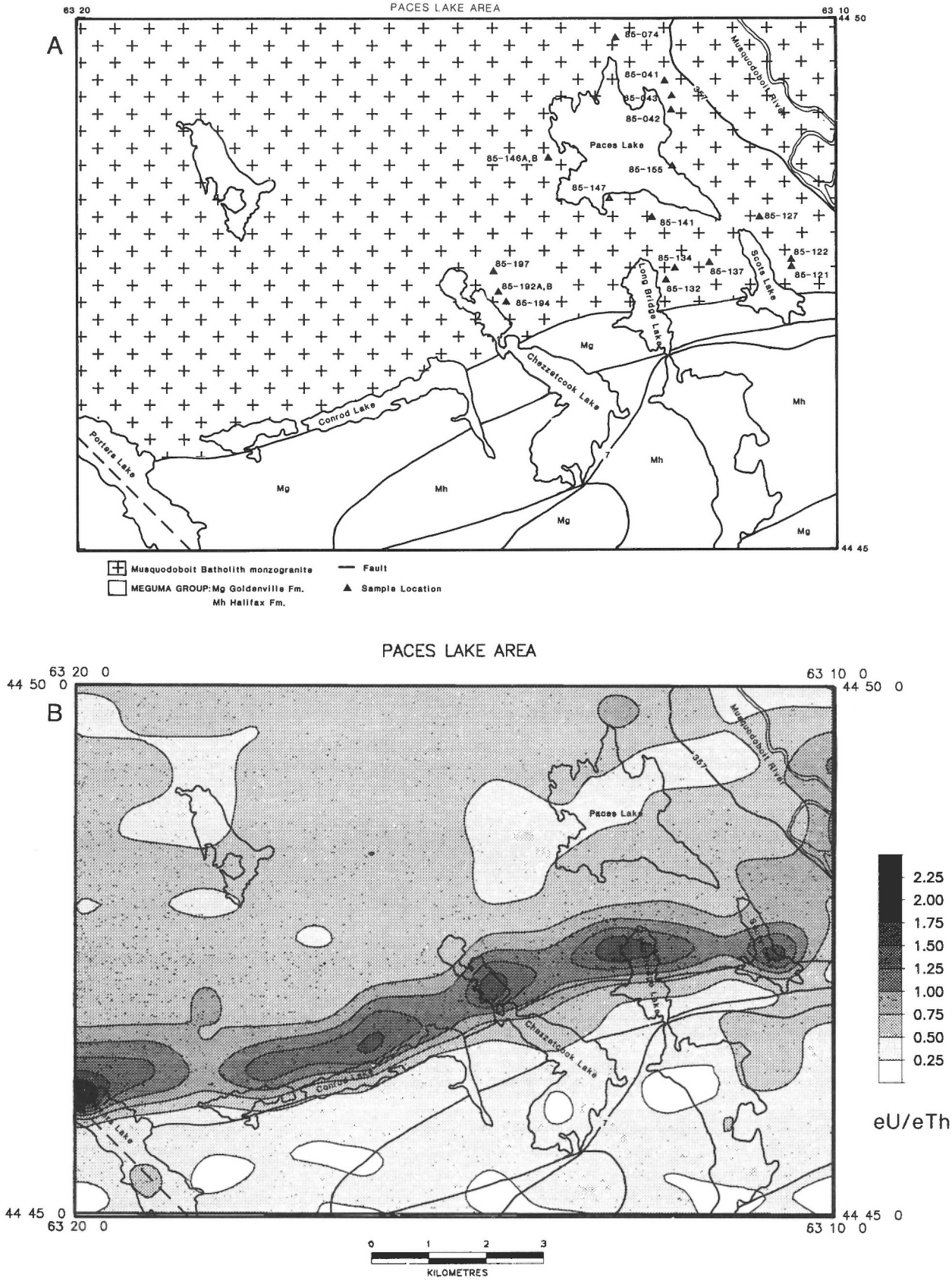

Figure 5. A) Geology of the Paces Lake area (Keppie, 1979) with B) airborne gamma ray spectrometric data for the eU/eTh ratio collected with a line spacing of 1 km (Geological Survey of Canada, 1982).

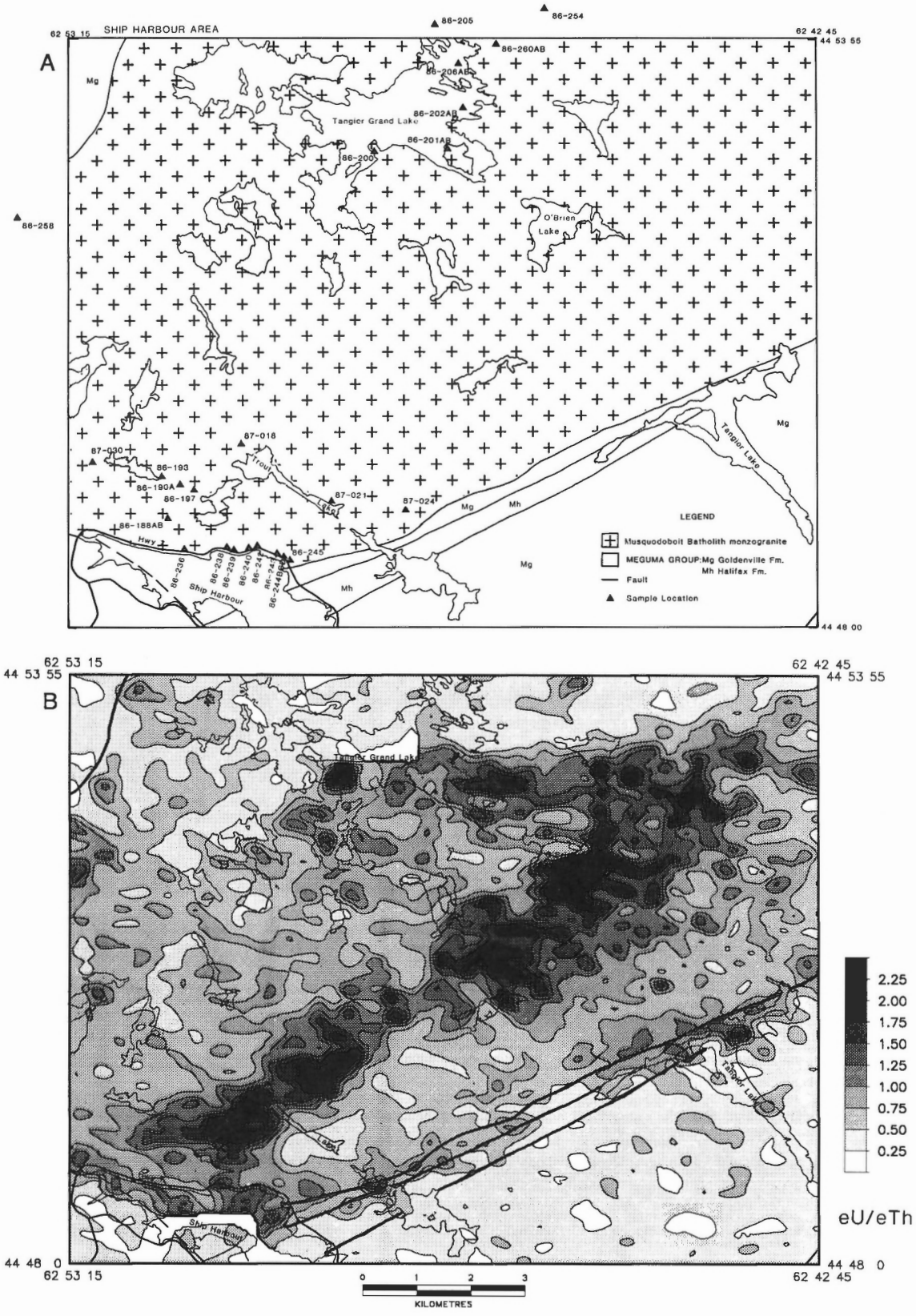

Figure 6. A) Geology of the Ship Harbour area (Keppie, 1979) with B) airborne gamma ray spectrometric data for the eU/eTh ratio, C) eU(ppm), and D) eTh(ppm) collected with a line spacing of 250 m (Geological Survey of Canada, 1987d).

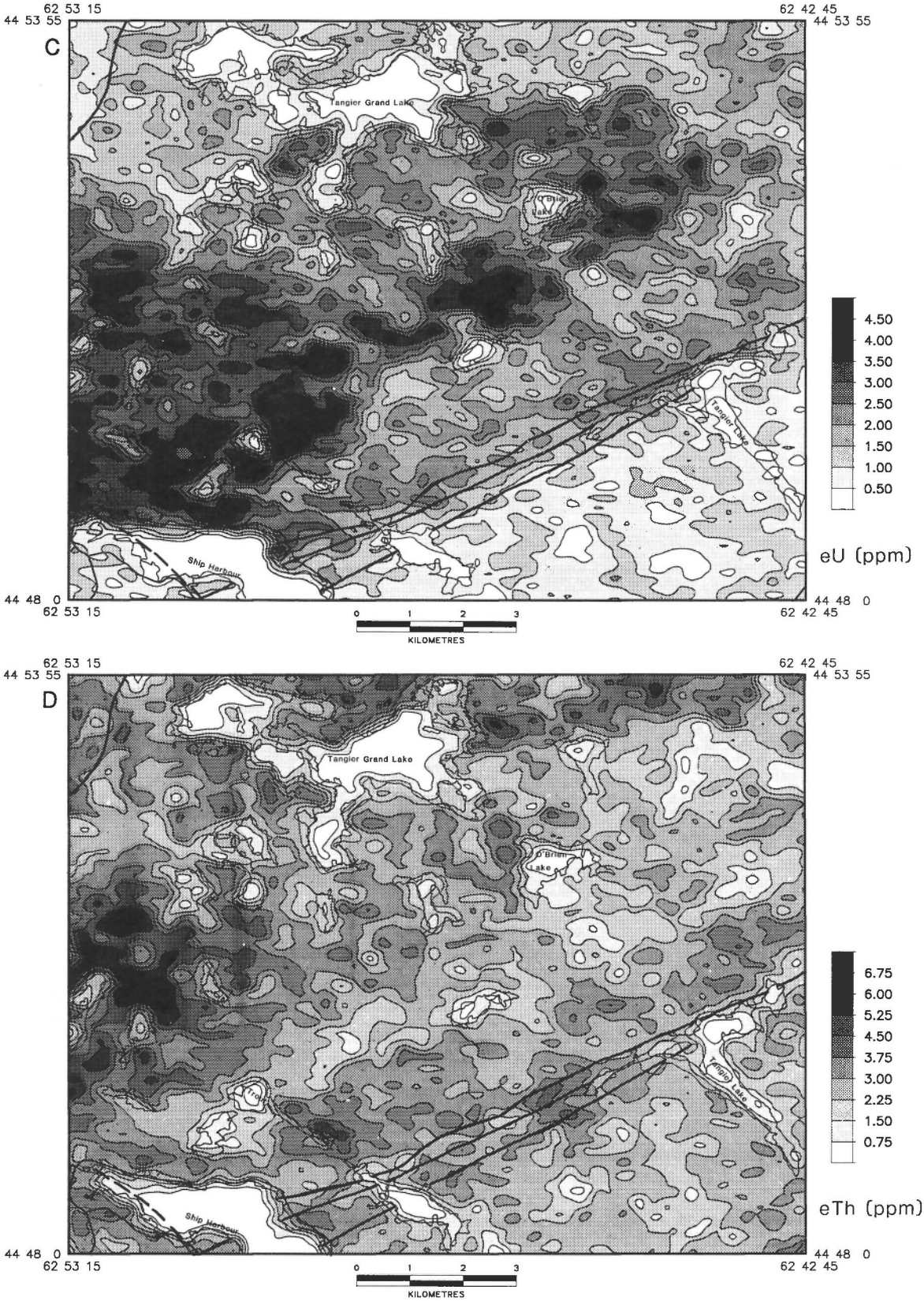
C
62 53 15
62 42 45
44 53 55
44 48 0
Tangier Grand Lake
O'Brien Lake
Tangier Lake
Ship Harbour
4.50
4.00
3.50
3.00
2.50
2.00
1.50
1.00
0.50
eU (ppm)
0 1 2 3
KILOMETRES
D
6.75
6.00
5.25
4.50
3.75
3.00
2.25
1.50
0.75
eTh (ppm)

Figure 6C, D

Minor rock types in the low ratio areas include aplite and aplite-pegmatite dykes, aplitic porphyry, fine- to medium-grained, equigranular biotite and muscovite-biotite monzogranite, and dykes and small intrusive bodies of leucomonzogranite. In the Ship Harbour and Tangier Grand Lake areas, aplite and aplite-pegmatite dykes are particularly abundant. Figure 6B shows a slight increase in eU/eTh ratio values along a part of Highway 7 that parallels Ship Harbour. This higher eU/eTh ratio area joins with the southern end of the main high eU/eTh ratio zone to the north and coincides with an area of abundant aplite and aplite-pegmatite dykes. Between the northeast corner of Paces Lake (Fig. 5A) and Highway 357 there are several large exposures of aplite with minor aplitic porphyry and a small unit of fine- to medium-grained, equigranular, muscovite-biotite leucomonzogranite. In the Granite Lake and Gibraltar Hill areas, minor rock types in the low eU/eTh ratio areas are restricted to a few, narrow aplite and aplite-pegmatite dykes.

In the Granite Lake area, monzogranite with a high eU/eTh ratio is typically light cream, massive, medium- to coarse-grained and weakly porphyritic (<5% alkali feldspar phenocrysts) to inequigranular and/or seriate. Figures 8A and 8B show the typical textural characteristics of monzogranite from the Granite Lake area with low and high eU/eTh ratios respectively. In general, the monzogranite with a high ratio shows a slight reduction in grain size and phenocryst content. A QAP plot (Fig. 7) of samples from areas with the high eU/eTh ratios indicates that all samples with high ratios are monzogranitic with respect to their modal mineralogy.

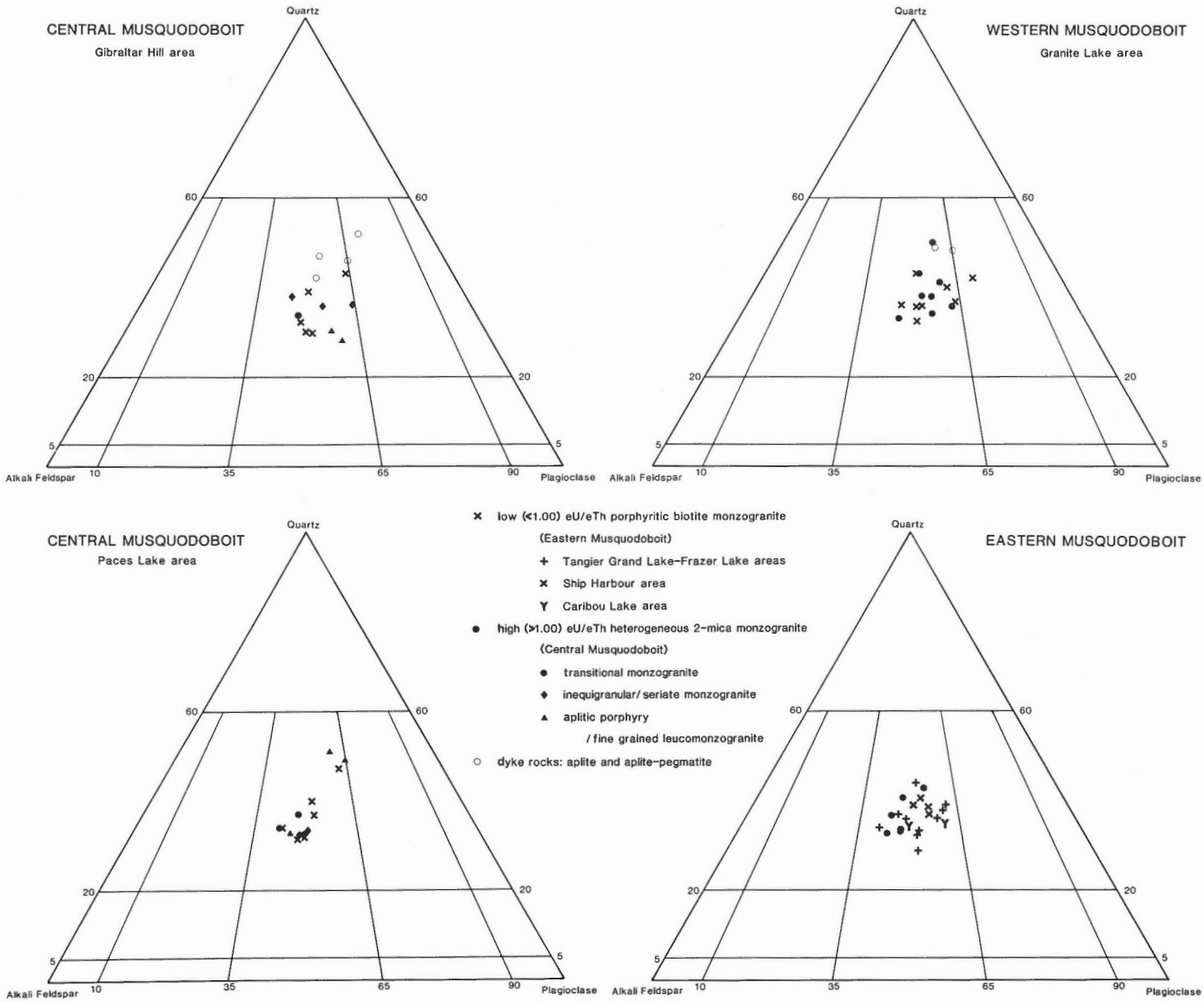

Figure 7. Modal compositions for the various low (<1.00) and high (>1.00) eU/eTh ratio monzogranites and associated dyke rocks from the Musquodoboit Batholith. Boundaries taken from Streckeisen (1976).

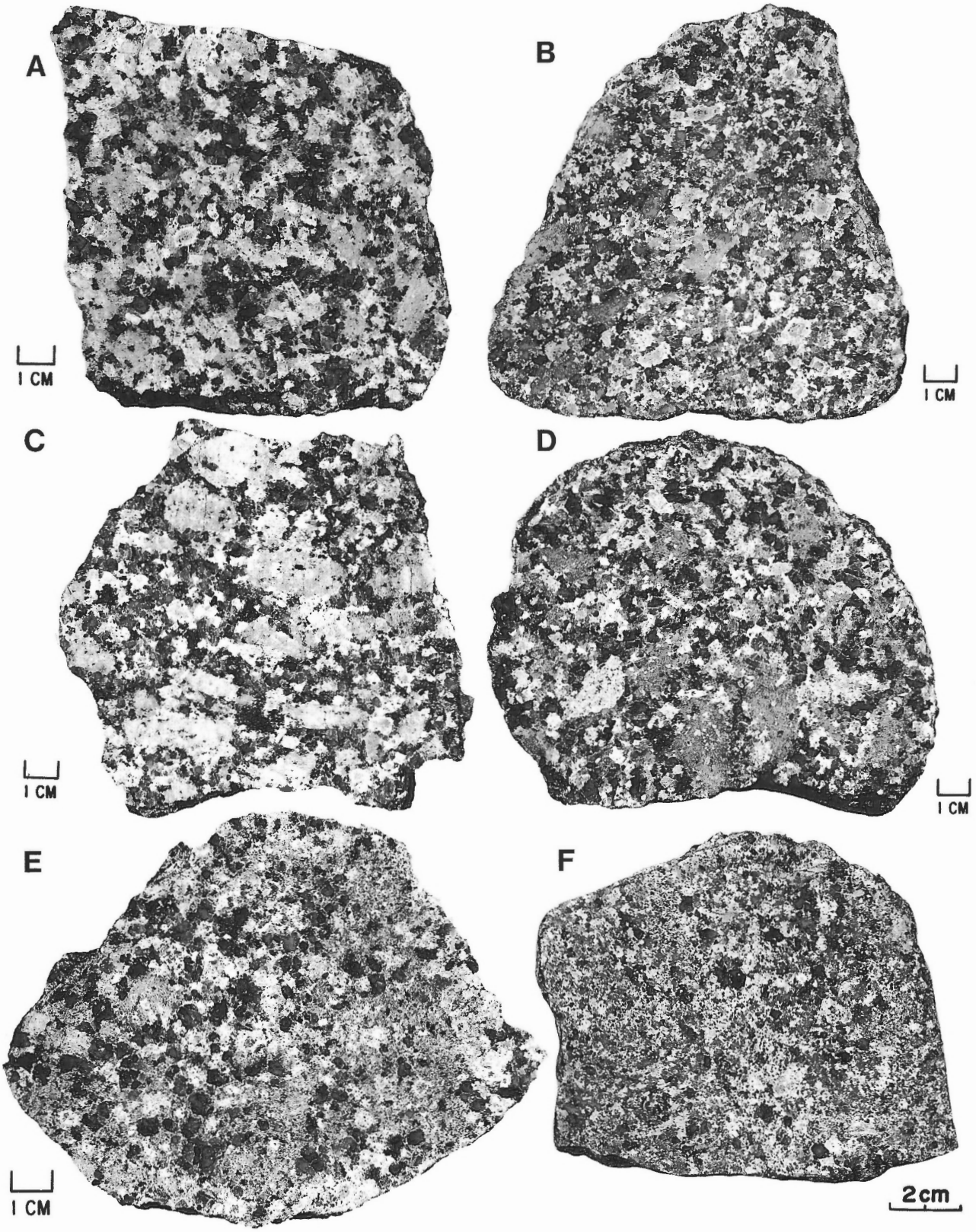

Figure 8. Stained slabs showing typical textural features for selected samples from the low (<1.00) and high (>1.00) eU/eTh ratio monzogranites and porphyries of the Musquodoboit Batholith A) Granite Lake, low eU/eTh ratio biotite monzogranite 85-002; B) Granite Lake, high eU/eTh ratio two-mica monzogranite 85-051; C) Gibraltar Hill, low eU/eTh ratio porphyritic, biotite monzogranite 85-109; D) Gibraltar Hill, high eU/eTh ratio, transitional two-mica monzogranite 85-076; E) F) Gibraltar Hill, high eU/eTh ratio, inequigranular to seriate monzogranite porphyry, E: 85-087; F: 87-009.

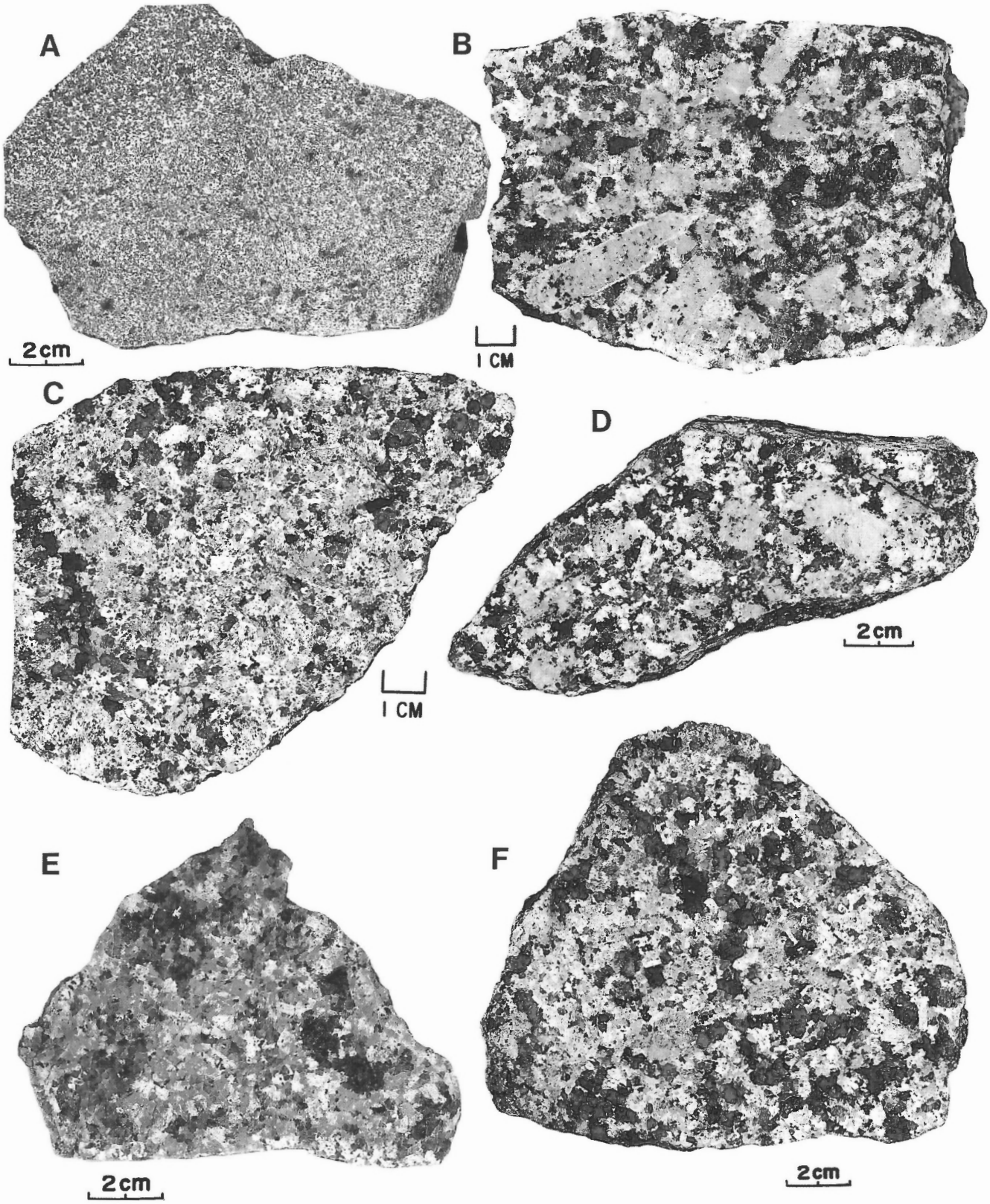

Figure 9. Stained slabs showing typical textural features for selected samples from the low (<1.00) and high (>1.00) eU/eTh ratio monzogranites and porphyries of the Musquodoboit Batholith, A) Gibraltar Hill, high eU/eTh ratio leucomonzogranite 87-005; B) Paces Lake, low eU/eTh ratio porphyritic, biotite monzogranite 85-141; C) Paces Lake, high eU/eTh ratio inequigranular monzogranite porphyry 85-192A; D) Ship Harbour area, low eU/eTh ratio, porphyritic, biotite monzogranite 85-202A; E), F) Ship Harbour area, high eU/eTh ratio two-mica monzogranite, E: 87-018; F: 86-258.

In the Gibraltar Hill and Paces Lake areas, monzogranite with a high ratio varies from grey to pale pink, is generally massive, and ranges from fine- to coarse-grained. In these areas, the granitic rocks are texturally heterogeneous and are grouped loosely into three types, based on their textural characteristics. The first is a transitional monzogranite (Fig. 8D), which in outcrop is often indistinguishable texturally from the porphyritic, biotite monzogranite with low eU/eTh ratios and appears to grade into the latter. This lithology varies texturally from medium- to coarse-grained, porphyritic (5% alkali feldspar phenocrysts) to medium grained, inequigranular and is similar to the monzogranite with high eU/eTh ratios from the Granite Lake area. A second type varies from fine- to medium-grained (in places coarse grained) and is typically inequigranular to seriate (Fig. 8E, F; 9C). This lithology appears to grade into the third type, an aplitic, quartz-feldspar porphyry, which is associated in some sites with a fine- to medium-grained, equigranular leucomonzogranite (Fig. 9A). The cores of many of the high eU/eTh ratio anomalies in the Gibraltar Hill and Paces Lake areas are occupied by a heterogeneous mixture of the three granitic rock types. The fine- to medium-grained, inequigranular to seriate monzogranite and porphyry, which are typical of the high eU/eTh ratio areas from Gibraltar Hill and Paces Lake, appear similar to the two small (<1 km^2) porphyritic aplite bodies described by MacDonald and Clark (1985). Correlations between these units and the airborne gamma ray spectrometric patterns suggest that they are more extensive than previously recognized, particularly in the Gibraltar Hill and Paces Lake areas, at or near the contacts between the Musquodoboit Batholith and Meguma Group.

In the eastern Musquodoboit Batholith, high ratio monzogranite is typically pale pink, massive, medium- to coarse-grained and generally inequigranular to weakly porphyritic (1-2% alkali feldspar phenocrysts; Fig. 9E, F). High ratio monzogranite from the eastern Musquodoboit Batholith does not show the same textural heterogeneity as monzogranite from the Gibraltar Hill and Paces Lake areas and is texturally similar to the transitional two-mica monzogranite from the Granite Lake area.

The major constituents of the high ratio monzogranite comprise quartz, alkali feldspar, plagioclase, muscovite, and less commonly biotite. In the fine- to medium-grained porphyry and seriate or inequigranular monzogranite, phenocrysts of quartz, alkali feldspar, less commonly plagioclase, and muscovite can occur in a fine- to medium-grained matrix of quartz, alkali feldspar, plagioclase, muscovite, and biotite. In the coarser grained, porphyritic to inequigranular (transitional) monzogranite, phenocrysts are composed primarily of alkali feldspar and less commonly plagioclase in a medium- to coarse-grained matrix of quartz, alkali feldspar, plagioclase, biotite, and muscovite. In the transitional monzogranite, typical of the Granite Lake, eastern Musquodoboit Batholith, and parts of the Gibraltar Hill and Paces Lake areas, the proportion of muscovite will generally be greater than or equal to the proportion of biotite. Biotite occurs as a minor constituent or is absent in the finer grained, seriate to inequigranular monzogranite and leucomonzogranite that occupy the core areas of many of the high ratio anomalies. Accessory phases include muscovite, biotite, cordierite, andalusite, garnet, tourmaline, zircon (monazite), apatite, and chlorite from alteration of biotite.

Lithogeochemistry

Several authors (Chatterjee and Muecke, 1982; Ford, 1982; Ford and Ballantyne, 1983; Ford and O'Reilly, 1985; Ford and Carson, 1986; Corey, 1987; O'Reilly, 1988; O'Reilly et al., 1988) have noted correlations between radioelement variations, in particular the U/Th ratio, and the enrichment or depletion of other major, minor, and selected trace elements. These correlations have generally been considered to be the result of the combined effects of magmatic differentiation and varying degrees of late- and/or postmagmatic alteration. Major and trace element variations from this study are consistent with these models.

The radioelement variations shown in Figure 10 verify the observed trends and patterns outlined by the airborne gamma ray spectrometric surveys. The mean values reflect the generally low eTh concentrations and high eU/eTh ratios which are characteristic of many of the Meguma Zone granites. Figure 10 shows a trend of generally increasing eU and decreasing eTh concentrations from the porphyritic, biotite monzogranite to the transitional two-mica monzogranite, porphyry, aplite, and aplite-pegmatite dyke rocks. The inequigranular and seriate phases have been included with the porphyry phase.

In general, the low ratio, porphyritic, biotite monzogranite from the Musquodoboit Batholith shows a restricted range of ratio values between 0.53 and 0.71. The biotite monzogranites from the Tangier Grand Lake and Frazer Lake areas of the eastern Musquodoboit Batholith are an exception, having a mean ratio value of 0.36, considerably less than other low ratio areas. The high ratio units, which include the transitional two-mica monzogranite, porphyry, aplite, and aplite-pegmatite dyke rocks, display a much greater range of ratio values than the low ratio porphyritic, biotite monzogranite. Mean ratio values range from 1.40 to 5.21, with the higher values associated with porphyry and dyke rocks. There is some overlap between individual analyses (Fig. 10) from the low and high ratio units. This overlap highlights the occurrence of gradational contacts between low ratio and high ratio units.

Tables 1 and 2 present analyses showing that all rock types from the Musquodoboit Batholith are peraluminous (A/CNK>1) and have major element chemistry and normative mineral compositions indicating that the low ratio porphyritic, biotite monzogranite is the least evolved rock type within the batholith (Fig. 11). Compared with the low ratio porphyritic, biotite monzogranite, the high ratio units show lower mean values for K_2O, CaO, total Fe, MgO, TiO_2, K/Rb, normative orthoclase, anorthite, enstatite, ferrosilite, magnetite, ilmenite, and colour index and higher mean values for SiO_2, Na_2O, P_2O_5, normative quartz, albite, apatite, differentiation index, and Na_2O/K_2O. Trace element variations show markedly lower mean values for Sr, Ba, Zr, Ce, La, and Th and higher mean values for Rb, Sn, and U in the high ratio units.

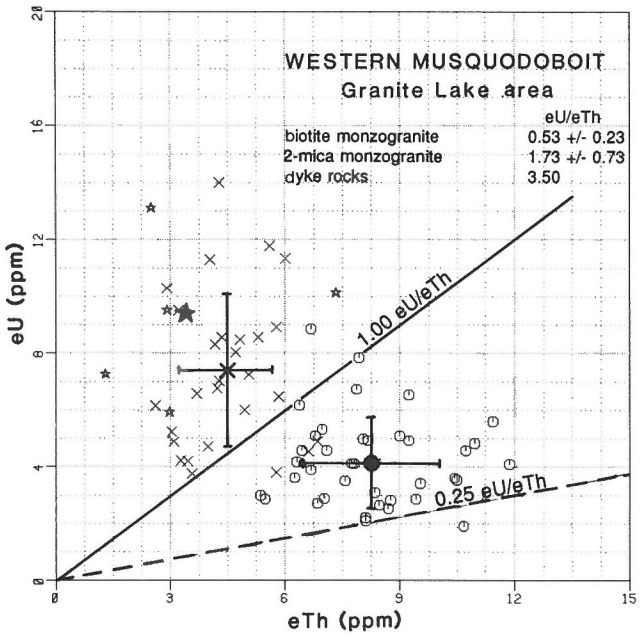

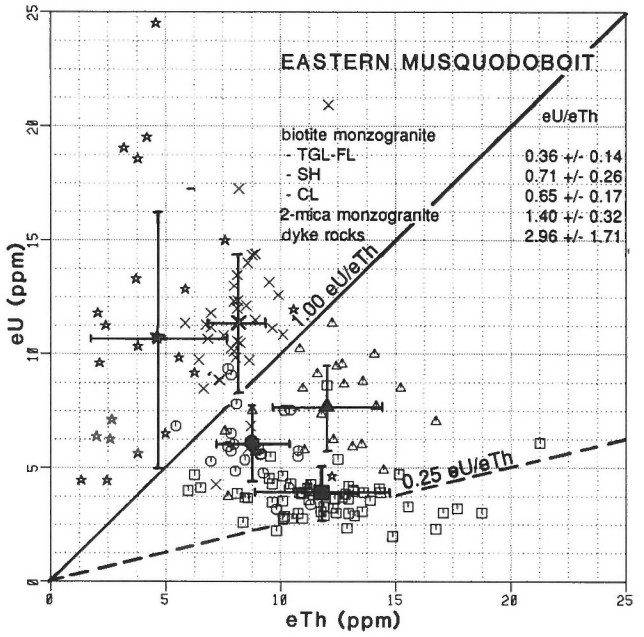

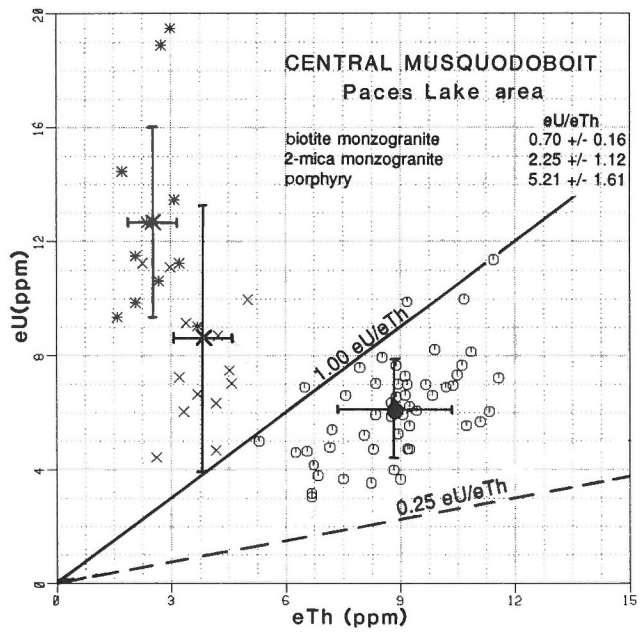

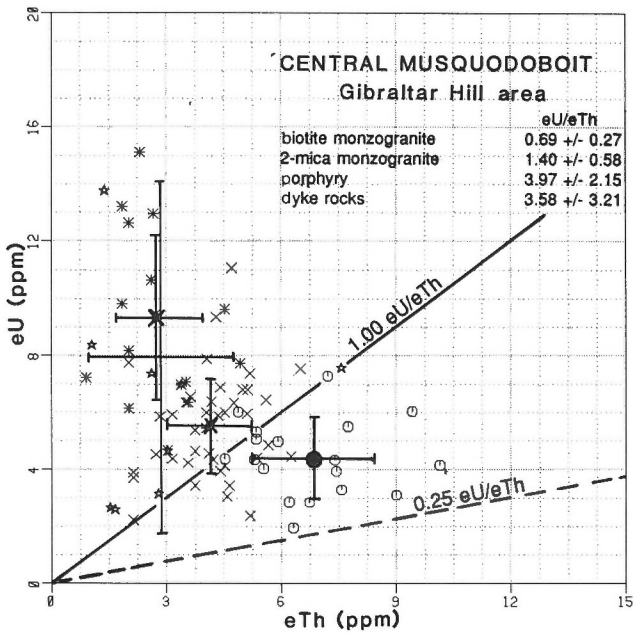

porphyritic biotite monzogranite

heterogeneous 2-mica monzogranite

porphyry

dyke rocks: aplite and aplite-pegmatite

Eastern Musquodoboit

porphyritic biotite monzogranite - Tangier Grand Lake - Frazer Lake areas

- Ship Harbour area

- Caribou Lake area

heterogeneous 2-mica monzogranite - Seal Cove Lake - Tangier Grand Lake areas

Figure 10. Plots of eU (ppm) versus eTh (ppm) concentrations as measured by in situ gamma ray spectrometry for the four study areas from the Musquodoboit Batholith.

Table 1. Major, trace element, and normative data for granitic rocks of the Musquodoboit Batholith.

	Gibraltar Hill				Granite Lake			Paces Lake			Ship Harbour						
	BKD N=5 X	TRANS N=1 X	PORPH N=5 X	DYKE N=4 X	BKD N=8 X	TRANS N=8 X	DYKE N=3 X	BKD N=6 X	TRANS N=3 X	PORPH N=5 X	TGL-FL N=10 X	TGL-FL N=10 SD	SH N=4 X	CL N=2 X	TRANS N=6 X	DYKE N=11 X	DYKE N=11 SD
SiO_2	73.10	72.10	74.10	74.30	71.33	75.39	74.53	71.32	74.70	75.06	70.56	1.02	72.18	71.80	73.50	74.38	0.55
Al_2O_3	14.10	15.10	14.16	14.73	14.94	13.63	14.73	15.27	14.07	14.06	14.81	0.33	14.63	14.25	14.28	14.41	0.44
Na_2O	3.63	3.95	4.22	4.62	3.72	3.59	4.53	3.81	3.78	4.13	3.60	0.17	3.81	3.64	4.01	4.45	0.53
K_2O	4.44	4.68	4.08	3.62	4.50	4.23	4.27	4.94	4.34	4.07	4.33	0.28	4.22	4.40	4.30	3.93	0.81
CaO	0.69	0.50	0.44	0.53	0.96	0.49	0.37	0.92	0.44	0.38	1.23	0.24	0.91	0.92	0.47	0.43	0.10
Fe_2O_3	0.55	0.83	0.42	0.32	0.97	0.45	0.37	0.61	0.53	0.33	0.70	0.14	0.40	0.58	0.46	0.41	0.09
FeO	1.12	0.70	0.48	0.23	1.00	0.51	0.07	1.03	0.67	0.34	1.75	0.34	1.30	1.30	0.72	0.26	0.17
MgO	0.47	0.32	0.20	0.08	0.70	0.29	0.05	0.44	0.20	0.06	0.91	0.16	0.60	0.49	0.24	0.17	0.08
MnO	0.50	0.07	0.05	0.05	0.06	0.05	0.03	0.05	0.06	0.04	0.07	0.01	0.06	0.06	0.05	0.10	0.16
TiO_2	0.25	0.18	0.11	0.06	0.31	0.15	0.06	0.26	0.16	0.07	0.40	0.07	0.27	0.30	0.15	0.08	0.03
P_2O_5	0.24	0.32	0.34	0.50	0.25	0.29	0.52	0.29	0.33	0.44	0.24	0.02	0.29	0.36	0.36	0.27	0.11
LOI	0.90	1.08	0.89	0.87	1.08	0.92	0.85	0.94	0.93	0.96	1.05	0.17	0.89	1.12	1.03	0.96	0.16
Total	99.78	100.00	99.60	99.98	100.00	100.14	100.43	100.10	100.30	100.00	99.97	0.54	99.75	99.45	99.78	100.03	0.39
Q	33.34	30.75	33.90	33.57	30.22	37.81	31.45	28.28	35.63	35.48	29.23	1.52	31.48	32.02	33.48	33.11	1.33
C	2.67	3.43	2.82	3.18	2.85	2.96	2.96	2.70	3.07	2.87	2.58	0.47	2.87	2.73	3.03	2.74	0.60
OR	26.59	28.00	24.43	21.44	26.80	25.20	23.99	29.49	25.84	24.27	25.91	1.76	25.28	26.52	25.77	23.17	3.95
AB	31.11	33.81	36.13	39.37	31.83	30.64	37.36	32.53	32.15	35.25	30.79	1.43	32.60	31.30	29.38	37.86	4.68
AN	1.88	0.39	0.07	0.14	3.21	0.56	0.83	2.70	0.26	0.00	4.58	1.18	2.65	2.27	0.09	0.50	0.79
EN	1.18	0.81	0.51	0.20	1.78	0.74	0.85	1.11	0.51	0.14	2.29	0.39	1.51	1.22	0.61	0.44	0.17
FS	1.17	0.35	0.40	0.20	0.59	0.35	0.18	0.95	0.56	0.29	1.97	0.44	1.62	1.43	0.70	0.26	0.43
MT	0.99	1.33	0.69	0.36	1.46	0.73	0.80	1.06	0.88	0.54	1.32	0.21	0.78	1.08	0.79	0.52	0.22
IL	0.49	0.35	0.21	0.11	0.60	0.29	0.34	0.50	0.30	0.14	0.76	0.14	0.51	0.57	0.30	0.16	0.05
AP	0.57	0.75	0.81	1.17	0.58	0.69	0.96	0.68	0.78	1.02	0.56	0.05	0.69	0.85	0.85	0.64	0.25
D.I.	91.04	92.57	94.48	94.53	88.85	93.66	92.80	90.29	93.62	95.00	85.93	1.84	89.37	89.85	93.63	94.78	0.90
C.I.	3.83	2.84	1.81	0.97	4.50	2.12	2.42	3.62	2.25	1.09	6.34	1.10	4.42	4.31	2.40	1.44	1.59
Rb	236	330	317	387	213	255	377	277	367	434	299	30	298	381	513	442	102
Sr	95	40	17	9	119	48	5	98	20	19	145	25	91	61	8	11	13
Ba	125	8	8	8	187	56	8	179	8	8	308	73	152	122	8	8	0
Zr	82	40	24	8	100	46	27	88	37	9	140	33	75	103	57	18	17
Cu	6	4	4	4	6	3	2	8	3	2	5	3	8	4	6	6	10
Pb	4	4	2	4	13	5	3	3	3	2	6	1	6	4	2	4	2
Zn	47	37	24	17	57	27	11	45	38	24	53	10	47	57	41	13	9
Sn	14	16	20	32	10	14	22	13	19	24	9	3	11	16	21	23	10
Be	3.2	5.5	3.1	2.5	3.0	2.7	0.3	3.4	2.0	1.1	4.5	1.4	2.5	2.3	2.3	4.0	2.7
Li	97	141	113	80	104	144	37	140	148	132	146	32	135	186	205	72	28
F	485	600	466	776	548	506	542	726	713	797	678	103	540	913	801	461	150
La	10	7	3	1	15	6	1	13	5	2	18	4	14	17	8	2	2
Ce	18	14	7	2	21	9	2	27	11	6	38	8	29	38	19	6	6
U	3.6	7.5	5.3	4.7	4.6	4.4	6.0	6.4	6.0	7.2	3.9	0.8	8.7	6.2	11.0	7.7	4.4
Th	5	4	1	1	7	3	1	7	6	1	9	2	8	10	5	2	2
A/CNK	1.17	1.21	1.17	1.18	1.17	1.21	1.15	1.15	1.20	1.18	1.16	0.03	1.17	1.14	1.18	1.17	0.07
U/Th	0.72	1.87	--	--	0.64	1.44	--	0.86	1.52	--	0.46	0.15	2.23	0.65	2.34	5.15	4.40
Na_2O/K_2O	0.82	0.84	1.06	1.30	0.84	0.86	1.10	0.77	0.87	1.02	0.84	0.08	0.90	0.83	0.93	1.20	0.41
K/Rb	156	118	110	91	176	138	115	149	101	79	121	15	121	97	71	78	24

BKD - low eU/eTh porphyritic, biotite monzogranite
TGL-FL - Tangier Grand Lake - Frazer Lake porphyritic, biotite monzogranite
SH - Ship Harbour porphyritic, biotite monzogranite
CL - Caribou Lake porphyritic, biotite monzogranite
TRANS - transitional two-mica monzogranite
PORPH - porphyry, including inequigranular to seriate monzogranite
DYKE - aplite and aplite pegmatite dyke rocks

To calculate the mean and standard deviation a value of 1/2 the detection limit was used for those samples below the detection limit.

Table 2. Average major, trace element, and normative data for granitic rocks of the Musquodoboit and South Mountain batholiths[1].

	Musquodoboit Batholith									South Mountain Batholith[1]					
	BKD N=35		TRANS N=18		PORPH N=10		DYKE N=18		bmg[2] N=7	gd N=57	bmg N=88	mbmg N=44	cglmg N=64	fglmg N=100	lg N=29
	X	SD	X	SD	X	SD	X	SD	X	X	X	X	X	X	X
SiO_2	71.48	1.50	74.48	2.08	74.58	1.44	74.39	0.56	71.92	67.10	69.51	71.46	73.22	73.90	73.51
Al_2O_3	14.76	0.64	14.00	0.98	14.11	0.71	14.53	0.41	14.58	15.51	14.82	14.62	14.23	14.27	14.67
Na_2O	3.68	0.19	3.78	0.36	4.17	0.48	4.50	0.50	3.60	3.48	3.41	3.52	3.41	3.51	3.79
K_2O	4.49	0.34	4.29	0.28	4.08	0.41	3.93	0.74	4.60	3.69	4.26	4.63	4.68	4.48	4.10
CaO	1.00	0.27	0.48	0.09	0.41	0.06	0.44	0.11	0.86	1.94	1.31	0.88	0.59	0.41	0.41
Fe_2O_3	0.68	0.28	0.49	0.15	0.38	0.10	0.39	0.09	1.72	4.54	3.51	2.51	1.89	1.45	1.23
FeO	1.30	0.44	0.62	0.15	0.41	0.18	0.22	0.17							
MgO	0.66	0.24	0.26	0.08	0.13	0.10	0.13	0.08	0.53	1.83	1.46	1.17	0.91	0.84	0.76
MnO	0.06	0.01	0.05	0.01	0.05	0.01	0.08	0.12	0.06	0.09	0.08	0.05	0.05	0.04	0.03
TiO_2	0.32	0.08	0.15	0.03	0.09	0.05	0.07	0.03	0.28	0.67	0.48	0.34	0.19	0.13	0.07
P_2O_5	0.26	0.04	0.32	0.05	0.39	0.08	0.35	0.18	0.25	0.21	0.20	0.25	0.23	0.27	0.44
LOI	1.01	0.18	0.97	0.16	0.92	0.16	0.92	0.15							
Total	99.90	0.45	100.04	0.31	99.82	0.49	100.10	0.42	99.68						
Q	30.17	2.75	35.62	4.62	34.69	3.22	32.93	1.62	30.62	26.72	29.23	30.52	33.70	35.08	34.91
C	2.70	0.44	3.03	0.36	2.85	0.41	2.87	0.54	2.75	2.81	2.73	2.84	3.05	3.49	4.02
OR	26.87	2.04	25.65	1.74	24.36	2.40	22.99	3.66	27.60	22.03	25.46	27.55	27.83	26.70	24.43
AB	31.49	1.60	32.31	3.15	35.69	4.16	38.11	4.55	30.94	29.70	29.09	29.22	29.03	29.85	0.00
AN	3.30	1.42	0.35	0.44	0.03	0.10	0.48	0.82	2.66	8.29	5.22	2.74	1.43	0.52	
EN	1.69	0.60	0.66	0.21	0.33	0.25	0.44	0.51							
FS	1.29	0.69	0.50	0.24	0.34	0.22	0.23	0.36							
MT	1.23	0.34	0.81	0.24	0.61	0.16	0.53	0.50							
IL	0.61	0.16	0.30	0.06	0.17	0.09	0.18	0.16	0.54	0.77	0.56	0.40	0.25	0.18	0.06
AP	0.61	0.09	0.76	0.12	0.91	0.18	0.81	0.37	0.59	0.50	0.47	0.58	0.55	0.62	1.04
D.I.	88.54	2.59	93.58	0.97	94.74	0.85	94.38	1.90	89.26	78.44	83.78	87.99	90.56	91.63	91.68
C.I.	4.84	1.47	2.27	0.49	1.44	0.63	1.50	1.25		9.38	7.40	5.57	4.28	3.67	3.21
Rb	269	51	364	124	376	89	419	117	294	149	184	255	301	338	589
Sr	115	33	29	22	19	17	10	11	97	170	118	80	48	31	19
Ba	209	97	29	44	8	0	8	0	253	667	491	351	196	146	61
Zr	107	34	43	10	16	19	16	18	91	193	159	123	82	60	39
Cu	6	4	4	3	3	2	5	8	13.8	7.0	5.3	2.3	0.4	2.7	0.6
Pb	7	7	4	2	2	1	4	2		17	20	22	19	20	13
Zn	52	16	36	7	24	7	13	7	54.3	78	66	60	51	45	62
Sn	11	3	17	6	22	5	25	15	11	5	7	10	13	18	27
Be	3.5	1.3	2.6	1.0	2.1	1.5	3.0	2.6	4.3						
Li	130	36	165	50	123	42	68	31	182.2	65	79	90	104	107	220
F	633	153	644	200	632	210	544	286	732	667	612	826	1013	960	2317
La	15	5	6	2	2	2	2	2	11.75	36	28	23	15	10	5
Ce	29	11	18	6	6	4	5	5	25.69						
U	4.7	2.2	7.0	3.5	6.2	5.0	7.1	6.3	5.9	2.9	3.8	4.5	5.4	7.8	3.9
Th	8	3	4	2	1	1	1	2	5.8	12.9	11.5	12.6	9.2	6.2	4
A/CNK	1.16	0.03	1.20	0.03	1.17	0.03	1.17	0.04		1.18	1.18	1.18	1.21	1.26	1.29
U/Th	0.63	0.26	1.78	0.62			---	--	2.20						
Na_2O/K_2O	0.82	0.08	0.88	0.10	1.04	0.19	1.21	0.38							
K/Rb	144	27	108	33	95	24	87	33	129						

BKD-low eU/eTh porphyritic, biotite monzogranite; TRANS-transitonal two-mica monzogranite; PORPH-porphyry, including inequigranular to seriate monzogranite; DYKE-aplite and aplite pegmatite dyke rocks.

1-Ham et al. 1989; gd-granodiorite; bmg-biotite monzogranite; mbmg-muscovite-biotite monzogranite; cglmg-coarse grained leucomonzogranite; fglmg-fine grained leucomonzogranite; lg-leucogranite
2-MacDonald and Clarke, 1985; bmg-biotite monzogranite

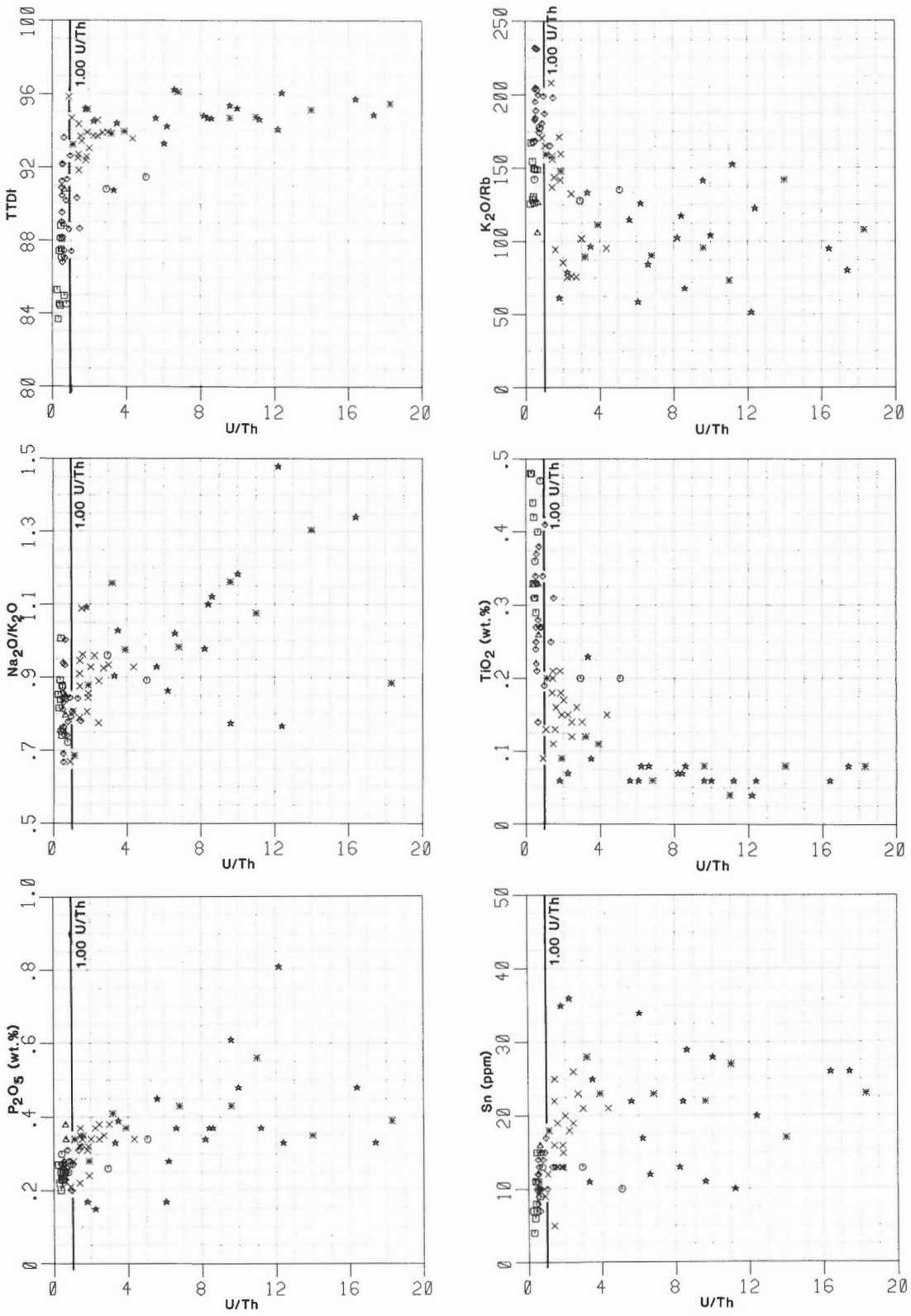

Figure 11. Selected variation plots for the Musquodoboit Batholith with mean values for the four most abundant rock types of the eastern half of the South Mountain Batholith (Ham et al., 1989).

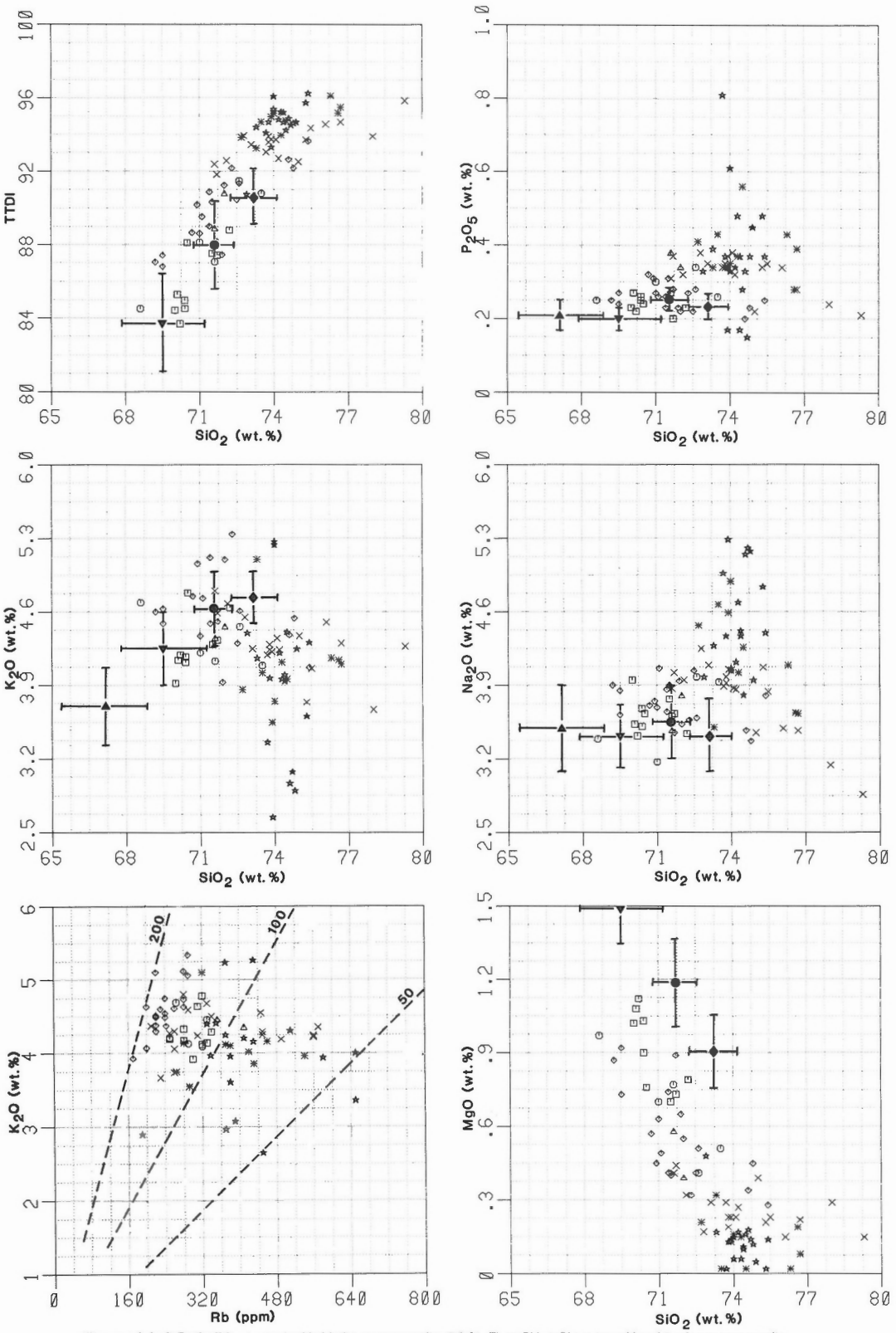

Musquodoboit Batholith ◇ porphyritic biotite monzogranite, ⊡ TGL-FL, ⊙ SH, △ CL; × transitional 2-mica monzogranite, ✳ porphyry, ★ dyke rocks; **South Mountain Batholith** ▲ granodiorite, ▼ biotite monzogranite, ● muscovite-biotite monzogranite, ◆ coarse grained leucomonzogranite.

Figure 11

The low ratio porphyritic, biotite monzogranite from the Musquodoboit Batholith has a major element composition comparable to the muscovite-biotite monzogranite from the South Mountain Batholith, although the spread of individual analysis encompasses both the biotite monzogranite and coarse grained leucomonzogranite compositions. The mean values for monzogranite samples from the Musquodoboit Batholith reported by MacDonald and Clarke (1985) (Table 2) are similar to mean values for the low ratio, porphyritic, biotite monzogranite from this study. Minor differences may be accounted for by the inclusion in MacDonald and Clarke's monzogranite unit of some transitional high ratio, two-mica monzogranite.

In contrast to the low ratio, porphyritic, biotite monzogranite, several elements from the high ratio units display trends that deviate from those established for the South Mountain Batholith. These include Na_2O and P_2O_5, which increase with increasing SiO_2, and K_2O which decreases with increasing SiO_2 (Fig. 11). Ford and Ballantyne (1983) first noted this trend towards sodium enrichment and its association with an increasing U/Th ratio in the Sangster Lake Pluton in the eastern Meguma Zone where they referred to it as an "albitization trend". O'Reilly (1988) later confirmed this association and also noted a strong positive correlation between this albitization trend and elevated P_2O_5 contents, which he attributed to increased late-stage hydrothermal alteration. This trend towards sodium enrichment is portrayed in Figures 11 and 12.

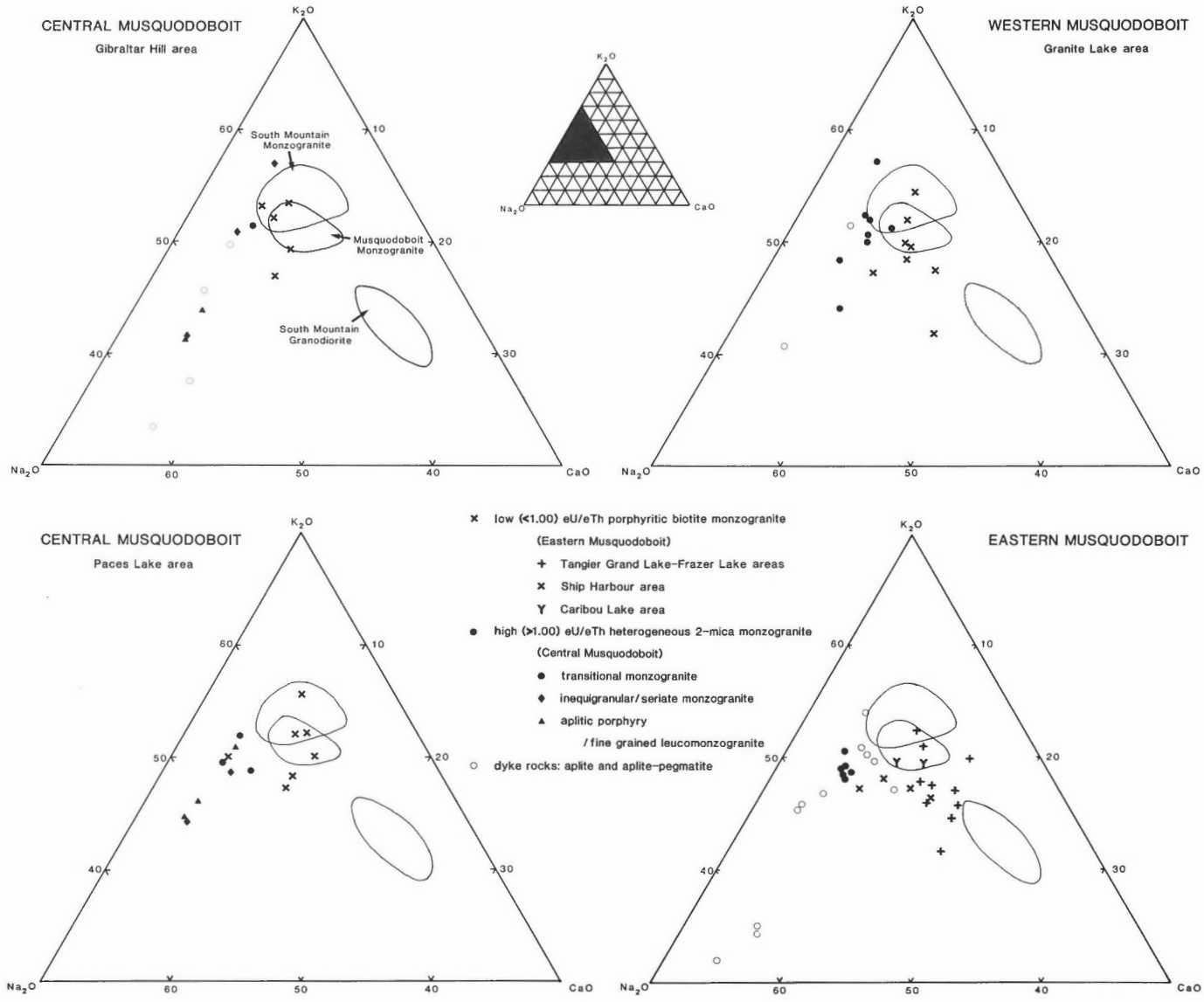

Figure 12. Plots of K_2O-Na_2O-CaO for geochemical data from the Musquodoboit Batholith showing trend towards sodium enrichment for high eU/eTh ratio samples.

The low ratio porphyritic, biotite monzogranite has a mean K/Rb ratio of 144 ± 27. The high ratio units have mean K/Rb values of: 108 ± 33 for the transitional two-mica monzogranite; 95 ± 24 for the porphyry and inequigranular/seriate phases, and 87 ± 33 for the dyke rocks. The correlation of lower K/Rb ratios with elevated U/Th ratios has also been noted for the Larry's River and Sangster Lake plutons from the eastern Meguma Zone (O'Reilly, 1988). O'Reilly suggested that this trend towards lower K/Rb ratios is a result of fluid-rock interaction.

Monzogranite with low ratios from the Tangier Grand Lake area have distinctly different radioelement characteristics compared with other low ratio areas of the batholith. Differentiation indices suggest that this monzogranite is the least evolved within the Musquodoboit Batholith, with a mean differentiation index of 85.93 ± 1.84 compared with other low ratio monzogranite areas, which range between 88.85 and 91.04. Variations in other elements, for example Ba, Sr, and Zr, also confirm the unique nature of these monzogranite samples.

The influence of fractional crystallization as a primary process of magmatic differentiation, and the varying intensities of late- and/or postmagmatic alteration on the radioelement contents, in particular the U/Th ratio, is indicated in Figure 11. The strong negative correlation with TiO_2 and strong positive correlation with differentiation index suggest that fractional crystallization of thorium-bearing phases strongly influences the variations in the U/Th ratio. On the other hand the generally weaker positive correlations with P_2O_5, Sn, and Na_2O/K_2O and negative correlation with K_2O/Rb highlight the role of late- and/or postmagmatic alteration.

The rare-earth element abundances for selected monzogranite samples with low and high eU/eTh ratios from the Musquodoboit Batholith are listed in Table 3 and plotted on Figure 13. Monzogranite with low eU/eTh ratios is characterized by the highest total REE levels (65.66 to 112.38), small negative europium anomalies (0.41 to 0.60), and La_N/Lu_N ratios which range between 6.69 and 8.82. For the monzogranite samples with low eU/eTh ratios, those from the Tangier Grand Lake (85-205) and Frazer Lake (86-225) areas, which were shown to have distinctly different radioelement signatures, also have noticeably different REE patterns with higher total REE values and La_N/Lu_N ratios. These and other indicators suggest that this monzogranite is the least evolved within the Musquodoboit Batholith. Compared with monzogranite with low eU/eTh ratios, the high ratio units are characterized by lower total REE, larger negative europium anomalies, and generally smaller La_N/Lu_N ratios. Rare-earth element levels for those units with high eU/eTh ratios from the Musquodoboit Batholith are similar to those of the medium and high eU/eTh response monzogranite from the Sangster Lake Pluton (O'Reilly, 1988) and with the leucogranite I suite from the South Mountain Batholith (Kontak et al., 1988). The low REE levels displayed by some leucogranite samples from the South Mountain Batholith and some leucogranite samples from the Sangster Lake Pluton are not evident in those units with high eU/eTh ratios from the Musquodoboit Batholith. This may be a reflection of the limited sampling from the Musquodoboit Batholith or an indication that the interaction with a late fluid phase did not proceed to the same degree in the Musquodoboit Batholith as it did in the South Mountain Batholith or Sangster Lake Pluton.

Table 3. Rare-earth element data for selected samples of the Musquodoboit Batholith.

	low eU/eTh porphyritic biotite monzogranite				high eU/eTh transitional two-mica monzogranite				high eU/eTh porphyry
Sample #	85-009	85-141	86-205	86-225	85-51	85-134	86-197	86-258	85-192
La	15.00	19.00	24.20	26.50	7.00	5.10	8.10	7.30	3.60
Ce	31.00	41.00	49.00	53.00	15.00	11.00	16.00	14.00	7.00
Nd	14.00	16.00	20.00	25.00	7.00	5.00	10.00	7.00	3.00
Sm	3.19	4.36	4.60	4.76	1.89	1.32	1.87	1.66	0.84
Eu	0.60	0.51	0.65	0.62	0.33	0.13	0.10	0.11	0.12
Tb	0.50	0.50	0.60	0.50	0.40	0.30	0.20	0.30	0.30
Yb	1.14	1.23	1.65	1.69	0.65	0.70	0.77	0.68	0.52
Lu	0.23	0.28	0.29	0.31	0.18	0.15	0.14	0.10	0.11
Sum 8 REE	65.66	82.88	100.99	112.38	32.45	23.70	37.18	31.15	15.49
La_N/Lu_N	6.69	7.02	8.62	8.82	4.00	3.50	5.98	7.62	3.40
Eu/Eu*	0.60	0.41	0.47	0.46	0.50	0.28	0.18	0.20	0.33

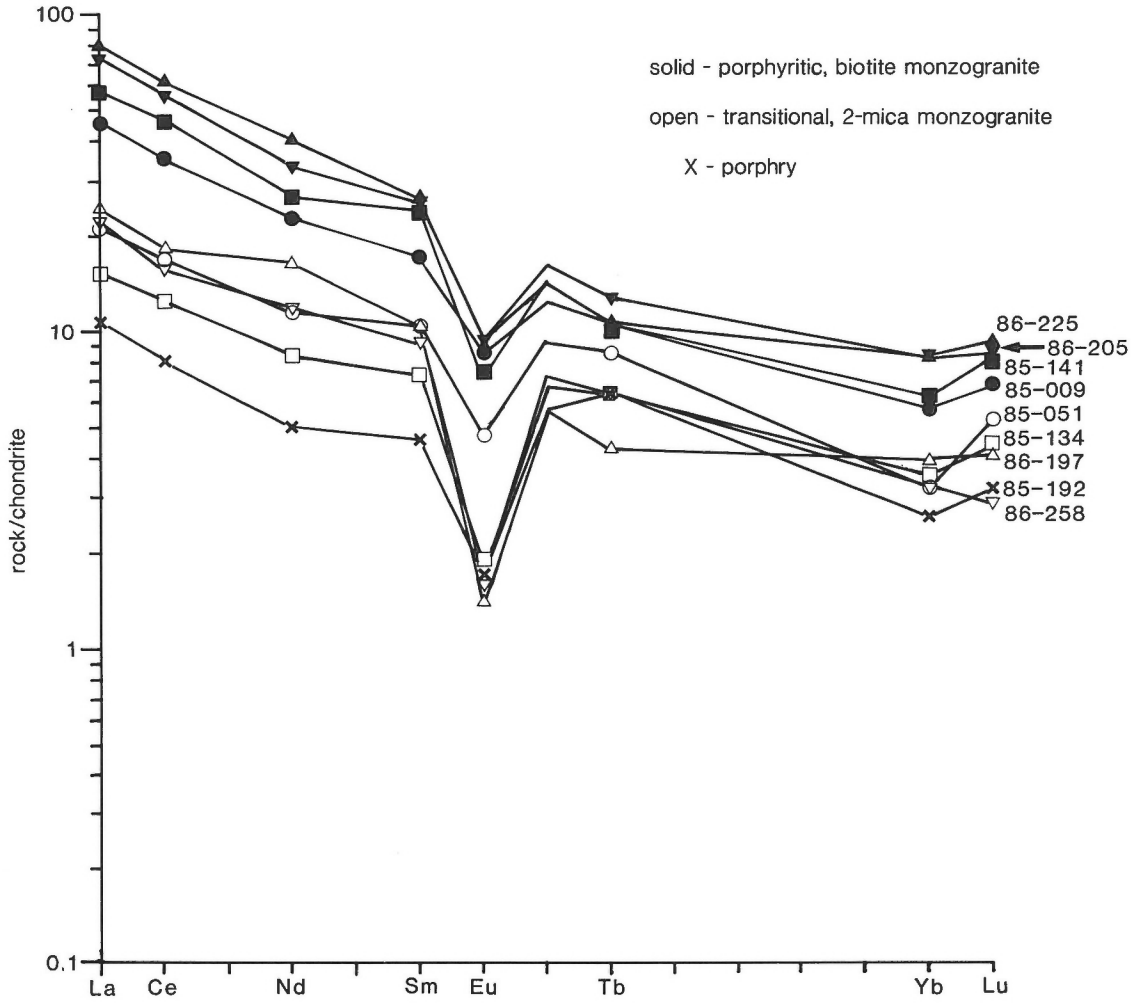

Figure 13. Chondrite-normalized REE patterns for selected low (solid symbols) and high (open symbols) eU/eTh ratio samples from the Musquodoboit Batholith.

LISCOMB COMPLEX

Regional airborne gamma ray spectrometric surveys

On the Radioactivity Maps of Nova Scotia (Ford et al., 1989) the radioelement characteristics of the Liscomb Complex are similar to those of other Meguma Zone granitic rocks. These include variable, but generally elevated K, eU, and eU/eTh ratio values combined with variable but generally low eTh and eTh/K ratios. There is a clear distinction between radioelement characteristics of the eastern and western portions of the complex; the granitic rocks of the eastern Liscomb Complex show a much wider range in radioelement signatures than those of the western part. This possibly results from the presence of fewer leucomonzogranitic intrusions and more granodioritic, gabbroic, and gneissic units in the western part of the complex than in the eastern part of the complex. For example, eU/eTh ratios generally range from less than 0.25 to greater than 2.25 in the eastern part of the complex and from less than 0.25 to no greater than 0.60 in the western part of the complex.

Detailed airborne gamma ray spectrometric surveys

As for the Musquodoboit Batholith, the part of the Liscomb Complex that displays the greatest range of radioelement variations was selected to evaluate correlations between the airborne radioelement distribution patterns and the associated petrographic and lithogeochemical variations. As part of this evaluation, a detailed airborne gamma ray spectrometric survey (Geological Survey of Canada, 1987a), with a line spacing of 250 m, was flown over the eastern half of the Liscomb Complex (Fig. 14A, B, C, D).

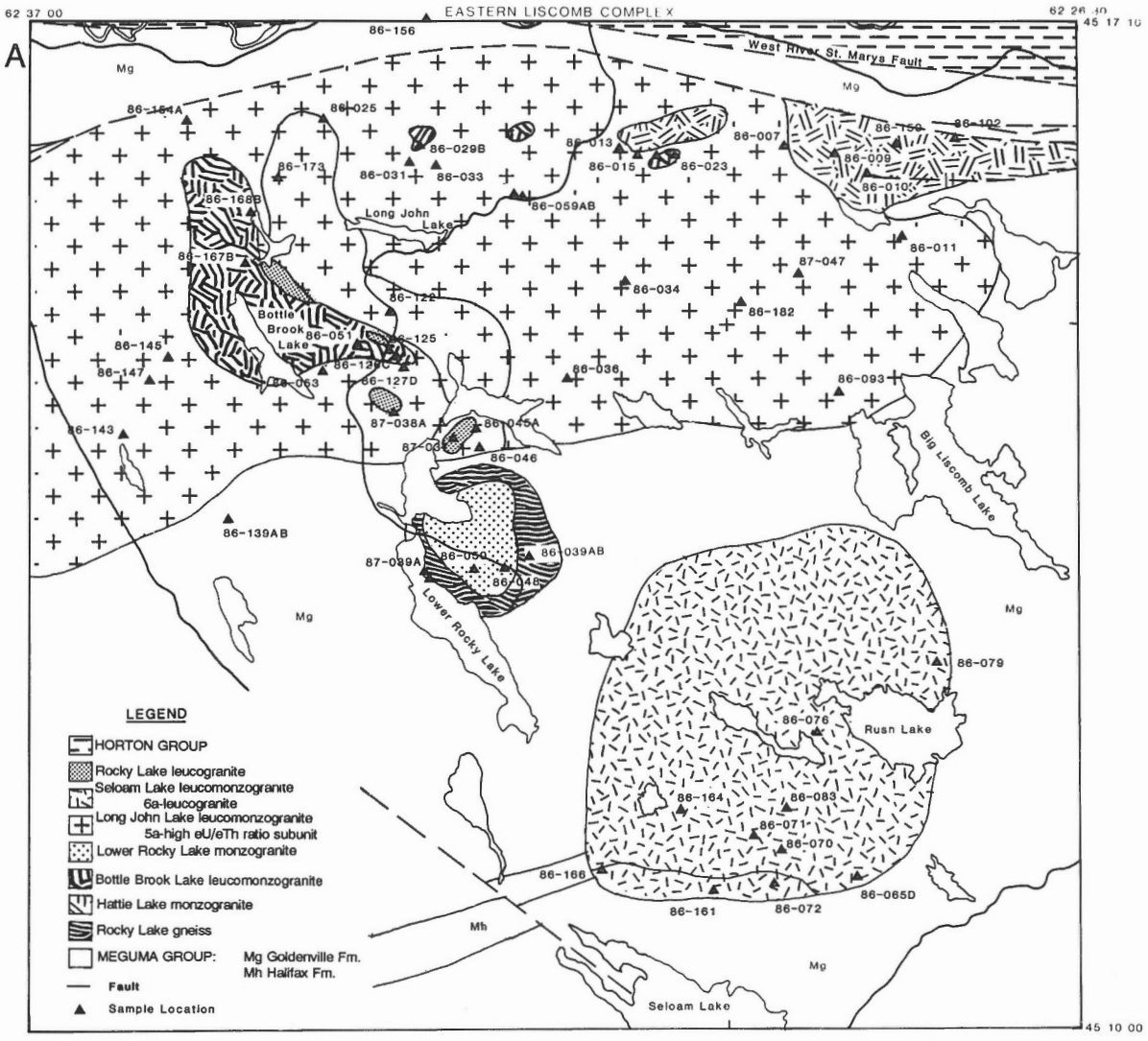

Figure 14. A) Geology of the eastern half of the Liscomb Complex with B) airborne gamma ray spectrometric data for eU/eTh ratio, C) eU (ppm), and D) eTh (ppm) collected with a line spacing of 250 m (Geological Survey of Canada, 1987a).

The Seloam Lake Pluton displays a prominent radioelement zonation characterized by: low (<0.50) eU/eTh ratios (Fig. 14B) and eU (Fig. 14C) in the central and northeastern portions of the pluton; moderate (0.50-1.00) eU/eTh ratios and eU along the western and eastern margins and high (>1.00) eU/eTh ratios and eU along the southern contact of the pluton. Maximum eU/eTh ratios and eU in this southern area exceed 2.50 and 6.5 ppm respectively. Equivalent thorium concentrations (Fig. 14D), commonly low throughout the pluton compared with other parts of the Liscomb Complex, are highest (maximum 4.0 ppm) in the central and northeastern parts of the pluton and lowest along the southern contact.

The eU/eTh ratio patterns for the Long John Lake Pluton (including the Hattie Lake monzogranite, the Bottle Brook Lake and Long John Lake leucomonzogranites, and the Rocky Lake leucogranite (Fig. 14A)) appear to define domains with low, moderate, and high ratios similar to the Seloam Lake Pluton. Low ratios are typical of the northern half and western extremities of the Long John Lake Pluton, whereas moderate ratios typify the southeastern half of the pluton and an arcuate zone west of Bottle Brook Lake. High ratios are restricted to a second arcuate zone east of Bottle Brook Lake and south of Long John Lake. Maximum eU/eTh levels attained in this area approach 2.50.

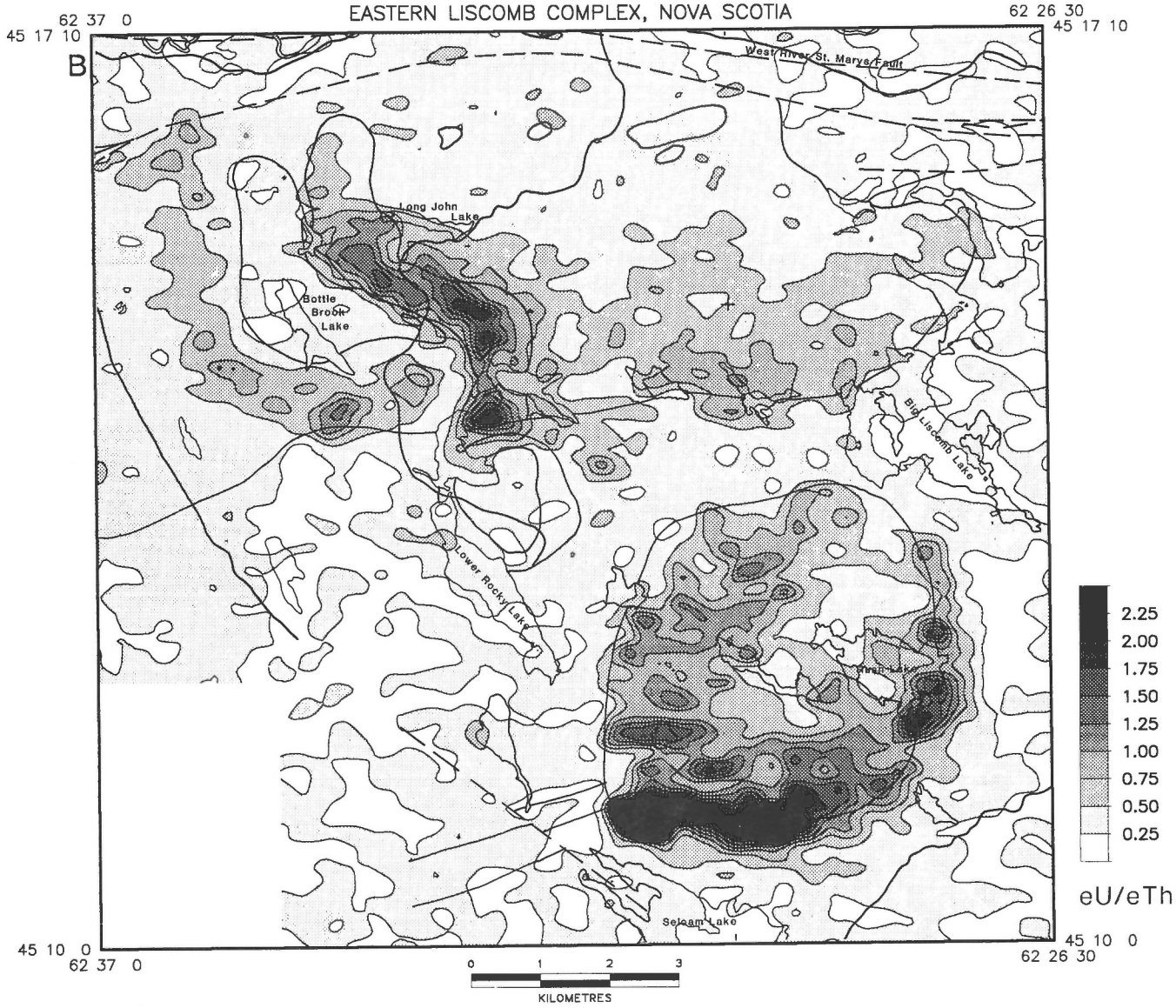

Figure 14B

In contrast to the generally indistinct patterns shown by eU (Fig. 14C), eTh patterns (Fig. 14D) show several distinct subdivisions. Low to very low concentrations are typical of the two arcuate, high eU/eTh ratio anomalies in the Bottle Brook Lake area. Low to intermediate concentrations are typical of much of the southeastern half of the pluton, east of Long John Lake, and the extreme northeastern part of the pluton. Intermediate to high concentrations occur over much of the northern half and extreme western part of the pluton. High to very high concentrations are found in the area around Bottle Brook Lake between the two arcuate ratio anomalies. Maximum eTh concentrations in this area reach 13.0 ppm compared with concentrations of between 8.0 and 9.0 ppm in adjacent, intermediate to high areas. It would appear that with the exception of areas with very high eU/eTh ratios, variations in the eU/eTh ratios are dominated more by variations in eTh than by variations in eU.

Confirmation of the relative variations in radioelement concentrations measured by airborne gamma ray spectrometry, using in situ gamma ray spectrometry and lithogeochemistry (see below), suggests that most of the glacial material over the eastern half of the Liscomb Complex is of local provenance. This is supported by surficial mapping of Stea and Fowler (1979). Figures 14B, C, and D suggest that there has been transport of granite-derived tills for a short distance (less than 1 km), east and south of the Seloam Lake Pluton and south of the Long John Lake Pluton. There would also appear to be a strong correlation between the occurrence of glaciofluvial sand, silt, and gravel deposits east of Long John Lake (Stea and Fowler, 1979), and low eU and eTh concentrations. Except for these minor interferences, the airborne radioelement patterns reflect the relative variations in bedrock concentrations.

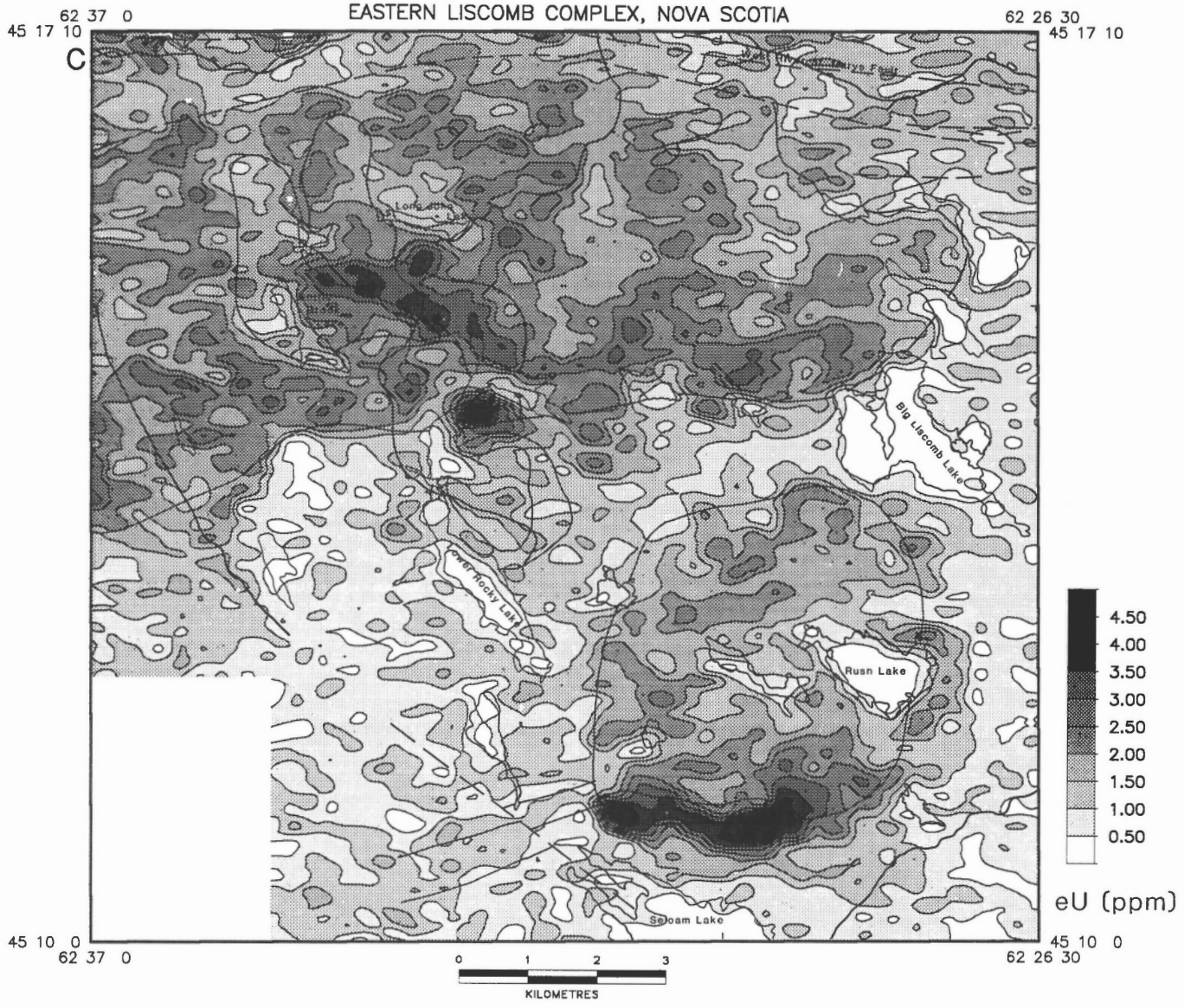

Figure 14C

Geology

The eastern half of the Liscomb Complex (Fig. 14A) contains three separate plutons: the Long John Lake pluton, which is the largest and most northerly of the three plutons; the Seloam Lake Pluton; and the Lower Rocky Lake Pluton. Based on radioelement characteristics, petrographic variations, and contact relationships, the Long John Lake Pluton is divisible into the Hattie Lake monzogranite, the Bottle Brook Lake and Long John Lake leucomonzogranites, a subunit of the Long John Lake leucomonzogranite with high eU/eTh ratios, and the Rocky Lake leucogranite. The Seloam Lake Pluton consists of the Seloam Lake leucomonzogranite and Seloam Lake leucogranite. The Hattie Lake monzogranite and Bottle Brook Lake leucomonzogranite occur as large, angular, sometimes polygonal to rounded xenolithic blocks and rafts within the Long John Lake leucomonzogranite (Fig. 15C, D) or are cut by dykes of the latter. Clusters of abundant xenoliths or large blocks of both the Hattie Lake monzogranite and Bottle Brook Lake leucomonzogranite are confined to the northeast part of the Long John Lake pluton north of Long John Lake. Relative age relationships between the Hattie Lake monzogranite and Bottle Brook Lake leucomonzogranite were not apparent even though xenoliths of both units occur in close (several metres) proximity to each other.

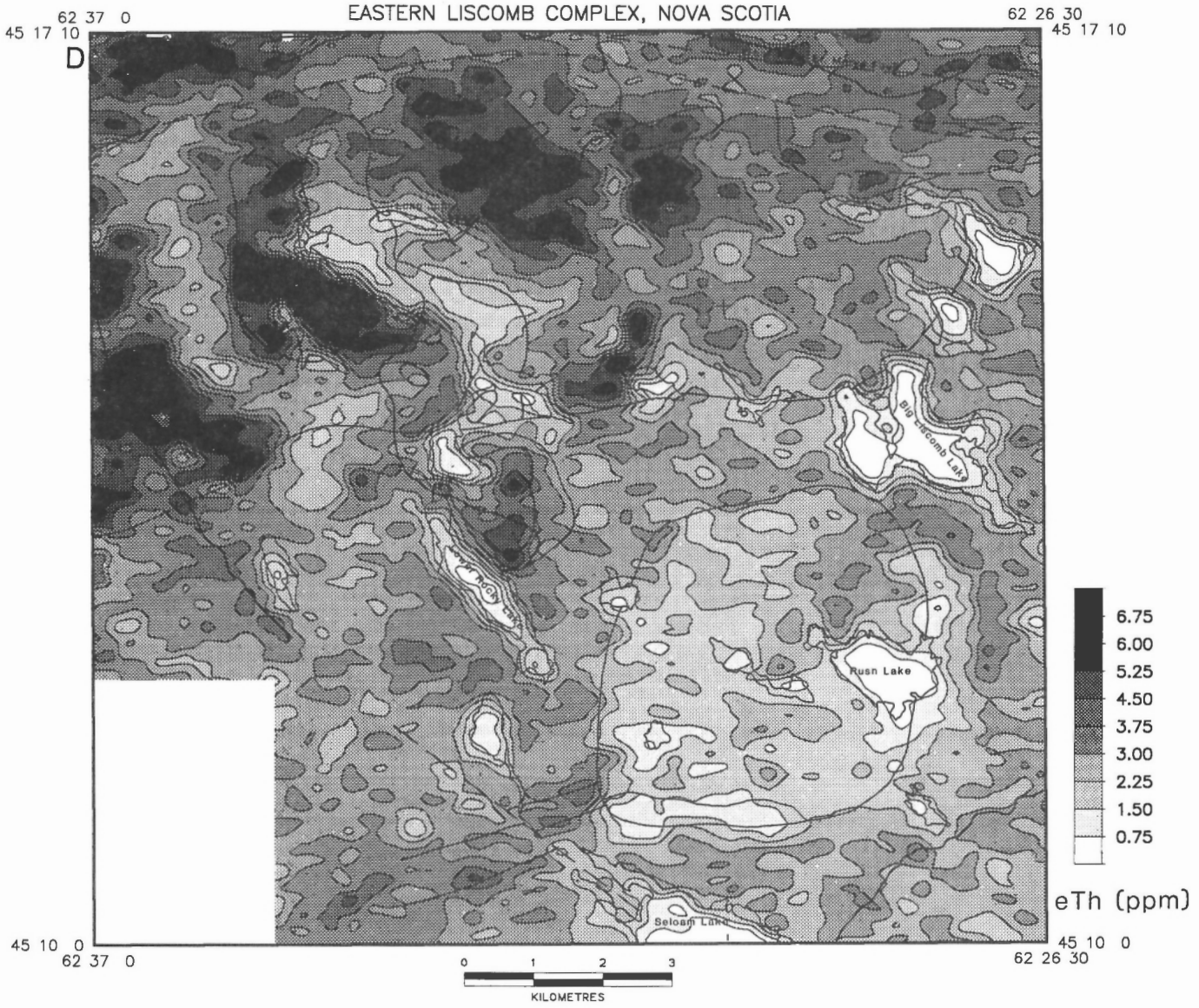

Figure 14D

The Hattie Lake monzogranite is a grey (colour index ranges from 5.85 to 7.04), medium- to coarse-grained, porphyritic biotite monzogranite. A QAP plot (Fig. 16) of modal abundances indicates the monzogranitic composition of three samples that plot close to the granodioritic field. Potassium feldspar phenocrysts up to 2 cm long constitute between 10 and 15% of the rock and are weakly perthitic. Accessory phases include muscovite, chlorite (after biotite), apatite, opaques, zircon, and monazite. The Hattie Lake monzogranite displays a foliation which ranges from weak to strong, with the development of a strong C and S fabric and locally an augen gneiss texture along the northeast contact with the Meguma Group. In areas where this foliation is weak the primary fabric is hypidiomorphic granular (Fig. 15A).

The Bottle Brook Lake leucomonzogranite is a light grey to pale pink (colour index ranges from 3.54 to 4.72), fine- to medium-grained, seriate to weakly porphyritic (5-10% small (<5 mm) alkali feldspar and quartz phenocrysts) biotite-muscovite leucomonzogranite (Fig. 15B). Textural variations are mainly the result of slight changes in grain size and phenocryst content, which in a few places may define a rudimentary layering. Accessory phases include chlorite (after biotite), apatite, and minor opaques.

The Long John Lake leucomonzogranite is a leucocratic (colour index ranges from 2.18 to 4.41), medium grained, equigranular, two-mica leucomonzogranite. Colour varies from pink, through buff, to locally greyish-white. The Long John Lake leucomonzogranite is similar in modal composition to the Bottle Brook Lake leucomonzogranite (Fig. 16). Both intrusions are distinctly more monzogranitic than the Hattie Lake monzogranite. Accessory phases include apatite, chlorite (after biotite), zircon, and minor opaques. The primary fabric is hypidiomorphic granular (Fig. 17C, D) although north of Long John Lake, a foliation is present which ranges from very weak just north of Long John Lake to very strong (C-S fabric) along its northeast contact.

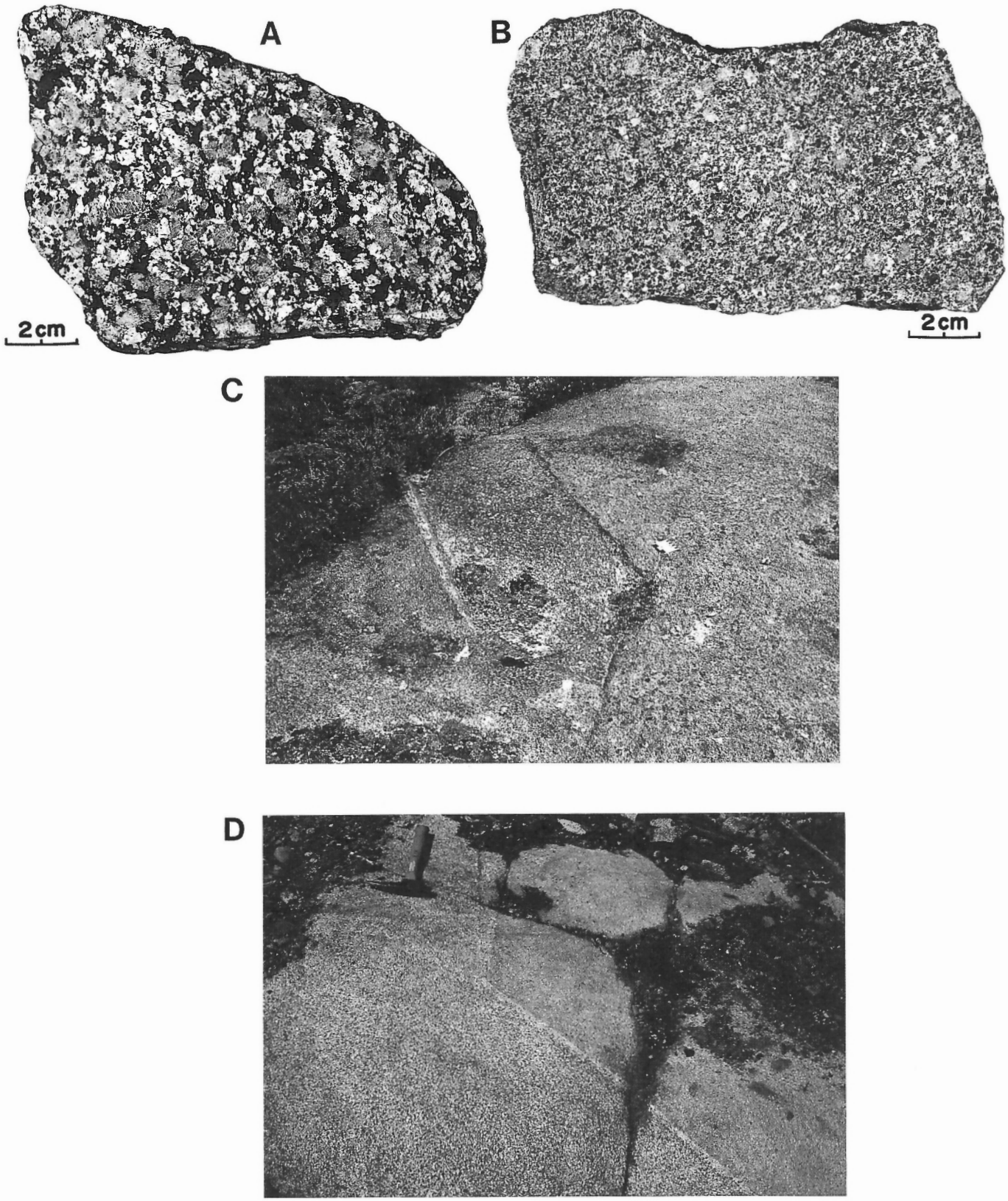

Figure 15. Stained slabs showing typical textural features for selected samples from the eastern half of the Liscomb Complex; A) Hattie Lake biotite monzogranite 86-009; B) Bottle Brook Lake biotite leucomonzogranite 86-167B; and photographs of large, xenolithic block of C) Hattie Lake monzogranite and D) Bottle Brook Lake leucomonzogranite in the Long John Lake leucomonzogranite.

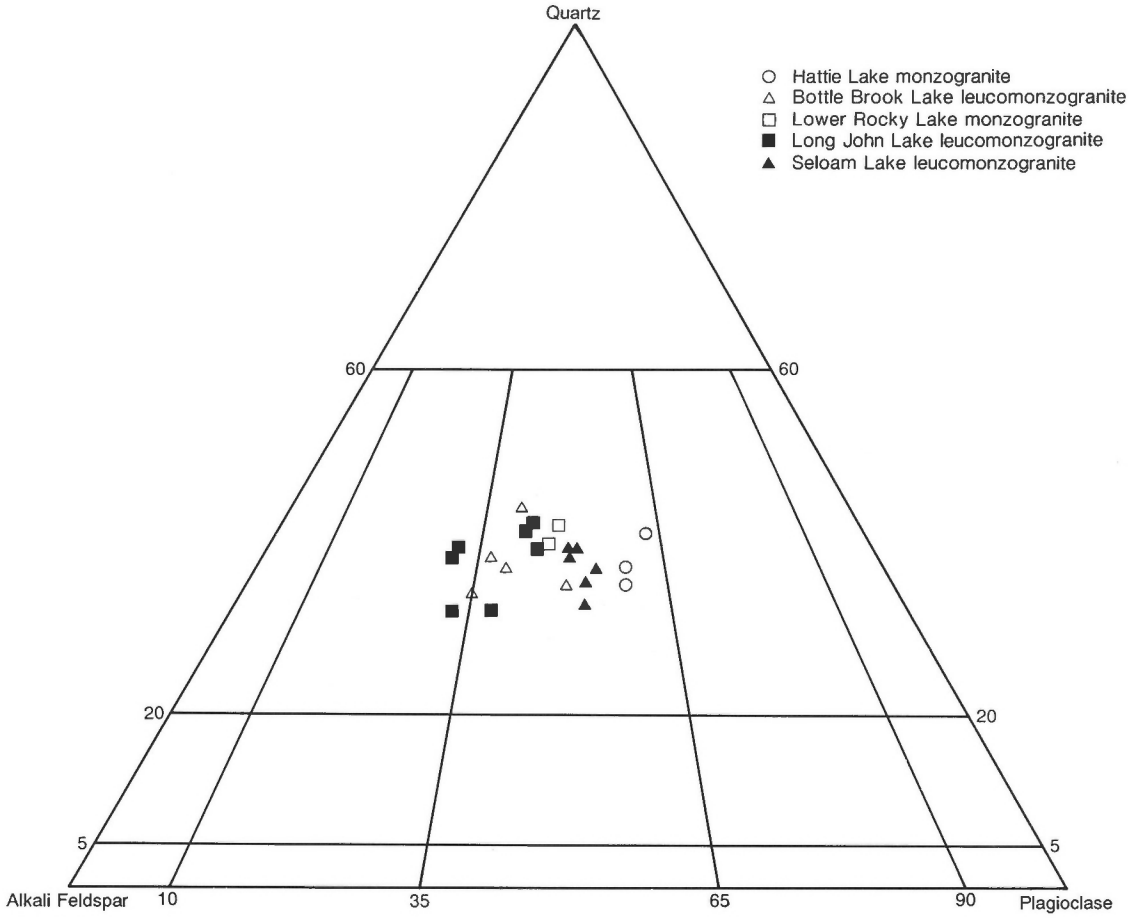

Figure 16. Modal compositions for the various low (<1.00) and some high (>1.00) eU/eTh ratio monzogranites from the eastern half of the Liscomb Complex. High eU/eTh ratio monzogranites which showed extensive metasomatism are not plotted.

The part of the Long John Lake leucomonzogranite that surrounds the Bottle Brook Lake leucomonzogranite, coincident with a high eU/eTh ratio anomaly, shows a slightly coarser grain size (Fig. 17E), is typically buff to greyish white, and shows a clear predominance of muscovite relative to biotite. This subunit is a leucocratic (colour index ranges from 1.12 to 1.89), medium grained, equigranular, muscovite-biotite leucomonzogranite. Accessory phases include chlorite (after biotite) and apatite. Modal abundances for this subunit of the Long John Lake leucomonzogranite are not plotted on Figure 16. This plot is designed as a classification scheme for "magmatic" rocks and should not be applied to rocks that have been extensively altered or have interacted with an evolved fluid phase. Modal abundances for samples from the subunit of the Long John Lake leucomonzogranite with high eU/eTh ratios would show a strong shift towards and into the granodiorite field. This is in contrast to monzogranite compositions for most major elements (see "Lithogeochemistry", below) and their more evolved appearance. As noted previously, phases with high ratios in other Meguma Zone granites commonly display strong, pervasive albitization (Ford and Ballantyne, 1983; Ford and O'Reilly, 1985; O'Reilly, 1988). This shift towards and into the granodiorite field is an indication of the altered nature of this unit.

The Rocky Lake leucogranite is a leucocratic (colour index ranges from 0.92 to 1.17), fine- to medium-grained, equigranular, saccharoidal leucogranite (Fig. 17F). These small leucogranite bodies are associated with, or occur in close proximity to, the subunit of the Long John Lake leucomonzogranite with high eU/eTh ratios, at or near the contact with the Bottle Brook Lake leucomonzogranite or the southern contact with the Meguma Group. It is not clear if these small bodies represent separate, and later intrusions, or extensively metasomatized equivalents of the subunit of the Long John Lake leucomonzogranite with high eU/eTh ratios.

The Seloam Lake leucomonzogranite is dominated by a leucocratic (colour index ranges from 1.14 to 2.12), medium grained, equigranular, muscovite-biotite leucomonzogranite (Fig. 17A). Colour ranges from pink, through buff, to greyish white. The Seloam Lake leucomonzogranite is similar in appearance to the Long John Lake leucomonzogranite, however, modal abundances

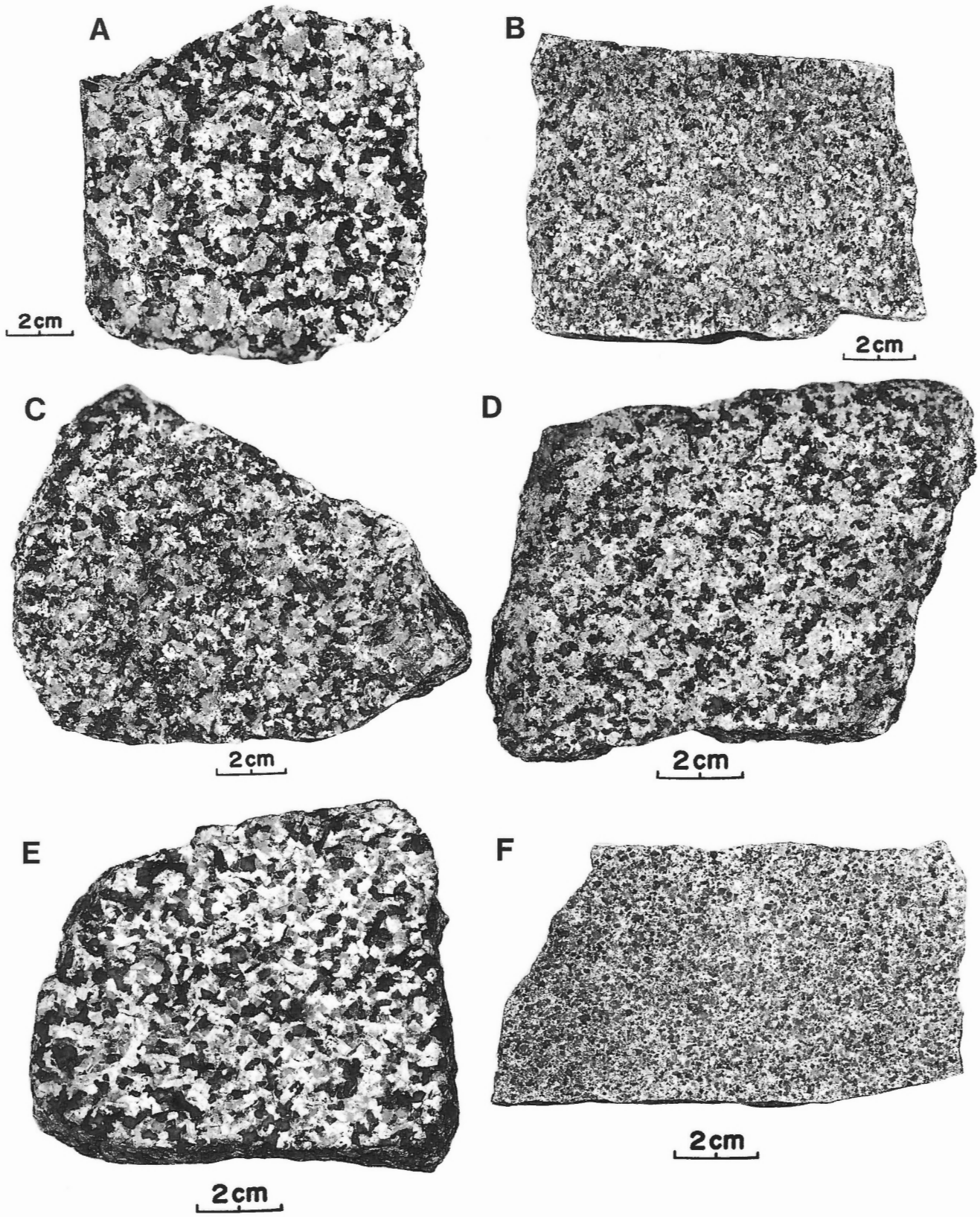

Figure 17. Stained slabs showing typical textural features of selected samples from the eastern half of the Liscomb Complex; A) Seloam Lake leucomonzogranite 86-070; B) Seloam Lake leucogranite 86-161; C), D) Long John Lake leucomonzogranite, C: 86-143; D: 86-093; E) Long John Lake leucomonzogranite, high eU/eTh ratio subunit 86-122; F) Rocky Lake leucogranite 87-038.

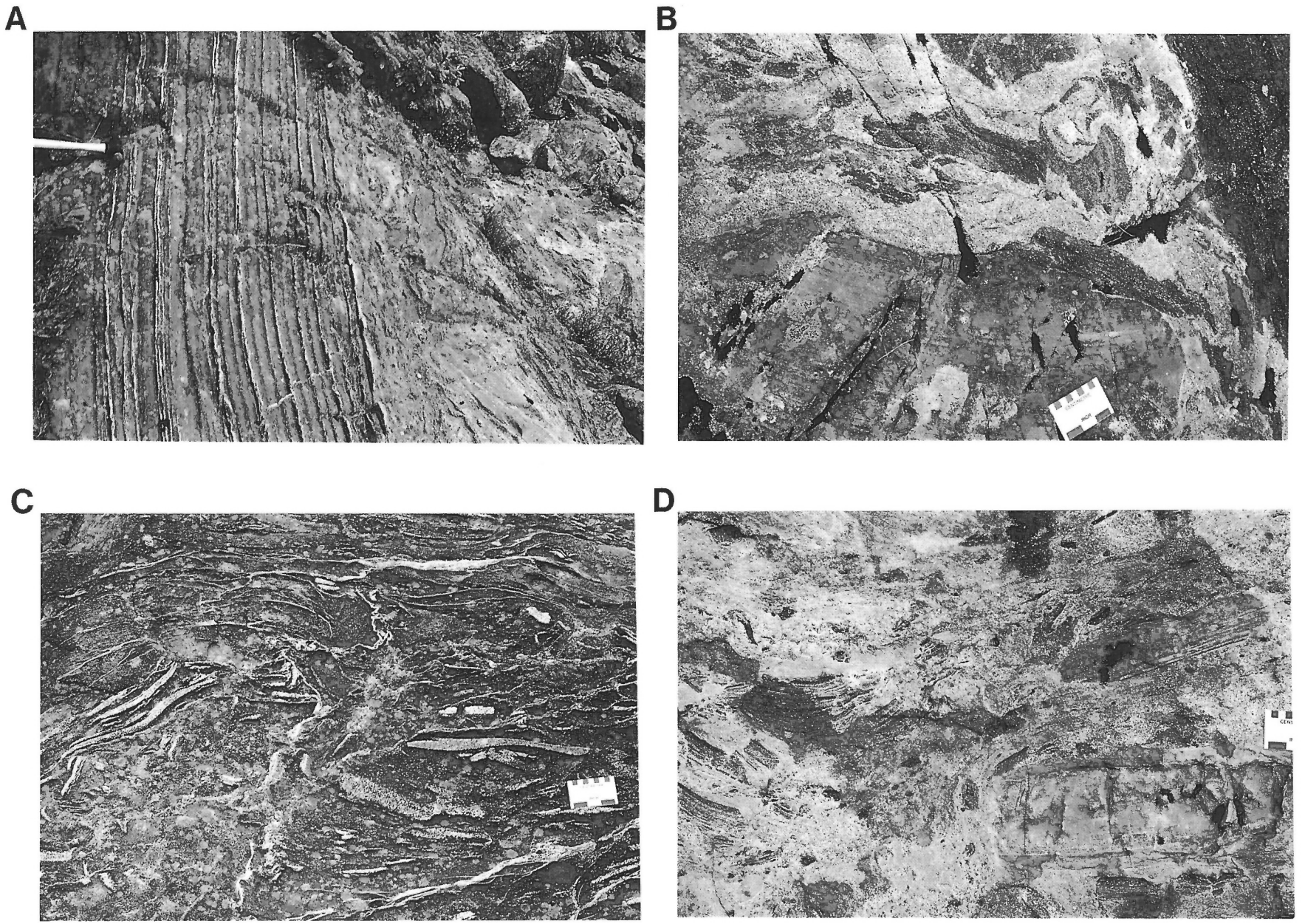

Figure 18. Photographs showing macroscopic features of the Rocky Lake gneiss from the northeast shore of Lower Rocky Lake.

for samples of the Seloam Lake leucomonzogranite show a slight shift towards the granodiorite field compared with samples of the Long John Lake leucomonzogranite (Fig. 16). This shift in modal abundance and the high eU/eTh ratio nature of these samples suggest that the Seloam Lake leucomonzogranite may have undergone some degree of interaction with an evolved fluid phase, although possibly not to the same degree as the subunit of the Long John Lake leucomonzogranite with high eU/eTh ratios. The predominant fabric of the pluton is massive, hypidiomorphic granular, although a single sample from the south-central part of the pluton displays a penetrative foliation.

The Seloam Lake leucogranite occurs along the southern contact of the Seloam Lake Pluton. It is similar in appearance (Fig. 17B) and mineralogy to the Rocky Lake leucogranite with a colour index that ranges from 0.59 to 0.73. It is not clear if this unit, which may be continuous along the southern contact coincident with the high eU/eTh ratio (Fig. 14B) anomaly, is a separate later intrusion or an extensively metasomatized equivalent of the Seloam Lake leucomonzogranite. Modal abundances for samples of the Seloam Lake and Rocky Lake leucogranites would show a strong shift towards the granodiorite field on Figure 16 characteristic of other high eU/eTh ratio units that have interacted with an evolved fluid phase (O'Reilly, 1988).

The Lower Rocky Lake Pluton is a small intrusion east of Lower Rocky Lake. It consists of a grey to pale pink (colour index ranges from 4.51 to 6.15), fine- to medium-grained, equigranular, biotite-muscovite monzogranite. Narrow leucomonzogranite and leucogranite dykes cut the Lower Rocky Lake monzogranite along the shores of Lower Rocky Lake and may be correlative with the Long John Lake Pluton.

The Rocky Lake gneiss surrounds the Lower Rocky Lake monzogranite, possibly as a continuous unit. It is predominantly a heterogeneous "gneissic breccia" unit (Fig. 18A, B, C, D) intruded by conformable to semiconformable, discontinuous lenses (Fig. 18B), sills, and dykes of the Lower Rocky Lake monzogranite. The "breccia" component of the Rocky Lake gneiss contains numerous psammitic and pelitic xenoliths and rafts that show various degrees of assimilation by the granitic component. This granitic component displays variable fabrics including massive, ghost- or schlieren-like and flow-like features (Fig. 18D). The variable fabric imparts a disrupted "migmatitic" appearance (Fig. 18A, C) to many of the outcrops. This gneissic unit is dominated by a fine grained, light greyish brown to dark grey, micaceous psammitic gneiss. The gneissosity is defined by alternating psammitic and pelitic bands (Fig. 18A) and a variable micaceous content in the psammitic unit. The gneissosity is commonly conformable to the contact with the Lower Rocky Lake monzogranite and disconformable to the east-northeast fabric of the Meguma Group.

Lithogeochemistry

Tables 4 and 5 summarize the radioelement, major, minor, and selected trace element analyses for the granitic rocks of the eastern half of the Liscomb Complex along with additional data for the granitic rocks of the western half of the Liscomb Complex supplied by Dr. A.K. Chatterjee of the Nova Scotia Department of Natural Resources.

The Hattie Lake and Lower Rocky Lake monzogranites have similar eU and eTh concentrations (Table 4, Fig. 19) and their eU/eTh ratio of 0.27 is close to the normal crustal ratio of 0.25 (Clarke et al., 1966) but is generally lower than most other Meguma Zone granitoids. The Bottle Brook Lake leucomonzogranite also has a low eU/eTh ratio (0.24) but has mean eU and eTh concentrations nearly twice those of the Hattie Lake and Lower Rocky Lake monzogranites.

Table 4. Average radioelement contents* of the granitic rocks of the eastern Liscomb Complex.

		K (pct)		U (ppm)		Th (ppm)		eU/Th		eU/K		eTh/K	
	N	X	SD	X	SD	X	SD	X	SD	X	SD	X	SD
Hattie Lake (HL) monzogranite	18	3.6	0.3	3.6	0.9	13.5	2.2	0.27	0.08	1.00	0.22	3.79	0.46
Lower Rocky Lake (LRL) monzogranite	8	3.9		3.9		14.6		0.27		0.97		3.74	
Bottle Brook Lake (BBL) leucomonzogranite	26	4.5	0.4	6.2	1.0	26.9	5.4	0.24	0.06	1.40	0.20	6.05	1.14
Long John Lake (LJL) leucomonzogranite	85	4.6	0.4	5.2	1.1	10.1	3.1	0.55	0.19	1.14	0.26	2.22	0.66
Long John Lake (LJLhr)** leucomonzogranite	28	4.0	0.4	7.7	2.2	4.0	0.9	1.96	0.53	1.92	0.54	0.99	0.15
Rocky Lake (RL) leucogranite	10	3.6	0.4	14.8	7.8	2.5	1.8	8.13	4.76	4.20	2.54	0.67	0.46
Seloam Lake (SL) leucomonzogranite	57	4.0	0.2	5.2	1.8	3.6	0.7	1.49	0.58	1.32	0.48	0.92	0.92
Seloam Lake (SLhr) leucogranite	6	3.5		14.2		1.9		7.56		4.06		0.55	

* radioelement concentrations measured by in situ gamma ray spectrometry
** altered equivalent of the Long John Lake leucomonzogranite
SD - standard deviation not calculated for N<9

Table 5. Major, trace element, and normative data for granitic rocks of the Liscomb Complex.

	Eastern Liscomb Complex										Western Liscomb Complex[1]					
	HLmg N=4	BBLImg N=9		LRLmg N=3	LJLImg N=13		LJLhr N=6	RLlg N=4	SLImg N=6	SLlg N=4	TLgd N=12		ELSmg N=12		NPSLMImg N=11	
	X	X	SD	X	X	SD	X	X	X	X	X	SD	X	SD	X	SD
SiO_2	70.65	71.47	0.32	70.13	72.54	0.66	73.38	72.05	73.18	73.52	68.76	2.40	72.34	1.70	72.62	0.41
Al_2O_3	14.92	14.96	0.21	15.10	14.83	0.29	15.08	15.58	15.05	15.35	15.77	0.66	14.81	0.44	15.15	0.13
Na_2O	3.43	3.53	0.20	3.49	3.59	0.18	4.26	5.01	4.33	5.30	3.41	0.10	3.46	0.28	3.74	0.35
K_2O	4.39	4.89	0.11	4.38	5.06	0.21	4.13	3.48	4.35	3.71	4.16	0.51	4.31	0.27	4.70	0.77
CaO	1.13	0.70	0.08	0.91	0.57	0.05	0.50	0.71	0.54	0.36	1.71	0.53	0.96	0.50	0.65	0.29
Fe_2O_3	0.69	0.55	0.13	0.74	0.60	0.22	0.39	0.41	0.31	0.36	3.84	1.04	2.32	0.92	1.46	0.26
FeO	1.70	1.04	0.21	1.63	0.75	0.21	0.35	0.25	0.35	0.10						
MgO	0.93	0.61	0.05	1.20	0.45	0.09	0.22	0.08	0.30	0.12	1.09	0.39	0.57	0.39	0.34	0.09
MnO	0.06	0.04	0.01	0.05	0.03	0.01	0.03	0.05	0.02	0.02	0.09	0.02	0.04	0.02	0.03	0.01
TiO_2	0.39	0.32	0.03	0.42	0.22	0.04	0.11	0.02	0.14	0.04	0.51	0.16	0.30	0.19	0.19	0.03
P_2O_5	0.20	0.30	0.02	0.22	0.33	0.02	0.41	0.86	0.34	0.40	0.17	0.08	0.23	0.06	0.25	0.05
LOI	1.20	1.20	0.21	1.20	1.08	0.19	1.20	0.96	1.08	1.14	0.82	0.13	1.00	0.19	0.84	0.06
Total	99.95	99.84	0.31	99.80	100.18	0.20	100.18	99.60	100.18	100.32						
Q	30.15	30.69	1.27	29.67	31.31	1.07	32.65	29.69	30.93	28.49	28.03	3.43	33.07	2.95	31.93	0.92
C	2.99	3.34	0.23	3.56	3.23	0.35	3.62	3.60	3.08	2.62	2.98	0.42	3.38	0.49	3.36	0.29
OR	26.34	29.37	0.65	26.29	30.21	1.30	24.68	20.77	25.99	22.12	24.80	3.03	25.71	1.67	28.97	5.49
AB	29.48	30.27	1.71	29.99	30.69	1.48	36.46	42.87	37.03	45.16	29.04	0.87	29.47	2.28	31.15	3.92
AN	4.30	1.55	0.49	3.08	0.68	0.25	0.03	0.00	0.42	0.00	7.40	2.42	3.07	2.51	1.56	1.60
EN	2.36	1.54	0.12	3.04	1.12	0.23	0.55	0.21	0.74	0.31	2.73	0.98	1.41	0.86	0.84	0.23
FS	1.95	0.91	0.43	1.66	0.55	0.34	0.22	0.16	0.15	0.02	0.77	0.98	1.68	1.61	0.00	0.00
MT	1.15	0.98	0.17	1.37	0.91	0.19	0.51	0.63	0.54	0.23	2.77	0.51	0.67	0.68	0.05	0.15
IL	0.76	0.62	0.05	0.81	0.41	0.08	0.20	0.04	0.26	0.08	0.97	0.32	0.56	0.40	0.09	0.12
AP	0.48	0.70	0.05	0.53	0.77	0.06	0.96	2.02	0.80	0.92	0.40	0.18	0.53	0.13	0.59	0.11
D.I.	85.97	90.34	0.86	85.96	92.30	0.99	93.89	93.33	93.95	95.77	81.90	5.00	88.25	4.44	92.02	1.76
C.I.	6.22	4.06	0.45	6.87	3.01	0.62	1.58	1.04	1.74	0.68	7.35	2.52	4.70	2.38	2.39	0.53
Rb	262	368	19	274	302	35	415	642	282	530	170	23	187	38	213	16
Sr	148	81	5	127	78	16	22	76	54	33	169	31	106	60	72	24
Ba	512	339	39	604	255	101	8	8	182	8	762	201	414	223	434	24
Zr	132	119	9	116	68	18	23	6	23	8	169	34	97	46	88	28
Cu	4	3	1	7	5	4	4	9	2	2	7	2	6	2	6	1
Pb	11	4	2	4	6	5	2	2	4	4	39	8	26	6	29	8
Zn	65	61	10	61	50	17	27	23	25	2	84	36	62	28	52	7
Sn	7	8	3	7	8	3	15	26	14	33	3	2	5	2	9	3
Be	5.9	4.6	2.1	4.7	5.7	2.2	6.5	3.5	3.5	8.0						
Li	75	96	24	89	86	40	134	58	124	99	56	11	83	34	80	20
F	478	840	116	655	436	160	656	1041	368	416	538	176	428	91	445	120
La	24	23	3	21	13	4	4	1	6	1	36	6	21	7	16	4
Ce	52	56	8	37	30	10	9	4	14	3						
U	4.0	6.5	1.0	3.6	6.1	1.0	5.3	30.3	5.1	12.0	3.4	0.6	4.0	0.6	5.3	1.0
Th	12	24	2	13	9	4	2	1	3	1	14	2	8	4	7	2
A/CNK	1.20	1.21	0.02	1.28	1.19	0.03	1.22	1.17	1.18	1.15						
U/Th	0.25	0.27	0.15	0.26	0.80	0.25	2.65	---	1.70	12.00	0.25	0.06	0.78	0.75	0.76	0.27
Na_2O/K_2O	0.78	0.72	0.05	0.80	0.71	0.06	1.03	1.45	1.00	1.44	0.83	0.14	0.81	0.09	0.84	0.29
K/Rb	139	111	5	135	143	21	84	45	128	59						

Eastern Liscomb Complex
HLmg-Hattie Lake biotite monzogranite; BBLImg-Bottle Brook Lake biotite-muscovite leucomonzogranite; LRLmg-Lower Rocky Lake biotite-muscovite monzogranite; LJLImg-Long John Lake two-mica leucomonzogranite; LJLhr-muscovite-biotite leucomonzogranite, high U/Th phase; RLlg-Rocky Lake leucogranite; SLImg-Seloam Lake muscovite-biotite leucomonzogranite; SLlg-Seloam Lake leucogranite
To calculate the mean and standard deviation a value 1/2 the detection limit was used for those samples below the detection limit.

1 - Western Liscomb Complex
Analysis for granitic rocks from the Western Liscomb Complex supplied by Dr. A.K. Chatterjee, Nova Scotia Department of Natural Resources
TLmg-Twin Lake biotite granodiorite; ELSmg-East Loon Lake and Sanctuary biotite-muscovite monzogranites; NPSLMImg-Nelson Lake, Porcupine Lake, South Loon Lake and Moose Lake equigranular, muscovite-biotite leucomonzogranites.

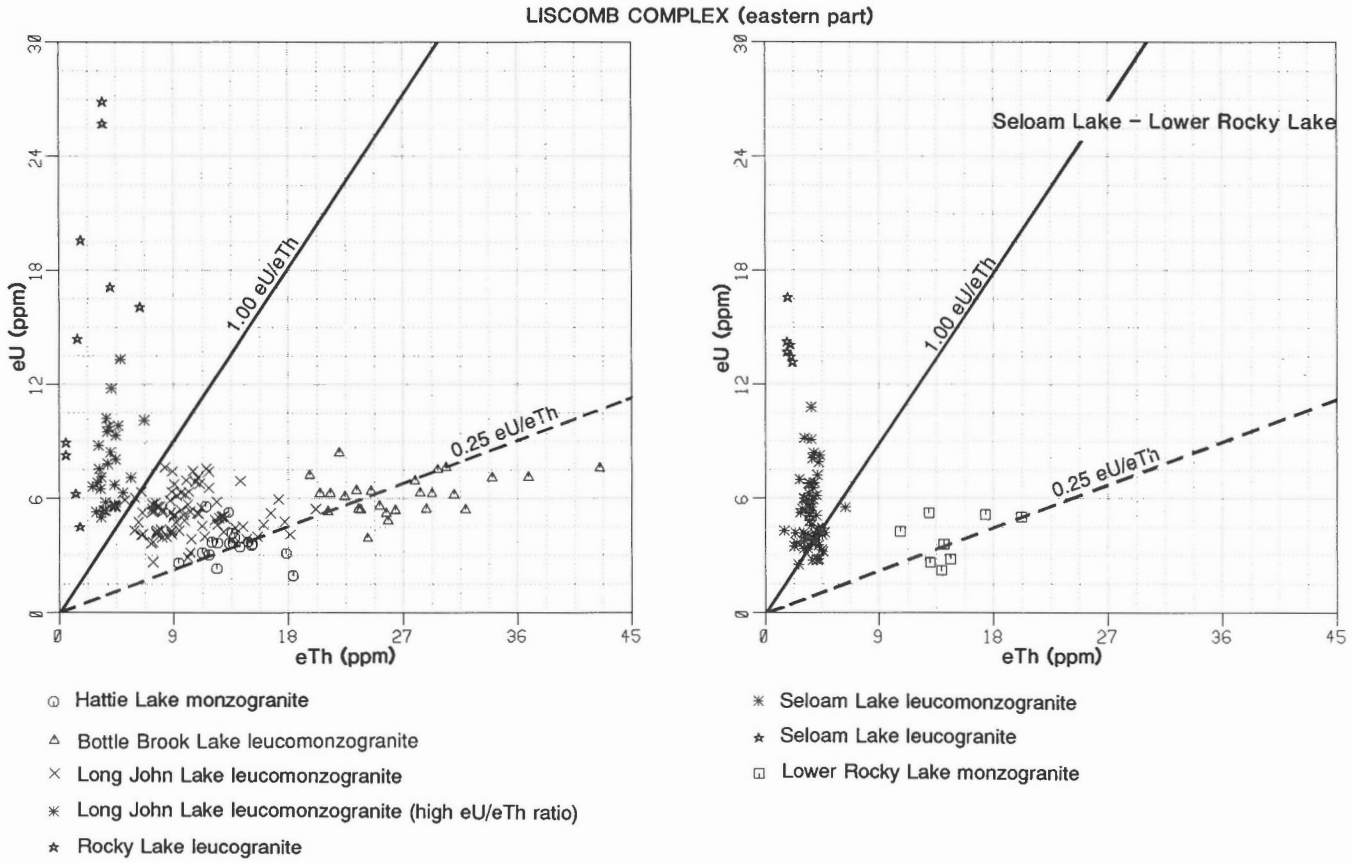

Figure 19. Plots of eU (ppm) versus eTh (ppm) concentrations as measured by in situ gamma ray spectrometry for the various granitic units of the eastern half of the Liscomb Complex.

In situ gamma ray spectrometric measurements from the northern and southern portions of the Long John Lake leucomonzogranite confirm the subtle increase in eU/eTh ratios (Fig. 14B) over the southern half of the intrusion. Mean radioelement concentrations range from 4.9 ppm eU and 10.4 ppm eTh with a mean eU/eTh ratio of 0.49 in the northern part of the intrusion to 5.4 ppm eU and 7.3 ppm eTh with a mean eU/eTh ratio of 0.77 in the southern part of the intrusion.

The K, eTh, and eU/eTh ratio values for the Seloam Lake leucomonzogranite are similar to the subunit of the Long John Lake leucomonzogranite with high eU/eTh ratios. Points that plot near or below the 1.00 eU/eTh ratio line (Fig. 19) are from within or near the low ratio core area of the pluton.

Potassium concentrations within the Long John Lake and Seloam Lake leucomonzogranites and associated leucogranites decrease progressively with increasing eU/eTh ratios (Table 4). This decrease in potassium concentration is a reflection of the pervasive "albitization" evident in other Meguma Zone granitoids.

All granitic rocks from the eastern part of the Liscomb Complex are peraluminous (A/CNK>1, Table 5). Major element chemistry and normative mineral compositions indicate that the low ratio units, in particular the Hattie Lake and Lower Rocky Lake monzogranites, are the least evolved rock types in this part of the complex. Compared with the low ratio units and the Long John Lake leucomonzogranite, the high ratio units (high ratio phase of the Long John Lake leucomonzogranite, Seloam Lake leucomonzogranite, Rocky Lake and Seloam Lake leucogranites) generally show lower mean values for K_2O, total Fe, MgO, TiO_2, normative orthoclase, anorthite, enstatite, ferrosilite, magnetite, ilmenite, and colour index, and higher mean values for SiO_2, Na_2O, P_2O_5, normative albite, apatite, and differentiation index. With a few exceptions trace element concentrations are lower for Sr, Ba, Zr, Zn, Ce, La, and Th, and higher for Rb and Sn in the high ratio units.

In general, the low ratio units have major element concentrations similar to the muscovite-biotite monzogranite of the South Mountain Batholith (Fig. 20). Exceptions to this relationship are found in mean concentrations of MgO and total Fe (Fig. 20) that are significantly lower than mean values for equivalent rock types of the South Mountain Batholith. The Long John Lake leucomonzogranite is intermediate between the low and high ratio units and has major element concentrations that generally span the muscovite-biotite monzogranite and coarse grained leucomonzogranite fields of the South Mountain Batholith.

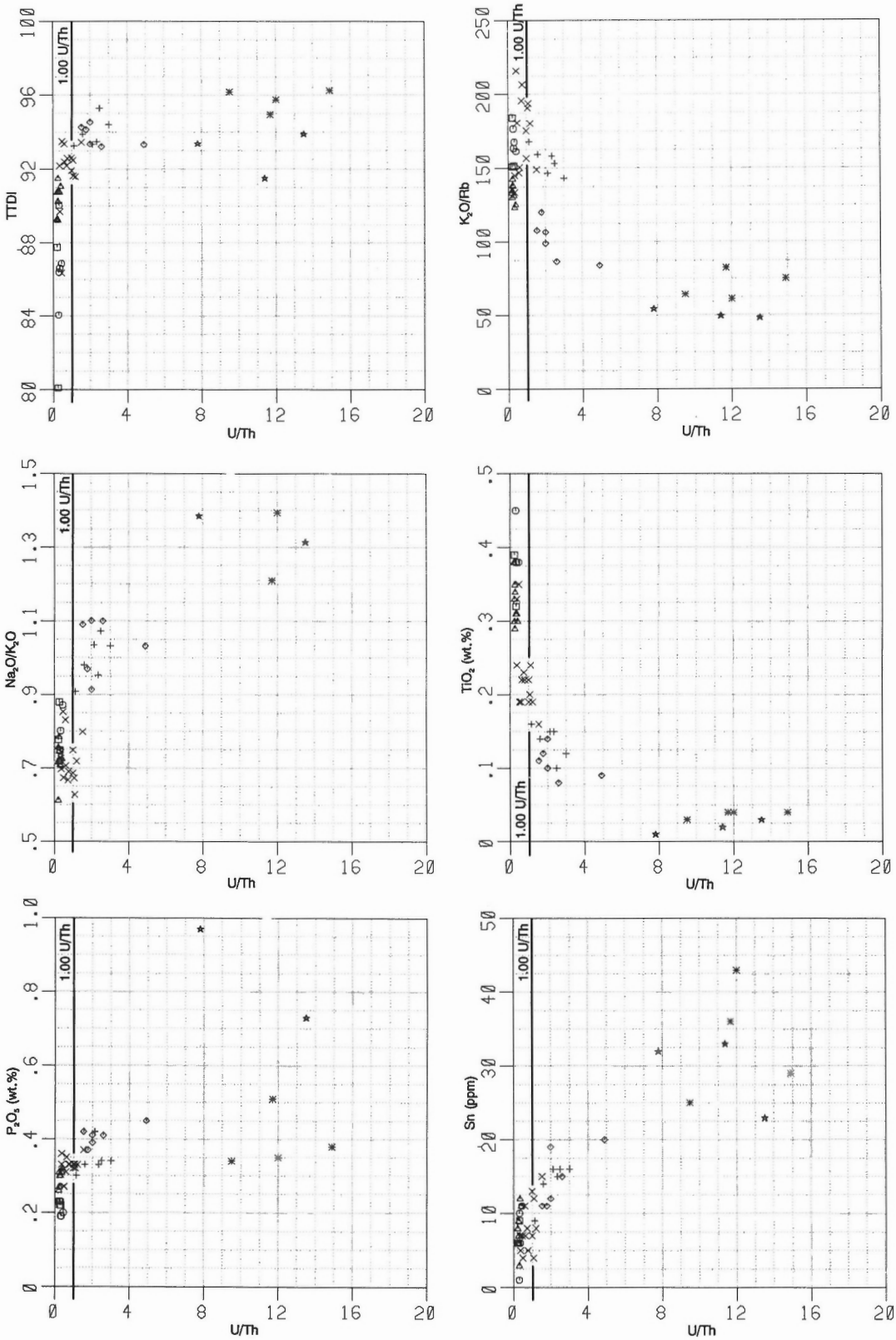

Figure 20. Selected variation plots for the eastern half of the Liscomb Complex with mean values for the four most abundant rock types of the South Mountain Batholith (Ham et al., 1989).

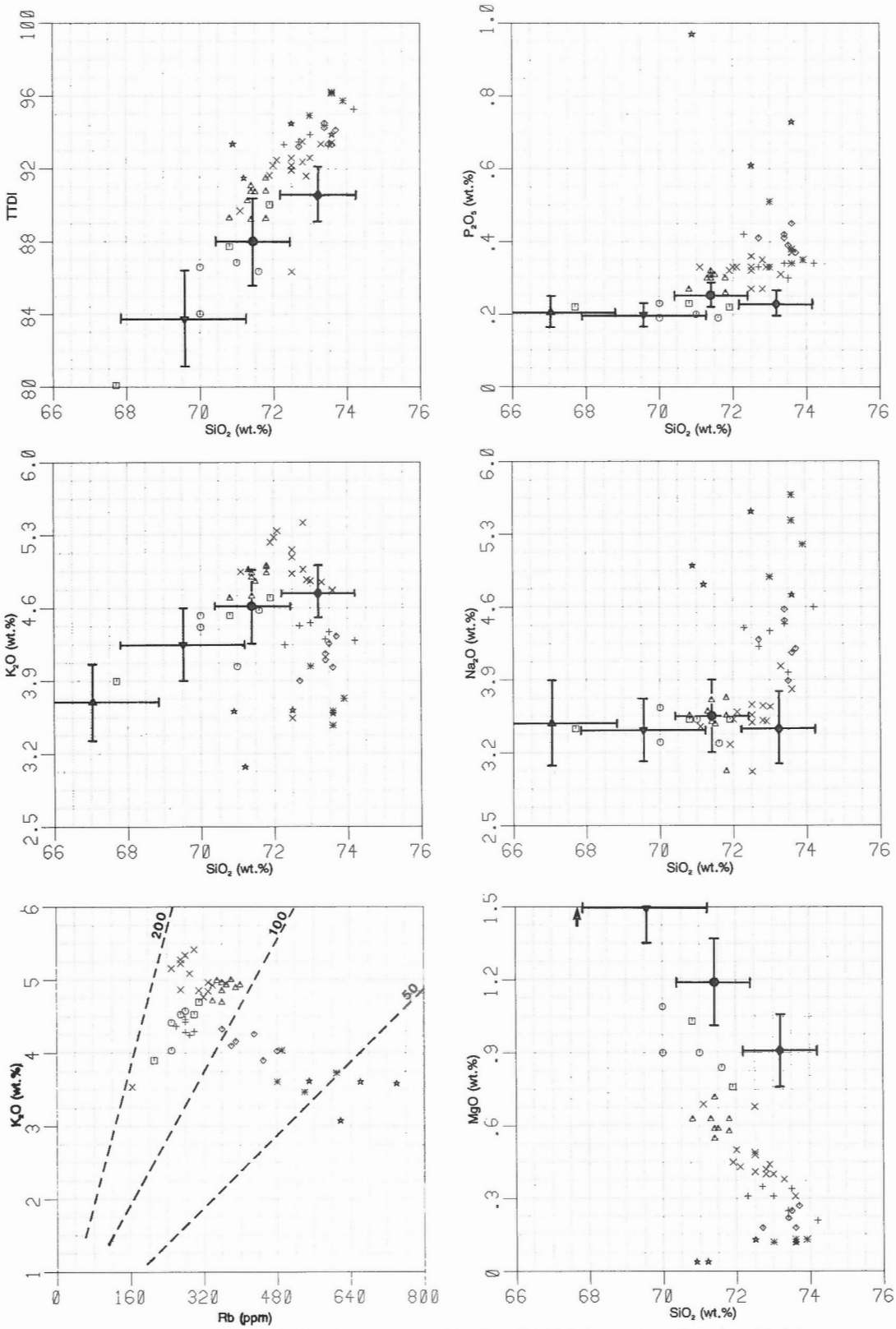

Liscomb Complex (East half) ⊙ Hattie Lake monzogranite, △ Bottle Brook Lake leucomonzogranite, × Long John Lake leucomonzogranite, ◇ Long John Lake leucomonzogranite (high eU/eTH ratio), ★ Rocky Lake leucogranite, + Seloam Lake leucomonzogranite, ✳ Seloam Lake leucogranite, ⊡ Lower Rocky Lake monzogranite; **South Mountain Batholith** ▲ granodiorite, ▼ biotite monzogranite, ● muscovite-biotite monzogranite, ◆ coarse grained leucomonzogranite

Figure 20

Geochemical characteristics of the high ratio units deviate from the trends established for the South Mountain Batholith and the low ratio units of the eastern half of the Liscomb Complex. These deviations include K_2O contents that decrease, and Na_2O and P_2O_5 that increase sharply with increasing U/Th ratios from the Long John Lake leucomonzogranite through the subunit of the Long John Lake high ratio leucomonzogranite to the Rocky Lake leucogranite and from the Seloam Lake leucomonzogranite to the Seloam Lake leucogranite. This trend towards sodium enrichment or "albitization trend", associated with increasing U/Th ratio (Fig. 20, 21) has been documented elsewhere (Ford and Ballantyne, 1983; O'Reilly, 1988).

The Seloam Lake leucomonzogranite has major element concentrations similar to those for the high ratio subunit of the Long John Lake leucomonzogranite. This may be a reflection of the sampling, because most samples from the Seloam Lake leucomonzogranite are from the high eU/eTh ratio margins. Samples from the low ratio core area of the Seloam Lake leucomonzogranite might be expected to fall closer to those for the Long John Lake leucomonzogranite. The Rocky Lake and Seloam Lake leucogranites have similar major element characteristics and plot as a separate group within the high ratio units. They display considerable spread in several elements, in particular those most involved in the late stage alteration; K_2O, Na_2O, and P_2O_5. This is also the case for the high ratio units from the Musquodoboit Batholith.

The low and high eU/eTh ratio units of the eastern half of the Liscomb Complex have variations in K/Rb ratios that are similar to the Larry's River and Sangster Lake plutons from the Eastern Meguma Zone, where O'Reilly (1988) has demonstrated a clear correlation between increasing U/Th ratio and decreasing K/Rb ratio. The low ratio units from the eastern half of the Liscomb Complex have mean K/Rb ratios that range from 139 to 111 whereas the high ratio units have mean K/Rb ratios that range from 128 to 45. While the Seloam Lake leucomonzogranite has been grouped with the high ratio units (mean eU/eTh ratio of 1.49 in Table 4), it has K/Rb ratios more typical of the Long John Lake leucomonzogranite and the low ratio units. Several other elements (Table 5) also show concentrations comparable to the Long John Lake leucomonzogranite and unlike the high ratio units, for example Rb, Sr, and Ba. This would suggest that caution should be exercised in the strict application of variations in eU/eTh ratio as a direct indicator of hydrothermal alteration and that high eU/eTh ratios may be generated by different processes (magmatic versus alteration) and by varying degrees of interaction between these different processes. However the overall correlation between increasing U/Th ratio and increasing Na_2O/K_2O ratio and decreasing K_2O/Rb ratio within the Long John Lake leucomonzogranite and other high ratio units illustrate the potential application of U/Th ratios as an indicator of the late stage albitization.

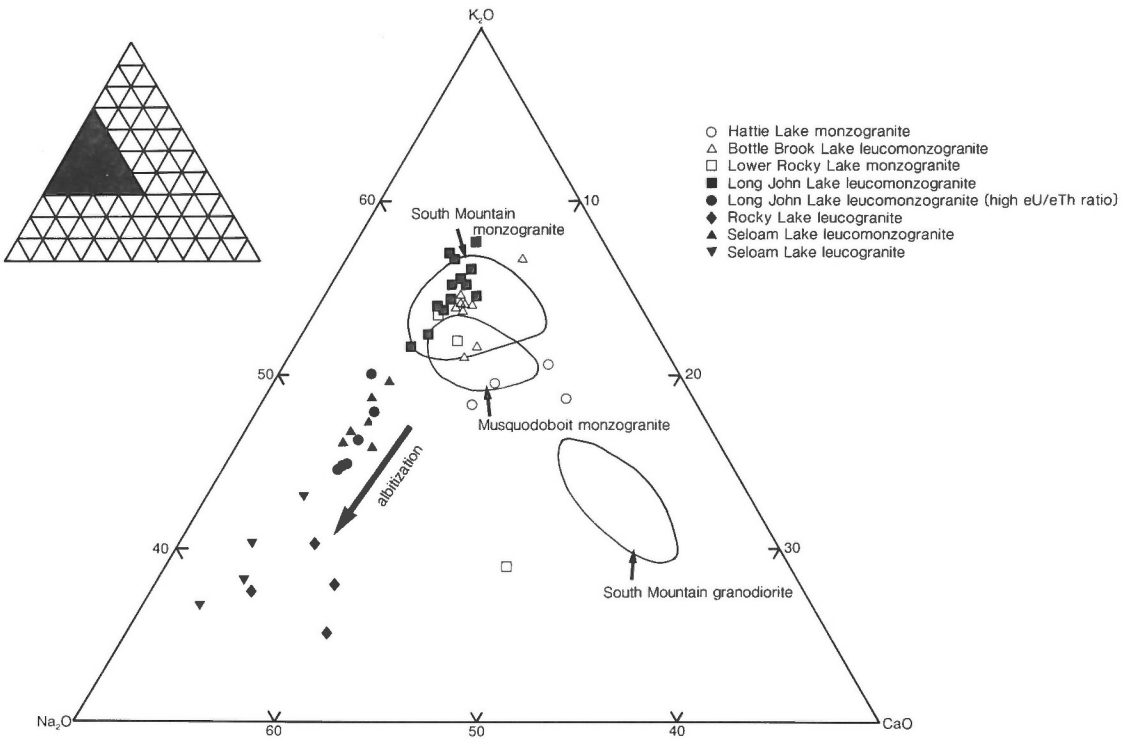

Figure 21. Plot of K_2O-Na_2O-CaO for geochemical data from the eastern half of the Liscomb Complex showing trend towards sodium enrichment for the high eU/eTh ratio samples.

SUMMARY

Results of ground follow-up studies conducted over portions of the Musquodoboit Batholith and Liscomb Complex of eastern Nova Scotia demonstrate that airborne gamma ray spectrometric surveys are a useful aid to both bedrock and surficial geological mapping and mineral exploration. Results from this and previous studies have shown that the radioelement distribution patterns measured by an airborne gamma ray spectrometric survey accurately reflect the relative variations in bedrock K, U, and Th concentrations and their associated ratios.

In the Musquodoboit Batholith, areas of low eU/eTh ratios are dominated by a less evolved, porphyritic, biotite monzogranite whereas areas of high eU/eTh ratios are dominated by fine- to coarse-grained, heterogeneous, two-mica monzogranite, porphyry, aplite, and aplitic-pegmatitic dyke rocks. These high ratio units display greater textural inhomogeneity, ranging from porphyritic to seriate, inequigranular, and equigranular. Correlations between the airborne gamma ray spectrometric patterns and the high eU/eTh ratio units suggest that these units may be more extensive than previously recognized. Whole-rock geochemical analyses of the high ratio units (monzogranite, porphyry, aplite, and aplitic-pegmatitic dyke rocks) indicate characteristics associated with increased magmatic differentiation, and as well, display features suggestive of increased fluid-rock or fluid-melt interaction, such as increased Na_2O, P_2O_5, and lower K_2O along with strong depletion of Sr and Ba and lower K/Rb ratios.

In the eastern part of the Liscomb Complex, monzogranite with low eU/eTh ratios is less evolved than adjacent units with intermediate or high eU/eTh ratios. Whole-rock geochemical analyses show that increased eU/eTh ratios correlate well with increased magmatic differentiation and increased late- and/or postmagmatic alteration (albitization) characterized by increased Na_2O/K_2O, Na_2O, and P_2O_5, and lower K_2O, Sr, Ba, and K/Rb.

Whereas the anomalously high eU/eTh ratio is perhaps the most obvious radioelement signature of the Musquodoboit Batholith and Liscomb Complex, other, commonly more subtle, variations in the eU/eTh ratio, and in other radioelement parameters, may also provide assistance to geological mapping. For example, low eU/eTh ratios correlate with low differentiation indices associated with monzogranite north of Tangier Grand Lake in the eastern Musquodoboit Batholith.

The lack of obvious petrological contrast between adjacent areas of strong radioelement variations emphasizes the important role that airborne gamma ray spectrometric surveys can play in geological mapping and mineral exploration. The ability to subdivide apparently homogeneous granitic intrusions, using radiometrics, may increase our understanding of the crystallization history of various granitic intrusions by outlining subtle petrological and sometimes cryptic compositional zonation that might not otherwise be recognized.

The results of this study and studies of other areas of the Meguma Zone demonstrate that airborne gamma ray spectrometric surveys can be a valuable aid to regional and detailed bedrock and surficial geological mapping and mineral exploration. Despite variable, commonly thick, overburden cover, these surveys can distinguish degrees of magmatic evolution in granitic rocks and can detect intrusions or parts of intrusions that have undergone late- and/or postmagmatic metasomatism and hydrothermal alteration. This last feature has important applications to mineral exploration because of the common association of granophile-element mineral deposits with these areas of pervasive alteration and anomalous radioelement signatures.

ACKNOWLEDGMENTS

This project, including the detailed (250 m line spaced) and some of the regional (1 km line spaced) airborne gamma ray spectrometric surveys, was carried out as a contribution to the Canada-Nova Scotia Mineral Development Agreement. The author wishes to acknowledge the capable assistance of J. Wills, S. Ross, and M. Moore during field studies. The project benefitted greatly from numerous discussions with M. MacDonald, A.K. Chatterjee, P. Giles, G.A. O'Reilly, L. Ham, M. Corey, D.J. Kontak, and P.K. Smith of the Nova Scotia Department of Natural Resources; D.R. Duncan, formerly of Seabright Resources Ltd.; and B.W. Charbonneau and R.B.K. Shives of the Geological Survey of Canada.

REFERENCES

Bristow, Q.
1979: Gamma-ray spectrometric methods in uranium exploration - airborne instrumentation; in Geophysics and Geochemistry in the Search for Metallic Ores, (ed.) P.J. Hood; Geological Survey of Canada, Economic Geology Report 31, p. 135-146.
1983: Airborne gamma-ray spectrometry in uranium exploration, principles and current practice; International Journal of Applied Radiation Isotopes, v. 34, p. 199-229.

Charbonneau, B.W., Killeen, P.G., Carson, J.M., Cameron, G.W., and Richardson, K.A.
1976: Significance of radioelement concentration measurements made by airborne gamma ray spectrometry over the Canadian Shield; International Atomic Energy Agency Symposium on Exploration for Uranium Ore Deposits, Vienna, Austria, p. 35-53.

Chatterjee, A.K. and Muecke, G.K.
1982: Geochemistry and the distribution of uranium and thorium in the granitoid rocks of the South Mountain Batholith, Nova Scotia; some genetic and exploration implications; in Uranium in Granites, (ed.) Y.T. Maurice; Geological Survey of Canada, Paper 81-23, p. 11-17.

Clark, S.P., Jr., Peterman, Z.E., and Heier, K.S.
1966: Abundance of uranium, thorium and potassium; in Handbook of Physical Constants, Geological Society of America, Memoir 97, p. 521-541.

Clarke, D.B. and Halliday, A.N.
1980: Strontium isotope geology of the South Mountain Batholith, Nova Scotia; Geochemica et Cosmochemica Acta, v. 44, p. 1045-1058.

Corey, M.C.
1987: A re-interpretation of U-Th ratios in the New Ross Area: Evidence for a zoned pluton; in Mines and Minerals Branch, Report of Activities 1987, Part A, (ed.) J.L. Bates and D.R. MacDonald; Nova Scotia Department of Mines and Energy, Report 87-5, p. 105-108.

Ford, K.L.
1982: Investigation of regional airborne gamma-ray spectrometric patterns in New Brunswick and Nova Scotia; in Current Research, Part B; Geological Survey of Canada, Paper 82-1B, p. 177-194.

Ford, K.L. and Ballantyne, S.B.
1983: Uranium and thorium distribution patterns and lithogeochemistry of Devonian granites in the Chedabucto Bay Area, Nova Scotia; in Current Research, Part A; Geological Survey of Canada, Paper 83-1A, p. 109-119.

Ford, K.L. and Carson, J.M.
1986: Application of airborne gamma-ray spectrometric surveys, Meguma Terrane, Nova Scotia; Maritime Sediments and Atlantic Geology, v. 22, p. 117-135.

Ford, K.L. and O'Reilly, G.A.
1985: Airborne gamma-ray spectrometric surveys as an indicator of granophile element specialization and associated mineral deposits in the granitic rocks of the Meguma Zone of Nova Scotia; in High Heat Production (HHP) Granites, Hydrothermal Circulation and Ore Genesis, Institution of Mining and Metallurgy, St. Austell, Cornwall, England, p. 113-133.

Ford, K.L., Carson, J.M., Grant, J.A., and Holman, P.B.
1989: Radioactivity Maps of Nova Scotia; Geological Survey of Canada, Map 35006G, scale 1:500 000.

Fyson, W.K.
1966: Structures in the Lower Paleozoic Meguma Group, Nova Scotia; Geological Society of America Bulletin, v. 77, p. 931-944.

Geological Survey of Canada
1982: Airborne gamma ray spectometric map, Musquodoboit Harbour, Nova Scotia, 11D/14; Geological Survey of Canada, G-Series Map 3541114G, scale 1:50 000.
1986a: Aeromagnetic total field maps, Musquodoboit Harbour, Nova Scotia, 11D/14; Geological Survey of Canada, Map C21284G, scale 1:50 000.
1986b: Aeromagnetic vertical gradient map, Musquodoboit Harbour, Nova Scotia, 11D/14; Geological Survey of Canada, Map C41284G, scale 1:50 000.
1987a: Airborne geophysical survey of the Eastern Liscomb Pluton, Nova Scotia, 11E/1, 2, 7, 8 (part of); Geological Survey of Canada, Open File 1473, 11 maps, scale 1:50 000.
1987b: Airborne geophysical survey of the Gibraltar Hill area, Nova Scotia, 11D/14 (part of); Geological Survey of Canada, Open File 1476, 11 maps, scale 1:50 000.
1987c: Airborne geophysical survey of the Granite Lake area, Nova Scotia, 11D/14 (part of); Geological Survey of Canada, Open File 1477, 11 maps, scale 1:50 000.
1987d: Airborne geophysical survey of the Ship Harbour area, Nova Scotia, 11D/15 (part of); Geological Survey of Canada, Open File 1472, 11 maps, scale 1:50 000.

Giles, P.S. and Chatterjee, A.K.
1987: Peraluminous granites of the Liscomb Complex; in Mines and Minerals Branch, Report of Activities, 1986; (ed.) J.L. Bates and D.R. MacDonald; Nova Scotia Department of Mines and Energy, Report 87-1, p. 95-98.

Grasty, R.L.
1979: Gamma-ray spectrometric methods in uranium exploration - theory and operational procedures; in Geophysics and Geochemistry in the Search for Metallic Ores, (ed.) P.J. Hood; Geological Survey of Canada, Economic Geology Report 31, p. 147-161.

Grasty, R.L., Mellander, H., and Parker, M.
1991: Airborne gamma ray spectrometer surveying; International Atomic Energy Agency, Technical Reports Series No. 323, Vienna, 97 p.

Grasty, R.L., Wilkes, P.G., and Kooyman, R.
1988: Background measurements in gamma-ray surveys; Geological Survey of Canada, Paper 88-11, 33 p.

Ham, L.J., Marsh, S.W., Corey, M.C., Horne, R.J., and MacDonald, M.A.
1989: Lithogeochemistry of the eastern portion of the South Mountain Batholith, Nova Scotia; Nova Scotia Department of Mines and Energy, Open File Report 89-001, 62 p.

Keppie, J.D.
1979: Geological map of Nova Scotia; Nova Scotia Department of Mines and Energy, scale 1:250 000.

Keppie, J.D. and Muecke, G.K.
1979: Metamorphic map of Nova Scotia; Nova Scotia Department of Mines and Energy, scale 1:1 000 000.

Killeen, P.G.
1979: Gamma-ray spectrometric methods in uranium exploration - application and interpretation; in Geophysics and Geochemistry in the Search for Metallic Ores, (ed.) P.J. Hood; Geological Survey of Canada, Economic Geology Report 31, p. 163-229.

Kontak, D.J., Cormier, R.F., and Reynolds, P.H.
1989: Preliminary results of Rb/Sr and $^{40}Ar/^{39}Ar$ geochronological investigations, East Kemptville leucogranite, southwestern Nova Scotia: Evidence for a ca. 370 Ma age of emplacement and multiple tectonothermal overprinting events; in Mines and Minerals Branch, Report of Activities, 1989, Part A, (ed.) D.R. MacDonald and K.A. Mills; Nova Scotia Department of Mines and Energy, Report 89-3, p. 41-48.

Kontak, D.J., Strong, D.F., and Kerrich, R.
1988: Crystal-melt+/-fluid phase equilibra versus late-stage fluid-rock interaction in granitic rocks of the South Mountain Batholith, Nova Scotia: Whole rock geochemistry and oxygen isotope evidence; Maritime Sediments and Atlantic Geology, v. 24, p. 97-110.

MacDonald, M.A. and Clarke, D.B.
1985: The petrology, geochemistry and economic potential of the Musquodoboit Batholith, Nova Scotia; Canadian Journal of Earth Sciences, v. 22, p. 1633-1642.

MacDonald, M.A., Horne, R.J., Corey, M.C., and Ham, L.J.
1992: An overview of recent bedrock mapping and follow-up petrological studies of the South Mountain Batholith, southwestern Nova Scotia, Canada; Atlantic Geology, v. 28, p. 7-28.

MacMichael, T.P.
1975: The origin of the lead-zinc-silver ores and the alteration of the surrounding granites in the Dunbrack mine, Musquodoboit Harbour, Nova Scotia; B.Sc. thesis, Dalhousie University, Halifax, Nova Scotia, 27 p.

O'Reilly, G.A.
1988: Geology and geochemistry of the Sangster Lake and Larrys River Plutons, Guysborough County, Nova Scotia; M.Sc. thesis, Dalhousie University, Halifax, Nova Scotia, 290 p.

O'Reilly, G.A., Corey, M.C., and Ford, K.L.
1988: The role of airborne gamma-ray spectrometry in bedrock mapping and mineral exploration: case studies from granitic rocks within the Meguma Zone, Nova Scotia; Maritime Sediments and Altantic Geology, v. 24, p. 47-60.

O'Reilly, G.A., Gauthier, G., and Brooks, C.
1985: Three permo-carboniferous Rb/Sr age determinations from the South Mountain Batholith; in Mines and Minerals Branch, Report of Activities 1984, (ed.) K.A. Mills and J.L. Bates; Nova Scotia Department of Mines and Energy, Report 85-1, p. 143-152.

Reynolds, P.H., Elias, P., Muecke, G.K., and Grist, A.M.
1987: Thermal history of the southwestern Meguma Zone, Nova Scotia, from an $^{40}Ar/^{39}Ar$ and fission track dating study of intrusive rocks; Canadian Journal of Earth Sciences, v. 24, p. 1952-1965.

Reynolds, P.H., Zentilli, M., and Muecke, G.K.
1981: K-Ar and $^{40}Ar/^{39}Ar$ geochronology of granitoid rocks from southern Nova Scotia: its bearing on the geological evolution of the Meguma Zone of the Appalachians; Canadian Journal of Earth Sciences, v. 18, p. 386-394.

Stea, R.R. and Fowler, J.H.
1979: Minor and trace element variations in Wisconsinan tills, Eastern Shore Region, Nova Scotia; Nova Scotia Department of Mines and Energy, Paper 79-4, 30 p.

Streckeisen, A.
1976: To each plutonic rock its proper name; Earth Science Review, v. 12, p. 1-33.

Williams, H.
1978: Tectonic lithofacies map of the Appalachian Orogen; Memorial University of Newfoundland, Map 1, scale 1:1 000 000.